Characterising Room Temperature Ionic Liquids With Acoustic Wave Devices

Nicola Doy

A thesis submitted in partial fulfilment of the requirements of
Nottingham Trent University for the degree of Doctor of Philosophy

April 2010

”Anybody who has been seriously engaged in scientific work of any kind realises that over the entrance to the gates of the temple of science are written the words: ‘Ye must have faith.’”

Max Planck

ACKNOWLEDGEMENTS

This work has been funded by the UK Engineering and Physical Sciences Research Council (EPSRC) under grant numbers EP/D03826X/1, EP/D038294/1 and EP/D038995/1 for which we are very grateful. In addition to this, funding for conference travel has been provided by the CR Barber Trust through the UK Institute of Physics.

I would like to say thank you to my Director of Studies, Glen McHale and supervisor Michael Newton for their knowledge, support, faith in my work and the incredible opportunities they have given me in presenting at both national and international conferences.

My parents Elizabeth and Jonathan Doy, partner Robert Morris, and his parents Kathleen and Dennis Morris who have provided unquestionable support, and made the completion of this work possible. Also to my siblings, Martin, Joanne and Claire who never really understood what I was trying to do but considered it to be very clever!

The work that has been carried out over the course of this project has relied on the assistance of many people to whom I wish to extend my thanks: David Parker of Nottingham Trent University, for making many sample holders. Rile Ge and Chris Hardacre at the Queens University Belfast, for supplying all of the knowledge and protocol required for handling room temperature ionic liquids along with the liquids themselves in much larger quantities than they ever really wanted to give. Jordan MacInnes, Ray Allen and Dmitriy Kuvshinov at the University of Sheffield for their assistance with microfluidics and design ideas. To Jordan I owe additional thanks for helping provide the understanding of the modelling and limitation calculations of the device, thank you for answering many emails!

Lastly, my fellow lab colleagues who provided endless support, information and well needed coffee breaks: Carl Evans, Shaun Atherton, Neil Shirtcliffe, Gary Wells, Christophe Trabi and David Willmer, thank you. A special thank you to Gary who was always on hand to discuss sling-backs and 80s fashion!

ABSTRACT

Data for the physical properties of Room Temperature Ionic Liquids (RTILs) as a function of chemical composition is limited due to the expense and difficulty of producing large volumes of pure samples for characterization. RTILs comprise solely of ions and are liquid at room temperature. These are becoming of increasing interest for an extensive range of applications. This thesis looks at developing small scale characterization processes to find low cost and efficient methods for processing smaller sample volumes.

Quartz crystal impedance analysis has been used to assess whether room temperature ionic liquids behave in a Newtonian manner to determine the values of their square root viscosity-density product using small volumes. Values are compared to traditional viscometer and densitometer measurements. A range of harmonics were studied for a 5 MHz fundamental crystal. The frequency shift of the third harmonic was found to provide the closest agreement between the two measurement methods with a limit seen at a square root viscosity-density product value of approximately 18 kg m^{-2} $s^{-0.5}$. Further characterisation of the liquid was performed to separate values of density and viscosity using dual Quartz Crystal Microbalance (QCM) with fabricated surface features on one QCM; this required a total sample volume of only 240 μL. Values were corroborated with standard measurement techniques demonstrating good agreement. A QCM was then incorporated into a microfluidic glass chip system to measure the square root of the viscosity-density product of RTILs. The QCM covers a central recess on the glass chip, with a seal formed by tightly clamping from above outside the sensing region. The change in resonant frequency of an 8 MHz QCM operating on the 3rd harmonic was shown to allow determination of the square root viscosity-density product of RTILs to a maximum limit of square root viscosity-density product of approximately 10 kg m^{-2} $s^{-0.5}$. This microfluidic technique reduced the sample size needed for characterisation from 1.5 ml to only 30 μL and allowed the measurement to be made in an enclosed system reducing the risk of water contamination.

In the final part of this work surface acoustic wave devices were studied. The most promising device, a Shear Horizontal Surface Acoustic Wave (SH-SAW) device with silicon dioxide guiding layer, provided good correlation between phase, insertion loss and the square root viscosity-density product. A maximum square root viscosity-density product limit was observed at approximately 10 kg m^{-2} $s^{-0.5}$ at which point the acoustic response becomes too damped for accurate results to be determined. This work provides a basis for further miniaturisation and characterisation which could develop a surface acoustic wave device based system for high throughput microfluidic characterisation of many properties of ionic liquids within a single chip.

CONTENTS

LIST OF FIGURES

LIST OF TABLES

LIST OF ABBREVIATIONS

IDT	InterDigiTated electrodes
PDMS	PolyDiMethylSiloxane
PEEK	PolyEtherEtherKetone
PTFE	PolyTetraFluoroEthylene
QCM	Quartz Crystal Microbalance
RTIL	Room Temperature Ionic Liquid
SAW	Surface Acoustic Wave
SH-APM	Shear Horizontal Acoustic Plate Mode
SH-SAW	Shear Horizontal Surface Acoustic Wave
SiO_2	Silicon Dioxide

I. INTRODUCTION

I.1 Motivation

The need for cleaner industrial processes is continuously rising. The past decade has led to the development of room temperature ionic liquids (RTILs) as alternative, environmentally friendly, solvents [1, 2]. They comprise solely of ions which are liquid at room temperature and can be considered designer solvents with over one million simple ionic liquids available. Ionic liquids have huge potential for a wide range of applications which include catalysis [3, 4], organic synthesis [5], electrochemistry [6], separations and extractions [7, 8], liquid crystals [9–11] and analytical solvents and coatings [12]. They can be specifically tailored to suit applications in chemical engineering for which they are finding novel applications. However, the available data on their physical properties as a function of chemical composition is limited and extending the range of known data is difficult due to the expense and difficulty of producing large volumes of pure liquids for characterization.

At the start of this study there was little reported work on the application of acoustic wave devices for measuring the properties of room temperature ionic liquids. Some preliminary data on the density and viscosity of the liquids was available in the literature but for a very limited number of RTILs.

Acoustic wave sensors, such as the quartz crystal microbalance (QCM), are widely used for studying the properties of small volume samples of liquids. The QCM is a thickness shear mode resonator and is a very popular and well established technique for mass or liquid sensing using the Sauerbrey or Kanazawa and Gordon equations respectively. Some applications include the attachment of mass from the liquid phase and for *in-situ* determination of the properties of surface coatings, such as electrodeposited polymers during deposition processes, with material parameters extracted using viscoelastic response models [13–17].

Surface Acoustic Wave (SAW) sensors are the natural next step for increased sensitivity and further miniaturisation. SAW sensors (such as the Rayleigh, Surface Skimming Bulk, Shear Horizontal SAW, Acoustic Plate Mode (APM), and the Love wave device) have been used for various sensing applications which include mass deposition [18], gas and vapour detection [19] and liquid identification [20]. The SAW sensor is a well known versatile device which has been evolving since the 1950s, seeing constant improvements to the selectivity, sensitivity and stability of the device. Their versatility makes them ideal sensors for integration into microfluidic experimental setups [21, 22] and makes them well suited to high throughput online laboratory-on-a-chip systems. Using high throughput, small volume liquid sensors in a microfluidic environment will make it possible

to characterise these liquids with microlitre sample volumes which will lower production costs and rapidly increase the rate of liquid characterisation, giving optimum information for use in potential chemical engineering applications.

I.2 Project Overview

The main objectives of this work were to: investigate acoustic wave techniques for characterising small volumes of Room Temperature Ionic Liquids (RTILs); obtain data for the viscosity-density product of RTILs; determine the Newtonian behaviour of RTILs experiencing high frequency perturbations and to integrate an acoustic wave device into a lab-on-a-chip set-up to further reduce sample volume needed to measure the viscosity-density product of RTILs.

To complete these objectives this project has overcome many challenges including: the high density and viscosity of RTILs; the limited volume of available material to work with; the need for an enclosed system due to their hygroscopic nature and the very limited range of chemically resistant engineering materials such as glass and polytetrafluoroethylene (PTFE) that can be used in producing flowcells and seals.

The layout of this thesis gives some background knowledge of acoustic wave technology (chapter 1), before looking at four self contained experimental studies.

The first experimental chapter looks at measuring the square-root viscosity-density product of RTILs using static pools of liquid with one sided contact on the Quartz Crystal Microbalance (QCM). It determines the range of Newtonian behaviour in relation to the QCM and makes a comparison of the responses of RTILs, polydimethylsiloxane (PDMS) oils and water-glycerol mixtures. A study varying the concentration of a water miscible and a water immiscible (miscible with methanol) RTIL has been completed, together with a further eighteen pure RTILs (minimal water content) characterised on both the fundamental and third harmonic of a QCM.

Experimental chapter 2 looks at separating the two parameters of the viscosity-density product using a dual QCM setup. This work is an extension to work published by Martin *et al.* [23] and uses SU8-10 photolithography to form a patterned surface on one of the QCMs. A comparison of frequency changes between the two QCMs makes it possible to separate the two parameters. Five patterned surfaces have been explored with viscosity and density determined for various concentrations of water-glycerol mixtures and eight pure RTILs.

The third experimental chapter looks at a further reduction in sample volume by integrating the QCM into an enclosed microfluidic setup to determine the viscosity-density product of RTILs whilst minimising hygroscopic issues. It looks at various concentrations of water-glycerol mixtures, concentrations of a water miscible

RTIL and many pure RTILs. Measurements are made on both the fundamental and third harmonic resonance on both an 8 and 9 MHz QCM.

The final experimental chapter looks at the challenges of using a Surface Acoustic Wave (SAW) device to measure the viscosity-density product of RTILs. The ionic content of RTILs has shown some conductivity challenges which lead to the investigation of a metallised propagation path on the Shear Horizontal SAW (SH-SAW) device. The addition of a silicon dioxide guiding layer onto a SH-SAW device (Love wave device) is also investigated as a possible improvement. Successful characterisation of a range of water-glycerol mixtures, dilutions of a water miscible RTIL and pure RTILs has been achieved by measuring the phase changes seen on a Love wave device. Finally, a short summary and ideas for further work concludes the contents of this work.

References

[1] M. Earle and K. Seddon, "Ionic liquids. Green solvents for the future," *Pure and Aplied Chemistry*, vol. 72, no. 7, pp. 1391–1398, 2000. Workshop on Sustainable Chemistry, Venice, Italy, Oct 15-17, 1998.

[2] C. Andrade and L. Alves, "Environmentally benign solvents in organic synthesis: Current topics," *Current Organic Chemistry*, vol. 9, no. 2, pp. 195–218, 2005.

[3] R. Sheldon, "Catalytic reactions in ionic liquids," *Chemical Communications*, no. 23, pp. 2399–2407, 2001.

[4] J. Dupont, R. de Souza, and P. Suarez, "Ionic liquid (molten salt) phase organometallic catalysis," *Chemical ReviewsDupont2002*, vol. 102, no. 10, pp. 3667–3691, 2002.

[5] G. Cave, C. Raston, and J. Scott, "Recent advances in solventless organic reactions: towards benign synthesis with remarkable versatility," *Chemical Communications*, no. 21, pp. 2159–2169, 2001.

[6] P. Chen, Y. Lin, and I. Sun, "Electrochemistry of gallium in the Lewis acidic aluminum chloride-1-methyl-3-ethylimidazolium chloride room-temperature molten salt," *Journal of the Electrochemical Society*, vol. 146, no. 9, pp. 3290–3294, 1999.

[7] G. Wei, Z. Yang, and C. Chen, "Room temperature ionic liquid as a novel medium for liquid/liquid extraction of metal ions," *Analytica Chimica Acta*, vol. 488, no. 2, pp. 183–192, 2003.

[8] H. Zhao, S. Xia, and P. Ma, "Use of ionic liquids as 'green' solvents for extractions," *Journal of Chemical Technology and Biotechnology*, vol. 80, no. 10, pp. 1089–1096, 2005.

[9] C. Bowlas, D. Bruce, and K. Seddon, "Liquid-crystalline ionic liquids," *Chemical Communications*, no. 14, pp. 1625–1626, 1996.

[10] D. Abdallah, A. Robertson, H. Hsu, and R. Weiss, "Smectic liquid-crystalline phases of quaternary group VA (especially phosphonium) salts with three equivalent long n-alkyl chains. How do layered assemblies form in liquid-crystalline and crystalline phases?," *Journal of the American Chemical Society*, vol. 122, no. 13, pp. 3053–3062, 2000.

[11] A. Bradley, C. Hardacre, J. Holbrey, S. Johnston, S. McMath, and M. Nieuwenhuyzen, "Small-angle X-ray scattering studies of liquid crystalline 1-alkyl-3-methylimidazolium salts," *Chemistry of Materials*, vol. 14, no. 2, pp. 629–635, 2002.

[12] W. Qin, H. Wei, and S. Li, "1,3-dialkylimidazolium-based room-temperature ionic liquids as background electrolyte and coating material in aqueous capillary electrophoresis," *Journal of Chromatography A*, vol. 985, no. 1-2, pp. 447–454, 2003. 25th International Symposium on Capillary Chromatography, Riva Del Garda, Italy, May 13-17, 2002.

[13] S. Martin, V. Granstaff, and G. Frye, "Characterization of a quartz crystal microbalance with simultaneous mass and liquid loading," *Analytical Chemistry*, vol. 63, no. 20, pp. 2272–2281, 1991.

[14] H. Bandey, A. Hillman, M. Brown, and S. Martin, "Viscoelastic characterization of electroactive polymer films at the electrode/solution interface," *Faraday Discussions*, vol. 107, pp. 105–121, 1997. Meeting on Interactions of Acoustic Waves with Thin Films and Interfaces, Leicester, England, Sep 08-10, 1997.

[15] K. Kanazawa and J. Gordon, "The oscillation of a frequency of a quartz resonator in contact with a liquid," *Analytica Chimica Acta*, vol. 175, pp. 99–105, 1985.

[16] S. Bruckenstein and M. Shay, "Experimental aspects of use of quartz crystal microbalance in solution," *Electrochimic Acta*, vol. 30, no. 10, pp. 1295–1300, 1985.

[17] G. Sauerbrey *Zeitschrift fr Physik*, pp. 206–222, 1959.

[18] K. Laenge, B. E. Rapp, and M. Rapp, "Surface acoustic wave biosensors: a review," *Analytical and Bioanalytical Chemistry*, vol. 391, no. 5, pp. 1509–1519, 2008.

[19] I. Esteban, C. Dejous, D. Rebiere, J. Pistre, R. Planade, and J. Lipskier, "Mass sensitivity of SH-APM sensors: potentialities for organophosphorous vapors detection," *Sensors and Actuators B-Chemical*, vol. 68, no. 1-3, pp. 244–248, 2000. Eurosensors XIII Meeting, The Hague, Netherlands, Sep 12-15, 1999.

[20] S. Jacesko, J. Abraham, T. Ji, V. Varadan, M. Cole, and J. Gardner, "Investigations on an electronic tongue with polymer microfluidic cell for liquid sensing and identification," *Smart Materials & Structures*, vol. 14, no. 5, pp. 1010–1016, 2005.

[21] D. Beyssen, L. Le Brizoual, O. Elmazria, and P. Alnot, "Microfluidic device based on surface acoustic wave," *Sensors and Actuators B-Chemical*, vol. 118, no. 1-2, pp. 380–385, 2006. 19th European Conference on Solid-State Transducers, Barcelona, Spain, Sep 11-14, 2005.

[22] D. Mark, S. Haeberle, G. Roth, F. von Stetten, and R. Zengerle, "Microfluidic lab-on-a-chip platforms: requirements, characteristics and applications," *Chemical Society Reviews*, vol. 39, no. 3, pp. 1153–1182, 2010.

[23] S. Martin, G. Frye, and K. Wessendorf, "Sensing liquid properties with thickness-shear mode resonators," *Sensors and Actuators A-Physical*, vol. 44, no. 3, pp. 209–218, 1994.

II. BACKGROUND AND THEORY

This work is based on three main areas: the Quartz Crystal Microbalance (QCM), Surface Acoustic Wave (SAW) sensors, and Room Temperature Ionic Liquids (RTILs). A brief overview of each of these topics are described.

II.1 Acoustic Wave Devices

The mode of operation of acoustic wave devices is determined by the piezoelectric nature of the material and its properties, which are described below.

II.1.1 Piezoelectricity

Piezoelectricity is the material property usual used to excite an acoustic wave in an acoustic wave device. For this reason, such devices are created using piezoelectric materials such as quartz, lithium tantalate and lithium niobate. Piezoelectricity is a property displayed by certain crystalline materials, in which a mechanical strain is produced in respose to an electric field [1] and vice versa. By applying an oscillating electric field to an acoustic wave device, a mechanical wave is created which propagates through the substrate before being converted back to an electric field for measurement. Each piezoelectric material has its advantages and disadvantages, including cost, temperature dependence, attenuation, and propagation velocity [2] which must be carefully considered for potential applications.

II.1.2 Crystal Orientation

An acoustic wave device is optimised for a given operational mode by choosing the crystal cut and wave propagation direction carefully for the application needed. AT-cut quartz (defined by its orientation - see Figure II.1) is the most popular cut for Thickness Shear Mode resonators (TSM, also referred to as QCM) and is considered to be temperature compensated. Various crystal cuts for quartz are shown in Figure II.1. Many specialised cuts and crystal types are available which present various elastic, piezoelectric and dielectric properties [3]. QCMs are commonly manufactured with fundamental frequencies between 1 and 32 MHz. For a QCM, the resonant frequency is dependent on crystal thickness. At high frequencies the crystal becomes extremely thin and hence very fragile, making it difficult to work with. Factors such as the density and shear modulus of the crystal also influence its operating frequency [4].

Applications that require frequencies higher than those given by the QCM use an alternative crystal cut and

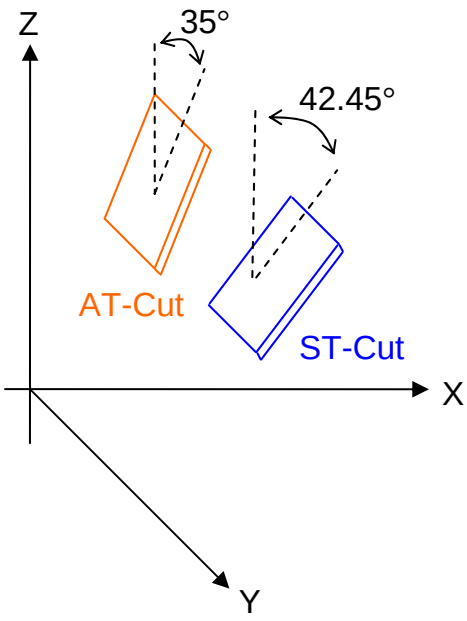

Figure II.1: Cuts of quartz shown relative to the crystal axes, showing the two crystal cuts used within this study, AT-cut - common for quartz crystal microbalances, and ST-cut - common for shear horizontal surface acoustic wave devices.

require a Surface Acoustic Wave (SAW) sensor. Again, the direction of crystalline orientation and hence propagation path of the surface acoustic wave is dependent on the wave needed and its application. The substrate and cut direction is initially chosen by the need for a Rayleigh wave if sensing a gas and Shear-Horizonatal Surface Acoustic Wave (SH-SAW) or Surface Skimming Bulk wave (SSBW) for liquid or mass sensing. Here the frequency is independent of substrate thickness and for this reason the SAW is generally more robust and capable of handling much greater applied pressures.

II.2 Quartz Crystal Microbalance

Quartz Crystal Resonators (QCR) or Thickness Shear Mode (TSM) devices operating with shear horizontal displacement are more commonly known as Quartz Crystal Microbalances (QCMs). This name is however a little misleading and implies it is only capable of sensing changes in mass which is not the case. The QCM is a well known small volume device and originated 40 years ago from the work of Sauerbrey [5] and King [6] investigating mass changes in the gas phase. More recently, applications have been found to measure properties in the liquid phase including bulk properties such as density, viscosity, conductivity [7], attachment of mass from the liquid phase [8] and *in-situ* determination of the properties of surface coatings such as online monitoring of electrodeposited polymers [9].

II.2.1 Quartz Crystal Microbalance Design

The QCM consists of a thin quartz disc operating between two electrodes (see Figure II.2). By applying an external electric potential to the piezoelectric material, an internal mechanical stress is induced resulting in an acoustic wave which propagates perpendicular to the crystal surface. Minimum impedance is seen when the

thickness of the device is an integer multiple of a half wavelength of the acoustic wave. By incorporating the QCM into an oscillation circuit the electric and mechanical oscillations will be at the fundamental frequency of the crystal. By measuring this frequency some of the properties of a liquid applied to the crystals surface can be determined.

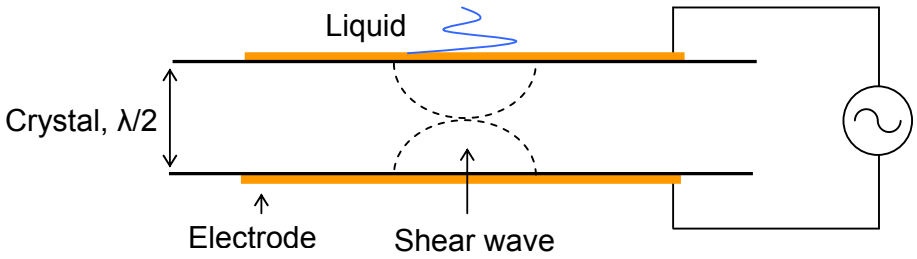

Figure II.2: Quartz Crystal Microbalance in oscillating circuit showing shear wave.

II.2.1.1 Harmonics

When the crystal is electrically excited over a broad frequency range it is possible to excite harmonics of the fundamental frequency. Standing shear wave patterns set up across the thickness of the crystal (see Figure II.3). Maximum displacement occurs at the crystal faces for each of the resonances [10] making the device sensitive to mass deposition and liquid parameters. Some studies have been completed on sensing using many harmonics of the QCM [11, 12]. Earlier work comparing resonant frequency shifts of various harmonics whilst testing the shear compliance of thin films has suggested that the third harmonic produces a more accurate frequency change response to mass/liquid loading [13].

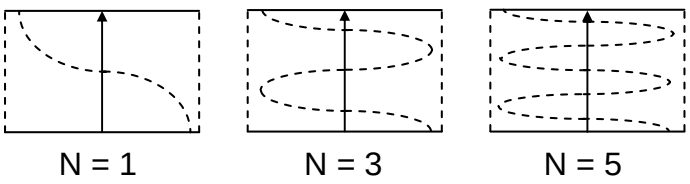

Figure II.3: Quartz Crystal Microbalance showing shear displacement profiles for the fundamental, third harmonic, and fifth harmonic resonances, where N is harmonic number.

II.2.2 Sensing

The Quartz Crystal Microbalance (QCM) was initially designed for mass deposition monitors in vacuum evaporators [5] sensing mass changes of roughly 1 ng.cm^{-2} [10]. Applications for the QCM have continued to grow following this. In 1982 it was found that the QCM could be made to oscillate in a liquid [14], which has since stimulated many useful applications. Subsequently it was found that polymers and viscoelastic films can be studied using a QCM. This section looks at mass and liquid sensing, and includes the effect of surface morphol-

ogy which can be designed to provide a further characterisation technique. A brief review of the Butterworth-Van Dyke (BVD) model [15] is given which can be used to assess many more properties.

II.2.2.1 Mass Sensing

Sauerbrey states that accumulation of mass on the surface of the QCM induces changes in the resonant frequency. Hence for detection of analytes in air, the frequency change is simply related to the change in mass [4] (Equation II.1, which can be reduced to Equation II.2 by collecting constants):

$$\Delta f = -\frac{2f_q^2}{\sqrt{\mu_q \rho_q}} \frac{\Delta M}{A} \tag{II.1}$$

where f_q is the fundamental resonant frequency of unloaded quartz, μ_q is the shear modulus of AT-cut quartz (2.497 x 10^{11} g $cm^{-1}s^{-2}$), ρ_q is the density of quartz (2.468 g cm^{-3}), A is surface area in cm^2 (one face), ΔM is the total mass change on both faces of the crystal. Thus,

$$\Delta f = K \Delta m \tag{II.2}$$

where K = -2.26 x 10^{-6} f_q^2 Hz $cm^{\,2}$ $g^{\,-1}$ and Δm is mass added per unit area in g cm^{-2}. For a 5 MHz crystal a frequency change of 1 Hz is the result of a mass change of 18 ng cm^{-2} [16].

The additional mass on the surface of the crystal can be thought of as a slight increase in its thickness resulting in an increase in wavelength corresponding to a decrease in frequency ($v = f\lambda$).

II.2.2.2 Liquid Sensing

A quartz crystal microbalance operates with a high frequency (typically 5 MHz) shear mode oscillation on its surface. When operated in a liquid environment, this surface oscillation entrains liquid (see Figure II.2). For a Newtonian liquid, this decays within a depth known as the penetration depth (0.25 μm in water at a fundametal frequency of 5 MHz) from the interface. The relationship for this depth is shown in Equation II.3.

$$\delta = \sqrt{(\eta / \pi f_s \rho)} \tag{II.3}$$

where ρ and η are the density and viscosity of the liquid and f_s is the resonant frequency [17].

When in contact with the liquid, the resonance is damped so that the frequency decrease is accompanied by an increase in bandwidth. The QCM can be used to measure either the accumulation of mass onto the surface of the crystal or properties of the liquid itself [1]. The QCM has become a very popular small volume device over the last fifty years and has had many applications some of which include; a sensitive solution phase microbalance [18, 19], deposition monitoring [20], chemical species detection [21], immunoassay [22], liquid chromatographic detection [23], corrosion monitoring [24], and electrochemical analysis [9].

Impedance analysis is a useful technique in which both the resonant frequency and bandwidth (B), of the crystal are measured which are both dependent on the liquid properties. The impedance of a circuit is its opposition to current. The bandwidth is a measure of the loss of energy over a range of frequencies. This corresponds to the damping of the shear mode oscillation caused by the liquid close to the solid-liquid interface. Some authors prefer to define dissipation $D = B/f_s$ (also equal to Q^{-1}). When the liquid is Newtonian, a frequency decrease (Δf), and a bandwidth increase (ΔB), occur in proportion to the square root of the viscosity-density product, see Equations II.4 and II.5. A single sided contact to a Newtonian liquid causes frequency and bandwidth shifts described by Equation II.4 and II.5.

$$\frac{\Delta f}{f_o} = -\frac{1}{Z_q}\left(\frac{f_s \eta \rho}{\pi}\right)^{1/2}, \tag{II.4}$$

$$\frac{\Delta B}{f_o} = \frac{2}{Z_q}\left(\frac{f_s \eta \rho}{\pi}\right)^{1/2}, \tag{II.5}$$

where the specific acoustic impedance of quartz is $Z_q = (\mu_q \rho_q)^{1/2} = 8.84 \text{ x } 10^6 \text{ kg m}^{-2} \text{ s}^{-1}$, f_o is the fundamental frequency and $f_s = nf_o$ is the overtone frequency at which the response is measured [1, 25]. By verifying that changes in resonant frequency and bandwidth are correlated, such that Δf = -$\Delta B/2$, Equations II.4 and II.5 allow determination of whether liquid has a Newtonian response. If the ionic liquid is Newtonian, either the frequency change (the Kanazawa and Gordon equation) or the bandwidth change can be used to determine the value of the viscosity-density product.

II.2.2.3 Polymers And Shear Moduli

A QCM is also a useful tool for applying a shear stress and studying the response on the shear modulus to measure properties of viscoelasticity, phase transition or cross-linking of thin films [26–28].

The viscoelasticity of a polymer can be described by how a polymer deforms in response to an applied stress. Polymers are defined as a compound made up of a large number of repeating units (monomers) joined together with covalent bonds creating a long chain [1]. The polymers chain length (molecular weight) relates directly to the degree of polymerisation. A polymer neither obeys the purely viscous nor the perfect elastic criteria and as such it is generally termed a viscoelastic material [26]. A viscoelastic material will not deform immediately when stresses are applied, equally the stress will not respond instantaneously to any imposed deformation.

Elastic behaviour implies a linear relationship between stress and strain with viscous behaviour implying a relationship between shear stress and the rate of strain. A rigid material behaves elastically, and a fluid or soft material displays viscous behaviour. A polymer exhibits a combination of these responses due to the chain structure, hence the term viscoelastic.

The properties of viscoelastic materials can be described by a complex modulus, where the shear modulus (measure of elasticity), G is given by Equation II.6.

$$G = G' + iG'' \tag{II.6}$$

where G' is the storage modulus (energy storage and release during periodic deformation), i is the $\sqrt{-1}$ and G'' the loss modulus (dissipation of energy, usually as heat) [1].

A film deposited on a QCM is subjected to shearing motion at the crystal-film interface. If the film is bonded well to the crystal surface it moves synchronously with the crystal, the top of the film however may experience some phase lag. If this is the case, elastic energy is stored and dissipated within the film. The crystal's resonant frequency and damping will subsequently depend on the film thickness, density and shear elastic properties. Studies have shown equivalent circuit models which describe how the film properties influence the resonant frequency and damping, and how they can be interpreted to obtain the film's shear storage and loss moduli [29].

When using a QCM to characterise a polymer, the polymer experiences a characteristic relaxation time, τ. If a stress is applied for a time period τ_s much shorter than the relaxation time ($\tau_s \ll \tau$) the polymer chains do not have enough time to move with respect to each other, hence the polymer behaves as an elastic solid characterised by a stiffness, μ. As temperature increases (viscosity decreases), relaxation time decreases until ($\tau_s \gg \tau$). At this point thermal energy permits chains to move with respect to each other allowing the polymer to behave as a viscous liquid characterised by a viscosity η. The temperature where $\tau_s \approx \tau$ can be described as the point at which the polymer deforms both elastically and viscously; giving rise to viscoelastic behaviour. The relaxation time is proportional to molecular weight [30]. Many studies have been completed to model surface loading conditions using the QCM [25, 31, 32]. Measurements of viscoelasticity have also been developed using shear horizontal acoustic plate mode (SH-APM) devices, Love wave devices and layer-guided SH-APM devices using the same principles [33, 34].

II.2.2.4 Newtonian Liquids

Viscosity is a measure of a fluids resistance to flow and is analogous to internal friction [35]. This friction is seen when a layer of fluid is forced to move past another layer. The greater the friction, the more force is needed to create movement (shear) and hence the more viscous the liquid, see Figure II.4.

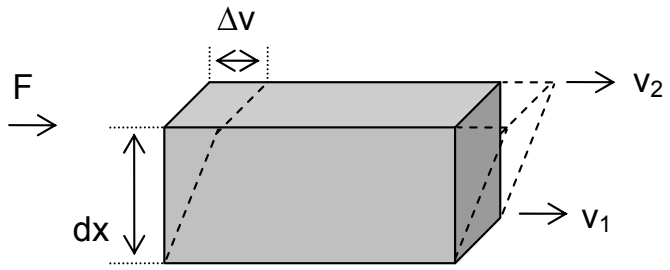

Figure II.4: Defining viscosity; the measure of internal friction of a fluid. Where F is the force applied, dx is distance between plates, v_1 and v_2 are velocities of the bottom and top plate respectively, and Δv is change in velocities.

Shear rate, shear stress and viscosity are defined by Equations II.7, II.8 and II.9, where F is force (N), A is area (m^2), σ is shear stress (Pa), γ is shear rate (s^{-1}), Δv is change in velocity (ms^{-1}), Δx is distance between top and bottom surface and η is viscosity (Pa.s).

$$\sigma = \frac{F}{A}, \tag{II.7}$$

$$\gamma = \frac{\Delta v}{\Delta x}, \tag{II.8}$$

$$\eta = \frac{\sigma}{\gamma}, \tag{II.9}$$

For a liquid to be Newtonian, viscosity must remain constant over a range of shear rates or shear rate is proportional to shear stress for a range of shear rates (see Figure II.5) [36]. Typical Newtonian fluids are water and thin oils [35] although no liquids are perfectly Newtonian over all shear rates.

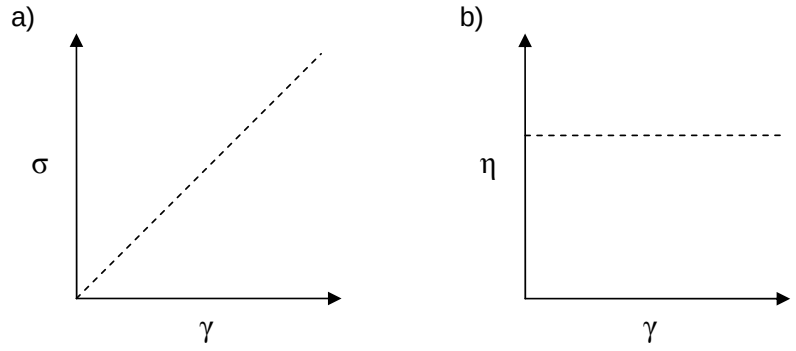

Figure II.5: Newtonian fluids a) Shear stress σ is proportional to shear rate γ, b) viscosity η is independent of shear rate.

If $\Delta f \neq -\Delta B/2$ and deviates significantly to that expected, the liquid is deemed non-Newtonian by the QCM technique [37,38]. It has recently been shown that liquids that are normally deemed Newtonian when measured on a rotational viscometer operating at much lower shear rates, are deemed non-Newtonian by the response of an acoustic wave device due to the high shear rates [39].

For a non-Newtonian liquid, viscosity will vary with shear rate. It is suggested that a non-Newtonian fluid is made up of a mixture of molecules of various shapes and sizes. At different shear rates the alignment of these molecules may alter (due to their size, shape and cohesiveness), hence the force needed to maintain motion may vary accordingly [35].

There are many types of non-Newtonian flow behaviour which have been modelled to show variations in fluid viscosity in relation to shear rate. These include pseudoplastic, plastic, dilatant, thixotropic and rheopexic [35]. In this study the liquids are simply defined as Newtonian or non-Newtonian based on the QCM or SAW device response.

In this study, measurements are compared to viscosity measurements taken on a DV-II+ Programmable viscometer (Brookfield, MA, USA) using a cone and plate geometry. Initially, measurements were completed by increasing the shear rate manually. Later in the study, Rheocalc 3.1 software (Brookfield, USA) was available to use with the viscometer and allowed the viscometer to record values of shear rate and shear stress in steps over a range of values. Where necessary the data is fit to the Bingham model, which is a two parameter model describing the fluid as having a Newtonian response above the Bingham yield stress response (Equation II.10).

$$\sigma = \sigma_o + \rho\gamma, \tag{II.10}$$

where σ is shear stress, σ_o is yield stress, ρ is plastic viscosity and γ is shear rate.

Due to the liquid being probed at such high frequencies in comparison to a traditional viscometer measurement, it may be necessary to consider the liquid as a liquid with a viscoelastic response.

This is modelled by considering the liquid to be a Maxwellian liquid which considers the finite reorientation time of molecules under stress [25] and uses a single relaxation time τ. When the Maxwellian fluid oscillates with $\omega\tau \ll 1$ (where $\omega = 2\pi f$), the liquid responds with Newtonian behaviour characterised by the shear viscosity, η. When the oscillation rate becomes close to the rate of molecular motion in the liquid, the energy ceases to dissipate in viscous flow and is instead stored elastically ($\omega\tau \gg 1$) [40].

By increasing the frequency, the high force causes the Maxwellian fluid to behave as an amorphous solid. Here, the shear properties are characterised by the shear modulus μ and the relaxation time τ, with the transition from viscous to elastic behaviour determined by Equation II.11 [40].

$$\tau = \frac{\eta}{\mu}, \tag{II.11}$$

The effect of τ becomes much more important with increasing liquid viscosity and as such the frequency of device used is often a trade off between sensitivity and the maximum measurable viscosity values [40]. When $\omega\tau \gg 1$, no apparent movement occurs and the upper limit of detection is reached.

II.2.2.5 Butterworth-Van Dyke Model

Changes in electrical behaviour are caused by variations in the acoustic properties at the surface of the quartz crystal and can be measured through changes in impedance, admittance spectra or changes in resonant frequency [41]. This behaviour is well studied [42, 43] with the electrical characteristics described by a lumped-element model known as the Butterworth-Van Dyke (BVD) circuit model [1]. This model is widely used for determining values such as the viscosity-density property where values correspond well to literature values [44] and simultaneous mass and liquid loading [7]. The model can be shown in Figure II.6. A full description of the BVD model can be seen in [45].

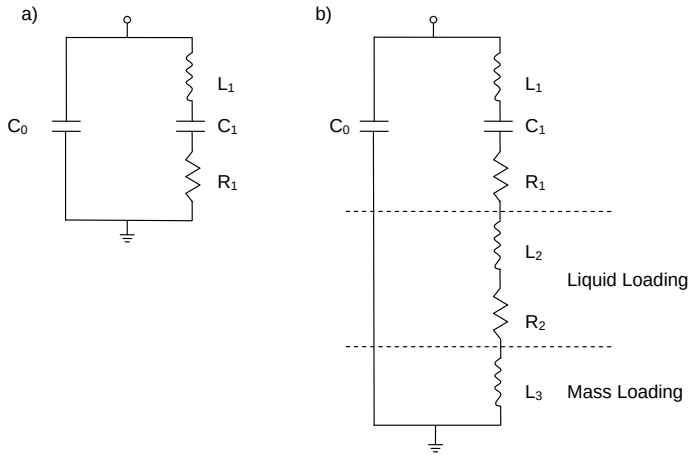

Figure II.6: Equivalent electrical circuit diagram for a) unperturbed QCM, b) QCM sensing liquid, mass or both, where C_0 is static capacitance between the electrodes and L_1, C_1, R_1 are motional contributions due to the electromechanical coupling from the piezoelectric material. When loaded with liquid an increase in both motional inductance L_2, and resistance R_2, is seen. If just mass loading occurs, only an increase in motional inductance L_3, is observed.

II.2.2.6 Compressional Waves

Some studies [46, 47] have been completed on compressional waves to model resonator responses to shear wave and compressional wave generation. These studies have been focused on non-uniform velocity profiles along the shear direction of the crystal. Acoustic wave devices are generally more vulnerable to compressional waves when enclosed in a small cell as in the lab-on-a-chip, see Figure II.7. This can however be overcome by acoustic absorbers/spoilers in the cell to prevent reflection of the acoustic wave [48, 49]. It has also been suggested that compressional waves are reduced by working with plano-plano crystals (flat both sides) rather than plano-convex (flat one side, curved second side) crystals and it is important to design experiments to avoid contributions from longitudinal waves which can travel distances much larger than the decay lengths of shear waves [50].

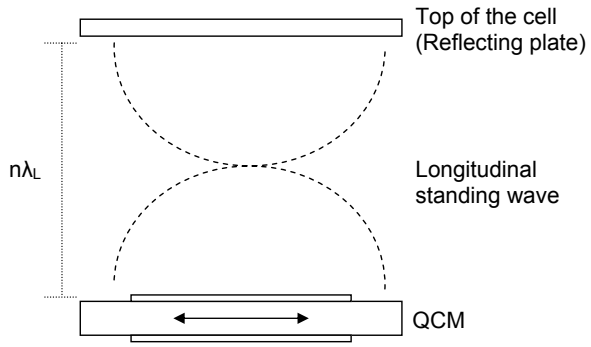

Figure II.7: A QCM showing shear wave motion, with longitudinal wave creating a standing wave (wavelength λ_L) setup due to reflection within a small cell.

II.3 Crystal Surface Morphology

When sensing with acoustic wave devices, surface morphology is critical. Surface roughness can create unwanted mass effects due to liquid trapped within the cavities. This effect can however be used advantageously by patterning a surface with features of known dimensions, making it possible to derive further properties [10, 51–54]. This section looks into the response of the QCM to rough surfaces, and the techniques used to separate the viscosity and density from the viscosity-density product using patterned surfaces.

II.3.1 Response To Rough Surfaces - Quartz Crystal Microbalance

It is well known that surface roughening can seriously affect the resonant frequency of a QCM, with 80% of the observed frequency shift caused by roughness effects [16]. A device with either a randomly textured surface or a regular pattern traps a quantity of fluid in excess of that viscously entrained by a smooth surface [10]. The liquid trapped in the surface features results in an enhanced frequency change, greater than expected for viscously entrained fluid alone [55].

The cavities formed by the rough surface trap additional fluid which moves synchronously with the surface of the crystal due to its vertical constraint. This trapped fluid has a mass effect which causes an additional frequency change. This additional change in frequency is not only dependent on the properties of the liquid constrained within the trap, but also on the type of microstructures on the crystal surface. By using a dual crystal arrangement containing one crystal with a rough surface and a second with a polished surface, it is possible to determine the viscosity and density values from the viscosity-density product [10]. The surface structure, dimensions and orientation influence the mass effect greatly which directly influences the accuracy of the liquid density measurement [56]. It is therefore important to consider the surface structures carefully. Zhang et al. [56] consider vertical line structures to be optimum when compared to a chess-board structure (see Figure II.8) as the vertical line structure is the simplest half closed structure and as such has the biggest volume of trapped liquid to aid density measurements.

Studies show that even if a standard unpolished QCM is considered for the rough surfaced QCM, the mass

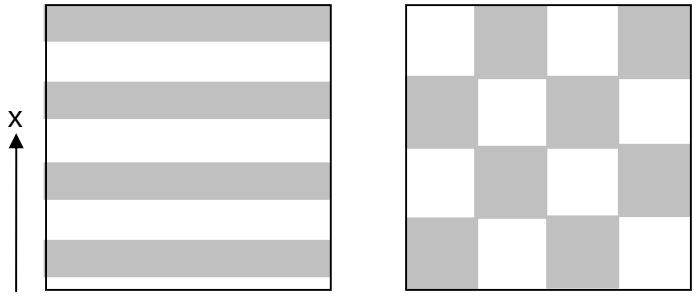

Figure II.8: Diagram of vertical line structure (left), and chess-board structure (right).

affect is still seen albeit very small [56–59]. This is due to the small amount of fluid which is constrained vertically in alignment with the crystalline structure's X-direction. For this reason development of a QCM with a randomly rough surface is not viable as a highly sensitive viscosity-density sensor.

If the degree of surface roughness needs to be known, it is suggested that changes in resonant frequency are not sufficient and a full impedance spectrum analysis is needed [58]. A major concern when looking at roughness or surface features, is how liquid fills the cavities, specifically how fluids wet into the troughs of a textured surface. The volume of fluid in the troughs is of high importance [60] and can alter the frequency change significantly. With thin surface features and low contact angles, the surface is seen to be fully wetted, i.e. no residual air at the QCM surface. At high contact angles, the wetting effect is less dominant and more residual air is retained. This volume will vary depending on the wetting properties of the liquid tested, causing variations in the frequency shift. A model can be used to describe some of these deviations [55].

II.3.2 Separating Viscosity and Density - Patterning Quartz Crystal Microbalance

In this work, the Martin *et al.* [10] study was closely followed using a dual QCM with one sided liquid contact, separating viscosity and density from the viscosity-density product. A dual sensor setup is required with micro structures fabricated on one crystal as shown in Figure II.9. Frequency change measurements between the two sensors give access to the separate properties as shown in Equations II.12 and II.13. The equations are derived from the original Sauerbrey (Equation II.1) and Kanazawa & Gordon (Equation II.4) equation, allowing for mass and liquid sensing. A derivation from the Sauerbrey and Kanazawa & Gordon equations to the forms stated below can be seen in Appendix I. The equivalent electrical circuit model is also described under mass and/or liquid loading by Martin *et al.* [7].

The liquid is trapped within the features causing an additional mass effect which causes an additional frequency change to that observed with the same liquid on a smooth crystal. Liquid below and level with the features is 'trapped' and moves with the crystal surface behaving as a mass layer. Liquid above this level has no constraints and is entrained undergoing a progressive phase lag. The response of liquid entrainment is seen on both crystals, and hence the additional frequency change seen on the patterned crystal is due to the mass effect. The crystal essentially weighs the trapped liquid (see Figure II.10), allowing density to be determined as in

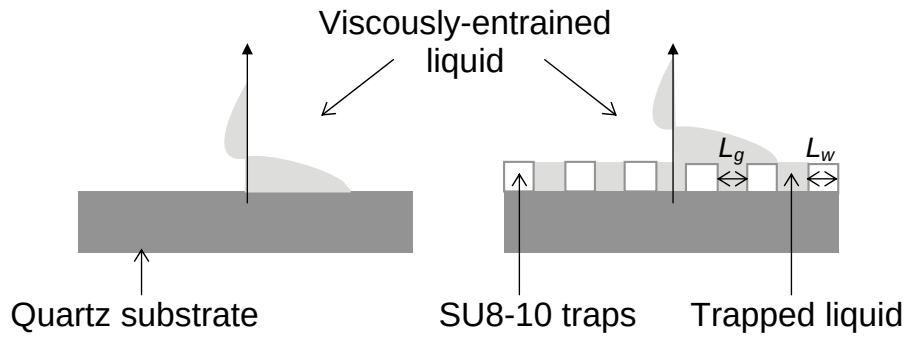

Figure II.9: Diagram of smooth (left) and patterned (right) quartz crystal microbalance, where L_g is length of trap gap, and L_w is length of trap width.

Equation II.12.

$$\rho = \frac{N(\mu_q \rho_q)^{0.5}}{2 f_s^2 h_{eff}} \mid \Delta f_t - \Delta f_s \mid, \tag{II.12}$$

where ρ is liquid density, η is liquid viscosity, N is harmonic number, μ_q is shear modulus of quartz, ρ_q is density of quartz, Δf_s is change in frequency of the smooth device, Δf_t is the change in frequency of the textured device.

Once density is found viscosity can then be determined using the change in frequency of the smooth device and density value found from Equation II.12 using Equation II.13:

$$\eta = \frac{2\pi h_{eff} N(\mu_q \rho_q)^{0.5} (\Delta f_s)^2}{f_s \mid \Delta f_t - \Delta f_s \mid}. \tag{II.13}$$

An effective height (h_{eff}) is considered to account for the design structure of the traps, and allows for the ratio of trap width to separation length to vary (see Equation II.14). The effective height is determined by working out the height when the liquid is spread equally across all traps creating an even mass layer (see Figure II.10). In this work, the reference crystal is a polished crystal with no mass layer. Ideally the reference crystal should have been a crystal with a flat SU8-10 mass layer.

$$h_{eff} = \left(\frac{L_g}{L_g + L_w} \right) h, \tag{II.14}$$

where h_{eff} is effective height, L_g is the length of trap gap, L_w is the length of trap width and h is the measured trap height.

A more recent study for simultaneous determination of density and viscosity, uses nanoporous alumina to create a rough surface [60]. Full impedance analysis relates frequency and bandwidth measurements to liquid viscosities. An advantage to this technique is that it does not require a reference crystal. A viscoelastic model which treats the nanopores as a viscoelastic layer with the exact same properties as quartz is used. As in the previous work [10] a calibrated volume per unit area for the pores and a combination of the Sauerbrey and

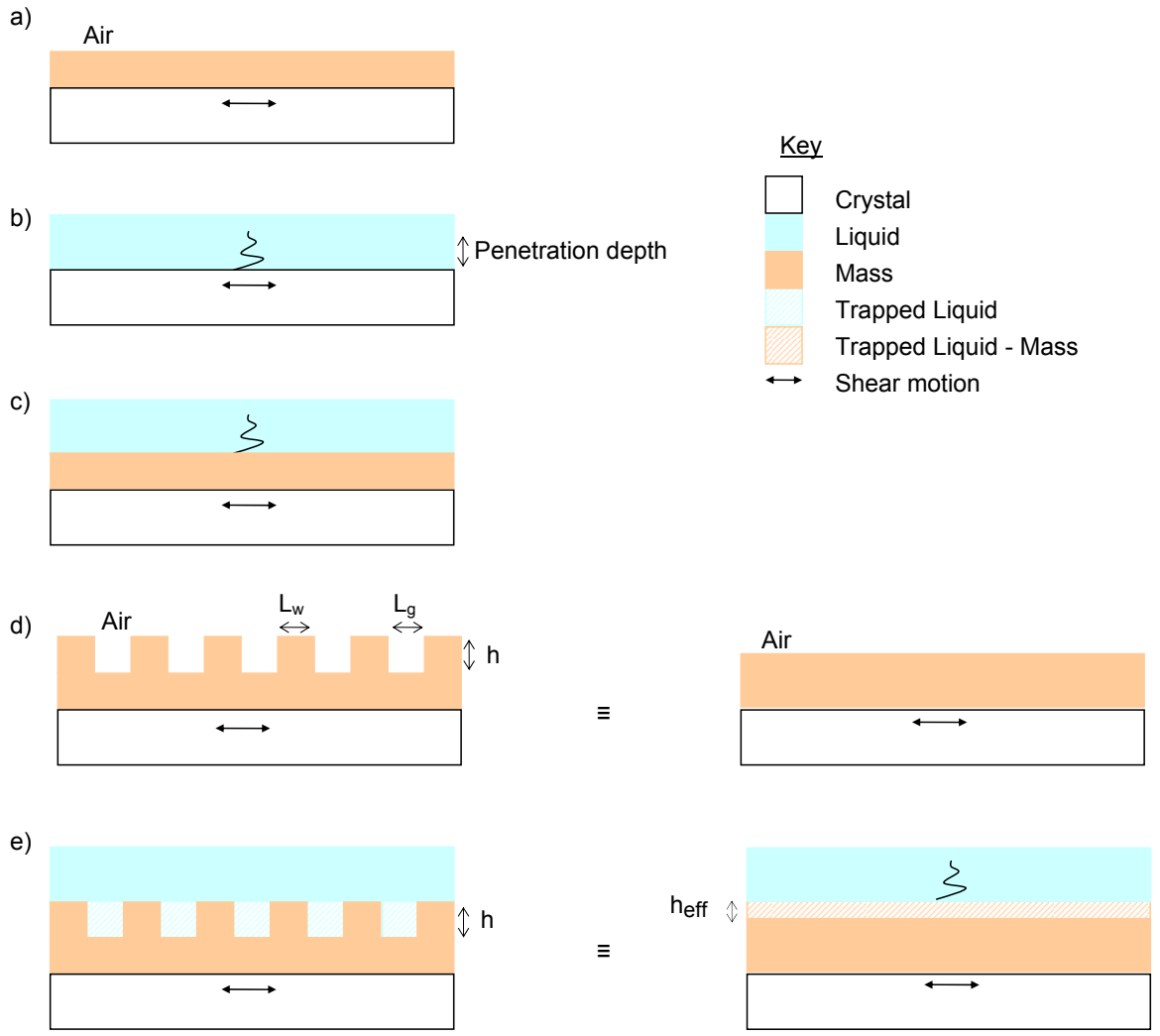

Figure II.10: Diagram of a quartz crystal a) mass sensing, b) liquid sensing, c) liquid sensing with initial mass layer, d) in air with fabricated traps on the surface (can be seen as a uniform mass layer), e) liquid sensing with a textured device showing trapped liquid acting as an additional mass layer (where h is the measured height of structures, L_g is length of groove, L_w is length of separation, and h_{eff} is effective height).

Kanazawa & Gordon equations allow density and viscosity to be derived.

This work extends the study of Martin *et al.* [10] where traps were fabricated from vertical gold strips (thickness 1.5 μm, cavities 5 μm wide) with measurements made of various wetting, low contact angle liquids such as hexane and butanol. The liquids studied had low viscosities and densities in comparison to measurements made herein. For more viscous liquids, the penetration depth of the shear wave into the liquid (Equation II.3) increases significantly. This means the height of the fabricated trap surface needs to be increased for higher viscosity liquids to successfully constrain the fluid within the cavities. It is well known that viscous fluids do not easily fill cavities as small as those described by Martin *et al.* and hence a larger cavity may be needed. Many studies [1, 55, 56, 61] have characterised responses to wetting characteristics and have suggested a 'trapping factor' to describe the level of filling. When working with more viscous liquids it is very difficult to see if the traps are filling completely. It is most likely they are filling with trapped air which may lead to the need for a filling factor.

In 1999 separate viscosity and density measurements evolved to use Surface Acoustic Wave (SAW) devices (see Section II.4). The advantage of the SAW sensor is that it can work at much higher frequencies and as such have increased sensitivity in relation to the QCM. Similarly to the QCM, a dual delay line is required containing both a structured and smooth device (see Figure II.11). Studies have been completed on the Shear Horizontal SAW (SH-SAW) [62] and the Love wave (layer guiding) device [53, 54, 63].

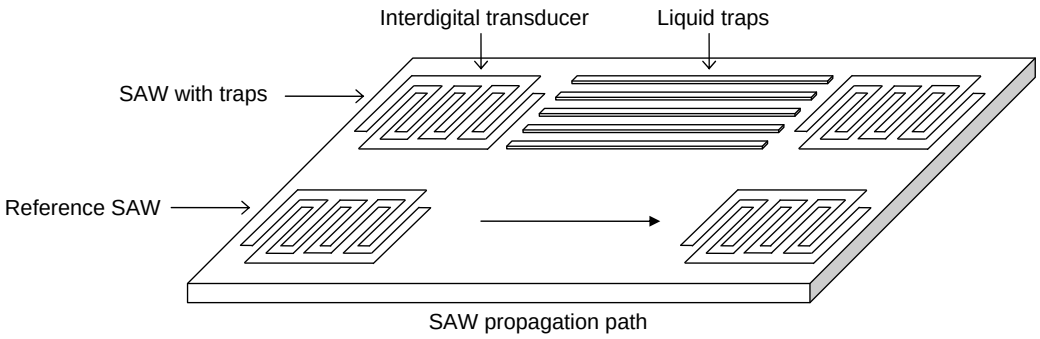

Figure II.11: Diagram of a dual SH-SAW device, showing placement of fabricated traps on ST-cut quartz.

One application of the dual Love wave SAW device, with one patterned device is to determine liquid composition for the food and beverage industry. The Love mode confines the acoustic energy to the top sensing surface giving it the highest sensitivity for acoustic wave devices. The guiding layer also provides added protection for the interdigital transducers (IDT) against chemically harsh environments. Analysis of the frequency changes of both the smooth and textured device with a known trapped volume and device sensitivity allows the viscosity and density values to be separated [63].

Similarly to the QCM, liquid is entrained by the shear wave on the surface of the SAW device which causes a

phase change response on the smooth crystal. On the structured device some liquid is constrained within the traps causing mass loading resulting in an additional frequency or phase shift. Again this mass loading is highly dependant on the dimensions of the liquid traps. Studies have shown a Love mode device operating at 125 MHz with a polymide waveguide layer to have sensitivities of 0.13 μg cm^{-3} Hz^{-1} for Bushmills whisky [63]. This is a significant improvement with a sensitivity over 700 times greater than the QCM. A silicon dioxide waveguide layer has also been explored and is shown to act as an excellent guiding layer for this technique with the advantage of being a chemically robust sensor with high sensitivity [53].

II.4 Surface Acoustic Wave Devices

For improved acoustic wave sensitivity, a high frequency device is needed. If the frequency of the QCM is increased too much it becomes fragile and near impossible to work with. For this reason we investigate the use of surface acoustic wave (SAW) devices. A SAW device also gives the opportunity for further miniaturisation of the sensor and fluid sample whilst providing alternative electrical connections. There are many types of SAW device, here is a short overview of the Shear-Horizontal SAW, Surface-Skimming Bulk Wave (SSBW), Rayleigh SAW, Acoustic Plate Mode (APM) which includes reverse sensing and Love wave devices, ranging in frequency from 10 MHz to 10 GHz [1] each with their own advantages. Batch fabrication techniques have seen many applications investigated for SAW devices due to their ease of production and low cost. Some of these applications include gas and vapour detection [64,65], thin film polymer characterisation [66], biosensing [67], liquid identification [68], chemical monitoring [69], and surface cleaning measurements [70].

II.4.1 Surface Acoustic Wave Design

A two port SAW device consists of a piezoelectric substrate with a set of interdigital transducers (IDT) deposited on the surface (see Figure II.13). When the device is probed, the acoustic mode propagation is restricted to the surface. The IDT consists of inter-locking fingers, the spacing of which determines the frequency of operation. The extent to which the fingers overlap (aperture) determines the electrical impedance [71]. The simplest finger design uses a single-single finger spacing (such as those shown in II.13). More complex designs can be used to optimise devices for specific applications. Some design modifications considered are in order to reduce reflections (such as split joined IDTs), consider the harmonic responses (use of a meander line design), and finger weighting/apodization [2].

The substrate cut and design of the device is chosen to match the wave required for the application, (whether it is liquid or gas sensing for example) and takes into consideration substrate temperature stability and velocity of wave. At higher frequencies surface perturbations are increased due to the increased acoustic energy at the surface of the substrate. There are many advantages to SAW devices [72] some of which include straight forward fabrication techniques, good repeatability, small size and weight and large frequency range. A SAW measurement can be made using an oscillator circuit [73] which uses the device as an amplifier feedback

loop, or a Network analyser. The response of the SAW is determined by the type and speed of the waves that propagate within the crystal and include bulk longitudinal (compressional waves), bulk transverse (shear waves), surface (Rayleigh waves) and plate waves (See Figures II.12 and II.13). The cut of the crystal is crucial in designing a specific SAW device.

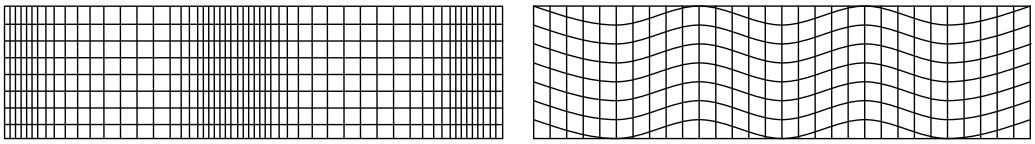

Figure II.12: Representation of waves seen in in solids: bulk longitudinal (compressional) and bulk transverse (shear) wave viewed from above.

II.4.2 Rayleigh Surface Acoustic Wave

The first confirmation of elastic vibrations in the surface of a solid material was by Lord Rayleigh in 1887 [1], and hence this propagation became known as the Rayleigh wave. The Rayleigh wave has some surface-normal displacement (see Figure II.13) and this is seen as an elliptical motion, containing both a compressional and shear wave component. The Rayleigh wave can not be used to detect liquids as the wave is rapidly damped by compressional waves. For this reason the Rayleigh wave has found many applications in gas phase sensing [74, 75].

II.4.3 Shear Horizontal Surface Acoustic and Surface Skimming Bulk Wave

The compressional waves produced when using a Rayleigh wave device can be avoided by designing a SAW device to operate with Shear Horizontal polarization (SH-SAW). This avoids any surface-normal displacement [76], making it useful for liquid sensing applications. The crystals shear mode oscillation entrains the liquid with an exponential penetration depth similar to that observed on the QCM, creating changes to observed electrical parameters (e.g. phase, frequency, power). From these changes in parameters it is possible to characterise chemical properties.

The SH-SAW has been used in many applications, some of which include perfume and flavour identification [77], detection of enzymes in responses to liquid phase [78, 79], detecting particles in liquids such as slurry [80] as well as liquid characterisation such as viscosity measurements [39].

The SH-SAW is sensitive to acoustoelectric interaction [81]. This has been studied for natural spring water on the surface of a SH-SAW which has also been modelled and compared well experimentally [82]. For low ionic concentration liquids, electric permittivity is negligibly small. However for higher ionic liquid concentrations, both the conductivity of the ionic solution and the viscous liquid can vary the resonant frequency [18]. These electroacoustic interactions are expected to be seen and cause particular challenges when testing some of the

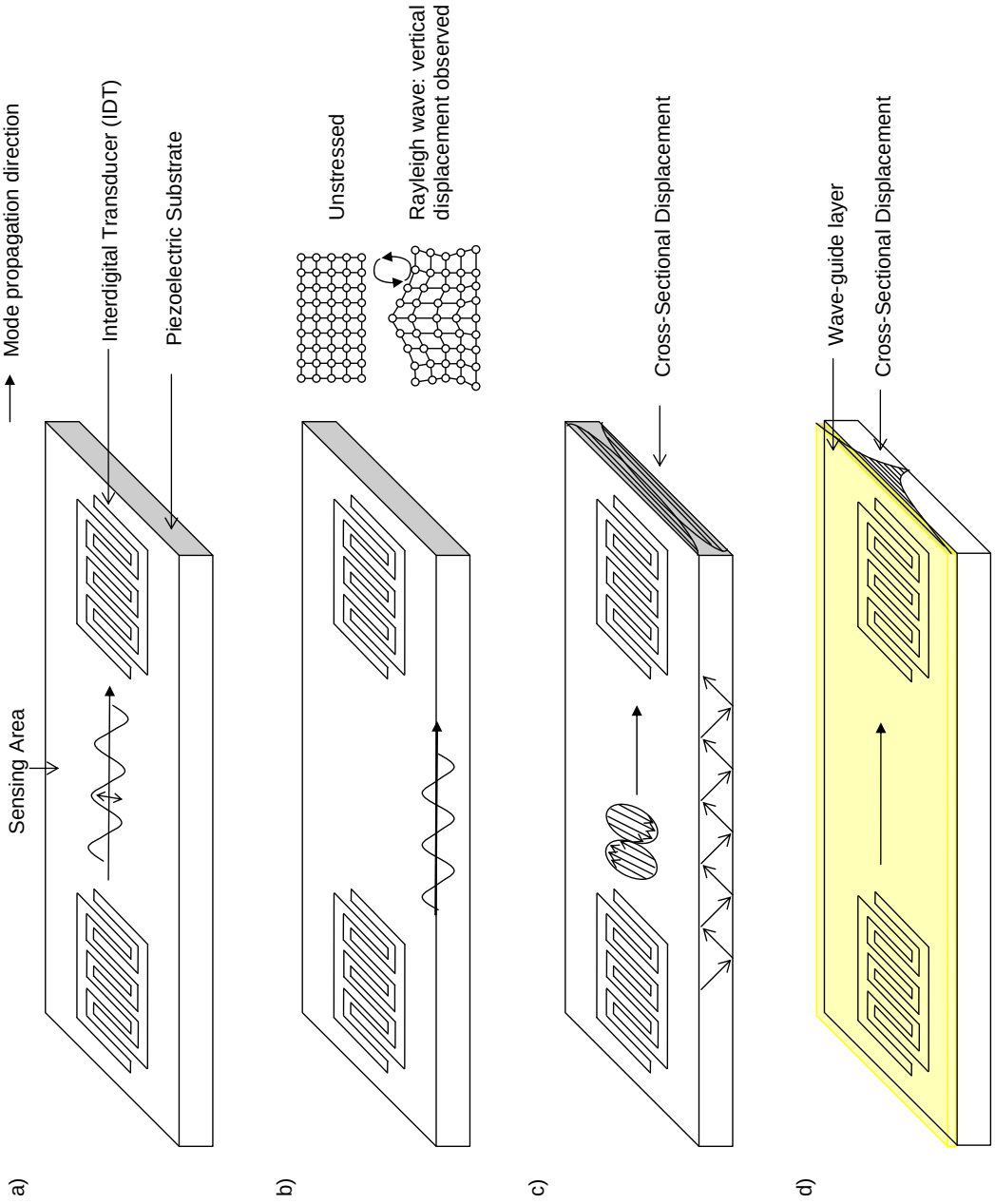

Figure II.13: Images of a) Shear-Horizontal Surface Acoustic Wave (SH-SAW), b) Rayleigh SAW, c) Shear-Horizontal Acoustic Plate mode (SH-APM) and d) Love wave sensor.

room temperature ionic liquids due to their chemical composition (discussed further in Section II.4.6).

II.4.3.1 Surface Skimming Bulk Wave

A Surface Skimming Bulk Wave device (SSBW) has shear horizontal polarisation similar to that of the SH-SAW. The direction of propagation from the IDT is however at a shallow angle slightly down into the bulk of the material (see Figure II.14). The SSBW device has been used in many applications including immunosensing [83] and temperature sensing [84], but is considered the least sensitive due the energy being transferred into the bulk rather than constrained to the surface.

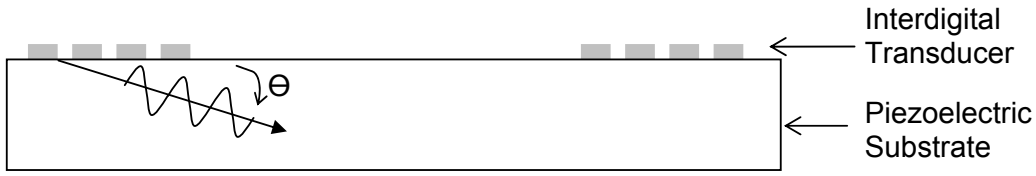

Figure II.14: Image of Surface Skimming Bulk Wave (SSBW), showing shear horizontal polarisation propogating at a shallow angle Θ, down into the bulk of the crystal.

II.4.4 Acoustic Plate Mode Devices

The Acoustic Plate Mode device is sensitive to either mass accumulation on the surface, the entrainment of liquid on the crystal-liquid interface or acoustoelectric coupling between evanescent plate mode electric fields and the liquid.

The Shear Horizontal APM is well designed for liquid sensing due to the absence of any surface normal displacement, allowing each mode to propagate in contact with the liquid without excessive damping. Energy is confined to the upper and lower boundary of the substrate and is concentrated within one wavelength of the surface. Each APM has displacement maxima at the top and bottom surfaces of the crystal (see Figure II.13) making it possible to sense on either side of the device.

Plate mode sensitivity is dependent upon the substrate thickness rather than frequency. For mass sensing, an APM device can have a mass sensitivity of 1.1 ng cm^{-2} Hz^{-1} for low order modes and 0.5 ng cm^{-2} Hz^{-1} on average for higher order modes [73] which makes it a good choice for a microbalance. With suitable surface chemistry it is also ideal for sensing specific species present in solutions.

When liquid sensing, the viscous loading on the plate modes causes both a change in the propagation velocity and attenuation of the mode as for the QCM. Due to the high frequency oscillation it is necessary to consider the viscoelastic response of the liquid such as that described in Section II.2.2.4. The velocity change occurs due to the mass loading by the liquid entrainment. The attenuation shift arises from the power dissipation in the liquid. If the liquid has a Newtonian response, the change in velocity or the change in attenuation of the

mode is proportional to the square root of the shear viscosity. It is expected that for viscosities greater than approximately 10 cP, when liquid sensing on a device of frequency 158 MHz, viscoelastic results are observed. The good sensitivity of these devices have enabled them to be used as microviscometers in the Newtonian regime ($\omega\tau \ll 1$) [40]. The SH-APM has been investigated for sensing the viscosity of liquids and has also been shown experimentally to have a maximum limit of viscosity. A limit of approximately 1000 cP has been observed for a device operating at a frequency of 18 MHz for glycerol solutions, at which point relaxation times become important [85].

The nature of the shear wave allows this sensor to operate on either side. The ability to sense on the opposite side to the electrodes has huge advantages which include the added protection of the IDTs to chemicals (prolonging their expected lifetime) making them excellent sensors for applications in harsh environments. Building polymer layers onto the surface of the substrate (opposite surface to the sensing side of the substrate) creates a layer guided SH-APM [86] which makes it possible to increase device sensitivity whilst still being able to sense on the opposite side to the electrodes [87].

II.4.5 Love Wave Devices

A Love wave device is created when a guiding layer is added to a SH-SAW or SSBW device. The Love wave will be supported if the guiding layer has a shear speed less than that of the device substrate [76]. The guiding layer must be thin compared with the wavelength on a thick substrate to support the Love wave. This idea was first reported for biosensing in 1992 [88]. Love waves are excellent as both gas and liquid sensors, and by measuring changes in insertion loss, phase, or both, the viscosity-density product of a liquid can be studied [76]. Various media for guiding layers have been studied including polyimide layers including SU8 [89], S1813 [90] and various solutions of polymethylmethacrylate (PMMA) [91]. Polymers have much lower shear velocities than quartz with high sensitivity although at the expense of large acoustic losses. Materials such as silicon dioxide (SiO_2), a hard elastic material, have also been extensively studied with great success [92–94] and present acoustic losses which are considered to be very low [91] . SiO_2 is resistant to water, most chemicals and is abrasion resistant [95] which makes it an ideal guiding layer. The thickness of the guiding layer has a dramatic effect on the response of the wave [93, 96] and as such an optimum thickness is required to achieve the greatest device sensitivity.

Love mode devices have been previously reported as viscosity sensors, and used with a wet cell which traps the fluid on the propagation path which avoids liquid contacting the IDTs. The Newtonian response of liquids is measured by the changes in phase and insertion loss. It has been previously shown that only low-viscosity measurements are possible with high accuracy and resolution, and many more viscous fluids show a non-Newtonian response at this high frequency [39, 97, 98].

Love mode devices have also been studied as liquid density sensors, where the viscosity-density product can be separated. A dual delay line structure with one smooth and one structured device is needed (similar to that needed for the QCM see Section II.3.2) [54, 63, 99]. The surface structures are aligned to the propagation path and are designed to trap an additional volume of liquid, to be treated as an ideal mass. One study has shown devices (frequency 124.7 MHz) to be sensitive to density changes of 0.36 μg cm^{-3} Hz^{-1} for various whisky-water solutions [63]. Viscous fluids remain the challenge however, due to high damping and high insertion losses which make it difficult to record frequency measurements. A clear limit at this frequency is seen for separating viscosity and density using the dual setup at a square root viscosity-density of 4.4 kg m^{-2} s$^{-0.5}$, restricting this technique to low viscosity liquids [63].

II.4.5.1 Guiding Layer Deposition

A guiding layer can be deposited onto the surface of a SAW device using two main techniques, spin processing and plasma deposition. A polymer such as SU8, S1813 or PMMA is generally spin coated at a certain speed to achieve a desirable thickness before being heated on a hotplate to harden it by cross-linking. The experimental work on SAW devices with guiding layers in this thesis, uses a thin film of silicon dioxide for a guiding layer. This is achieved using a modified vacuum evaporator (Edward 306), containing an R301 RF power supply and TORUS HV Circular sputter head (Kurt J. Lesker, UK) to produce SiO_2 guiding layers of various thicknesses. A QCM thickness monitor within the system determines the thickness of mass deposition. This was considered the most chemically robust material to use with RTILs it is also well characterised and is the simplest material to deposit for use to act as a guiding layer.

II.4.6 Acoustoelectric Interactions

Acoustoelectric interactions are also experienced when liquid sensing with each of the devices. Like the entrainment of liquid, ionic involvement decays exponentially with distance from the solid-liquid interface with an electric decay length of $\lambda/2\pi$. This acoustoelectric interaction can lead to perturbations in plate mode velocity and attenuation which can be related to the solution conductivity [100]. To eliminate these acoustoelectric interactions, deposition of a conductive metal layer on the substrate surface moves the electric fields slightly resulting in the decoupling of ions in solution with no effect on mass sensitivity [100]. Alternatively solutions can be buffered so that solution conductivity does not vary significantly over measurements [73]. However these interactions can be very useful in determining electrical conductivity of solutions and further detecting metal ions in liquids by studying frequency and attenuation changes [101, 102].

II.4.7 Microfluidics - Acoustic Wave Technology

The small size and high sensitivity of acoustic wave technology makes it ideal for use in microfluidic experimental setups. This technology is only just beginning to be explored and is already finding many uses in chemical and biological areas [103]. Arrays of devices have been studied for distinguishing different liquid

characteristics, producing a useful system for liquid identification [104, 105]. More commercially, SAW encapsulation techniques have been investigated to provide completely disposable chips incorporating a SH-SAW device with a fluid channel making them ideal for biological studies [106]. SAW devices have also been used to transport and mix droplets within a lab-on-a-chip setup ready for further characterisation. The SAW device allows small nano-litre sized volumes of samples to be measured [107].

II.5 Room Temperature Ionic Liquids

Over the past decade, ionic liquids have been developed within many publications as alternative, environmentally friendly solvents [108–111]. The drive for cleaner industrial processes has led to the emergence of ionic liquids as preferable solvents for a range of reactions previously considered harmful, and show potential applications in clean synthesis, electrochemistry and liquid crystals. Unfortunately, ionic liquids have yet to prove their full-scale viability. This is largely due to the fact that almost all of the available research has focussed on the chemistry rather than the development of physical data. It has however been established that the diversity of physical properties that are available in ionic liquid solvents give them the potential to be the engineering solvent of choice. These factors also allow the properties and structure of the solvent to be systematically changed allowing entire processes to be optimised. This would enable plants to be designed without limitations imposed by solvent choice. Despite the enormous potential of this designer solvent approach to optimising reactions, only a handful of ionic liquids are commonly used in current investigations. One of the major reasons is the limited physical property data available as a function of chemical composition. This information is time consuming to collect and requires many expensive measurements requiring decilitre quantities of ionic liquid whose purity and exact provenance is known. If ionic liquids are to be tailored to each individual application the physical property database [112] needs to be expanded substantially to include both thermal effects and the variation with added secondary solvent (either another ionic liquid, water or an organic material). In particular, the amount of material necessary for a complete physical property analysis to be competitive needs to be brought down by a factor of 100 or more allowing data collection at a negligible cost [113]. One technique for characterising RTILs on chip has already been developed for studying solution phase synthesis [114].

II.5.1 Applications and Characteristics

Ionic liquids have been a focal point in green chemistry for the past decade as applications for these materials are becoming more diverse [111]. Possible applications for RTILs include separation techniques [115], catalysis [116], organic synthesis [117], pharmaceutical solvents [118], fuels cells [119, 120], solar cells, heat transfer fluids, lubricants and anti-corrosion coatings [121]. Ionic Liquids are defined as molten salts with a melting point below 100°C. This report looks at room temperature ionic liquids (RTIL) which are ionic liquids that are liquid at room temperature. They are organic salts, whose cations, substituents, and anions can be varied virtually at will to change their chemical and physical properties [113]. Changing the design of the liquid allows a wide variety of physical properties to be made available and therefore materials are being

designed with specific applications in mind, making them more desirable than traditional organic solvents. These liquids have many characteristics providing the opportunity to reduce, or even completely eliminate, hazardous and toxic emissions to the atmosphere, thus addressing health and safety concerns whilst benefiting the environment [121]. Some of the characteristics of ionic liquids are summarised below:

- Liquid phase temperature range of approx 300°C, giving a wide range of thermal stability. This allows for large kinetic control of chemical processes.
- No measurable vapour pressure means solvent evaporation is eliminated, reducing the need for respiratory protection and exhaust systems.
- Non-flammable permits safe use as solvents for exothermic reactions.
- Can be used as catalysts.
- Capable of influencing highly selective reactions and producing new chemistries.

More recently these characteristics have been challenged [122, 123] due to more intense research and it has become clear these properties are not seen in all ionic liquids. It has been stated that the only properties you are guaranteed to see are:

- It is liquid below 100°C.
- It contains ions, and therefore will show ionic conductivity.

Even with just these two properties, some liquids are so viscous at these temperatures that liquid may not fall within the traditional definition [124]. However, when their properties are known these materials have huge application potential [125].

More recent studies have looked into molecular simulations and modelling techniques to predict expected liquid properties rather than using experimental studies alone. Models of intra- and inter-molecular structures, dynamic and transport behaviour [126] and simulated values of density [127] have been firmly established. However this is relatively new and further properties need to be studied.

The most popular liquids are undoubtedly the di-alkylimidazolium salts, probably due to their ease of synthesis and attractive physical properties [113]. The number of possible combinations, and the complexity of the liquids being synthesised, has the disadvantage of being costly. It is for this reason there is little, but growing literature on this characterisation. By making these processes easier and less costly, the liquids will soon become more widely available.

II.5.1.1 Room Temperature Ionic Liquids Investigated in this Study

All RTILs used in this project were supplied by a PhD student at the Queen's University Belfast, Rile Ge under supervision of Prof. Chris Hardacre. A complete list of the Room Temperature Ionic Liquids used

within this work and their chemical names can be seen in Table II.1. [C_4mimpyrr][FAP], [C_4mim][TFA], [C_4mim][DCA], [C_4mpyrr][DCA], [C_2mim][SCN], [C_4mim][$MeSO_4$], [C_4mim][$OctSO_4$] and [$N_{1,8,8,8}$][TFA] were obtained from Merck (98%). [C_2mim][$EtSO_4$] was prepared by reacting 1-methylimidazole with diethyl sulfate according to previously reported procedures [128]. All other ionic liquids were prepared in house using standard literature methods from the appropriate organic halide salt [129, 130].

Room Temperature Ionic Liquid	Chemical Name
[C_2mim][NTf_2]	1-ethyl-3-methylimidazolium bis(trifluoromethylsulfonyl)imide
[C_4mim][NTf_2]	1-butyl-3-methylimidazolium bis(trifluoromethylsulfonyl)imide
[C_6mim][NTf_2]	1-hexyl-3-methylimidazolium bis(trifluoromethylsulfonyl)imide
[C_8mim][NTf_2]	1-octyl-3-methylimidazolium bis(trifluoromethylsulfonyl)imide
[C_{10}mim][NTf_2]	1-decyl-3-methylimidazolium bis(trifluoromethylsulfonyl)imide
[C_4dmim][NTf_2]	1-butyl-2,3-dimethylimidazolium bis(trifluoromethylsulfonyl)imide
[$P_{6,6,6,14}$][NTf_2]	trihexyltetradecylphosphonium bis(trifluoromethylsulfonyl)imide
[C_4mpyrr][NTf_2]	1-butyl-1-methylpyrrolidium bis(trifluoromethylsulfonyl)imide
[C_2mim][SCN]	1-ethyl-3-methylimidazolium thiocyanate
[C_4mim][SCN]	1-butyl-3-methylimidazolium thiocyanate
[C_{10}mim][SCN]	1-decyl-3-methylimidazolium thiocyanate
[C_4mpyrr][SCN]	1-butyl-1-methylpyrrolidinium thiocyanate
[C_4mim][DCA]	1-butyl-3-methylimidazolium dicyanamid
[C_4mpyrr][DCA]	1-butyl-1-methylpyrrolidinium dicyanamid
[C_4mpyrr][$MeSO_4$]	1-butyl-1-methylpyrrolidinium methylsulfate
[C_1mim][$MeSO_4$]	1,3-dimethylimidazolium methylsulphate
[C_4mim][$MeSO_4$]	1-butyl-3-methylimidazolium methylsulfate
[C_4mim][$OctSO_4$]	1-butyl-3-methylimidazolium octylsulfate
[$N_{1,8,8,8}$][TFA]	Methyl trifluoroacetate
[C_4mim][TFA]	1-butyl-3-methylimidazolium trifluoroacetate
[C_4mim][AcO]	1-butyl-3-methylimidazolium acetate
[C_4mim][OTf]	1-butyl-3-methylimidazolium trifluoromethylsulfonyl
[C_2mim][$EtSO_4$]	1-ethyl-3-methylimidazolium ethylsulfate
[C_4mpyrr][FAP]	1-butyl-1-methylpyrrolidinium tris(pentafluoroethyl)trifluorophosphate

Table II.1: Complete list of Room Temperature Ionic Liquids used within this work.

II.5.2 Technical Challenges

Most ionic liquids are highly hygroscopic and therefore need to be dried under vacuum before use to remove any water contamination. This is extremely important when measuring values of viscosity where viscosity varies exponentially with water concentration [131]. For this reason all measurements need to be carried out in a controlled environment taking into account temperature and humidity.

Ionic liquids can be very corrosive, and as such anything that comes into contact with the liquids must have a high chemical resistance. The liquids currently under test are not hazardous, but for long term use and exposure, the testing device and set-up must be chemically robust. For this reason materials are limited to glass, quartz, sapphire, polytetrafluoroethylene (PTFE) and polyetheretherketones (PEEK). Any adhesive materials

must be cautiously considered due to possible chemical and physical degradation, contaminating the sample and environment [110].

References

[1] D. S. Ballantine, R. M. White, S. J. Martin, A. J. Ricco, E. T. Zellers, G. C. Frye, and H. Wohltjen, *Acoustic Wave Sensors: Theory, Design, & Physico-Chemical Applications (Applications of Modern Acoustics)*. Academic Press, 1996.

[2] C. K. Campbell, *Surface Acoustic Wave Devices for Mobile and Wireless Communications*. Academic Press, 1998.

[3] M. Thompson and D. C. Stone, *Surface-Launched Acoustic Wave Sensors: Chemical Sensing and Thin-Film Characterization*. Wiley-Interscience, 1997.

[4] C. O'Sullivan and G. Guilbault, "Commercial quartz crystal microbalances - theory and applications," *Biosensors & Bioelectronics*, vol. 14, no. 8-9, pp. 663–670, 1999.

[5] G. Sauerbrey *Zeitschrift fr Physik*, pp. 206–222, 1959.

[6] W. King, "Piezoelectric sorption detector," *Analytical chemistry*, vol. 36, p. 1735, 1964.

[7] S. Martin, V. Granstaff, and G. Frye, "Characterization of a quartz crystal microbalance with simultaneous mass and liquid loading," *Analytical Chemistry*, vol. 63, no. 20, pp. 2272–2281, 1991.

[8] H. Bandey, A. Hillman, M. Brown, and S. Martin, "Viscoelastic characterization of electroactive polymer films at the electrode/solution interface," *Faraday Discussions*, vol. 107, pp. 105–121, 1997. Meeting on Interactions of Acoustic Waves with Thin Films and Interfaces, Leicester, England, Sep 08-10, 1997.

[9] S. Bruckenstein and M. Shay, "Experimental aspects of use of quartz crystal microbalance in solution," *Electrochimic Acta*, vol. 30, no. 10, pp. 1295–1300, 1985.

[10] S. Martin, G. Frye, and K. Wessendorf, "Sensing liquid properties with thickness-shear mode resonators," *Sensors and Actuators A-Physical*, vol. 44, no. 3, pp. 209–218, 1994.

[11] M. Ferrari and V. Ferrari, "An oscillator circuit for dual-harmonic tracking of frequency and resistance in quartz resonator sensors," *Measurement Science and Technology*, vol. 20, no. 12, 2009.

[12] M. Yoshimoto, S. Tokimura, K. Shigenobu, S. Kurosawa, and M. Naito, "Properties of the overtone mode of the quartz crystal microbalance in a low-viscosity liquid," *Analytica Chimica Acta*, vol. 510, pp. 15–19, 2004.

[13] D. Johannsmann, "Derivation of the shear compliance of thin films on quartz resonators from comparison of the frequency shifts on different harmonics: A perturbation analysis," *Journal of Applied Physics*, vol. 89, no. 11, Part 1, pp. 6356–6364, 2001.

[14] T. Nomura and M. Okuhara, "Frequency-shifts of piezoelectric quartz crystals immersed in organic liquids," *Analytica Chimica Acta*, vol. 142, pp. 281–284, 1982.

[15] P. Roach, G. McHale, C. R. Evans, N. J. Shirtcliffe, and M. I. Newton, "Decoupling of the liquid response of a superhydrophobic quartz crystal microbalance," *Langmuir*, vol. 23, no. 19, pp. 9823–9830, 2007.

[16] M. Thompson, A. Kipling, W. Duncan-Hewitt, L. Rajakovic, and B. Cavicvlasak, "Thickness-shear-mode acoustic-wave sensors in the liquid-phase - a review," *Analyst*, vol. 116, pp. 881–890, Sep 1991.

[17] K. Kanazawa and J. Gordon, "The oscillation of a frequency of a quartz resonator in contact with a liquid," *Analytica Chimica Acta*, vol. 175, pp. 99–105, 1985.

[18] T. Nomura, A. Saitoh, and Y. Horikoshi, "Measurement of acoustic properties of liquid using liquid flow SH-SAW sensor system," *Sensors and Actuators B - Chemical*, vol. 76, no. 1-3, pp. 69–73, 2001. 8th International Meeting on Chemical Sensors (IMCS-8), Basel, Switzerland, Jul 02-05, 2000.

[19] P. Kao, A. Patwardhan, D. Allara, and S. Tadigadapa, "Human serum albumin adsorption study on 62-MHz miniaturized quartz gravimetric sensors," *Analytical chemistry*, vol. 80, pp. 5930–5936, 2008.

[20] W. Shin, M. Nishibori, T. Itoh, N. Izu, and I. Matsubara, "Monitoring of dispensed fluid with the quartz crystal microbalance (qcm) for the better control of inkjet or dispenser machine," *Journal of the Ceramic Society of Japan*, vol. 116, no. 1351, pp. 459–461, 2008.

[21] M. Atashbar, B. Bejcek, A. Vijh, and S. Singamaneni, "QCM biosensor with ultra thin polymer film," *Sensors and Actuators B-Chemical*, vol. 107, no. 2, pp. 945–951, 2005.

[22] N. Adanyi, M. Varadi, N. Kim, and I. Szendro, "Development of new immunosensors for determination of contaminants in food," *Current Applied Physics*, vol. 6, no. 2, pp. 279–286, 2006. Conference on Engineering Aspects of Nanomaterials and Technologies, Budapest, Hungary, Jan 24-27, 2005.

[23] F. Dickert, P. Lieberzeit, P. Achatz, C. Palfinger, M. Fassnauer, E. Schmid, W. Werther, and G. Horner, "Qcm array for on-line-monitoring of composting procedures," *Analyst*, vol. 129, no. 5, pp. 432–437, 2004.

[24] C. Kleber, U. Hilfrich, and M. Schreiner, "In situ QCM and TM-AFM investigations of the early stages of degradation of silver and copper surfaces," *Applied Surface Science*, vol. 253, no. 7, pp. 3712–3721, 2007.

[25] H. Bandey, S. Martin, R. Cernosek, and A. Hillman, "Modeling the responses of thickness-shear mode resonators under various loading conditions," *Analytical Chemistry*, vol. 71, no. 11, pp. 2205–2214, 1999.

[26] R. Lucklum and P. Hauptmann, "The quartz crystal microbalance: mass sensitivity, viscoelasticity and acoustic amplification," *Sensors and Actuators B-Chemical*, vol. 70, no. 1-3, pp. 30–36, 2000.

[27] D. Johannsmann, K. Mathauer, G. Wegner, and W. Knoll, "Viscoelastic properties of thin-films probed with a quartz-crystal resonator," *Physical Review B*, vol. 46, no. 12, pp. 7808–7815, 1992.

[28] M. Herrscher, C. Ziegler, and D. Johannsmann, "Shifts of frequency and bandwidth of quartz crystal resonators coated with samples of finite lateral size," *Journal of Applied Physics*, vol. 101, no. 11, 2007.

[29] S. Martin and G. Frye, "Polymer film characterization using quartz resonators," in *IEEE 1991 Ultrasonics Symposium: Proceedings, Vols 1 and 2* (B. Mcavoy, ed.), pp. 393–398, 1991. 1991 Ultrasonics Symp, Lake Vista, FL, Dec 08-11, 1991.

[30] C. Reed, K. Kanazawa, and J. Kaufman, "Physical description of a viscoelastically loaded at-cut quartz resonator," *Journal of Applied Physics*, vol. 68, no. 5, pp. 1993–2001, 1990.

[31] E. Nwankwo and C. Durning, "Mechanical response of thickness-shear mode quartz-crystal resonators to linear viscoelastic fluids," *Sensors and Actuators A-Physical*, vol. 64, no. 2, pp. 119–124, 1998.

[32] E. Nwankwo and C. Durning, "Fluid property investigation by impedance characterization of quartz crystal resonators Part II: Parasitic effects, viscoelastic fluids," *Sensors and Actuators A-Physical*, vol. 72, no. 3, pp. 195–202, 1999.

[33] G. McHale, M. Newton, and F. Martin, "Theoretical mass, liquid, and polymer sensitivity of acoustic wave sensors with viscoelastic guiding layers," *Journal of Applied Physics*, vol. 93, no. 1, pp. 675–690, 2003.

[34] G. McHale, R. Lucklum, M. Newton, and J. Cowen, "Influence of viscoelasticity and interfacial slip on acoustic wave sensors," *Journal of Applied Physics*, vol. 88, no. 12, pp. 7304–7312, 2000.

[35] I. Brookfield Engineering Labs., "More solutions to sticky problems," 11 Commerce Blvd., Middleboro, MA 02346 USA.

[36] TA Instruments, Lukens Drive, New Castle, DE 19720, *TA Instruments Thermal Analysis & Rheology, Software Manual*, June 1995.

[37] J. Kuntner, G. Stangl, and B. Jakoby, "Analyzing the non-Newtonian behavior of oil-based liquids using microacoustic sensors," in *Proceedings of the IEEE Sensors 2003, Vols 1 and 2*, (345 E 47TH ST, New York, NY 10017 USA), pp. 956–960, IEEE Sensors Council, IEEE, 2003. 2nd IEEE International Conference on Sensors, Toronto, Canada, Oct 22-24, 2003.

[38] N.-J. Cho, J. N. D'Amour, J. Stalgren, W. Knoll, K. Kanazawa, and C. W. Frank, "Quartz resonator signatures under Newtonian liquid loading for initial instrument check," *Journal of Colloid and Interface Science*, vol. 315, no. 1, pp. 248–254, 2007.

[39] T. Morita, M. Sugimoto, and J. Kondoh, "Measurements of standard-viscosity liquids using shear horizontal surface acoustic wave sensors," *Japanese Journal of Applied Physics*, vol. 48, 2009.

[40] A. Ricco and S. Martin, "Acoustic-wave viscosity sensor," *Applied Physics Letters*, vol. 50, pp. 1474–1476, 1987.

[41] R. Lucklum and P. Hauptmann, "Thin film shear modulus determination with quartz crystal resonators: A review," in *Proceedings of the 2001 IEEE International Frequency Control Symposium & PDA Exhibition*, (345 E 47TH ST, New York, NY 10017 USA), pp. 408–418, 2001. IEEE International Frequency Control Symposium and PDA Exhibition, Seattle, WA, Jun 06-08, 2001.

[42] H. Muramatsu, E. Tamiya, and I. Karube, "Computation of equivalent-circuit parameters of quartz crystals in contact with liquids and study of liquid properties," *Analytical Chemistry*, vol. 60, pp. 2142–2146, 1988.

[43] A. Kipling and M. Thompson, "Network analysis method applied to liquid-phase acoustic-wave sensors," *Analytical Chemistry*, vol. 62, pp. 1514–1519, 1990.

[44] H. Valimaki, J. Lekkala, and H. Helle, "Prediction ability of a lumped-element equivalent-circuit model for thickness-shear mode resonators in liquids," *Sensors and Actuators A-Physical*, vol. 60, pp. 80–85, May 1997. Eurosensors X Meeting, Louvain, Belgium, Sep 08-11, 1996.

[45] J. Rosenbaum, *Bulk Acoustic Wave Theory and Devices (Artech House Acoustics Library)*. Artech Print on Demand, 1988.

[46] T. Schneider and S. Martin, "Influence of compresional wave generation on thickness-shear mode resonator response in a fluid," *Analytical Chemistry*, vol. 67, pp. 3324–3335, 1995.

[47] R. Lucklum, S. Schranz, C. Behling, F. Eichelbaum, and P. Hauptmann, "Analysis of compressional-wave influence on thickness-shear-mode resonators in liquids," *Sensors and Actuators A-Physical*, vol. 60, no. 1-3, pp. 40–48, 1997. Eurosensor X Meeting, Louvain, Belgium, Sep 08-11, 1996.

[48] L. Tessier, F. Patat, N. Schmitt, G. Feuillard, and M. Thompson, "Effect of the generation of compressional waves on the response of the thickness-shear mode acoustic-wave sensor in liquids," *Analytical Chemistry*, vol. 66, pp. 3569–3574, 1994.

[49] F. Eggers and T. Funck, "Method for measurement of shear-wave impedance in the mhz region for liquid samples of approximately 1ml," *Journal of Physics E-Scientific Instruments*, vol. 20, pp. 523–530, 1987.

[50] Z. Lin and M. Ward, "The role of longitudinal-waves in quartz-crystal microbalance applications in liquids," *Analytical Chemistry*, vol. 67, no. 4, pp. 685–693, 1995.

[51] S. Martin, G. Frye, A. Ricco, and S. Senturia, "Effect of surface-roughness on the response of thickness-shear mode resonators in liquids," *Analytical Chemistry*, vol. 65, no. 20, pp. 2910–2922, 1993.

[52] S. Martin, K. Wessendorf, C. Gebert, G. Frye, R. Cernosek, L. Casaua, and M. Mitchell, "Measuring liquid properties with smooth-surface and textured-surface resonators," in *Proceedings of the 1993 IEEE International frequency control symposium*, (345 E 47TH ST, New York, NY 10017), pp. 603–608, 1993. 1993 IEEE International Frequency Control Symposium (the 47th Annual Symposium), Salt Lake City, UT, Jun 02-04, 1993.

[53] F. Herrmann, D. Hahn, and S. Buttgenbach, "Separate determination of liquid density and viscosity with sagittally corrugated Love-mode sensors," *Sensors and Actuators A-Physical*, vol. 78, no. 2-3, pp. 99–107, 1999.

[54] F. Herrmann, D. Hahn, and S. Buttgenbach, "Separation of density and viscosity influence on liquid-loaded surface acoustic wave devices," *Applied Physics Letters*, vol. 74, no. 22, pp. 3410–3412, 1999.

[55] L. Theisen, S. Martin, and A. Hillman, "A model for the quartz crystal microbalance frequency response to wetting characteristics of corrugated surfaces," *Analytical Chemistry*, vol. 76, no. 3, pp. 796–804, 2004.

[56] C. Zhang, S. Schranz, R. Lucklum, and P. Hauptmann, "Mass effects of quartz resonant sensors with different surface microstructures in liquids," *IEEE Transactions on ultrasonics ferroelectrics and frequency control*, vol. 45, pp. 1204–1210, Sep 1998.

[57] M. Yang and M. Thompson, "Surface-morphology and the response of the thickness-shear mode acoustic-wave sensor in liquids," *Langmuir*, vol. 9, no. 8, pp. 1990–1994, 1993.

[58] L. Daikhin, E. Gileadi, G. Katz, V. Tsionsky, M. Urbakh, and D. Zagidulin, "Influence of roughness on the admittance of the quartz crystal microbalance immersed in liquids," *Analytical Chemistry*, vol. 74, no. 3, pp. 554–561, 2002.

[59] M. Urbakh and L. Daikhin, "Surface morphology and the quartz crystal microbalance response in liquids," *Colloids and Surfaces A-Physicochemical and Engineering Aspects*, vol. 134, pp. 75–84, Mar 15 1998. Symposium on Electrochemical Surface Science at the 212th Meeting of the American-Chemical-Society, Orlando, Florida, Aug 25-29, 1997.

[60] C. Goubaidoulline, J. Reuber, F. Merz, and D. Johannsmann, "Simultaneous determination of density and viscosity of liquids based on quartz-crystal resonators covered with nanoporous alumina," *Journal of Applied Physics*, vol. 98, no. 1, 2005.

[61] C. Zhang, S. Schranz, and P. Hauptmann, "Surface microstructures of tsm resonators and liquid properties measurement," *Sensors and Actuators B - Chemical*, vol. 65, no. 1-3, pp. 296–298, 2000. 7th International Meeting on Chemical Sensors (IMCS-7), Beijing, Peoples R China, Jul 27-30, 1998.

[62] J. Kondoh, S. Hayashi, and S. Shiokawa, "Simultaneous detection of density and viscosity using surface acoustic wave liquid-phase sensors," *Japanese Journal of Applied Physics Part 1- Regular Papers Brief Communications & Review Papers*, vol. 40, pp. 3713–3717, 2001.

[63] A. Turton, D. Bhattacharyya, and D. Wood, "Love-mode surface acoustic wave liquid sensors using a polyimide waveguide layer," in *Proceedings of the 2004 IEEE International Frequency Control Symposium and Exposition* (Yuhas, MP, ed.), (345 E 47TH ST, New York, NY 10017 USA), pp. 250–

256, IEEE, IEEE, 2005. IEEE International Frequency Control Symposium and Exposition, Montreal, Canada, Aug 23-27, 2004.

[64] B. J. Meulendyk, M. C. Wheeler, B. Segee, and M. P. da Cunha, "Generalized and pure shear horizontal SAW sensors on quartz for hydrogen fluoride gas detection," in *2007 IEEE Ultrasonics Symposium Proceedings, Vols 1-6*, (345 E 47th St, New York, NY 10017 USA), pp. 480–483, 2007. IEEE Ultrasonics Symposium, New York, NY, Oct 28-31, 2007.

[65] G. Hansford, R. Freshwater, L. Eden, K. Turnbull, D. Hadaway, V. Ostanin, and R. Jones, "Lightweight dew-/frost-point hygrometer based on a surface-acoustic-wave sensor for balloon-borne atmospheric water vapor profile sounding," *Review of Scientific Instruments*, vol. 77, no. 1, 2006.

[66] J. Kondoh, S. Shiokawa, M. Rapp, and S. Stier, "Simulation of viscoelastic effects of polymer coatings on surface acoustic wave gas sensor under consideration of film thickness," *Japanese Journal of Applied Physics Part 1 - Regular Papers Short Notes & Review Papers*, vol. 37, no. 5B, Sp. Iss. SI, pp. 2842–2848, 1998. 18th Symposium on Ultrasonic Electronics (USE97), Chiba, Japan, Nov 12-14, 1997.

[67] G. Papadakis, A. Tsortos, and E. Gizeli, "Triple-helix DNA structural studies using a Love wave acoustic biosensor," *Biosensors & Bioelectronics*, vol. 25, no. 4, pp. 702–707, 2009.

[68] M. Cole, G. Sehra, J. Gardner, and V. Varadan, "Development of smart tongue devices for measurement of liquid properties," *IEEE Sensors Journal*, vol. 4, no. 5, pp. 543–550, 2004.

[69] C. Chuanzhi, M. Jinyi, Z. Boli, J. Hongmin, and Z. Hongxing, "Surface acoustic wave sensing detection system for chemical warfare agents," in *Proceedings of the First International Symposium on Test Automation & Instrumentation, Vols 1 - 3* (Qi, J and Cui, JP, ed.), (137 Chaonei Dajie, Beijing 100010, Peoples R China), pp. 1946–1949, China Instrument & Control Soc; Chinese Measurement Soc, Foreign Instrument Technol Comm, World Publishing Corporation, 2006. 1st International Symposium on Test Automation and Instrumentation, Beijing, Peoples R China, Sep 13-16, 2006.

[70] D. Galipeau, P. Story, K. Vetelino, and R. Mileham, "Surface acoustic wave microsensors and applications," *Smart Materials & Structures*, vol. 6, no. 6, pp. 658–667, 1997.

[71] G. Calabrese, H. Wohltjen, and M. Roy, "Surface acoustic-wave devices as chemical sensors in liquids - evidence disputing the importance of rayleigh-wave propagation," *Analytical Chemistry*, vol. 59, no. 6, pp. 833–837, 1987.

[72] D. Morgan, "Surface acoustic-wave devices and applications - 1 introductory review," *Ultrasonics*, vol. 11, no. 3, pp. 121–131, 1973.

[73] S. Martin, A. Ricco, T. Niemczyk, and G. Frye, "Characterization of SH acoustic plate mode liquid sensors," *Sensors and Actuators*, vol. 20, no. 3, pp. 253–268, 1989.

[74] H. Wohltjen and R. Dessy, "Surface acoustic-wave probes for chemical-analysis, 2 - gas chromatography detector," *Analytical Chemistry*, vol. 51, no. 9, pp. 1465–1470, 1979.

[75] M. Penza and L. Vasanelli, "Saw nox gas sensor using WO3 thin-film sensitive coating," *Sensors and Actuators B - Chemical*, vol. 41, no. 1-3, pp. 31–36, 1997.

[76] G. McHale, "Generalized concept of shear horizontal acoustic plate mode and Love wave sensors," *Measurement Science & Technology*, vol. 14, no. 11, pp. 1847–1853, 2003.

[77] T. Nakamoto, A. Fukuda, and T. Moriizumi, "Perfume and flavor identification by odor-sensing system using quartz-resonator sensor array and neural-network pattern-recognition," *Sensors and Actuators B - Chemical*, vol. 10, no. 2, pp. 85–90, 1993. 6th International Conference on Solid State Sensors and Actuators (Transducers 91), San Francisco, CA, Jun 24-28, 1991.

[78] J. Kondoh and S. Shiokawa, "New application of shear horizontal surface-acoustic-wave sensors to identifying fruit juices," *Japanese Journal of Applied Physics Part 1 - Regular Papers Short Notes & Review Papers*, vol. 33, no. 5B, pp. 3095–3099, 1994. 14th Symposium on Ultrasonic Electronics (USE 93), Yokohama, Japan, Dec 07-09, 1993.

[79] J. Kondoh, T. Imayama, Y. Matsui, and S. Shiokawa, "Enzyme biosensor based on surface acoustic wave device," *Electronics and Communications in Japan Part II - Electronics*, vol. 79, no. 7, pp. 69–75, 1996.

[80] J. Kondoh, T. Oyama, and S. Shiokawa, "Influence of particles in liquid on SH-SAW sensors," in *Proceedings of the IEEE Sensors 2004, Vols 1-3* (Rocha, D and Sarro, PM and Vellekoop, MJ, ed.), (345 E 47th St, New York, NY 10017 USA), pp. 119–122, 2004. IEEE Sensors 2004 Conference, Vienna, Austria, Oct 24-27, 2004.

[81] J. Kondoh, Y. Matsui, and S. Shiokawa, "New biosensor using shear horizontal surface-acoustic-wave device," *Japanese Journal of Applied Physics Part 1 - Regular Papers Short Notes & Review Papers*, vol. 32, no. 5B, pp. 2376–2379, 1993.

[82] A. Campitelli, W. Wlodarski, and M. Hoummady, "Identification of natural spring water using shear horizontal SAW based sensors," *Sensors and Actuators B-Chemical*, vol. 49, no. 3, pp. 195–201, 1998.

[83] D. Deobagkar, V. Limaye, S. Sinha, and R. Yadava, "Acoustic wave immunosensing of Escherichia coli in water," *Sensors and Actuators B-chemical*, vol. 104, no. 1, pp. 85–89, 2005.

[84] C. Wold, J. Sternhagen, R. Mileham, K. Mitzner, and D. Galipeau, "Temperature measurement using surface skimming bulk waves," in *1999 IEEE Ultrasonics Symposium Proceedings, Vol 1 and 2* (Schneider, SC and Levy, M and McAvoy, BR, ed.), pp. 441–444, 1999.

[85] F. Teston, G. Feuillard, L. Tessier, L. Hue, and M. Lethiecq, "Analysis of the coupling between shear horizontal plate waves and liquids: Application to the measurement of the shear rigidity modulus of glycerol solutions," *Journal of Applied Physics*, vol. 87, no. 2, pp. 689–694, 2000.

[86] M. Newton, G. McHale, and F. Martin, "Layer-guided shear acoustic plate mode sensor," *Applied Physics Letters*, vol. 82, no. 13, pp. 2181–2183, 2003.

[87] C. R. Evans, S. M. Stanley, C. J. Percival, G. McHale, and M. I. Newton, "Lithium tantalate layer guided plate mode sensors," *Sensors and Actuators A-Physical*, vol. 132, no. 1, Sp. Iss. SI, pp. 241–244, 2006. 19th European Conference on Solid-State Transducers, Barcelona, Spain, Sep 11-14, 2005.

[88] G. Kovacs, G. Lubking, M. Vellekoop, and A. Venema, "Love waves for (bio)chemical sensing in liquids," in *IEEE 1992 Ultrasonics Symposium : Proceedings, Vols 1 and 2* (Mcavoy, BR, ed.), pp. 281–285, 1992. IEEE 1992 Ultrasonic Symp, Tucson, AZ, Oct 20-23, 1992.

[89] M. I. Newton, P. Roach, and G. McHale, "ST quartz acoustic wave sensors with sectional guiding layers," *Sensors*, vol. 8, no. 7, pp. 4384–4391, 2008.

[90] M. Newton, G. McHale, and F. Martin, "Experimental study of Love wave devices with thick guiding layers," *Sensors and Actuators A-Physical*, vol. 109, no. 3, pp. 180–185, 2004.

[91] E. Gizeli, A. Stevenson, N. Goddard, and C. Lowe, "A novel love-plate acoustic sensor utilizing polymer overlayers," *IEEE Transactions on Ultrasonics Ferroelectrics and Frequency Control*, vol. 39, no. 5, pp. 657–659, 1992.

[92] F. Herrmann, M. Weihnacht, and S. Buttgenbach, "Properties of shear-horizontal surface acoustic waves in different layered quartz-SiO2 structures," *Ultrasonics*, vol. 37, no. 5, pp. 335–341, 1999.

[93] J. Du, G. Harding, J. Ogilvy, P. Dencher, and M. Lake, "A study of love-wave acoustic sensors," *Sensors and Actuators A-Physical*, vol. 56, no. 3, pp. 211–219, 1996.

[94] B. Jakoby and M. Vellekoop, "Properties of Love waves: applications in sensors," *Smart Materials & Structures*, vol. 6, no. 6, pp. 668–679, 1997.

[95] J. Du, G. Harding, A. Collings, and P. Dencher, "An experimental study of Love-wave acoustic sensors operating in liquids," *Sensors and Actuators A-Physical*, vol. 60, no. 1-3, pp. 54–61, 1997. Eurosensors X Meeting, Louvain, Belgium, Sep 08-11, 1996.

[96] M. Newton, G. McHale, F. Martin, E. Gizeli, and K. Melzak, "Generalized Love waves," *Europhysics Letters*, vol. 58, no. 6, pp. 818–822, 2002.

[97] B. Jakoby and M. Vellekoop, "Viscosity sensing using a Love-wave device," *Sensors and Actuators A-Physical*, vol. 68, no. 1-3, pp. 275–281, 1998. Eurosensors XI Meeting, Warsaw, Poland, Sep 21-24, 1997.

[98] B. Jakoby, M. Scherer, M. Buskies, and H. Eisenschmid, "An automotive engine oil viscosity sensor," *IEEE Sensors Journal*, vol. 3, no. 5, pp. 562–568, 2003.

[99] A. Turton, D. Bhattacharyya, and D. Wood, "Liquid density analysis of sucrose and alcoholic beverages using polyimide guided Love-mode acoustic wave sensors," *Measurement science & Technology*, vol. 17, no. 2, pp. 257–263, 2006.

[100] T. Niemczyk, S. Martin, G. Frye, and A. Ricco, "Acoustoelectric interaction of plate modes with solutions," *Journal of Applied Physics*, vol. 64, no. 10, Part 1, pp. 5002–5008, 1988.

[101] S. Liew, F. Josse, D. Haworth, Z. Shana, U. Kelkar, and M. Grunze, "Applications of lithium-niobate acoustic plate modes as sensor for conductive liquids," in *IEEE 1990 Ultrasonics Symposium: Proceedings, Vols 1-3* (B. Mcavoy, ed.), pp. 285–290, IEEE, Ultrason Ferroelect & Frequency Control Soc, 1990.

[102] R. Dahint, Z. Shana, F. Josse, S. Riedel, and M. Grunze, "Identification of metal-ion solutions using acoustic plate mode devices and pattern-recognition," *IEEE Transactions on Ultrasonics Ferroelectrics and Frequency Control*, vol. 40, no. 2, pp. 114–120, 1993.

[103] D. Beyssen, L. Le Brizoual, O. Elmazria, and P. Alnot, "Microfluidic device based on surface acoustic wave," *Sensors and Actuators B-Chemical*, vol. 118, no. 1-2, pp. 380–385, 2006. 19th European Conference on Solid-State Transducers, Barcelona, Spain, Sep 11-14, 2005.

[104] S. Jacesko, J. Abraham, T. Ji, V. Varadan, M. Cole, and J. Gardner, "Investigations on an electronic tongue with polymer microfluidic cell for liquid sensing and identification," *Smart Materials & Structures*, vol. 14, no. 5, pp. 1010–1016, 2005.

[105] I. I. Leonte, G. Sehra, M. Cole, P. Hesketh, and J. W. Gardner, "Taste sensors utilizing high-frequency SH-SAW devices," *Sensors and Actuators B - Chemical*, vol. 118, no. 1-2, pp. 349–355, 2006. 19th European Conference on Solid-State Transducers, Barcelona, Spain, Sep 11-14, 2005.

[106] K. Laenge, G. Blaess, A. Voigt, R. Goetzen, and M. Rapp, "Integration of a surface acoustic wave biosensor in a microfluidic polymer chip," *Biosensors & Bioelectronics*, vol. 22, no. 2, pp. 227–232, 2006.

[107] D. Mark, S. Haeberle, G. Roth, F. von Stetten, and R. Zengerle, "Microfluidic lab-on-a-chip platforms: requirements, characteristics and applications," *Chemical Society Reviews*, vol. 39, no. 3, pp. 1153–1182, 2010.

[108] K. Harris, M. Kanakubo, and L. Woolf, "Temperature and pressure dependence of the viscosity of the ionic liquids 1-methyl-3-octylimidazolium hexafluorophosphate and 1-methyl-3-octylimidazolium tetrafluoroborate," *Journal of Chemical and Engineering Data*, vol. 51, no. 3, pp. 1161–1167, 2006.

[109] C. Jin, C. Ye, B. Phillips, J. Zabinski, X. Liu, W. Liu, and J. Shreeve, "Polyethylene glycol functionalized dicationic ionic liquids with alkyl or polyfluoroalkyl substituents as high temperature lubricants," *Journal of Materials Chemistry*, vol. 16, no. 16, pp. 1529–1535, 2006.

[110] S. Forsyth, J. Pringle, and D. MacFarlane, "Ionic liquids - An overview," *Australian Journal of Chemistry*, vol. 57, no. 2, pp. 113–119, 2004. Ionic Liquid Workshop, Melbourne, Australia, May, 2003.

[111] K. Seddon, "Ionic liquids - A taste of the future," *Nature Materials*, vol. 2, no. 6, pp. 363–365, 2003.

[112] H. Zhao, "Current studies on some physical properties of ionic liquids," *Physics and Chemistry of Liquids*, vol. 41, no. 6, pp. 545–557, 2003.

[113] J. Brennecke and E. Maginn, "Ionic liquids: Innovative fluids for chemical processing," *Aiche Journal*, vol. 47, no. 11, pp. 2384–2389, 2001.

[114] P. Dubois, G. Marchand, Y. Fouillet, J. Berthier, T. Douki, F. Hassine, S. Gmouh, and M. Vaultier, "Ionic liquid droplet as e-microreactor," *Analytical Chemistry*, vol. 78, no. 14, pp. 4909–4917, 2006.

[115] A. Berthod, M. Ruiz-Angel, and S. Carda-Broch, "Ionic liquids in separation techniques," *Journal of Chromatography A*, vol. 1184, no. 1-2, pp. 6–18, 2008.

[116] V. I. Parvulescu and C. Hardacre, "Catalysis in ionic liquids," *Chemical Reviews*, vol. 107, no. 6, pp. 2615–2665, 2007.

[117] W. Miao and T. H. Chan, "Ionic-liquid-supported synthesis: A novel liquid-phase strategy for organic synthesis," *Accounts of Chemical Research*, vol. 39, no. 12, pp. 897–908, 2006.

[118] H. Mizuuchi, V. Jaitely, S. Murdan, and A. T. Florence, "Room temperature ionic liquids and their mixtures: Potential pharmaceutical solvents," *European Journal of Pharmaceutical Sciences*, vol. 33, no. 4-5, pp. 326–331, 2008.

[119] J.-W. Choi, G. Cheruvally, Y.-H. Kim, J.-K. Kim, J. Manuel, P. Raghavan, J.-H. Ahn, K.-W. Kim, H.-J. Ahn, D. S. Choi, and C. E. Song, "Poly(ethylene oxide)-based polymer electrolyte incorporating room-temperature ionic liquid for lithium batteries," *Solid State Ionics*, vol. 178, no. 19-20, pp. 1235–1241, 2007.

[120] P. R. V. Rao, K. A. Venkatesan, and T. G. Srinivasan, "Studies on applications of room temperature ionic liquids," *Progress in Nuclear Energy*, vol. 50, no. 2-6, pp. 449–455, 2008. COE-INES 2nd International Symposium on Innovative Nuclear Energy Systems for Sustainable Development of the World, Yokohama, Japan, Nov 26-30, 2006.

[121] J. Holbrey, "Industrial applications of ionic liquids," *Chimica Oggi-Chemistry Today*, vol. 22, no. 6, pp. 35–37, 2004.

[122] M. Deetlefs and K. Seddon, "Ionic liquids: fact and fiction," *Chimca Oggi-Chemistry Today*, vol. 24, no. 2, pp. 16+, 2006.

[123] M. Earle, J. Esperanca, M. Gilea, J. Lopes, L. Rebelo, J. Magee, K. Seddon, and J. Widegren, "The distillation and volatility of ionic liquids," *Nature*, vol. 439, no. 7078, pp. 831–834, 2006.

[124] D. R. MacFarlane and K. R. Seddon, "Ionic liquids - Progress on the fundamental issues," *Australian Journal of Chemistry*, vol. 60, no. 1, pp. 3–5, 2007.

[125] M. Armand, F. Endres, D. R. MacFarlane, H. Ohno, and B. Scrosati, "Ionic-liquid materials for the electrochemical challenges of the future," *Nature materials*, vol. 8, no. 8, pp. 621–629, 2009.

[126] B. L. Bhargava, S. Balasubramanian, and M. L. Klein, "Modelling room temperature ionic liquids," *Chemical Communications*, no. 29, pp. 3339–3351, 2008.

[127] J. Jacquemin, R. Ge, P. Nancarrow, D. W. Rooney, M. F. C. Gomes, A. A. H. Padua, and C. Hardacre, "Prediction of ionic liquid properties. I. Volumetric properties as a function of temperature at 0.1 MPa," *Journal of Chemical and Engineering Data*, vol. 53, no. 3, pp. 716–726, 2008.

[128] P. Bonhote, A. Dias, N. Papageorgiou, K. Kalyanasundaram, and M. Gratzel, "Hydrophobic, highly conductive ambient-temperature molten salts," *Inorganic Chemistry*, vol. 35, no. 5, pp. 1168–1178, 1996.

[129] M. Earle, S. Katdare, and K. Seddon, "Paradigm confirmed: The first use of ionic liquids to dramatically influence the outcome of chemical reactions," *Organic Letters*, vol. 6, no. 5, pp. 707–710, 2004.

[130] W. Xu, L. Wang, R. Nieman, and C. Angell, "Ionic liquids of chelated orthoborates as model ionic glassformers," *Journal of Physical Chemistry B*, vol. 107, no. 42, pp. 11749–11756, 2003.

[131] J. Jacquemin, P. Husson, A. Padua, and V. Majer, "Density and viscosity of several pure and water-saturated ionic liquids," *Green Chemistry*, vol. 8, no. 2, pp. 172–180, 2006.

III. EXPERIMENTAL I: QUARTZ CRYSTAL IMPEDANCE ANALYSIS OF ROOM TEMPERATURE IONIC LIQUIDS

In this chapter the results of a standard small volume impedance analysis technique using a Quartz Crystal Microbalance (QCM) to characterise Room Temperature Ionic Liquids (RTILs) are presented [1]. This technique gives access to the square root viscosity-density product, calculated through analysis of changes in the crystal's resonant frequency when loaded with a liquid. This is compared to values obtained with traditional viscometer and densitometer methods. The advantage of this method is that it allows the required volume of liquid to be reduced significantly.

The Newtonian behaviour of two RTILs with varying concentration, nineteen pure RTILs, and polydimethylsiloxane (PDMS) oils (1 - 100,000 cP) which are known to be non-Newtonian at high viscosity at high frequency [2] are also studied by analysing the changes in the impedance spectra of the quartz crystal and fitting with a Butterworth Van Dyke (BVD) model [3] [4].

The values obtained for the square root of the viscosity-density product using this technique are consistent with those measured using traditional methods. The third harmonic frequency response has also been studied and provides improved agreement with the traditionally measured values in comparison to the fundamental response, with the largest difference of around 10%.

Throughout this study, the RTILs have been supplied by The Queens University Belfast who produced most liquids 'in-house'. Protocols for their use were also advised along with safe handling.

III.1 Method

A quartz crystal with single sided electrode contact is operated within a standard holder. These holders use seals made from rubber which is not chemically compatible with RTILs. For this study a device holder was machined 'in house' directly from Polytetrafluoroethylene (PTFE) leaving a 20 mm diameter chamber with a 2.5 mm wide raised lip acting as seal, negating the need for the o-ring. The holder has a screw ring which clamps around the rim of the device as shown in III.1.

A quartz crystal (Testbourne Ltd, UK) with a 5 MHz resonant frequency, clamped within the holder was used

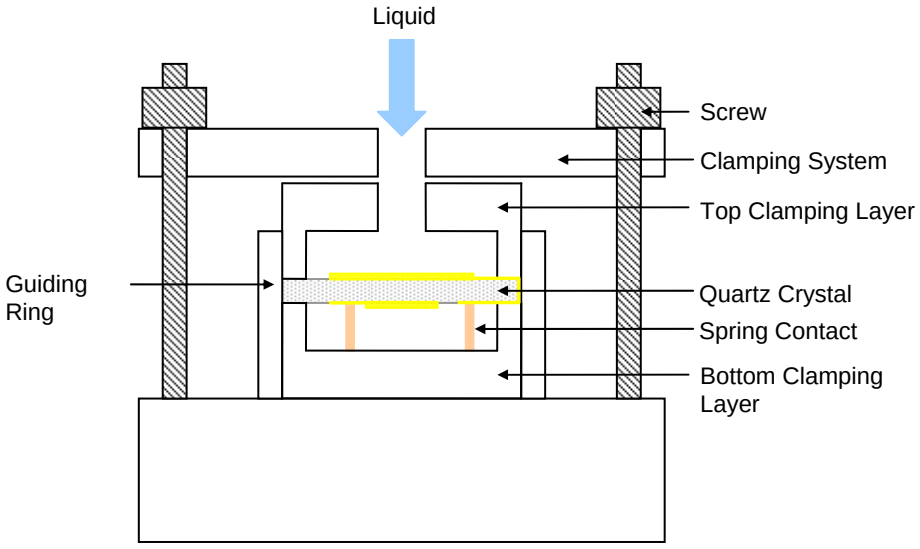

Figure III.1: Schematic 'In-house' machined PTFE Quartz Crystal Microbalance holder.

with a calibrated E5061A network analyser (Agilent, CA) to measure the resonant frequency. Reflected power measurements are made in which radio frequency energy excites the crystal at a range of different frequencies. Less power is reflected at resonance thus allowing the resonant frequency to be determined as the minimum of this plot. The ratio of power reflected to that transmitted is presented on the screen as a reflected power plot against frequency.

Spectra were recorded for the unloaded (air) and liquid loaded QCM for both the fundamental and third harmonic resonant frequencies (N = 1, 3) as it has been suggested in the literature that the third harmonic may provide a more accurate frequency change measurement [5].

The Network analyser allows the storage of this data in comma seperated variable (.csv) ASCII files. The collected data is imported into LabView^{TM} (National Instruments, CA,USA) and fitted using a Butterworth Van Dyke (BVD) model described in Section II.2.2.5. When the crystal is loaded with liquid, the resonance is rapidly damped causing a frequency decrease and bandwidth increase (as seen in the results section Figure III.5). The BVD model allows a load impedance to be extracted as a series combination of a resistance and an inductance. From the fit (see Figure III.2), the resonant frequency and bandwidth are obtained [4].

The RTILs are very hygroscopic, and hence uptake water from the atmosphere changing their viscosity rapidly. It is for this reason that all RTILs are dried under vacuum (1 Torr) in a heated oil bath (60 °C) before use to minimise water contamination. The liquids were characterised using a DV-II+ Programmable viscometer (Brookfield, MA, USA), and a DMA 4500 Density/specific gravity/concentration meter (Anton Parr, Austria, Europe) immediately prior to use with a QCM requiring a total of 2.0 ml sample liquid. The temperature for both density and viscosity measurements were controlled with a water bath and were set to 25°C, which was the room temperature at the time the QCM measurements were made. Measurements for this chapter were

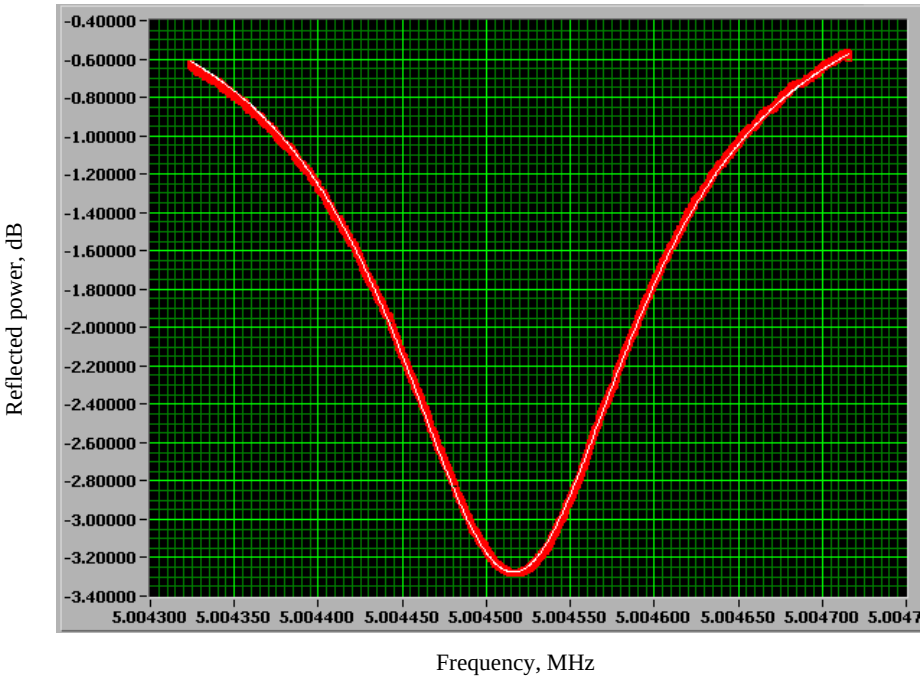

Figure III.2: Labview^{TM} screen shot of a BVD fit for an unloaded quartz crystal, where red represents the raw data and the thin white line is the fit.

made during an extended visit to the Queens University Belfast where water content measurements could be recorded using a Cou-Lo Compact Coulometric Karl Fischer titrator (GR Scientific, UK). Measurements of halide content to ensure the liquids were of suitable purity were also made at Queen's University Belfast using chromatography [6] prior to use.

To ensure the QCM and 'in-house' manufactured device holder were functioning correctly, concentrations of water-glycerol mixtures (0% to 90%) were made. Water-glycerol solutions were chosen as a calibrating fluid as these liquid are known to behave according to the frequency and bandwidth changes predicted by Kanazawa and Gordon [7]. They are also well known for being hygroscopic at higher concentrations and are considered to behave in a Newtonian manner within the chosen concentrations. A second series of comparison fluids, PDMS oils (Aldrich), which are known to be strongly non-Newtonian at high molecular weight were measured covering viscosities from 1 cP to 100,000 cP.

Table III.1 shows the nineteen Room Temperature Ionic Liquids used in the these experiments. A water immiscible ionic liquid [C_4mim][NTf_2] is diluted to various concentrations with methanol, and a water miscible ionic liquid [C_4mim][OTf] is varied with water to change the viscosity of the liquids. By varying their concentration with water or methanol viscosity decreases rapidly.

Crystals were cleaned in distilled water and methanol before blow drying with nitrogen prior to each measurement. Cleaning the QCM after testing PDMS oils required an additional cleaning step of rinsing the crystals with a cleaning agent, 5% v/v Decon90 (Decon Laboratories Limited, UK) with distilled water at 60 °C to

Ionic Liquid - Water Miscible	Ionic Liquid - Water Immiscible
$[C_2mim][SCN]$	$[C_2mim][NTf_2]$
$[C_{10}mim][SCN]$	$[C_4mim][NTf_2]$
$[C_4mim][DCA]$	$[C_6mim][NTf_2]$
$[C_4mpyrr][DCA]$	$[C_8mim][NTf_2]$
$[C_4mim][TFA]$	$[C_{10}mim][NTf_2]$
$[N_{1,8,8,8}][TFA]$	$[C_4mpyrr][NTf_2]$
$[C_4mim][ACO]$	$[P_{6,6,6,14}][NTf_2]$
$[C_4mim][OTf]$	$[C_4mpyrr][FAP]$
$[C_2mim][EtSO_4]$	$[C_4mim][OctSO_4]$
$[C_4mim][MeSO_4]$	

Table III.1: Nineteen room temperature ionic liquids investigated, showing liquids to be miscible or immiscible with water.

remove all traces of the oil on the surface, it was sometimes necessary, especially for the highly viscous oils to gently rub the surface of the crystal with a lens cloth. Crystals were rinsed and dried until the resonant frequency returned to its original unloaded frequency (within 50 Hz).

Because the liquids are hygroscopic, and water content considerably changes the viscosity of the liquids, all measurements were made in a two handed zipper-lock glove bag (Z530212-1EA, Sigma-Aldrich, UK) under an argon atmosphere to reduce the absorption of moisture. A typical measurement time for introducing the liquid to the cell and taking the resonance spectra for a range of harmonics (N = 1 to 11) was under two minutes. Only the fundamental and third harmonic are presented herein, a full set of harmonics is available in reference [8]. A sample volume of 40 μL was needed for the QCM to operate satisfactorily. This sample volume of liquid results in a film with a thickness of 1270 μm covering the sensing region of the crystal which is much greater than the expected maximum shear wave penetration depth for the most viscous liquid (maximum penetration depth 7.5 μm).

III.2 Results and Discussion

Results were obtained for water-glycerol solutions, two RTILs with varying concentrations and nineteen pure RTILs. Spectra showing changes in frequency and bandwidth are shown, providing information on the Newtonian response and the square root viscosity density product of each liquid. Each point is an average of three QCM measurements each made with new liquid samples, and where appropriate error bars of the minimum and maximum values obtained are shown.

III.2.1 Water-Glycerol Results

Figure III.3 shows the square-root viscosity-density product values obtained from the QCM for water-glycerol solutions on the fundamental, against those measured using traditional measurements. These measurements were made to ensure the 'in-house' manufactured device holder was functioning correctly, according to the re-

lationship predicted by Kanazawa and Gordon [7]. Excellent agreement is found. Measurements were recorded for change in bandwidth and change in frequency as shown in III.4 and show that the range of water-glycerol concentrations measured have strong Newtonian behaviour (defined as $\Delta f = -\frac{\Delta B}{2}$).

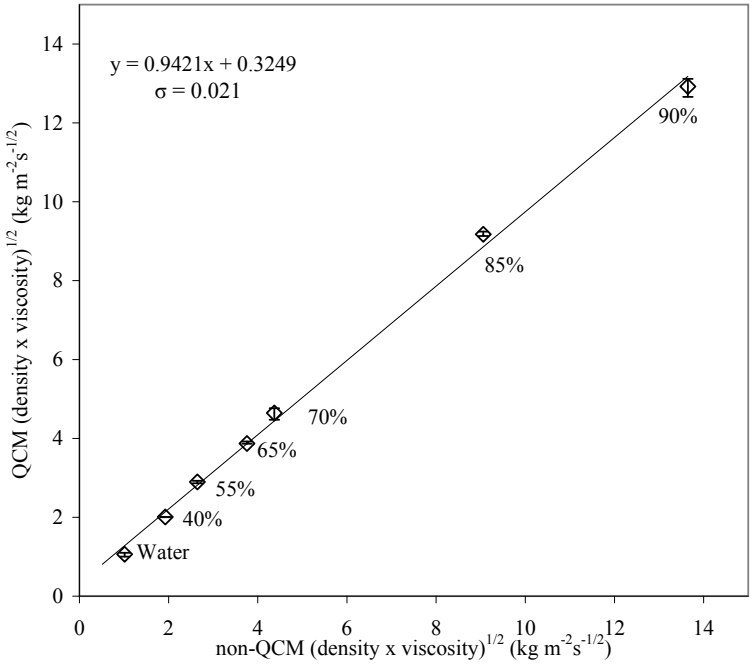

Figure III.3: Comparison of the square root viscosity-density product ($\sqrt{(\rho\eta)}$) determined from the quartz crystal operating on the fundamental resonance and from separate measurements using a viscometer and density meter at 25 °C for varying concentrations of water-glycerol (v/v).

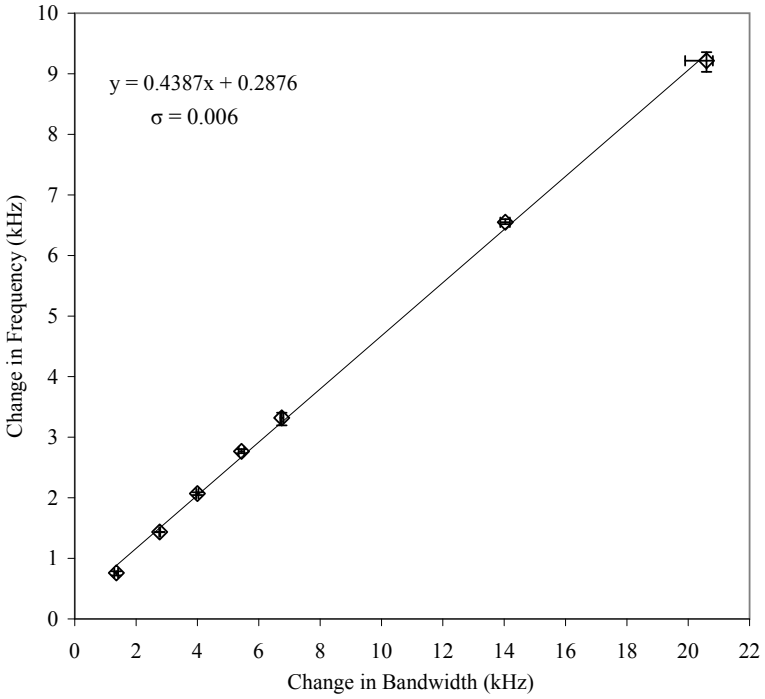

Figure III.4: QCM measurements of various concentrations for varying concentrations of water-glycerol data presented as change in frequency against change in bandwidth to test for Newtonian response.

III.2.2 Power Spectra for Room Temperature Ionic Liquids on a Loaded Quartz Crystal Microbalance

Figure III.5 shows a standard quartz crystal power spectra response for an unloaded crystal and the same crystal then loaded with $[C_2mim][NTf_2]$. This is a typical result for a QCM; with an unloaded crystal having a strong, sharp resonant peak, which when loaded becomes broad and damped. From the changes seen in these spectra it is possible to determine the change in frequency and bandwidth, to calculate the viscosity-density product. If the change in frequency equals half the change in bandwidth, the liquid is considered Newtonian however if this is not the case, the liquid is considered non-Newtonian with more non-Newtonian behaviour demonstrated further from this value.

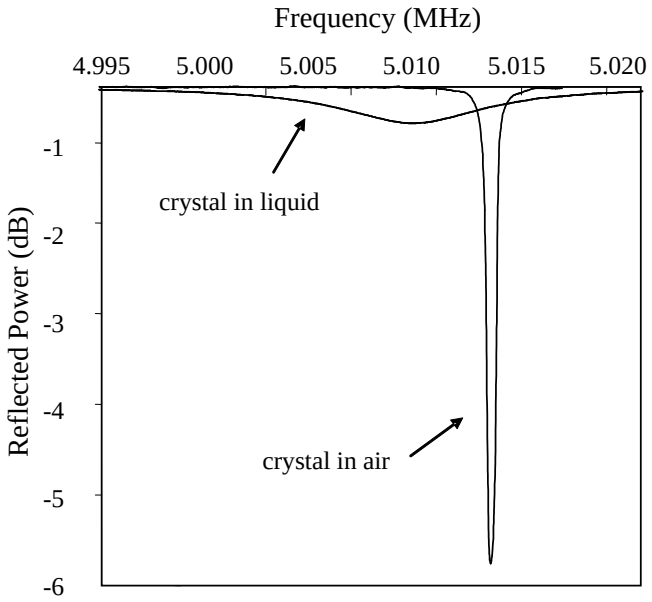

Figure III.5: Quartz crystal power spectra for crystal unloaded and loaded with $[C_2mim][NTf_2]$.

III.2.3 Newtonian Response

It is clear from Figure III.6(a) and III.6(b) both the water miscible and water immiscible ionic liquid tested relate well to the Kanazawa and Gordon relationship [7]. Both the change in frequency and bandwidth response varies linearly with the square root viscosity-density product. It is clear this is not the case for the PDMS oils, which deviate from the linear response significantly for both the change in frequency and bandwidth. This result is expected because the oils are known to be strongly non-Newtonian at high molecular weights [2]. When this data is plotted as the change in frequency against change in bandwidth to test for Newtonian behaviour, see Figure III.7(a) it is possible to see the PDMS oils deviate considerably from Newtonian behaviour at high molecular weights, confirming the PDMS oils to be non-Newtonian as expected. At low concentrations (Figure III.7(b)) the response of both ionic liquids between the change in frequency and bandwidth lie in agreement with that expected for Newtonian behaviour, however the higher concentrations lie slightly below this line. It is unclear if these liquids are slightly non-Newtonian or if this is a degree of error seen with more viscous liquids.

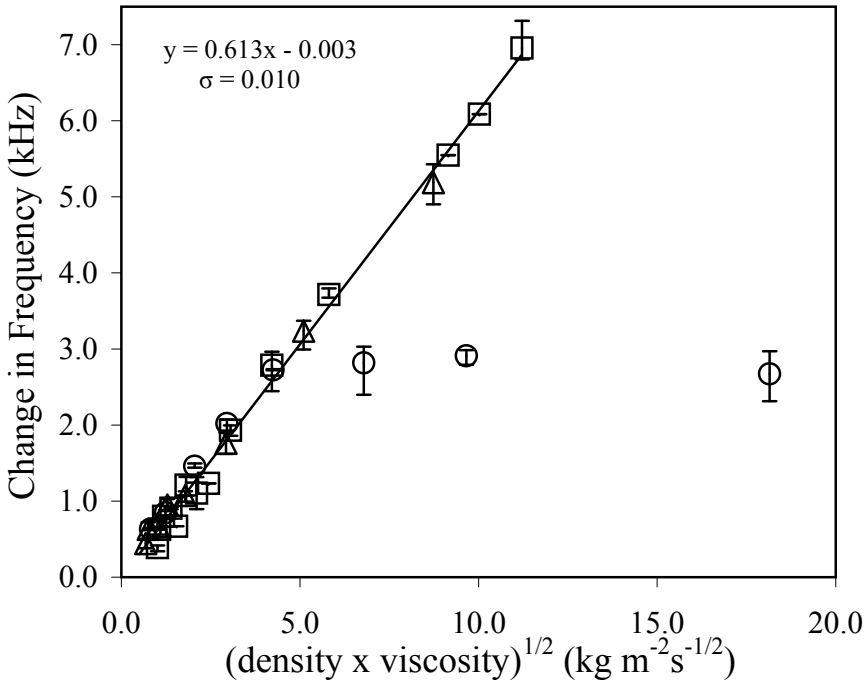

(a)

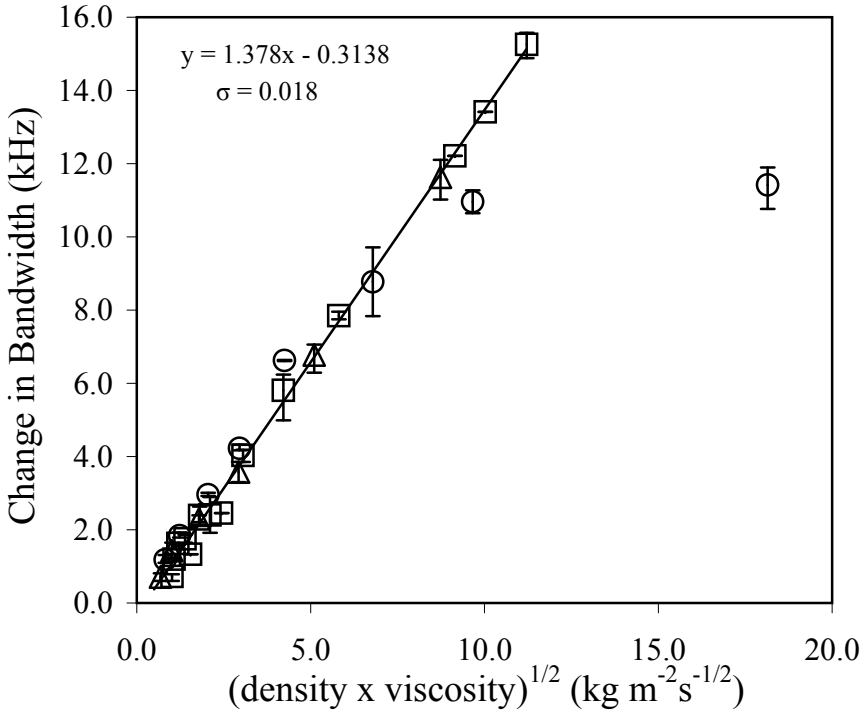

(b)

Figure III.6: Changes in (a) resonant frequency and (b) bandwidth as a function of viscosity-density product. Data shows [C_4mim][OTf] up to 100% concentration in water (□), [C_4mim][NTf_2] up to 100% concentration in methanol (△), and a range of PDMS oils (○).

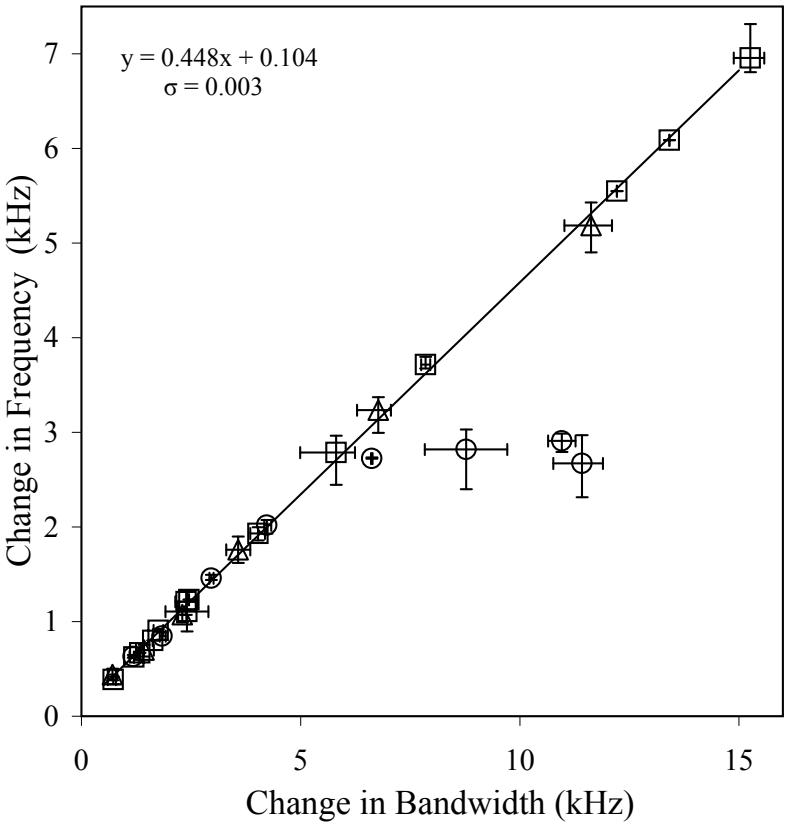

(a)

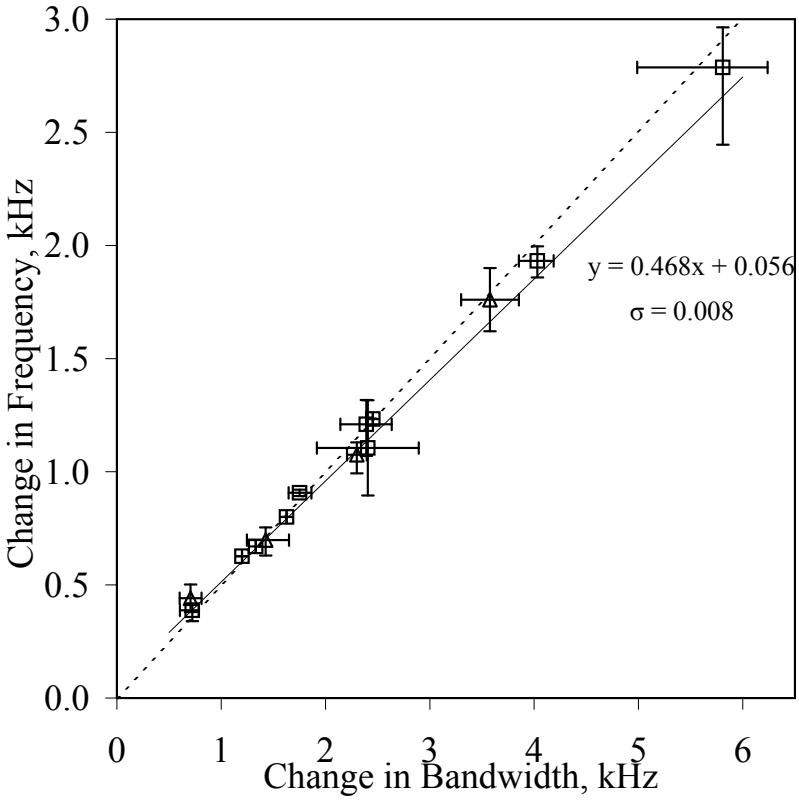

(b)

Figure III.7: (a) Data presented as change in frequency against change in bandwidth to test for Newtonian response. The polydimethylsiloxane oils (○) deviate significantly from Newtonian behaviour (Kanazawa and Gordon equation shown by the dashed line) at high molecular weight, but the [C_4mim][OTf] (□) and [C_4mim][NTf_2] (△) remain Newtonian. Also presented with a reduced viscosity density range in (b).

III.2.4 Viscosity-Density Dependence on Water Content

Both the fundamental and third harmonic frequency response to liquid loading with various concentrations of ionic liquids have been studied. Figure III.8(a) and III.9(a) show the calculated square root viscosity-density product from the change in resonant frequency using the Kanazawa and Gordon equation [7] for both the fundamental, and third harmonic resonances, for varying concentrations of a water miscible ($[C_4mim][OTf]$) and water immiscible ($[C_4mim][NTf_2]$) liquid. Figures III.8(b) and III.9(b) show how the QCM calculated values vary from those measured with traditional methods. The fundamental values have a best fit line with an average slope of 0.83, this agreement is improved by measurements made on the third harmonic resonance (with an average slope of 0.93). The largest error from the averaged measurements on the third harmonic resonance is around ±10%. This is seen with the pure ionic liquids, which when considering their hygroscopic nature and dependence of viscosity on liquid composition is expected.

III.2.5 Pure Room Temperature Ionic Liquids on the Fundamental Resonance

To understand what is happening with the higher viscosity liquids, nineteen pure RTILs with minimal water content have been studied on the fundamental resonance to determine the Newtonian response. See Table III.2 for a full list of RTILs measured with corresponding traditionally measured properties including water content, halide content, viscosity and density.

Figures III.10 and III.11 shows the change in fundamental frequency and bandwidth data for eleven of the nineteen liquids tested (see Table III.3). There is a clear correlation between the change in frequency and change in bandwidth, demonstrating Newtonian behaviour for these liquids. When this change in frequency is plotted against the square-root viscosity-density product the linear relationship maintains upto a square root viscosity-density product approximately equal to 18 kg $m^{-2}s^{-1/2}$.

Above this threshold, two ionic liquids, $[P_{6,6,6,14}][NTf_2]$ and $[C_4mim][TFA]$, deviate slightly from the linear prediction and a further two, $[C_4mim][OctSO_4]$ and $[N_{1,8,8,8}][TFA]$, deviate significantly from the linear prediction. At high viscosities the resonant curves are very broad and difficult to fit accurately. However it was possible to fit the resonant curve for $[C_4mim][OctSO_4]$, which was found to satisfy the Newtonian criteria given by, $\Delta f = -\Delta B/2$. This would indicate that all ionic liquids tested for which the quartz crystal method was able to provide accurate results (i.e. up to $\sqrt{\rho\eta} \approx 18$ kg $m^{-2}s^{-1/2}$) were Newtonian.

III.2.6 Pure Room Temperature Ionic Liquids on the Third Harmonic Resonance

The frequency change response of the third harmonic resonance has been studied to see if the agreement with traditional measurements can be improved.

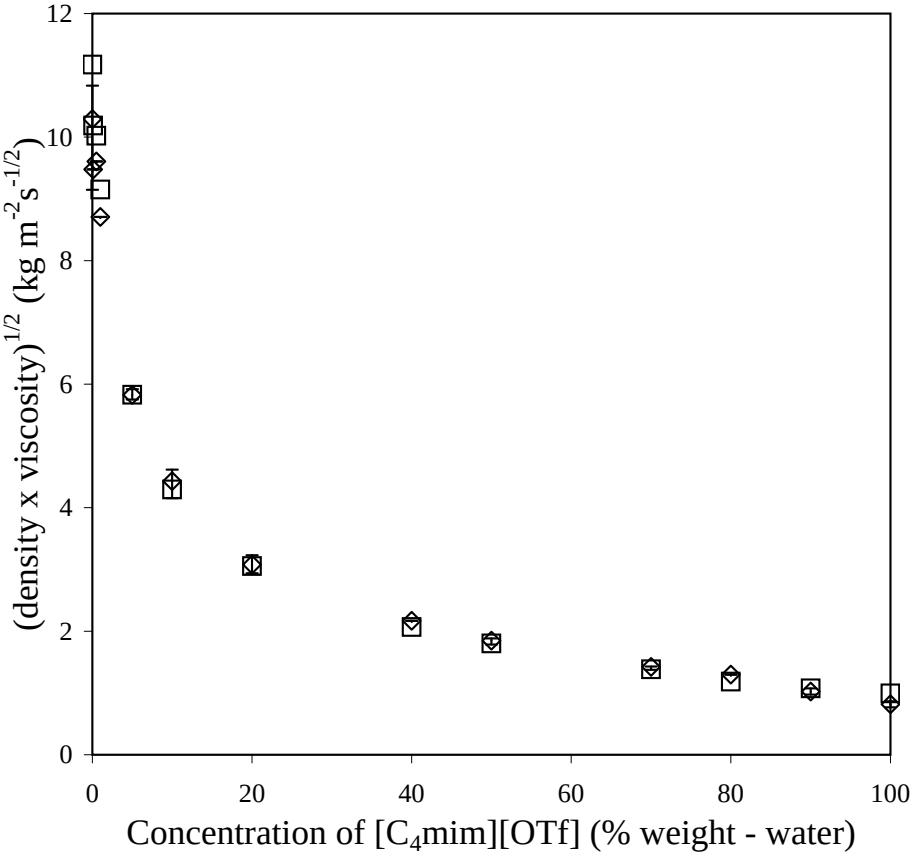

(a)

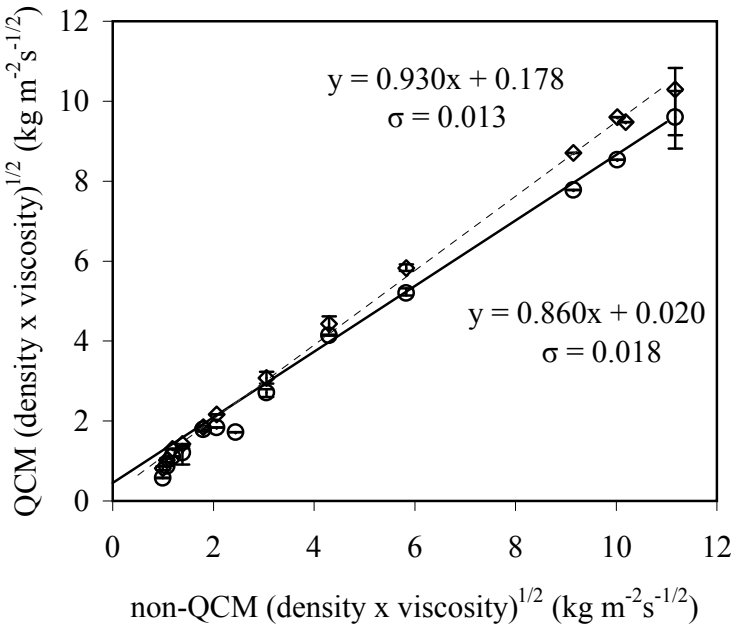

(b)

Figure III.8: (a) Viscosity-density dependence on concentration for the water miscible ionic liquid [C_4mim][OTf] determined by viscometer (□) and the third harmonic of the quartz crystal (◊). (b) Comparison of the quartz crystal data from the fundamental (○) and third harmonic (◊).

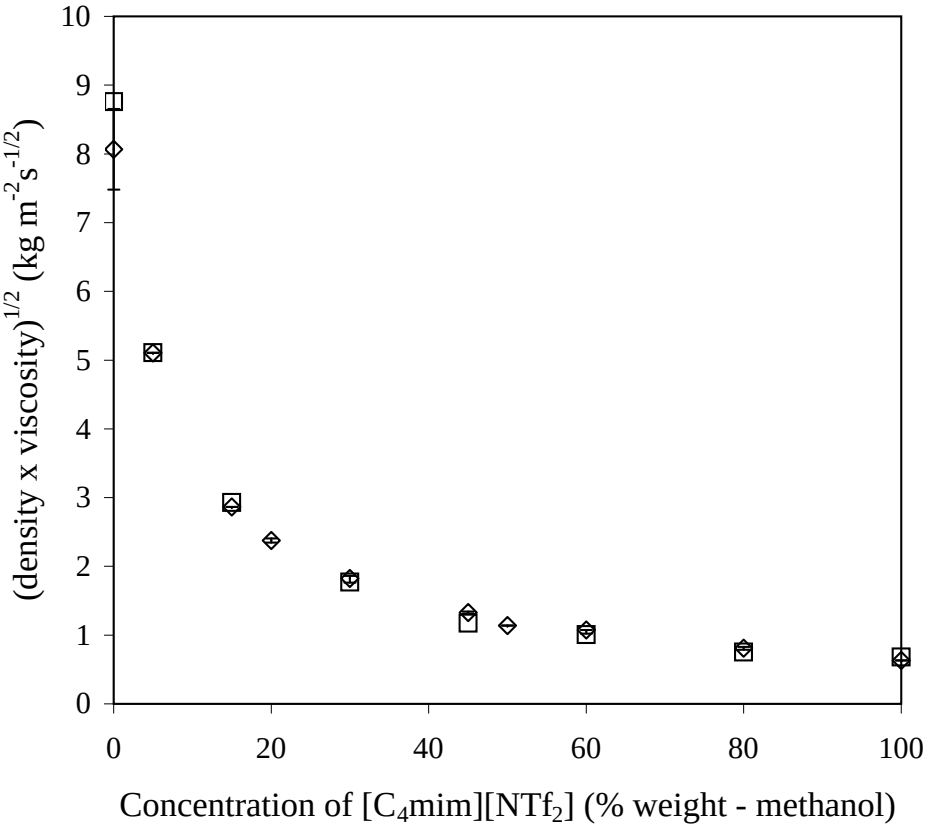

(a)

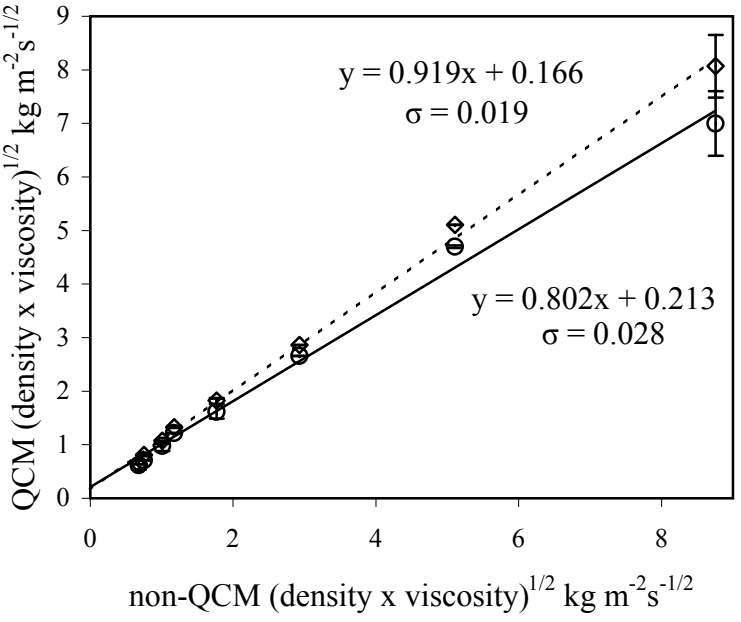

(b)

Figure III.9: (a) Viscosity-density dependence on concentration for the water immiscible ionic liquid [C_4mim][NTf_2] determined by viscometer (□) and the third harmonic of the quartz crystal (◊). (b) Comparison of the quartz crystal data from the fundamental (○) and third harmonic (◊).

Ionic Liquid	Viscosity (cP)	Density (g cm^{-3})	H_2O Content (wt%)	Halide Content (ppm)
$[C_2mim][SCN]$	23.6	1.118	0.0307	<5
$[C_4mim][DCA]$	28.8	1.059	0.0256	1830
$[C_4mpyrr][DCA]$	36.5	1.013	0.0235	1790
$[C_2mim][NTf_2]$	36.5	1.520	0.0100	<5
$[C_4mim][NTf_2]$	50.5	1.436	0.0096	<5
$[C_4mim][OTf]$	83.2	1.292	0.0681	<5
$[C_4mpyrr][NTf_2]$	79.3	1.395	0.0010	<5
$[C_6mim][NTf_2]$	80.1	1.357	0.0013	<5
$[C_2mim][EtSO_4]$	98.4	1.237	0.0279	0
$[C_8mim][NTf_2]$	95.0	1.321	0.0032	<5
$[C_{10}mim][NTf_2]$	120.2	1.279	0.0052	<5
$[C_4mim][AcO]$	139.7	1.243	0.0746	<10
$[C_4mim][MeSO_4]$	188.0	1.208	0.0067	<5
$[C_4mpyrr][FAP]$	221.0	1.580	0.0132	<100
$[P_{6,6,6,14}][NTf_2]$	335.9	1.065	0.0095	<5
$[C_4mim][TFA]$	418.5	1.068	0.0744	<5
$[C_4mim][OctSO_4]$	888.6	1.072	0.0113	<7
$[N_{1,8,8,8}][TFA]$	1708.0	0.966	0.0108	<5
$[C_{10}mim][SCN]$	683.7	1.011	0.0307	<5

Table III.2: Measured ionic liquid properties including halide content, water content in mass fractions (wt%), traditionally measured viscosity and density(at 25 °C).

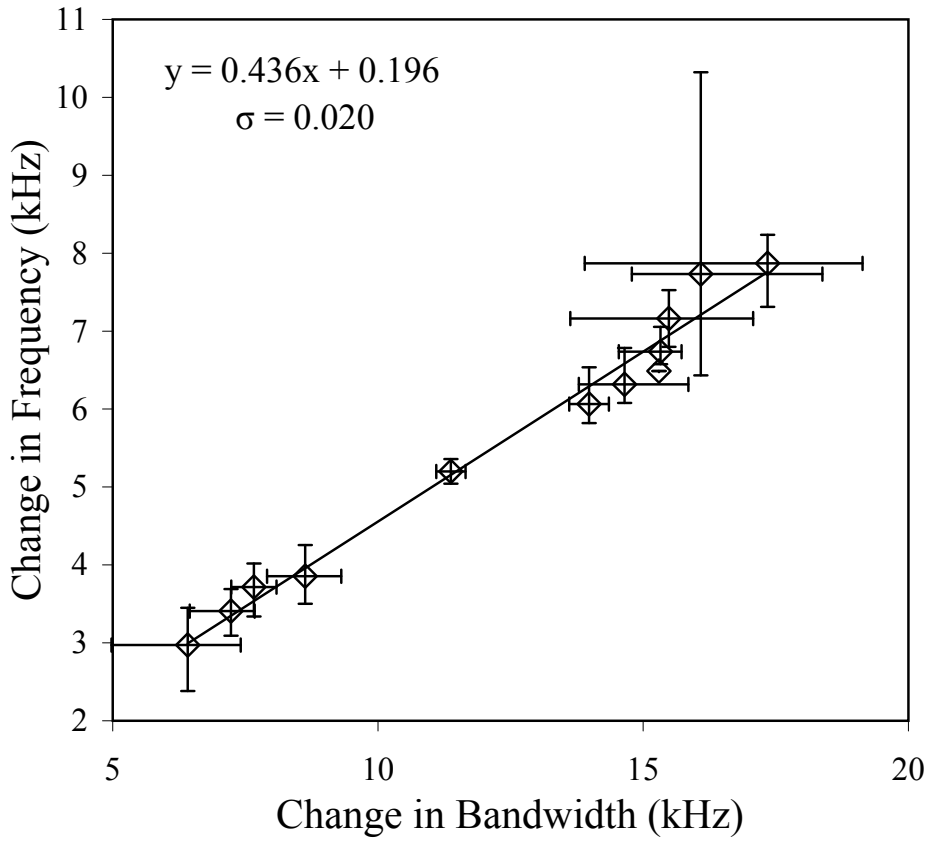

Figure III.10: Fundamental mode data for twelve pure ionic liquids showing the correlation between change in resonant frequency and change in bandwidth demonstrating Newtonian behaviour.

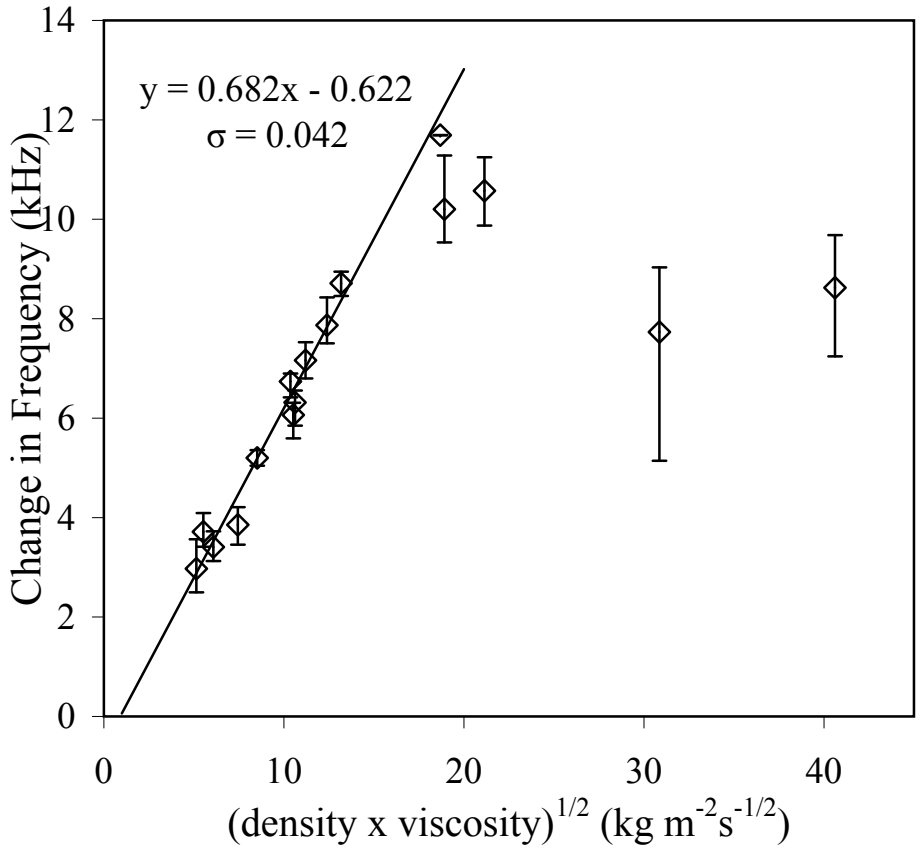

Figure III.11: Fundamental mode data for pure ionic liquids showing change in resonant frequency as a function of viscosity-density product; the data is described by a linear relationship up to $\sqrt{(\rho\eta)} \approx 18$ kg m^{-2} s$^{-1/2}$.

Ionic liquid	**Included in Newtonian Test Figure ***	**$(\rho\eta)^{1/2}$ (kg m^{-2} s$^{-1/2}$) Third Harmonic of Quartz Crystal**	**$(\rho\eta)^{1/2}$ (kg m^{-2} s$^{-1/2}$) Viscometer-Density Meter**
[C_2mim][SCN]	√	(4.5±0.6)	5.1
[C_4mim][DCA]	√	(5.6±0.1)	5.5
[C_4mpyrr][DCA]	√	(5.5±0.1)	6.1
[C_2mim][NTf_2]	√	(6.4±0.6)	7.4
[C_4mim][NTf_2]	√	(8.2±0.2)	8.5
[C_4mim][OTf]	√	(10.0±0.9)	10.4
[C_4mpyrr][NTf_2]	√	(10.1±0.3)	10.5
[C_6mim][NTf_2]	√	(9.8± 0.5)	10.4
[C_2mim][$EtSO_4$]	√	(10.7±0.6)	11.0
[C_8mim][NTf_2]	√	(9.6±0.9)	11.2
[C_{10}mim][NTf_2]	√	(10.9±0.5)	12.4
[C_4mim][AcO]	X	(11.8±0.2)	13.2
[C_4mim][$MeSO_4$]	X	(13.8±0.8)	15.1
[C_4mpyrr][FAP]	X	(15.3±2.1)	18.7
[$P_{6,6,6,14}$][NTf_2]	X	(10.6±0.6)	18.9
[C_4mim][TFA]	X	(14.6±0.1)	21.1
[C_4mim][$OctSO_4$]	X	(10.9±1.1)	30.9
[$N_{1,8,8,8}$][TFA]	X	(15.3±3.6)	40.6

Table III.3: Comparison of the square root viscosity-density product ($\sqrt{(\rho\eta)}$) determined from the third harmonic of quartz crystal and from separate measurements using a viscometer and density meter at 25 °C, where * represents the liquid is included in Figure III.10 which shows the test for Newtonian behaviour.

Figure III.12 shows the correlation of the square root viscosity-density product estimated using the shift in third harmonic frequency. The linear relationship seen with the fundamental QCM response is repeated here, with the calculated value for the square root viscosity-density value in good agreement with the value derived from traditional methods until a clear threshold $\sqrt{\rho\eta} \approx 18$ kg m^{-2}s$^{-1/2}$. For data points up to this threshold the data can be fitted by $\sqrt{\rho\eta}_Q = 0.86\sqrt{\rho\eta}_T$, (where $_Q$ and $_T$ represent QCM and traditional measurements respectively) thus indicating around a 10% underestimate by the quartz crystal impedance method compared to the values obtained by the viscometer and densitometer. This underestimate could be corrected however, by using a calibrated value for the numerical coefficient in Equation II.4 rather than the theoretical value from the Kanazawa and Gordon equation [7].

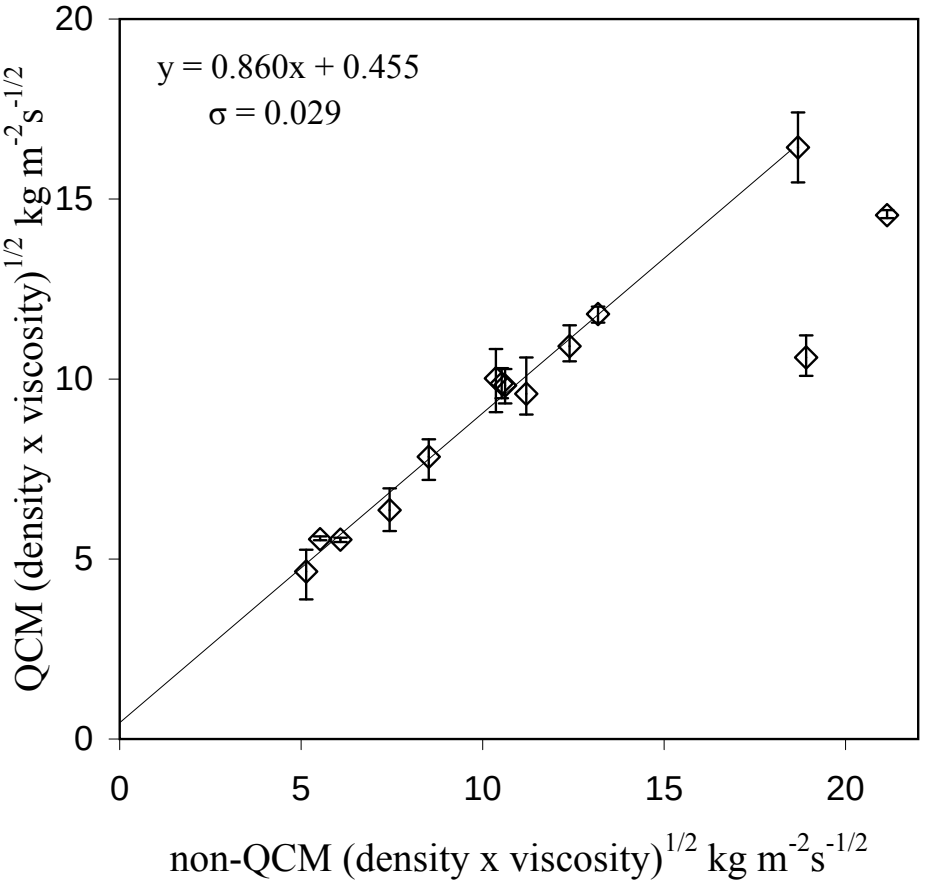

Figure III.12: Correlation between density-viscosity product for thirteen pure ionic liquids determined using viscometer and density meter and by using the change in resonant frequency of the quartz crystal at the third harmonic. The linear correlation breaks down for the highest viscosity ionic liquids at around $\sqrt{\rho\eta} \approx 18$ kg m^{-2} s$^{-1/2}$.

III.3 Conclusion

It is clear from these results that quartz crystal impedance analysis can be used to determine whether room temperature ionic liquids and various concentrations of these liquids behave in a Newtonian manner when subjected to a high frequency oscillation. For liquids which have Newtonian behaviour it is apparent that the square root viscosity-density product of these liquids can be obtained using this small volume technique. The

third harmonic response is seen to show better correlation to those obtained with the viscometer and densitometer over the full range of liquids tested. From the nineteen room temperature ionic liquids with minimal water content tested, the correlated shifts in frequency and bandwidth show twelve liquids to be Newtonian. A clear limit was seen at $\approx$18 kg $m^{-2}s^{-1/2}$, where a breakdown in the relationship of change in frequency and square root viscosity density product takes place. It is unclear if liquids with square-root viscosity density products above this had reached the limit of detection for the QCM or if they are showing non-Newtonian behaviour.

This technique has allowed the sample volume to be reduced significantly and Newtonian behaviour to be determined. The square root viscosity density product value has limited use as a characterisation tool and often the separate values are needed. This technique could be much more valuable if used with a predictive modelling technique such as those described by Jacquemin *et al.* [9] to predict density measurements. This is a significant advance and would allow the sample size to be reduced from a traditional volume of 1.5 ml to only 40 μl of liquid to obtain values for both viscosity and density separately.

References

[1] G. McHale, C. Hardacre, R. Ge, N. Doy, R. W. K. Allen, J. M. Maclnnes, M. R. Bown, and M. I. Newton, "Density-viscosity product of small-volume ionic liquid samples using quartz crystal impedance analysis," *Analytical Chemistry*, vol. 80, no. 15, pp. 5806–5811, 2008.

[2] V. Raimbault, D. Rebiere, C. Dejous, M. Guirardel, and V. Conedera, "Acoustic Love wave platform with PDMS microfluidic chip," *Sensors and Actuators A-Physical*, vol. 142, no. 1, Sp. Iss. SI, pp. 160–165, 2008. 20th Eurosensors Conference, Goteborg, Sweden, Sep 17-20, 2006.

[3] P. Roach, S. Atherton, N. Doy, G. McHale, and M. I. Newton, "SU-8 guiding layer for love wave devices," *Sensors*, vol. 7, no. 11, pp. 2539–2547, 2007.

[4] D. S. Ballantine, R. M. White, S. J. Martin, A. J. Ricco, E. T. Zellers, G. C. Frye, and H. Wohltjen, *Acoustic Wave Sensors: Theory, Design, & Physico-Chemical Applications (Applications of Modern Acoustics)*. Academic Press, 1996.

[5] D. Johannsmann, "Derivation of the shear compliance of thin films on quartz resonators from comparison of the frequency shifts on different harmonics: A perturbation analysis," *Journal of Applied Physics*, vol. 89, no. 11, Part 1, pp. 6356–6364, 2001.

[6] C. Villagran, M. Deetlefs, W. Pitner, and C. Hardacre, "Quantification of halide in ionic liquids using ion chromatography," *Analytical Chemistry*, vol. 76, no. 7, pp. 2118–2123, 2004.

[7] K. Kanazawa and J. Gordon, "Frequency of a quartz crystal microbalance in contact with liquid," *Analytical Chemistry*, vol. 57, no. 8, pp. 1770–1771, 1985.

[8] N. Doy, G. McHale, P. Roach, M. I. Newton, C. Hardacre, R. Ge, R. W. Allen, J. M. MacInnes, and M. R. Bown, "Small volume determination of the viscosity-density product for ionic liquids using quartz crystal harmonics," in *2008 IEEE International Frequency Control Symposium, Vols 1 and 2*, pp. 440–442, 2008. IEEE International Frequency Control Symposium, Honolulu, HI, May 19-21, 2008.

[9] J. Jacquemin, R. Ge, P. Nancarrow, D. W. Rooney, M. F. C. Gomes, A. A. H. Padua, and C. Hardacre, "Prediction of ionic liquid properties. I. Volumetric properties as a function of temperature at 0.1 MPa," *Journal of Chemical and Engineering Data*, vol. 53, no. 3, pp. 716–726, 2008.

IV. EXPERIMENTAL II: SEPARATING VISCOSITY AND DENSITY

Following on from chapter III, this chapter looks at using a dual crystal setup to obtain viscosity and density separately using a sample volume of only 240 μL in comparison to traditional methods which use a total sample volume of 1.5 ml. This is an extension to work completed by Martin *et al.* [1], and utilises a dual QCM setup with the fabrication of SU8-10 polymer traps onto the sensing area of one QCM with the second operating as a reference. Martin *et al.* have previously looked at highly wetting low viscosity liquids with the fabrication of gold traps on QCMs. This study looks at both water-glycerol mixtures and a range of pure RTILs, which are considerably more viscous and have considerably lower wettability, on five SU8-10 polymer traps of different widths.

IV.1 Methodology

To separate the components of viscosity and density from the viscosity-density product of a liquid using small volume quartz crystal impedance analysis two QCMs were used. Photolithography is used to pattern the surface of one of the crystals thus forming liquid traps (see Section II.3.2, Figure II.9). This creates an additional frequency response so that when compared to the change in frequency of a reference crystal, viscosity and density can be separated from the viscosity-density product. This section describes fabrication of the patterned device using photolithography, and considers both mask design and lithography protocol as well as methods for imaging the trap profile and experimental procedure.

IV.1.1 Fabrication of Textured Device

The fabrication of a patterned device is achieved in two stages, first a mask is designed and produced with the desired parameters, followed by a photolithography process for SU8-10 which has been developed based on the standard SU8 protocol [2] for the thickness needed.

IV.1.1.1 Mask Design

The trap structures are formed by photolithography using a photoresist which requires a mask for exposure. The mask allows only certain areas of a sample to be exposed to UV light causing a chemical change. SU8-10 is a negative photoresist, therefore the areas exposed to UV light remain once the process is complete whilst the areas left unexposed to UV light are removed.

For this application the design of the mask is critical. It has been well established [3, 4] that there are certain

limits to the trap dimensions which allow successful determination of viscosity and density from the QCM measurements.

If the trap dimensions are too large, the liquid trapped within the surface is not sufficiently restricted and will still experience shearing motion from the entrained liquid on the crystal. As such, the liquid does not behave as a rigid mass layer and hence does not cause only an additional frequency change. Comparatively, if the trap dimensions are too small, problems arise with incomplete filling and trapped air results in spurious frequency shifts.

An experiment was designed to find the optimum trap dimensions to separate viscosity and density measurements RTILs with various viscosity and density values. Ethanol and water-glycerol mixtures were also investigated as possible calibration liquids. The mask needed to create the structures was produced in AutoCAD® (Autodesk, USA) and manufactured by JD Photo-Tools (Oldham, UK) on (5 x 5)" soda lime glass. Masks were produced with five trap designs, the trap dimensions studied are described in Figure IV.1.

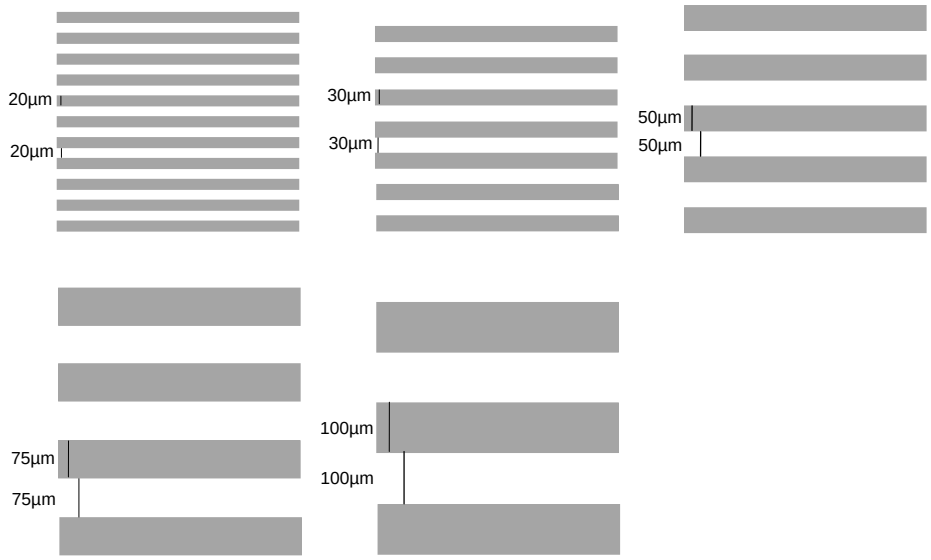

Figure IV.1: Exposure mask dimensions for fabrication of the surface traps for the patterned Quartz Crystal Microbalance.

For the most viscous RTIL the depth of the traps needed to be at least 7.3 μm to completely contain the entrained penetration depth. However, in retrospect, the most viscous liquid tested only needed a trap depth of 2.6 μm for the penetration depth to be completely entrained.

IV.1.1.2 SU8-10 Photolithography Protocol

To fabricate the traps on the surface of the QCMs a standard SU8-10 photolithography lift off process [2] was utilised with spin speeds adjusted to obtain the required thickness. The protocol for generating structures on gold surfaces [5] was closely followed.

Before use, the QCMs were cleaned in 5% v/v Decon90 in water at 80 °C for 20 mins, rinsed with deionised water and washed in 80 °C deionised water for 20 mins to remove all dust particles. Finally the crystals were rinsed in ethanol (Sigma-Aldrich, UK) and dried in a jet of Nitrogen to ensure a dry, clean surface for the photolithography process.

The gold electrodes on the surface of the crystal can cause problems with reflections when exposing the polymer with UV light. To improve patterning on a reflective surface, an antireflective base coat of XHRIC-16 (Brewer Science, MO, USA) was used [6].

SU8-10 can be very challenging to remove. Omnicoat™ (Micro.Chem, USA) is used as a second base layer to allow SU8-10 to be removed should it be necessary. It has also been suggested that Omnicoat™ acts as a support when producing pillars or tall structures [6] and prevents the photoresist layer (SU8-10) mixing with the antireflective layer. The complete photolithography process is described in Figure IV.2. All spin processes were completed using a WS-650 spin processor (Laurell®, PA) with a two step spin program.

The samples were aligned and exposed using a MJB4 Mask Aligner (Suss, MicroTech AG, Germany). The structures are considered tall features which require long exposure time. A filter to reduce the UV intensity of the mask aligner by approximately half was used to give more control over the exposure time. An exposure time of 21 seconds, with total energy = 546 mJ/cm^2 was used to give a patterned polymer of approximate depth 8.5 μm.

The traps are orientation specific and need to be aligned according to the x-flat of the QCM. This ensures the liquid within the traps experience no shearing motion, making the liquid behave as a rigid mass layer (described in section II.3.2).

Once the fabrication is complete the dimensions of the traps were checked using a profilometer and measured to be 8.4 μm with a Dektak (Veeco, USA). Further images were taken with a scanning electron microscope (see Figures IV.3(a) to IV.3(e)). Some earlier measurements were made using a different method which included no omnicoat layer, and the addition of a final gold film as described in [7], but this method was refined to give this protocol offering the most reliable and consistent method.

IV.1.2 Trap Surface Profiles

At the start of this work access to a Xyris 4000 WL (TaiCaan Technologies, Southampton, UK) optical profilometer (courtesy of the EPSRC Engineering Instrument Pool) was available. This allowed the surface struc-

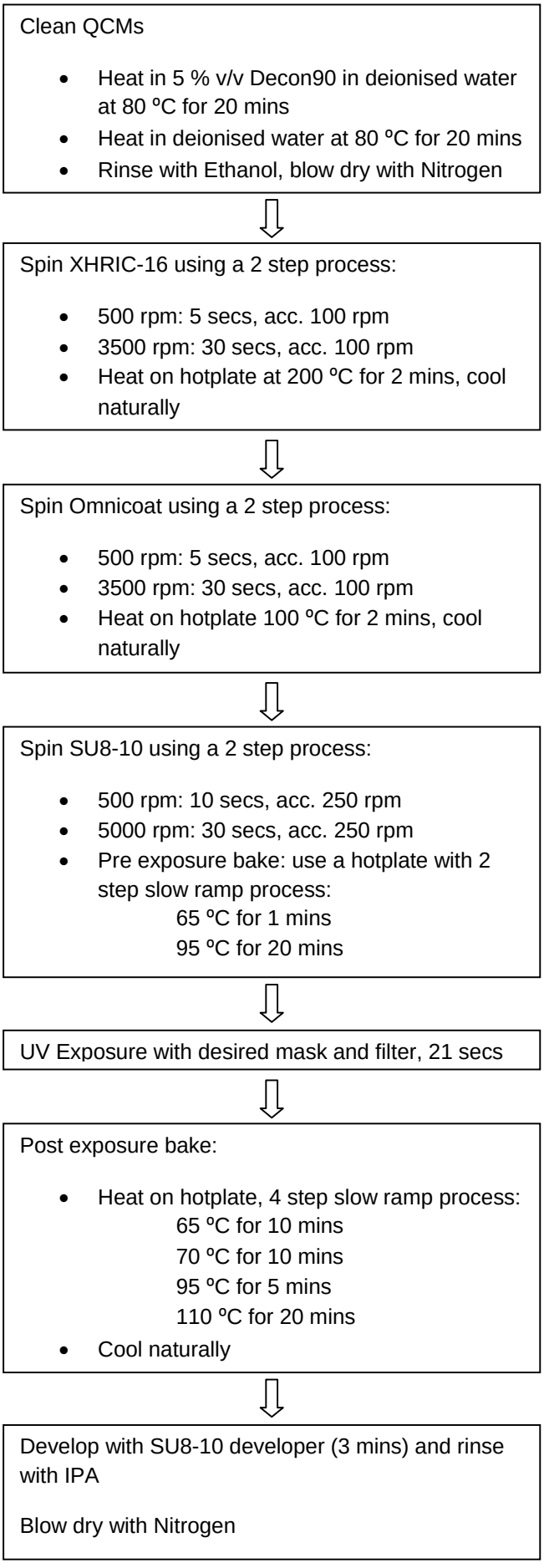

Figure IV.2: Photolithography process for pattern fabrication onto the surface of a Quartz Crystal Microbalance.

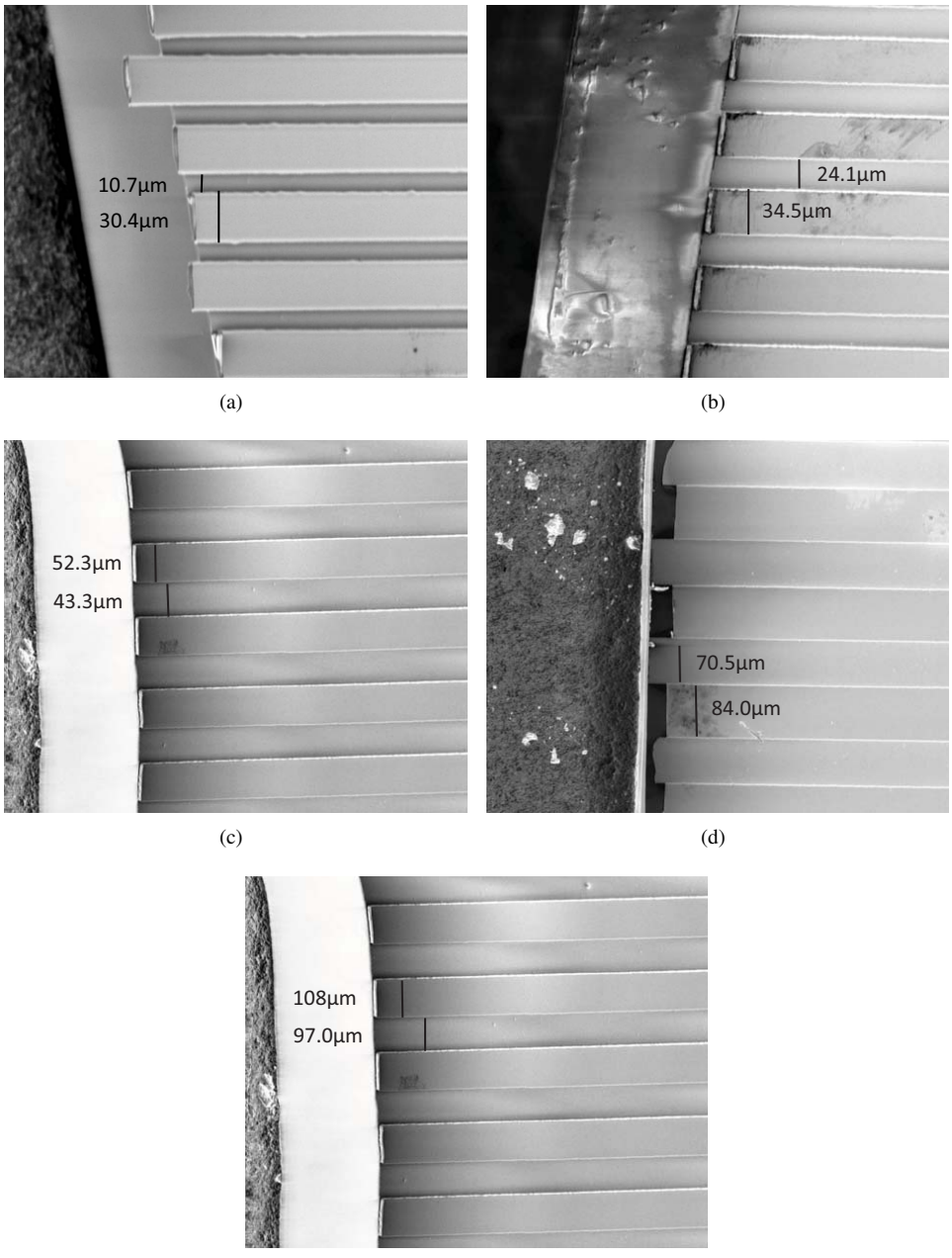

Figure IV.3: Scanning electron microscope image of (a) Trap design 1 - trap width 10.7 μm, separation width 30.4 μm, (b) Trap design 2 - trap width 24.1 μm, separation width 34.5 μm, (c) Trap design 3 - trap width 43.4 μm, separation width 52.5 μm, (d) Trap design 4 - trap width 70.5 μm, separation width 84.0 μm, (e) Trap design 5 - trap width 108.0 μm, separation width 97.0 μm (L_g is trap width, and L_w is separation width).

tures to be investigated both before and after an ionic liquid was left on the surface for a long period of time. Due to the chemical reactivity of RTILs it was unknown whether SU8-10 was a suitable material for trap fabrication. The high viscosity of some of the ionic liquids required depths greater than 8.5 μm to ensure the entrained wave penetration depth was constrained within the structures.

SU8-10 polymer was a good alternative to solid gold traps due to its chemical robustness and the time needed to deposit a gold film of such a great thickness. To test the resistance to chemical reactivity of the SU8-10 polymer traps a pure RTIL ($[C_6mim][NTf_2]$) was left on the trap surface for 48 hours. A comparison of profiles before and after show no significant damage to the trap surface structures. Figures IV.4(a) and IV.4(b) show images of a set of traps before and after the RTIL was left on the surface using the optical profilometer. A single measurement of RTIL made on the QCM takes only a couple of minutes before it is removed from the surface, so the traps are considered suitable.

All further characterisation and measurements of the traps were made on a Dektak (Veeco, USA.) stylus profilometer which gave a line profile of the surface structures, making it possible to determine the height and widths of the surface structures.

IV.1.3 Equipment Setup

In order to separate the square root viscosity-density product into single viscosity and density measurements, a QCM setup arrangement with two standard 1" (2.54 cm) 5 MHz quartz crystals (Tangidyne, NY) were used. One crystal was patterned over the sensing region with SU-8 10 photoresist (Micro.Chem, USA) using standard photolithography as described in Section IV.1.1.2. The second crystal was left blank as a reference. The combination of both frequency changes allows the viscosity and density to be determined.

The resonant frequency changes of both the reference and patterned crystals were recorded on the fundamental resonant frequency using a E8012 Network Analyser (Agilent, CA) in reflected power mode (see section III.1) using the same QCM clamping system made from PTFE as seen in Figure III.1.

The frequencies of the crystals in both air and liquid were recorded. Measurements of the reference crystal and the patterned crystal were made directly after one another using the same device holder. Full BVD fitting of the resonant peaks was not required as the frequency was recorded (described as the frequency point at which the minimum power is reflected) using the 'track minimum' function on the network analyser.

The change in resonant frequencies from both the reference and patterned crystal were analysed in Excel^{TM} (Microsoft, WA) using Equations II.12 and II.13 to obtain separate measurements of viscosity and density from the viscosity-density product (these are described in more detail in Section II.3.2).

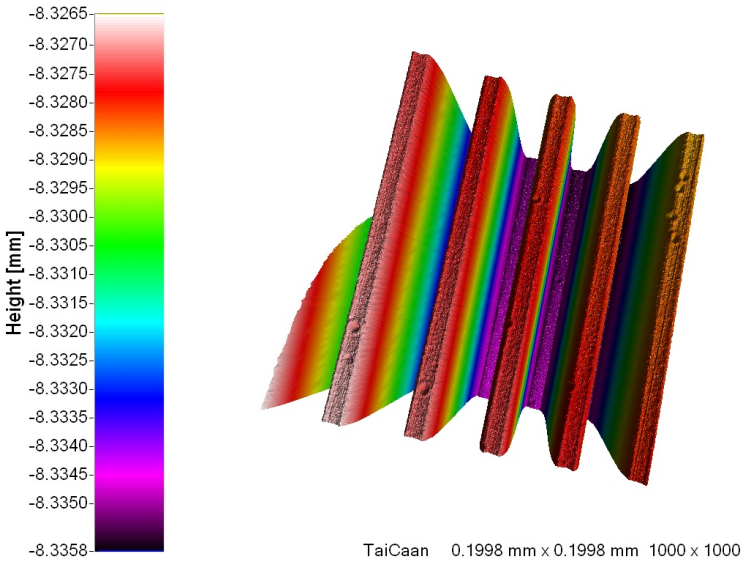

(a)

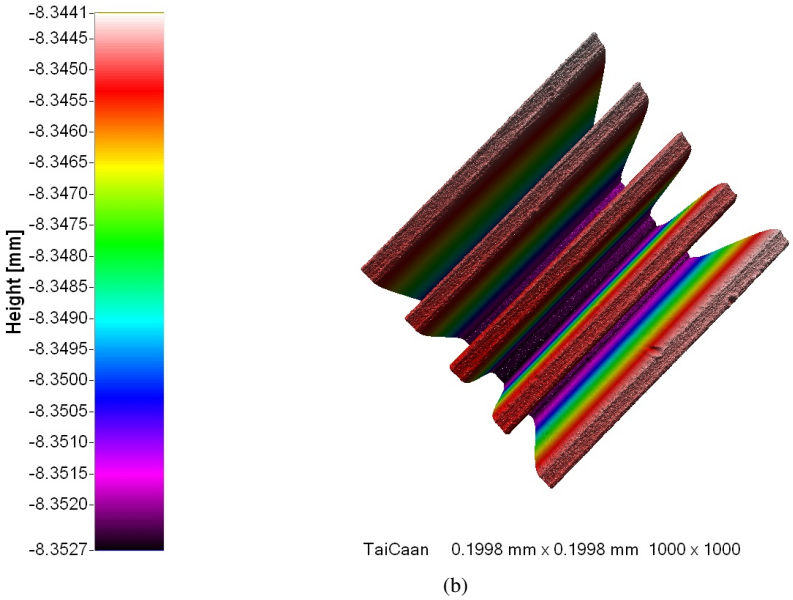

(b)

Figure IV.4: Optical profilometer scan (a) before, and (b) after the surface structures are exposed to a Room Temperature Ionic Liquid ($[C_6mim][NTf_2]$) for 48 hours.

Five trap designs were investigated, all trap heights were measured to be 8.4 μm deep using a Dektak (Veeco, NY) stylus profilometer. A calibrated Pipetman traditional shaft pipette (Gilson, WI) was used to give a sample volume of 120 μL on each QCM measurement to ensure there was sufficient liquid to fill each trap and allow for a height of 57 μm above their surface (for the largest trap volume). The penetration depth of the most viscous liquid tested corresponds to around 2.5 μm. This method requires a total volume of 240 μL to calculate a single measurement of viscosity and density.

All measurements were made using an 'in house' dry box (see Figure IV.5) with an argon atmosphere to minimise water contamination to the ionic liquids. This was created from a heavy duty sand blast cabinet (Machine Mart Ltd, UK), with PTFE sheet floor, arms length gloves (Dunlop's, UK) and a gas line. This was an improvement on the glove bag used in chapter 3 as it was a more rigid setup allowing for increased movement inside.

Figure IV.5: 'In-house' dry box used for separate density viscosity measurements.

Water and ethanol were used to clean the surface of the QCMs after each test (care was taken to avoid damaging the surface of the traps). The traps were rinsed and nitrogen dried until the resonant frequency returned to its original frequency within ~ 50 Hz.

Various concentrations of water-glycerol mixtures (0 to 85% v/v concentration) and nine pure RTILs (See Table IV.1) were tested on each of the trap geometries with RTIL densities ranging between 1.013 and 1.519 g/cm^3 and viscosities ranging between 22 to 134 cP. In addition, ethanol was investigated as it is highly wetting and so expected to fully penetrate into the traps. Measurements were repeated at least three times and an average taken.

Measurements were recorded at room temperature and a direct comparison was made to those collected on traditional equipment including a DV-II+ (Brookfield, MA) Programmable viscometer (0.5 mL required volume) and a DMA 4500 (Anton Parr, Germany) Density meter (1.0 mL required volume) measured immediately prior

RTIL	Densitometer measured Density g.cm^{-3} (± 0.0005)	Viscometer measured Viscosity cP (± 4%)
[C_4mpyrr][DCA]	1.013	34
[C_4mim][DCA]	1.059	27
[C_4mim][SCN]	1.118	22
[C_2mim][$EtSO_4$]	1.238	88
[C_4mim][ACO]	1.248	134
[C_{10}mim][NTf_2]	1.279	118
[C_6mim][NTf_2]	1.372	66
[C_4mpyrr][NTf_2]	1.395	74
[C_2mim][NTf_2]	1.519	29

Table IV.1: Room Temperature Ionic Liquids measured for separation of viscosity and density properties from the viscosity-density product (raw frequency change values observed on the quartz crystals from these liquids can be found in Appendix B).

to using the QCM setup.

These two pieces of lab equipment were purchased especially for this project making it possible to carry out the remaining experiments at Nottingham Trent University rather than at the Queens University Belfast. The viscometer requires a smaller volume (0.5 ml) than the viscometer previously used (1.0 ml).

IV.2 Results and Discussion

Results are discussed for separating the viscosity and density from the square root viscosity-density product for each trap size. The addition of a gold film on the surface of the traps has also been explored.

IV.2.1 Varying Trap Size

Figures IV.6(a), IV.7(a), IV.8(a), IV.9(a) and IV.10(a) show separate density measurements for all trap sizes considered. Figures IV.6(b), IV.7(b), IV.8(b), IV.9(b) and IV.10(b) show separate viscosity measurements for each trap size. A geometrical fitting parameter for each trap was implemented in the formula as the 'experimental effective height' (see Table IV.2). This parameter is based on the density measurement and is calculated using ethanol to give y = x (see Figures IV.6(a), IV.7(a), IV.8(a), IV.9(a) and IV.10(a)). The same effective height is then used to calculate the viscosity. Initially water-glycerol mixtures were used as calibration liquids although the results demonstrated that these liquids were not penetrating into the smallest traps resulting in incomplete filling. To avoid this, ethanol was chosen for the calibration liquid because of its good wetting of SU8-10.

Trap Design	Trap Width (μm)	Separation Width (μm)	Experimental Effective Height (μm)	Theoretical Effective Height (μm)
1	10.7	30.4	1.68	2.19
2	24.1	34.5	2.22	3.45
3	43.4	52.5	1.85	3.80
4	70.5	84.0	1.53	3.83
5	108.0	97.0	1.44	4.43

Table IV.2: Measured Quartz Crystal Microbalance trap parameters, with effective height considered as a geometrical fitting factor (used to calibrate measurements of density to traditionally measured values) and theoretical effective height.

Density and viscosity results for all liquids were determined using the effective height calculated from the ethanol density measurement. From the change in frequency of the smooth and textured QCM, and the measured density from the densitometer, it is possible to calculate the experimental effective height (see Figure IV.2) using Equation II.12. The effective height should be the same for all liquids that penetrate into the traps. This height is then used in Equation II.13 to calculate the viscosity for ethanol using the changes in smooth and textured frequency measurements. Using this same value, the densities and viscosities of RTILs were calculated using the frequency changes seen on the smooth and textured QCMs. This same method of calibration has been used for the water-glycerol solutions although some challenges with liquid penetration were seen.

When looking at the RTIL measurements of viscosity and density on each trap design, a linear relationship between the QCM derived values and the traditionally measured values is seen. Trap designs 1, 2 and 3 (Figures IV.6(a), IV.6(b), IV.7(a), IV.7(b), IV.8(a) and IV.8(b)) show good agreement between the QCM derived density and viscosity values and those measured traditionally with only small deviances from y = x. Trap 4 (Figure IV.9(a) and IV.9(b)) is in reasonable agreement although more scatter is seen on the density line of best fit (Figure IV.9(a)), a discontinuity at approximately 1.248 g cm^{-3} is starting to emerge. Above this density value, all measured liquids contain [NTf_2] suggesting further investigation is necessary to determine if this influences their behaviour. It is clear the largest trap design (Figures IV.10(a) and IV.10(b)) shows the largest deviance between the expected and derived values, with a significant step seen within the density results at approximately 1.248 g cm^{-3}. It is expected however to see a limit at which the traps no longer act to confine the liquid as a rigid mass [3] which may have been seen here. Additional calibration of the QCMs with known liquid densities greater than this may be required to ensure a density to trap dimension limit has not been found. It would also be possible to use a known RTIL as an alternative calibrating fluid.

For water-glycerol solutions, it is clear there is a problem with the smallest liquid traps (Figures IV.6(a) and IV.6(b)). The smallest trap design is much larger than the trap dimensions used by Martin *et al.* [8] although the liquids described have very low densities and viscosities with good wetting properties. Water-glycerol solutions are much more viscous, fairly dense and also have much poorer wetting properties. Each of

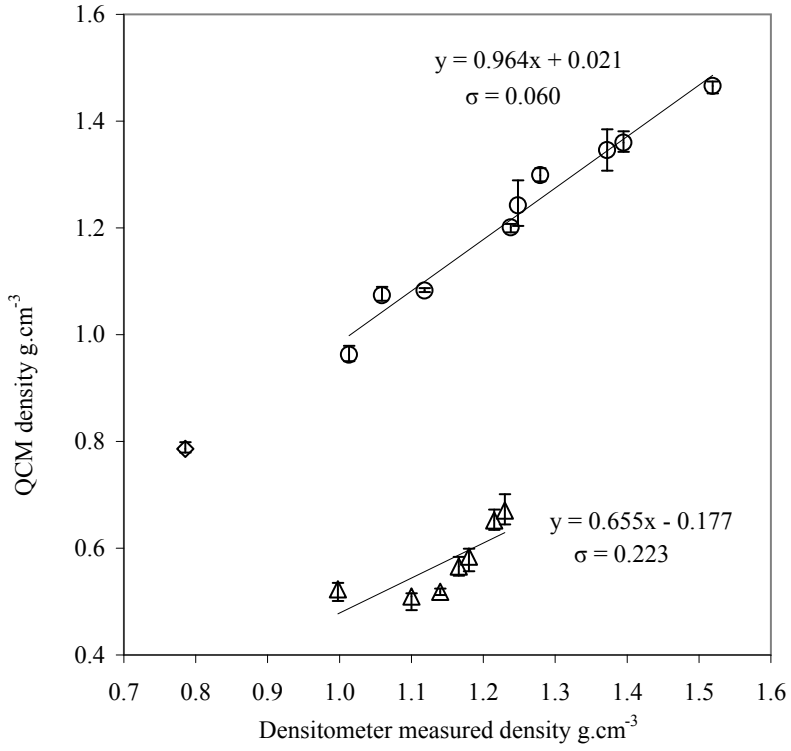

(a)

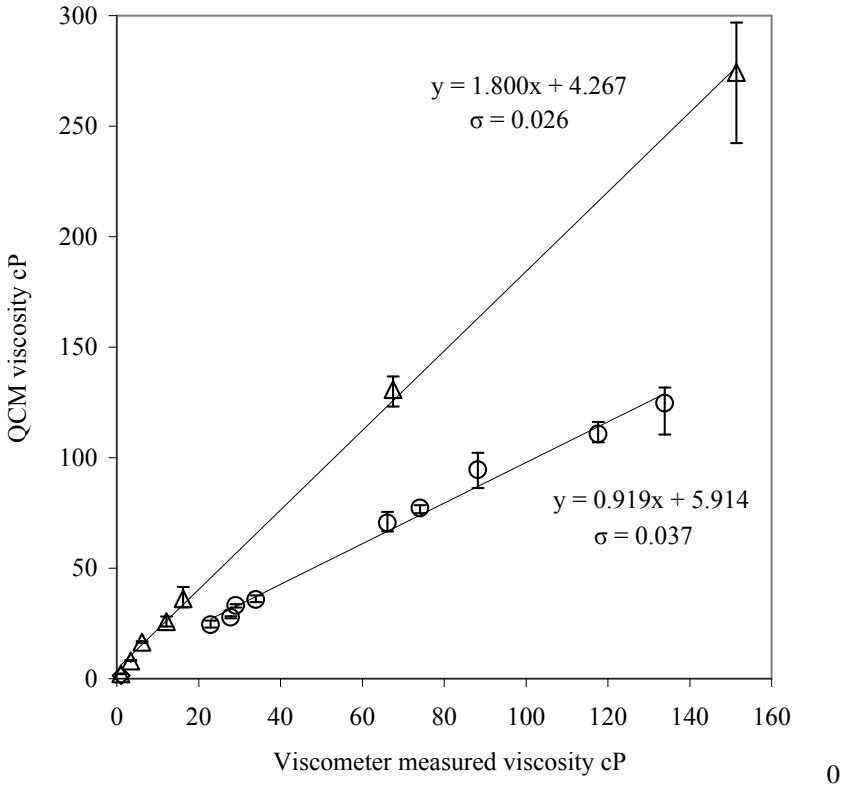

(b)

Figure IV.6: (a) Density and (b) Viscosity measurements for Trap 1, showing varying concentration of water-glycerol △, 9 pure Room Temperature Ionic Liquids ○ (Shown in Table IV.1), and Ethanol ◇.

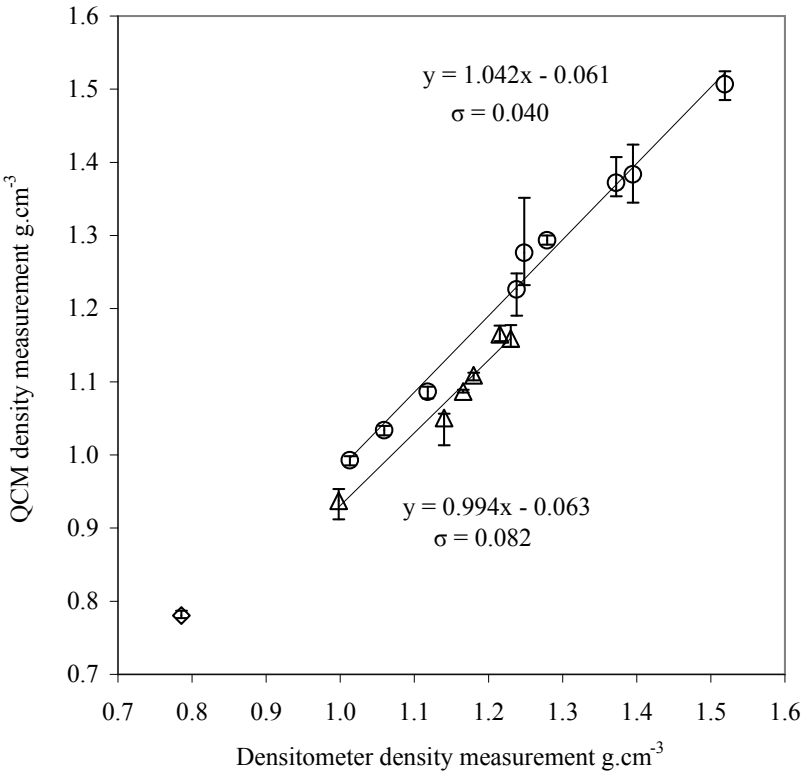

(a)

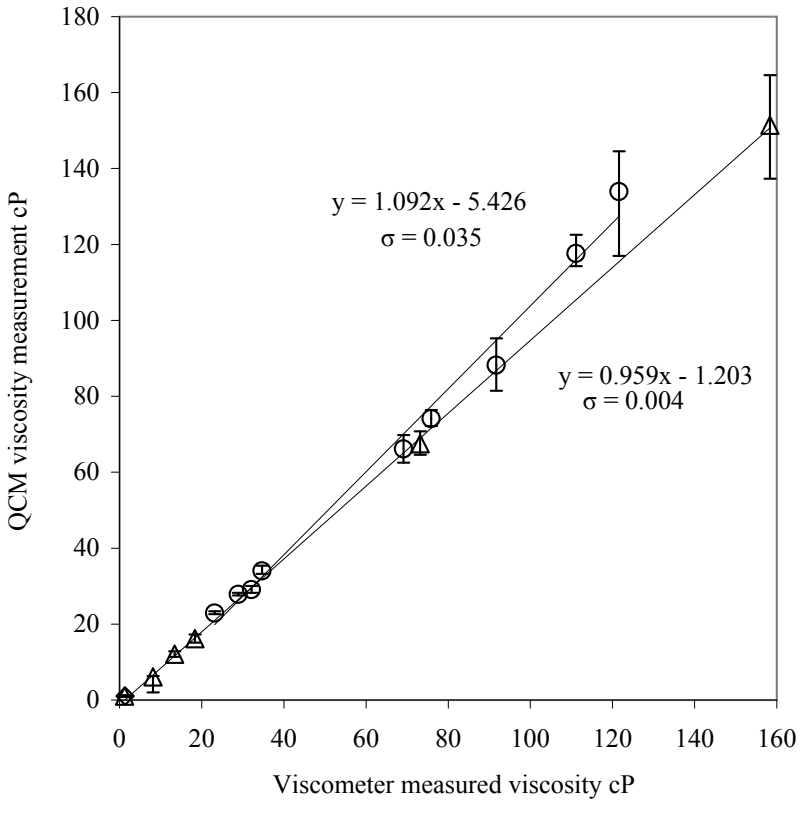

(b)

Figure IV.7: (a) Density and (b) Viscosity measurements for Trap 2, showing varying concentration of water-glycerol △, 9 pure Room Temperature Ionic Liquids ○ (Shown in Table IV.1), and Ethanol ◇.

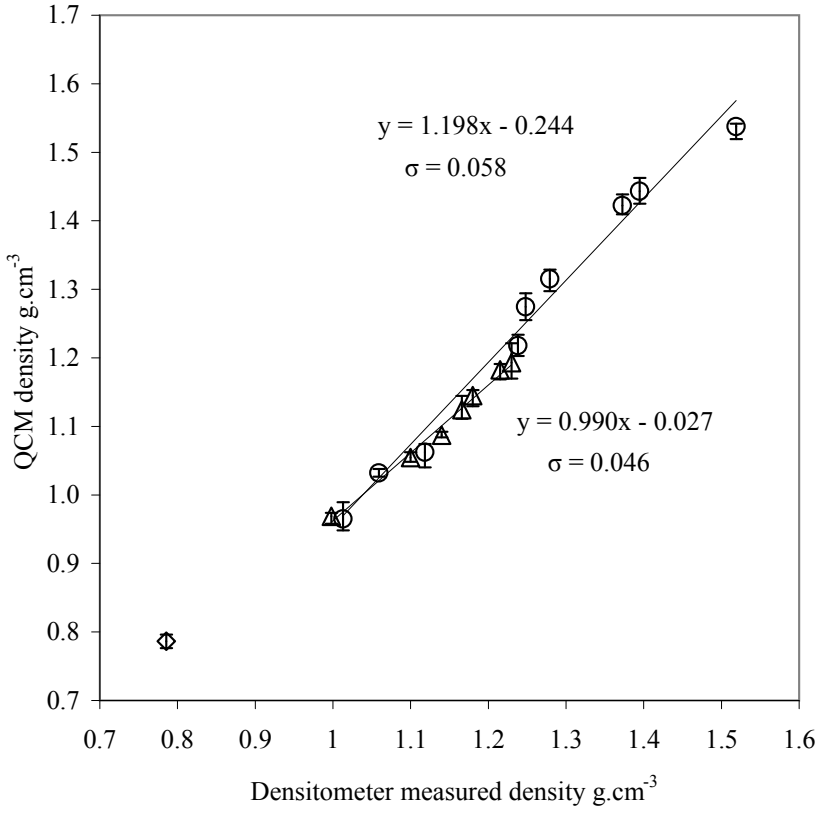

(a)

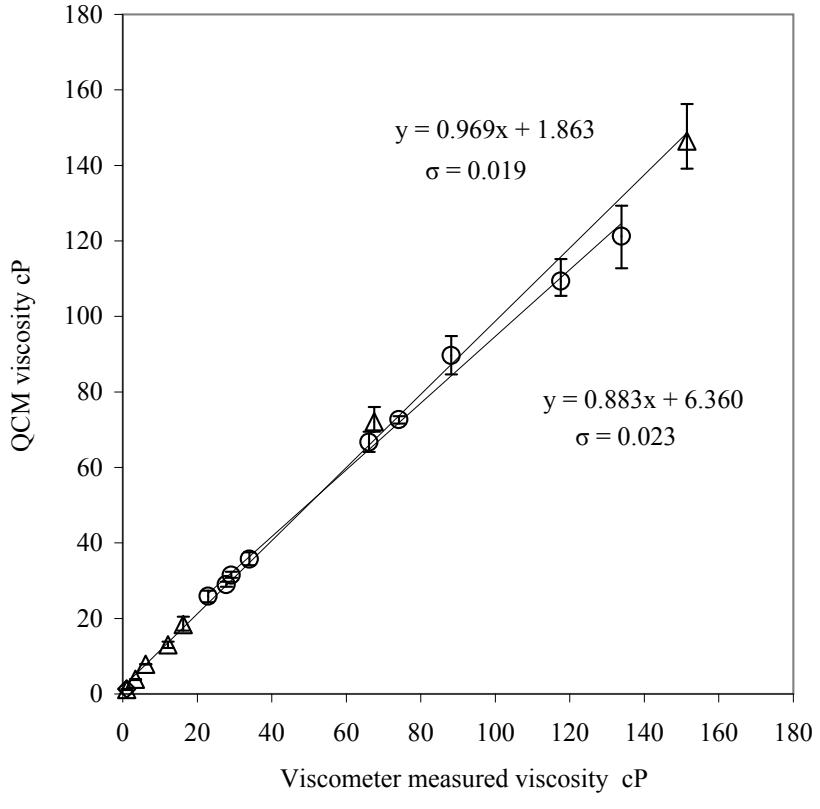

(b)

Figure IV.8: (a) Density and (b) Viscosity measurements for Trap 3, showing varying concentration of water-glycerol △, 9 pure Room Temperature Ionic Liquids ○ (Shown in Table IV.1), and Ethanol ◇.

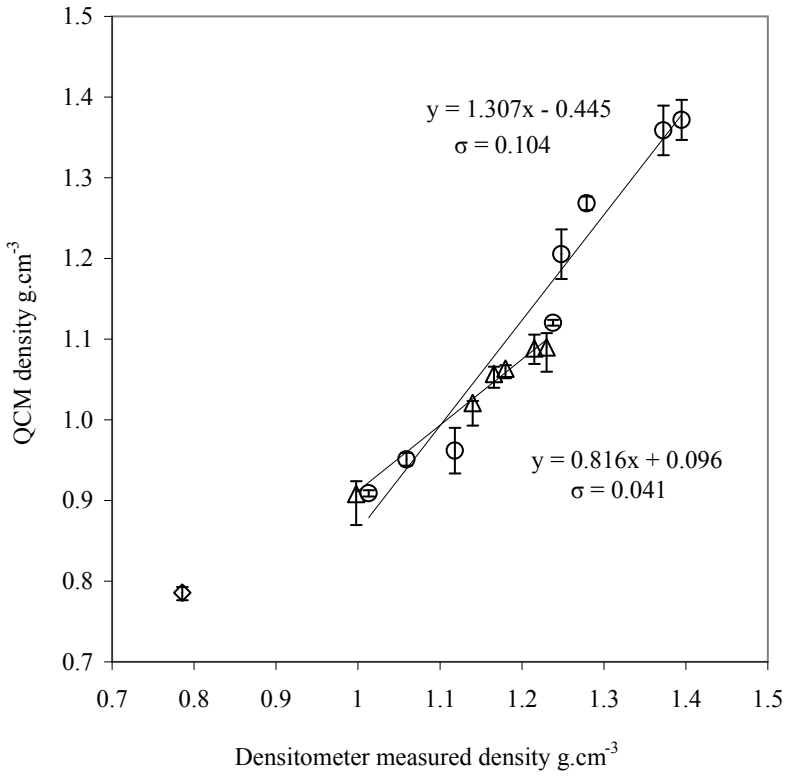

(a)

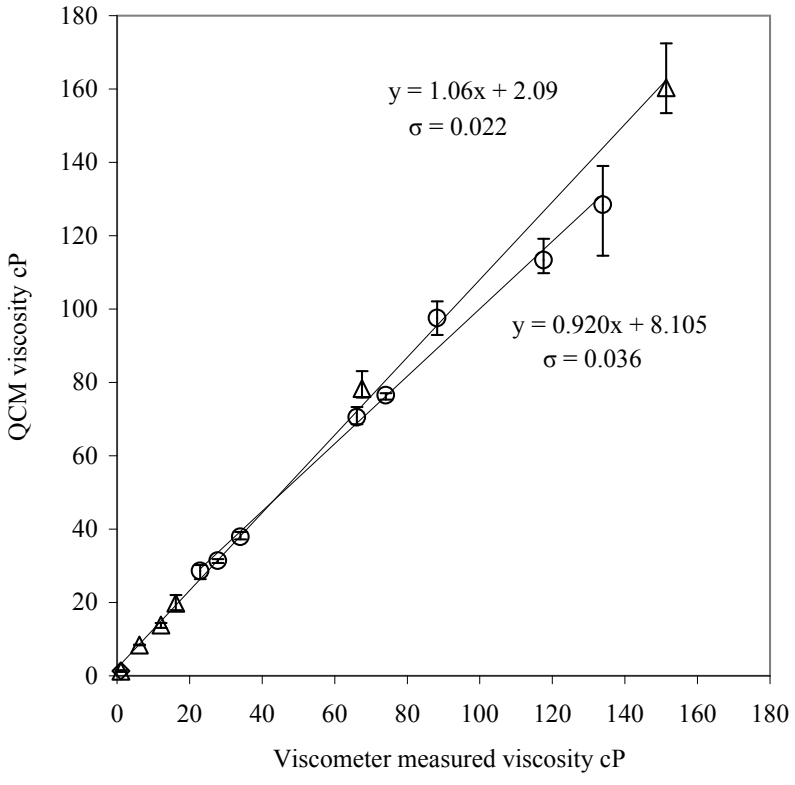

(b)

Figure IV.9: (a) Density and (b) Viscosity measurements for Trap 4, showing varying concentration of water-glycerol △, 9 pure Room Temperature Ionic Liquids ○ (Shown in Table IV.1), and Ethanol ◇.

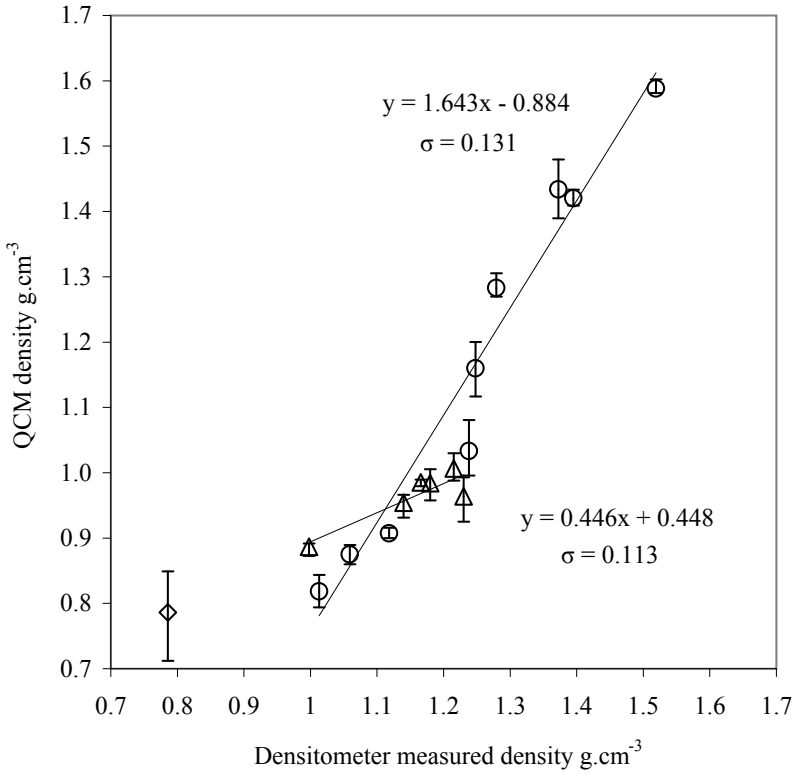

(a)

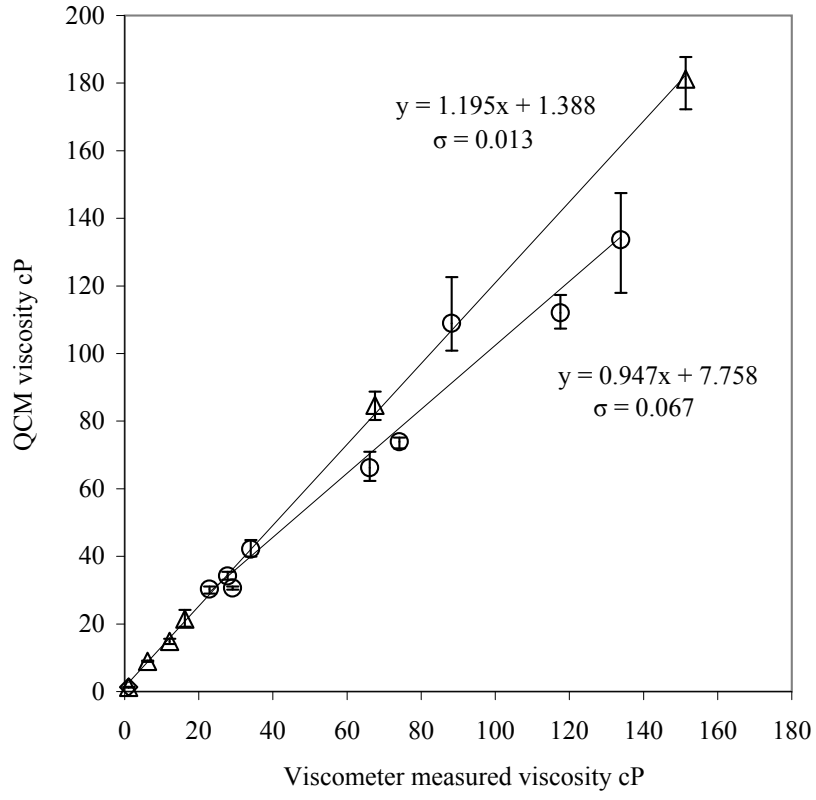

(b)

Figure IV.10: (a) Density and (b) Viscosity measurements for Trap 5, showing varying concentration of water-glycerol △, 9 pure Room Temperature Ionic Liquids ○ (Shown in Table IV.1), and Ethanol ◇.

these factors could result in incomplete filling retaining some amount of air below the liquid within the trap. Problems can be seen with the smallest traps, which have independent correlations for both water-glycerol solutions and measured RTILs, suggesting incomplete filling. If this was taking place, it would be expected that the QCM measured density values would be much lower than those measured with the traditional densitometer (due to a lower volume of liquid being effectively weighed). This effect is seen in Figure IV.6(a) and IV.6(b) where density values are half those expected (respectively this then causes a problem with the viscosity values). The three remaining trap sizes have very good agreement for both density and viscosity values. For the liquids tested, the closest agreement between QCM derived values and those measured traditionally occurs for trap dimensions of 30 and 50 μm. Investigation into further trap sizes and ratios around these may further optimise the agreement.

With problems such as incomplete filling, chemical coatings are often used to improve the wettability of the surface [6]. However, it is very difficult to add a coating onto the surface of the traps to lower the contact angle. An over layer of gold was explored to see if it could increase the wettability of the trap surface as water is known to have a lower contact angle on gold than on SU8-10 [5, 9]). The results are shown in Section IV.2.2 and give a good indication of liquid contact angle, although the differences between gold and SU8-10 are not significant.

IV.2.2 Addition of a Gold Film onto the Surface of SU8-10

Having completed the experiments on SU8-10 traps, the addition of a gold layer onto their surface was considered as it was suggested that it may provide a lower contact angle. This may encourage liquid penetration into the smallest traps. The contact angle of SU8-10 varies slightly depending on the protocol used for its fabrication. Here the measurements for contact angle have been made on a flat SU8-10 reference sample and a second sample of SU8-10 coated with 10 nm of titanium and 100 nm of gold. Various concentrations of water-glycerol solutions and nine pure RTILs (detailed in Table IV.3) were measured. These measurements were intended to be indicative, and for this reason the RTIL measurements have not been made under a dry atmosphere. In consequence the liquids are not considered to be pure with respect to water contamination but pure in the sense they were not diluted intentionally before measurements. Measurements were made using the sessile drop method to determine the contact angle formed between the liquid/solid and liquid/vapour interface (see Figure IV.11) on an 8-bit black and white DSA Mk 10 camera (Kruss, Hamburg, Germany). A pipette was used to place a sample volume of 3 μl onto the surfaces. Three measurements were made for each liquid on each surface and the mean plotted on Figure IV.12.

Comparison between the two surfaces show slightly higher contact angles for the gold coating. The difference is not however sufficiently large and is within experimental error so coating the trap surface was deemed unnecessary. For RTILs these contact angle measurements are very interesting, and show on average that the

Liquid	$(\rho\eta)^{1/2}$ (kg m^{-2} $s^{-1/2}$) Viscometer-Density Meter (±5%)	Contact Angle, ±5°	
		SU8-10	Gold Coated SU8-10
Water	1.01	76	86
40% v/v water glycerol	1.92	73	81
50% v/v water glycerol	2.47	72	77
70% v/v water glycerol	4.37	71	71
80% v/v water glycerol	9.02	70	69
85% v/v water glycerol	13.64	62	64
$[C_4mim][SCN]$	5.06	47	50
$[C_4mim][DCA]$	5.43	30	41
$[C_4mpyrr][DCA]$	5.87	35	37
$[C_2mim][NTf_2]$	6.69	31	46
$[C_6mim][NTf_2]$	9.52	35	44
$[C_4mpyrr][NTf_2]$	10.17	26	43
$[C_2mim][EtSO_4]$	10.44	38	42
$[C_{10}mim][NTf_2]$	12.26	8	14
$[C_4mim][ACO]$	12.93	29	31

Table IV.3: Liquids measured using the sessile drop method on an 8-bit black and white DSA Mk 10 camera to give an estimate of contact angle on SU8-10 and SU8-10 coated with gold.

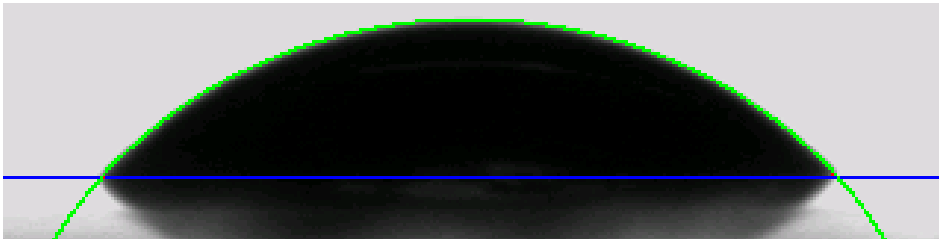

Figure IV.11: Contact angle (≈ 47°) seen on SU8-10 for $[C_2mim][SCN]$.

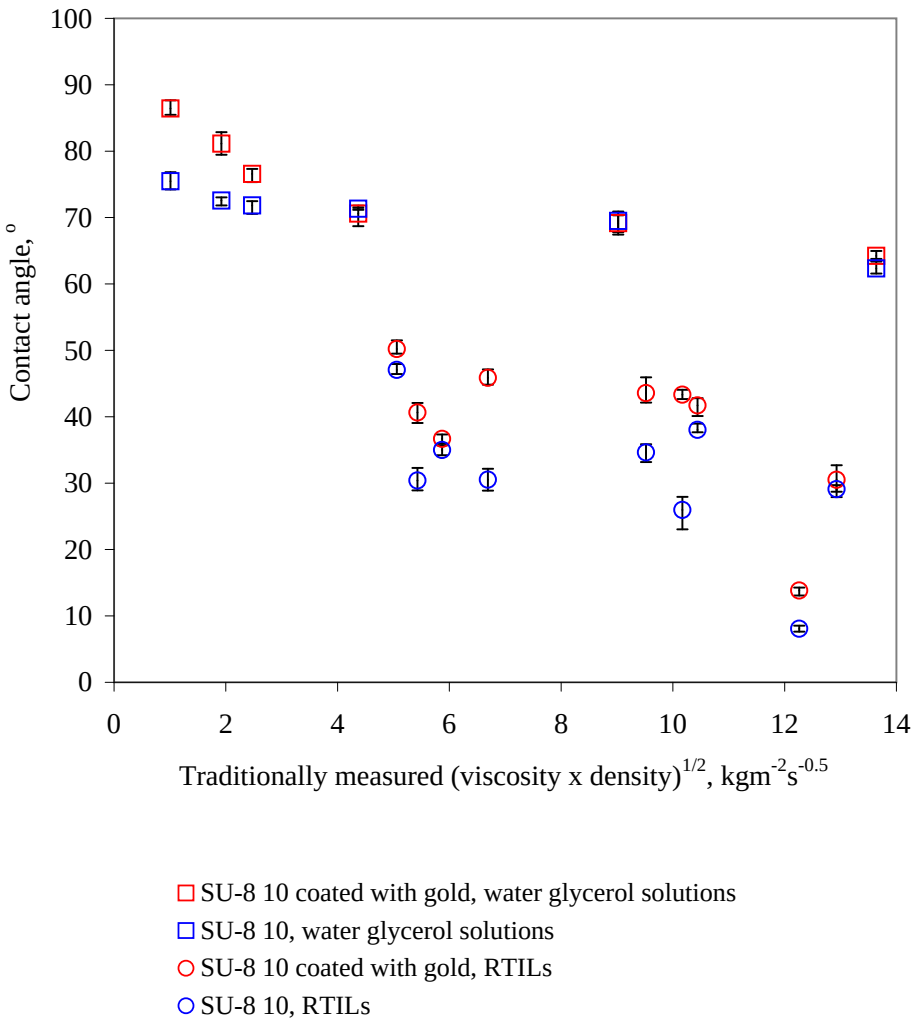

Figure IV.12: Contact angles measured using the sessile drop method for various the concentrations of water-glycerol and 9 Room Temperature Ionic Liquids (shown in Table IV.1) on a flat SU8-10 surface, and a flat SU8-10 surface coated with 10 nm of titanium and 100 nm of gold.

RTIL samples generally have a much lower contact angle (almost half) than the water-glycerol solutions tested. This confirms the results seen on the narrowest traps (Figure IV.6(a)) for water-glycerol solutions. Given their high contact angle it is highly likely the traps were partially filled with air therefore lowering the value seen on the QCM. PDMS oils may have offered a better range of calibration liquids than water-glycerol mixtures, although they would have been very challenging to remove from the traps. The calibration could be further improved by using a range of highly wettable liquids such as methanol, n-propanol and n-butanol.

IV.3 Conclusion

Separate viscosity and density measurements have been made using a dual QCM set-up with SU8-10 fabricated structures, using a total sample volume of only 240 μl. This has reduced the current volume needed to measure the viscosity and density separately by a factor of six, and could result in further reduction if smaller diameter crystals were used. From the trap dimensions investigated, the optimum size has been shown to be either 30 or 50 μm, although this may be improved by exploring different sizes and ratios in this range. Further calibration liquids with higher densities are needed to fully characterise the devices. For the range of liquids tested it is shown that a gold layer would not reduce the contact angle of the liquids significantly enough to explore with the smallest trap dimensions. This was however only a problem for the water-glycerol solutions and the smallest trap dimension worked well for the RTILs. With further optimisation of the trap geometry, the dual QCM separation technique may offer a viable alternative to larger volume methods. This could potentially allow new liquids to be added to the RTIL physical property database [10] using smaller (and hence lower cost) sample volumes.

References

[1] S. Martin, G. Frye, and K. Wessendorf, "Sensing liquid properties with thickness-shear mode resonators," *Sensors and Actuators A-Physical*, vol. 44, no. 3, pp. 209–218, 1994.

[2] MicroChem Corp, "www.microchem.com/products/pdf/su8_2-25.pdf."

[3] F. Herrmann, D. Hahn, and S. Buttgenbach, "Separation of density and viscosity influence on liquid-loaded surface acoustic wave devices," *Applied Physics Letters*, vol. 74, no. 22, pp. 3410–3412, 1999.

[4] F. Herrmann, D. Hahn, and S. Buttgenbach, "Separate determination of liquid density and viscosity with sagittally corrugated Love-mode sensors," *Sensors and Actuators A-Physical*, vol. 78, no. 2-3, pp. 99–107, 1999.

[5] N. Shirtcliffe, S. Aqil, C. Evans, G. McHale, M. Newton, C. Perry, and P. Roach, "The use off high aspect ratio photoresist (SU-8) for super-hydrophobic pattern prototyping," *Journal of micromechanics and microengineering*, vol. 14, no. 10, pp. 1384–1389, 2004.

[6] G. McHale, P. Roach, C. R. Evans, N. J. Shirtcliffe, S. J. Elliott, and M. I. Newton, "Sensor Response of Superhydrophobic Quartz Crystal Resonators," in *2008 IEEE International Frequency Control Symposium, Vols 1 and 2*, (345 E 47TH ST, New York, NY 10017 USA), pp. 698–704, IEEE, IEEE, 2008. IEEE International Frequency Control Symposium, Honolulu, HI, May 19-21, 2008.

[7] N. Doy, G. McHale, M. Newton, C. Hardacre, R. Ge, R. Allen, and J. MacInnes, "Density and viscosity measurements of room temperature ionic liquids using patterned quartz crystal microbalances," in *Frequency Control Symposium, 2009 Joint with the 22nd European Frequency and Time forum. IEEE International*, pp. 1043 – 1045, 2009.

[8] S. Martin, G. Frye, A. Ricco, and S. Senturia, "Effect of surface-roughness on the response of thickness-shear mode resonators in liquids," *Analytical Chemistry*, vol. 65, no. 20, pp. 2910–2922, 1993.

[9] H. Notsu, W. Kubo, I. Shitanda, and T. Tatsuma, "Super-hydrophobic/super-hydrophilic patterning of gold surfaces by photocatalytic lithography," *Journal of Materials Chemistry*, vol. 15, pp. 1523–1527, 2005.

[10] H. Zhao, "Current studies on some physical properties of ionic liquids," *Physics and Chemistry of Liquids*, vol. 41, no. 6, pp. 545–557, 2003.

V. EXPERIMENTAL III: MICROFLUIDICS: QUARTZ CRYSTAL INTEGRATION

This chapter looks at incorporating a Quartz Crystal Microbalance (QCM) into an enclosed microfluidic device. By reducing the size of the QCM from a diameter of 1" to 0.538", the QCM becomes much more desirable for use 'on-chip' and allows measurements of viscosity-density product to be determined with a much smaller sample volume. The microfluidic system is a sealed environment which reduces the risk of contamination, or water uptake for hygroscopic liquids such as Room Temperature Ionic Liquids (RTILs). This method reduces the sample size needed for characterisation from 1.5 ml using a traditional viscosity and density meter to 30 μL. This setup has been designed in collaboration with the University of Sheffield and is intended to eventually form part of an integrated lab-on-a-chip system designed for use with RTILs to investigate many properties including thermal conductivity, specific heat capacity, water concentration and electrical conductivity. This chapter looks experimentally at measurements of the square root viscosity-density product for RTILs on 8 and 9 MHz QCM.

V.1 Methodology

The design of the microfluidic glass chip has been carefully considered to allow incorporation of a QCM. The change in frequency of the QCM enclosed in the system allows determination of the square root viscosity-density product for small volume liquid characterisation by applying the Kanazawa and Gordon equation [1]. This section includes the design of the microfluidic chip, initial microfluidic flow cell setup, liquid characterisation and cleaning protocol, QCM design and limitations of the flow cell setup including pressure and flow rate models and an estimation of the flow cell leakage rate.

V.1.1 Microfluidic Chip and Chip Holder Design

The custom made microfluidic device was designed in collaboration with The University of Sheffield. The device consists of a glass chip (3 cm by 3 cm by 1 mm) fabricated by Micronit Microfluidics BV (The Netherlands). The glass chip design is shown in Figure V.1. The chip consists of an open top circular cell of radius 5 mm with depth 300 μm and flow passages to and from the cell formed by wet etching (depth 125 μm), giving an open top cell volume of 23 μL.

One of the main challenges when working with harsh chemicals such as RTILs is the limited number of chemically resistant materials available which create a good seal against glass. Here, a clamping system similar to that used in Section III with a specially designed top plate was manufactured from polyether ether ketone

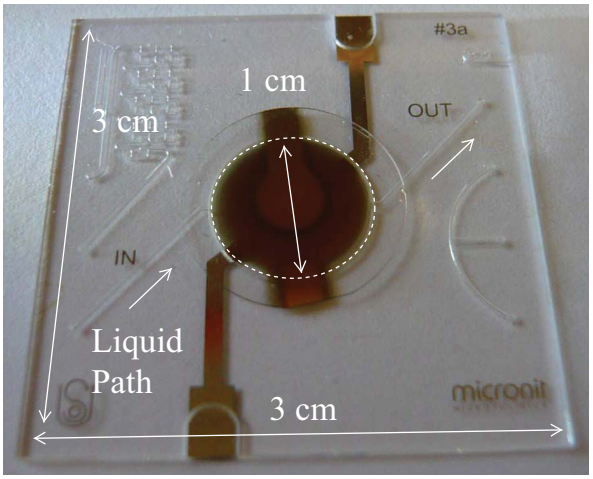

Figure V.1: Custom made glass chip produced by Micronit Microfluidics BV (The Netherlands) showing placement of the QCM.

(PEEK) which has excellent chemically resistant properties. The QCM sits on the open top circular glass chip which is constrained in the base layer of the holder as in Figure V.2, the top plate (see figure V.3) then clamps onto the QCM outside the sensing region creating a pressure seal. Clamping the PEEK against the QCM and the glass chip forms a very good seal although a minimal leakage will still occur; this is a designed-in feature of the chip system. A leakage model has been calculated and described in Section V.1.5.2. The QCM is designed for one sided connection via spring contacts outside the circular cell as shown in Figure V.4).

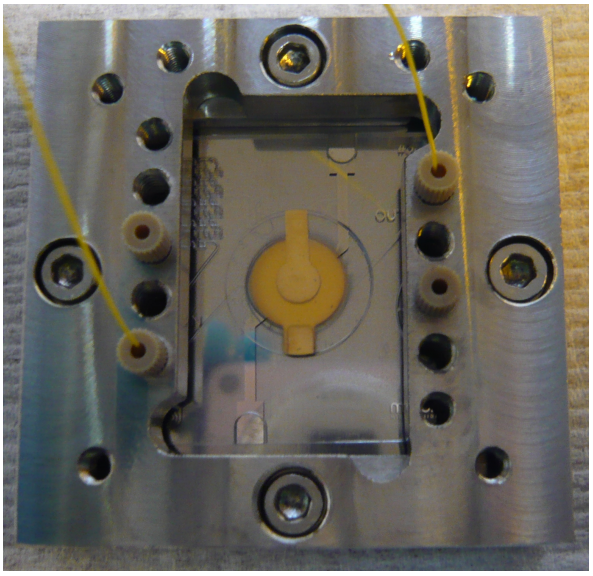

Figure V.2: Microfluidic glass chip held in the base layer of the device holder with the spacer layer and quartz crystal (capillary tubing and headless nuts can also be seen).

To connect to the flow cell standard Upchurch (WA, USA) microfluidic connectors were used, see Table V.1. A Nemesys syringe pump (Cetoni, Germany) with a gastight syringe (Hamilton, Switzerland) controlled the flow rate of the system. Flow rates ranged from 0.04 μl/s for highly viscous samples (100 cP) to 2 μl/s for cleaning (discussed further in Section V.1.5.1). The capillary tubing for the inlet (length = 15 cm) and outlet (length = 15 cm) were considered to be longer than necessary due to the chip set-up being in an Octagon 10 incubator

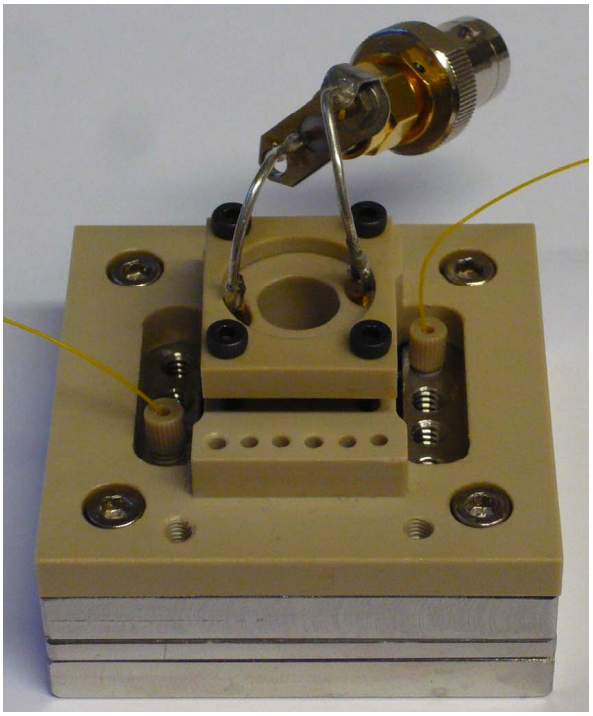

Figure V.3: Lab-on-a-chip setup showing the top clamping mechanism, with inlet and outlet capillary tubing.

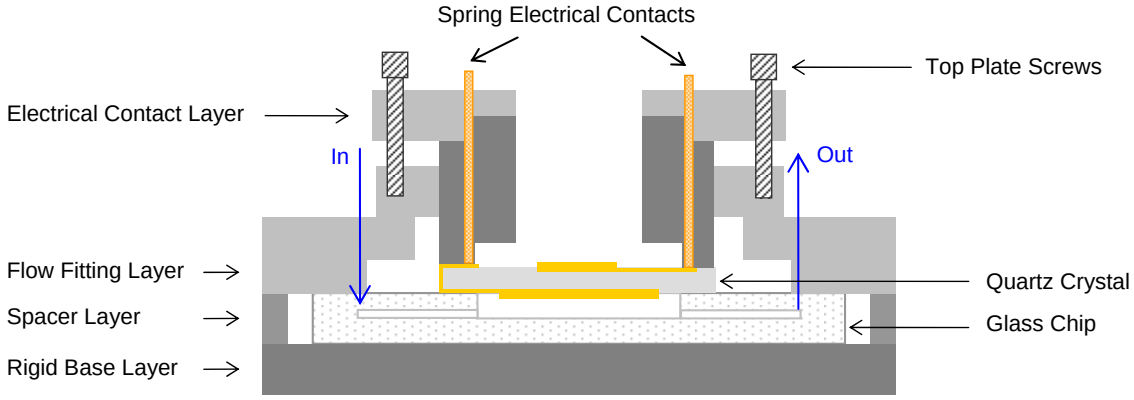

Figure V.4: Cross-section of the clamping system: containing the glass chip and Quartz Crystal Microbalance, creating an enclosed microfluidic system.

(Brinsea, UK) to maintain a steady temperature (25/30 °C, see Figure V.5 for equipment set up), and this could be reduced to optimise sample size and cell pressure if needed.

Upchurch Connectors (WA, USA)	Stock number
PEEK capillary tubing (inner 150µm and outer diameter 360µm)	1572
Headless nuts (outer diameter 360µm)	F-123Hx
Ferrules (outer diameter 360µm)	N-123-03x
2µm Filter capsule assembly	M-542

Table V.1: Standard UpChurch (WA, USA) microfluidic connections needed with stock numbers.

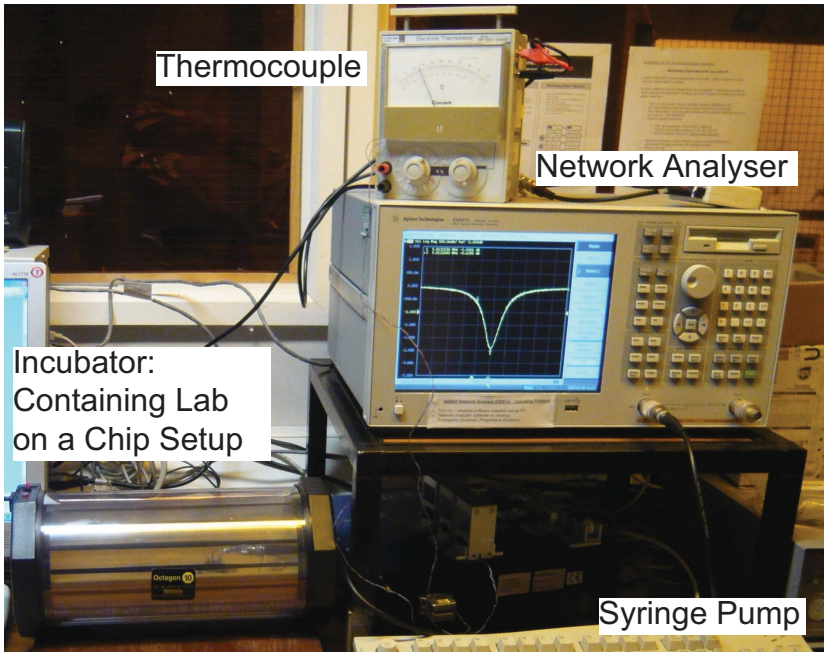

Figure V.5: Lab-on-a-chip equipment setup to measure changes in frequency from the quartz crystal microbalance on a network analyser via the PC.

V.1.2 Microfluidic Chip Setup

With a microfluidic device setup such as this, it is very important that the glass chip and its surroundings are clean and put together precisely. Both sides of the glass chip must be cleaned with methanol and lens cloth tissues removing any dust particles from the surfaces. The glass chip is placed on the base plate of the holder ensuring the flow inlet and outlet are aligned correctly. The spacer is placed around the chip before adding the upper plate, the screws are gently tightened avoiding contact with the glass chip. To loosely hold the glass chip in place, two spare ferrules with nuts are inserted gently into holes that are not used for the inlet and outlet, this allows for placement of the connections to be double checked for alignment in the case that the glass chip is not square to the holder. The alignment is then checked by holding the chip setup to the light. The ferrules may need loosening and adjustments may need to be made to ensure alignment. There is a tolerance of between 50 and 500 μm for the ferrule and the inlet/outlet holes to be truly aligned (see Figure V.6). To make the connections, a ferrule and tubing is needed. The ferrule needs to be placed onto the end of the capillary

tubing and, the tubing pushed through until the tip is just visible. An inlet and outlet connection is made, with a headless nut to hold the ferrule and tubing in place.

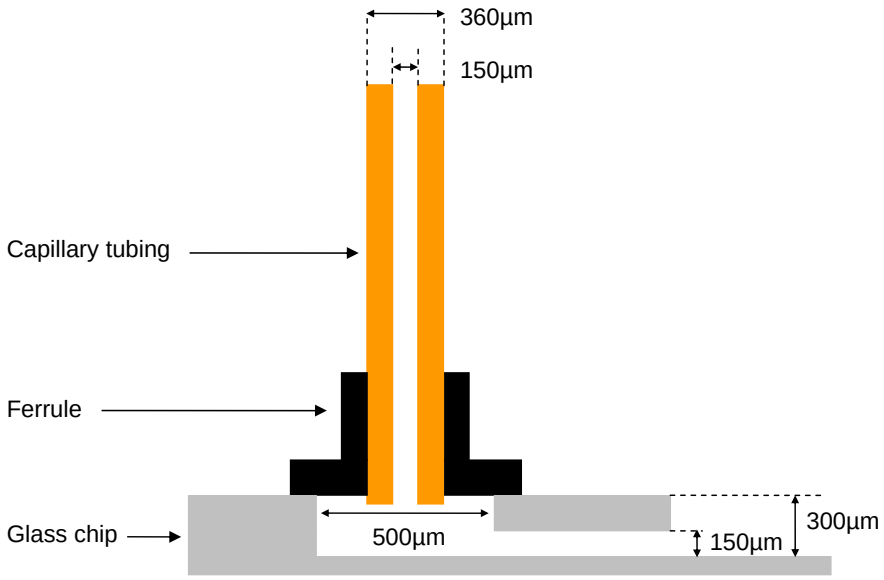

Figure V.6: Schematic of microfluidic glass chip with ferrule and capillary tubing to show alignment.

The QCM is placed with the large sensing electrode facing down over the centre of the well in the glass chip. The capillary tubing is threaded thorough the holes in the upper plate of the holder which is then placed onto the setup and held in place by tightening the four bolts. The PEEK clamp with electrical contacts is inserted into the centre aligned with the electrodes of the QCM. Once the PEEK clamp is fully lowered, the final cap is placed on top. It is essential that the cap is tight and sits flat once secured with four bolts using a torque driver. An extender tool is used for headless fittings to ensure they are all tight.

A micro filter assembly is fitted to the inlet of the capillary tubing to avoid potential blockages in the tubing or glass chip. If the filter capsule becomes blocked it is cleaned by sonicating in methanol. A 1/32" tipped syringe is placed into the filter assembly nut and tightened, ensuring it gently touches the filter disc minimising any dead volume. The outlet tubing is left open to the atmosphere and placed in a waste container.

To check the setup is correct, the spectrum for the QCM is viewed on the network analyser to ensure a strong, symmetrical resonant peak. Once this is seen, the setup is left overnight for stresses in the QCM, chip and holder to equilibriate. The resonant frequency of the crystal in air is then recorded at the desired temperature and the cell setup initially checked with methanol to ensure it is sealed with minimal leakage; methanol is used because it is very wetting and reduces the risk of bubbles within the system.

V.1.3 Liquid Characterisation and Cleaning Protocol

The microfluidic device requires a liquid sample volume of 30 μl, a direct non-microfluidic comparison of measurements has been made using a DVII+ Programmable viscometer (Brookfield, MA), temperature con-

trolled via a water bath and a DMA4500 Density/specific gravity/concentration meter (Anton Parr, Germany) which require a combined volume of 1.5 ml.

Preliminary measurements were made with water-glycerol mixtures (0 to 85% v/v) to ensure a response that agrees with Kanazawa and Gordon [1]. Further measurements were made for varying concentrations of a single RTIL miscible with water [C_2mim][$EtSO_4$], followed by a number of pure RTILs.

The cleaning protocol varies depending on the RTILs miscibility (see Table V.2). It requires six fluid volume changes to ensure there is no residue remaining from the sample. This was the volume required which returned the resonant frequency of the QCM to its original value (to within ~ 50 Hz) after a liquid sample had been tested. Two QCMs of different frequencies, (8 and 9 MHz) have been tested. Table V.2 shows which RTILs have been tested on each crystal along with the traditionally measured viscosity and density meter values. The 9 MHz crystal measurements were collected at 25 °C and the 8 MHz crystal measurements recorded at 30 °C, to work at stable temperatures slightly above room temperature.

RTILs Measured	**$(\rho\eta)^{1/2}$ (kg m^{-2} $s^{-1/2}$) Viscometer-Density Meter at 25°C**	**$(\rho\eta)^{1/2}$ (kg m^{-2} $s^{-1/2}$) Viscometer-Density Meter at 30°C**	**Water Miscible?**
[C_2mim][$EtSO_4$] 10%	1.19	1.08	√
[C_2mim][$EtSO_4$] 25%	1.29	1.27	√
[C_2mim][$EtSO_4$] 50%	2.55	1.77	√
[C_2mim][$EtSO_4$]75%	3.70	2.75	√
[C_2mim][$EtSO_4$] 80%	x	3.36	√
[C_2mim][$EtSO_4$] 85%	4.65	x	√
[C_2mim][$EtSO_4$] 90%	9.18	5.53	√
[C_2mim][$EtSO_4$] 100%	11.19	9.23	√
[C_4mim][DCA] 100%	5.64	x	√
[C_2mim][SCN] 100%	5.24	x	√
[C_6mim][NTf_2] 100%	10.47	8.51	x
[C_{10}mim][NTf2] 100%	x	11.05	x
[C_2mim][NTf_2] 100%	x	6.43	x
[C_4dmim][NTf_2] 100%	x	9.23	x
[C_4mim][NTf_2] 100%	x	7.60	x
[C_8mim][NTf_2] 100%	x	9.43	x
[C_4mpyrr][NTf_2] 100%	x	8.84	x
[C_4mpyrr][DCA] 100%	x	5.36	√

Table V.2: Room temperature ionic liquids measured on the 8 and 9 MHz quartz crystal with measured viscometer and densitometer values of (viscosity x density)$^{1/2}$.

One potential concern in this system is that the crystal is most sensitive in the centre of the sensing region. Although the cleaning protocol may have been followed and the frequency of the crystal returned to its original frequency, a small quantity of residue may still be present at the outer rim of the crystal which is not necessarily detected. These residues could build up over time causing erroneous measurements. For this application

however, it was found that six fluid volume changes gave repeatable, consistent results, suggesting the cell was sufficiently clean so this was not cause for concern.

V.1.4 Fabrication of Quartz Crystals

Two polished quartz discs (0.538" diameter) with a thickness related to a fundamental frequency of 8 MHz and 9 MHz were purchased from International Crystal Manufacturing (OK, USA). Wrap around electrodes with top and bottom diameters of 9 mm and 4.5 mm respectively, were fabricated with 10 nm titanium and 150 nm gold using an K575X sputter coater (Emitech, Quorom Technologies) to give single sided electrical contact access. These were fabricated using an acrylic mask with the electrode pattern designed in CorelDRAW®. The acrylic was cut out using a M-300 laser (Universal Laser System, OH). Resonant frequency changes of the final QCMs mounted in the chip were monitored by tracking the frequencies of the minimum reflected power using an E5061A network analyser (Agilent, CA), operating in reflection mode outputting the frequency changes to a PC controlled via Matlab® (Mathworks, MA). Liquid flow was stopped to allow the frequency measurements to be recorded without the influence of fluid motion. Frequency measurements were made on both the fundamental and third harmonic. BVD fitting (see Section II.2.2.5) was not performed as the frequency measurements were deemed sufficient. Since the completion of these experiments, QCMs have been sourced from ICMFG (OK, USA) with smaller electrodes having diameters 0.159" and 0.324" negating the need to deposit electrodes onto the crystals, making QCMs for any future work more consistent.

V.1.5 Limitations

There are two limitations that should be considered when working with this microfluidic cell setup. The first is the pressure, and hence flow rate which the system can withstand. This has been modelled in Comsol Multiphysics® and is determined by the thickness of the quartz crystal. The second is the leakage between the QCM and the glass chip; the leakage rate has been estimated.

V.1.5.1 Theoretical Maximum Pressure and Flow Rate Calculations

A model of the clamped QCM has been created according to the schematic shown in Figure V.7. This includes the glass flow chip, the quartz disc and PEEK clamping system.

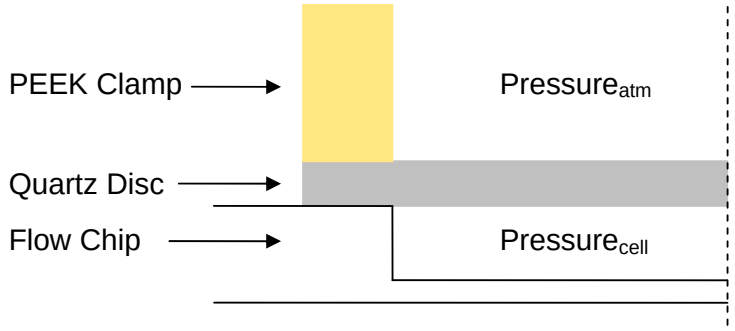

Figure V.7: Schematic of the system modelled in Comsol Multiphysics®.

The model has been completed in Comsol Multiphysics® using the 2D axial symmetry; structural mechanics module in the stress-strain application mode. This module assumes axis symmetry both in load and geometry and studies the displacement, stresses and strain in an axially symmetric loaded body. The objects are specified and the subdomains set to the material properties of quartz, glass, and PEEK which include the Young's modulus (E), Poisson's ratio (ν) and density (ρ). The properties included in the simulation are:

1) Quartz: E = 73.1 GPa, ν = 0.17, ρ = 2650 kg/m^3,
2) Glass: E = 73.1 GPa, ν = 0.17, ρ = 2203 kg/m^3,
3) PEEK: E = 2.0 GPa, ν = 0.33, ρ = 7850 kg/m^3.

Boundary conditions are fixed for the top edge of the clamp and the bottom edge of the flow chip as these are constrained and hence unable to move. A force is applied to the underside of the quartz as a distributed load with a force which has been determined by the known design tensile stress of quartz (48 MPa [2]). With a force applied to the crystal, the mesh is refined and the solution is determined. Once solved, post processing is completed by looking at the surface principal stress and the deformed shape of the quartz disc. The force applied to the crystal was adjusted and the model updated until a maximum principal stress greater than the design tensile stress was achieved. It would be at this point experimentally that the crystal would break (see Figure V.8). A pressure of -2 $\times$ 10^5 N/m^2 (2 bar) was applied to achieve this maximum stress as in Figure V.9 (actual value at 2 bar = 54 MPa). The solved model shows the weakest point of the setup to be the underside of the crystal near the clamp.

This model confirms that the QCM is the weakest point in the enclosed system regarding pressure. This is due to the crystal thickness and the clamping method. Ideally, a thicker crystal is needed to increase the pressure the set up can withstand. If the flow rates are too high and pressure builds up the device will fail around the outer rim of the QCM according to the model. This has also been confirmed experimentally (Figure V.10). The QCM has cracked on several occasions leaving the Miconit glass chip undamaged. This is hugely beneficial as the quartz crystals are inexpensive (~ £13/crystal, at time of study) and are easily replaceable, whilst the glass chip is considerably more expensive and must be remade to specification in order to be replaced.

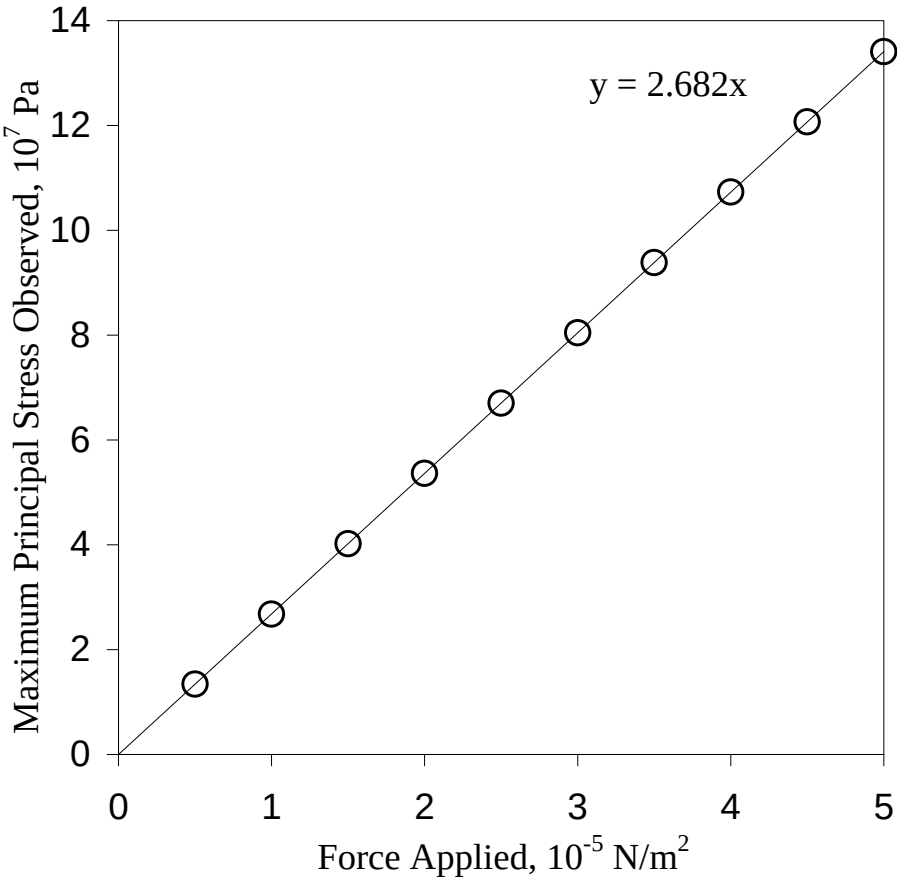

Figure V.8: The results of a Comsol Multiphysics® model of the clamped QCM, solved for varying force applied to the underside of the crystal. The plot shows how the maximum principal stress changes with the force applied. The design tensile stress of quartz is 48 MPa, relating to a pressure applied of 1.8×10^{-5} N/m^2 ($\sim$ 2 bar).

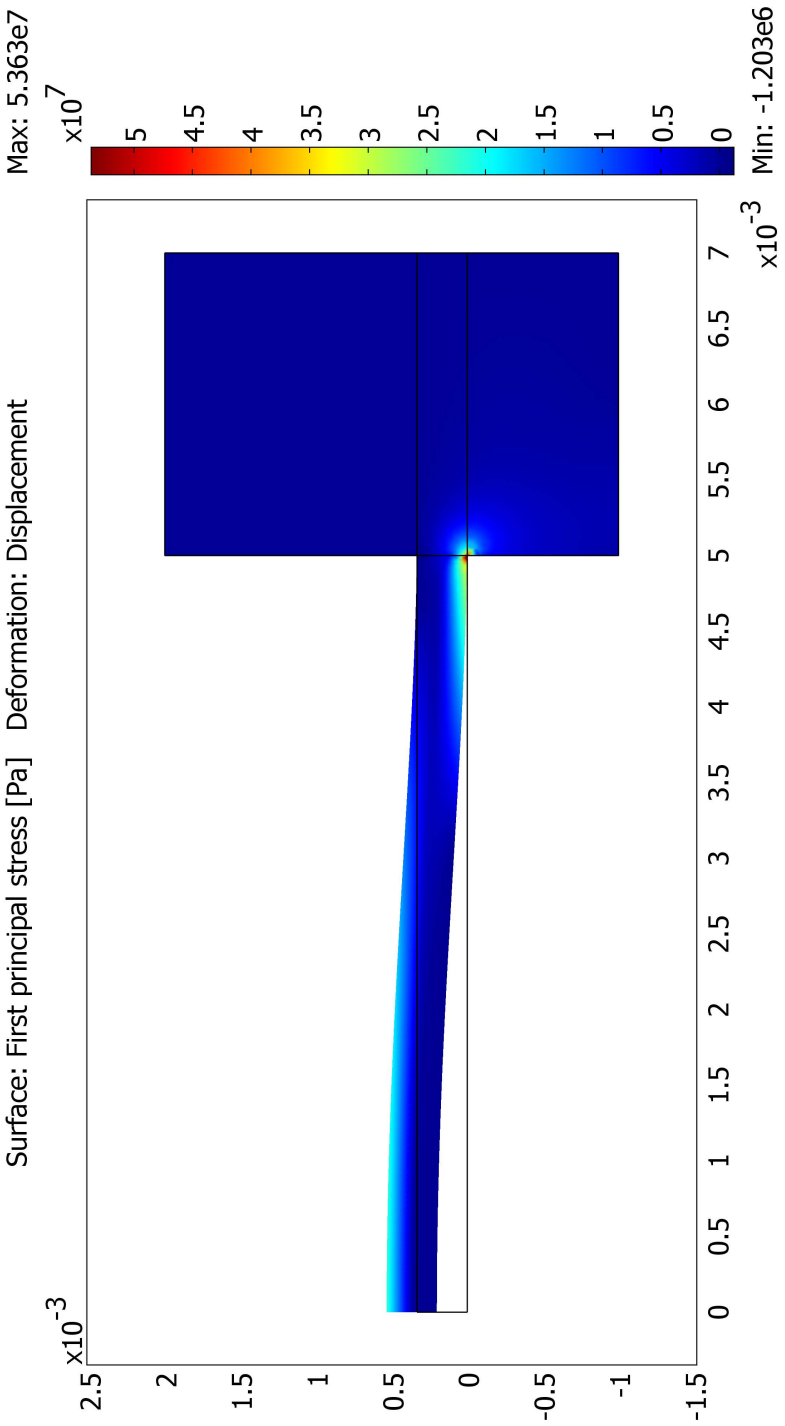

Figure V.9: A Comsol model of the principal stress and deformation of the QCM when clamped in the cell setup, showing the point of weakness in the setup (the red region).

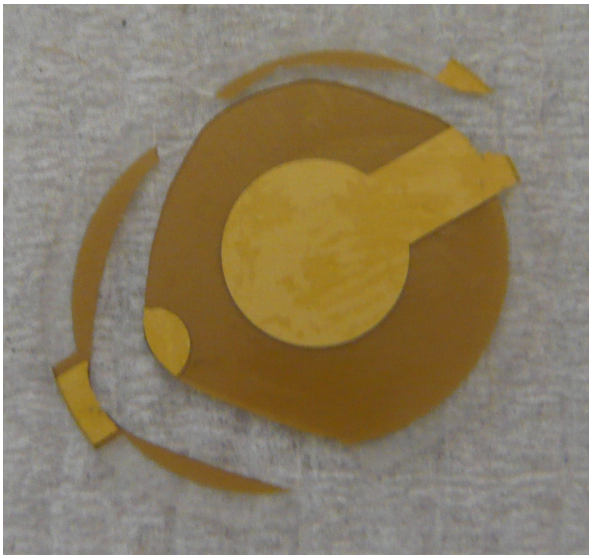

Figure V.10: A failed Quartz Crystal: the pressure within the lab-on-a-chip device has exceeded the crystal's limit which has cracked around its weakest point.

A rough guide to the maximum pressure and flow rate within the cell can be calculated from the Hagen-Poiseuille equation (Equation V.1) [3].

$$\Delta P = \frac{128 Q \eta L}{\pi D^4}, \tag{V.1}$$

where ΔP is the change in pressure in the system (2×10^5 Pa) calculated above, L is length of outlet tubing (0.3 m), D is inner diameter of the outlet tubing (1.5×10^{-4} m), η is dynamic viscosity (Pa.s) and, Q is the volumetric flow rate (m^3/s). From the known maximum pressure drop (before the quartz crystal fractures) it is possible to calculate the volumetric flow rate flowing through a pipe (assuming flow is laminar viscous and incompressible). A system schematic is shown in Figure V.11 to help identify the necessary parameters.

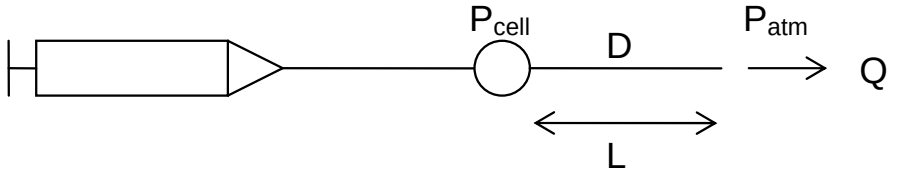

Figure V.11: Schematic of chip system showing relevant parameters, where: P_{cell} is the pressure in the cell, P_{atm} is the atmospheric pressure, L is length of tubing, D is inner diameter of tubing and Q is volumetric flow rate.

For a liquid with a low viscosity such as methanol (η = 0.54 cP at 25 °C), a maximum flow rate Q, can be calculated to be 11.8 μL/s. By reducing the flow rate by approximately 50% to 6 μL/s in the above example, it is possible to reduce the cell pressure to 1 bar hence reducing the maximum stress in the QCM giving a safety margin. For a more viscous liquid (e.g. 100 cP), a maximum flow rate of 0.08 μL/s is calculated. For safety,

a flow rate equal to or less than half the maximum flow rate (0.04 μL/s) has always been used experimentally. However by decreasing the flow rate of the sample, the time taken for an average measurement is increased considerably due to the additional cell loading and cleaning time and hence this must be considered when discussing a high-throughput device.

V.1.5.2 Seal Leakage Rate

When designed, it was known that a contact seal was not optimum, but due to the nature of the liquids being tested and the need for small volumes it was considered to be a good choice. Since a small amount of leakage was expected to occur the limitations of the seal were calculated using a model of radial flow in a space of uniform height, illustrated in Figure V.12. This gives an estimate of the expected leakage rate through the seal.

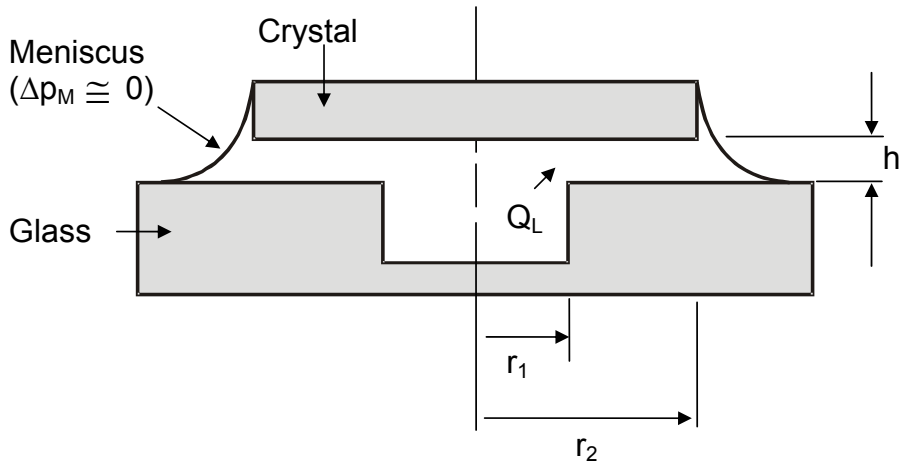

Figure V.12: Model geometry used to characterise seal leakage rate.

Determination of the velocity and pressure distribution p in the gap is relatively straightforward since the height of the gap h is small in relation to the radial distance r (hence $r \gg h$ or $\frac{h}{r} \approx 0$) [4]. For a Newtonian liquid with steady laminar flow in such a system, the equation for radial pressure gradient in terms of leakage volume flow rate Q_L, gap height h, liquid viscosity η, and radius r, can be expressed as in Equation V.2 [5, 6],

$$\frac{dp}{dr} = -\frac{6\eta Q_L}{\pi h^3 r}. \tag{V.2}$$

Integration from r_1 to r_2 then yields a relation between pressure differential and leakage flow rate in;

$$Q_L = \frac{\pi h^3 (p_1 - p_2)}{6\eta ln(r_2/r_1)}. \tag{V.3}$$

In practice, the gap is not uniform and varies according to the surface undulations in the glass and quartz surfaces. For polished, optical-quality surfaces such as those involved in this seal, the surface undulations are expected to be less than 0.1 μm. Using this value for the height, and a pressure difference of 1 bar, Equation V.3 gives a leakage flow rate of 1.5 pL/s for a liquid with 0.1 Pa.s viscosity. For continuous operation over

one day, if the leaked liquid (total volume, V = $1.296 \times 10^{-10} m^3$) formed a quarter-circular fillet around the perimeter of the quartz crystal with diameter d, the total radius of the quarter-circular fillet can be determined using Pappus' centroid theorm [7] (see Equation V.4, rearranged to give distance travelled x, in Equation V.5).

$$V = (x^2 - \frac{1}{4}\pi x^2)\pi d, \tag{V.4}$$

$$x = \sqrt{\frac{4V}{\pi d(4-\pi)}}. \tag{V.5}$$

This equation takes a cross sectional area of a revolved solid to determine the volume. For this example, the fillet radius would be about 100 μm assuming the liquid wets glass and quartz completely (contact angle of zero). A fillet of about 100 μm would be very visible, in contrast to that seen experimentally (very little liquid could be detected over similar periods of operation). This suggests that in fact the gap corresponded to a smaller size than the 0.1 μm assumed above, which is entirely possible.

V.2 Results and Discussion

The results have been separated into two sections. They show the response of the 9 MHz and the 8 MHz QCM operating on both the fundamental and third harmonic for determination of the square root viscosity-density product. Water-glycerol mixtures, various concentrations of a diluted RTIL ($[C_2mim][EtSO_4]$) and a range of pure RTILs have been investigated.

When obtaining measurements on the QCM, the pressure within the cell needs to be considered. Pressure in the cell was kept well below the crystals breaking stress. Frequency measurements were made at the same time relative to that at which the flow of liquid was stopped to minimise changes in pressure and changes due to increasing viscosities. An average of three measurements was recorded to allow deviations to be seen which maybe related to pressure. The results obtained were very consistent and as such the pressure effects were considered negligible in comparison to the frequency shifts obtained for the liquids. If stress effects were dominant, a crystal orientation which is stress compensated such as SC-Cut, which still behaves as a thickness shear mode resonator, would have been considered.

V.2.1 9 MHz Quartz Crystal Microbalance

Results for the 9 MHz quartz crystal have all been obtained within an incubator at 25 °C, an average of three measurements were recorded, with the minimum and maximum values also displayed as error bars on all figures. The liquids tested are described in Table V.2.

V.2.1.1 Temperature Characterisation

AT-Cut Quartz crystal resonant properties are considered to be relatively temperature insensitive, however minimal frequency changes may occur over high temperature changes. To test this response a temperature characterisation plot is produced (see Figure V.13). The temperature was circulated between 20 °C and 60 °C and shows a change in frequency of ~50 Hz / °C in air. If the crystal was not kept at a steady temperature it would be much more difficult to use the frequency response to show the crystal is clean. Here a change in frequency of ~50 Hz corresponds to a difference in the square root viscosity-density product measurement of ~0.03 kg m^{-2} $s^{-1/2}$. This reinforces the need for working with the chip system in an incubator. The plot V.13 shows interesting behaviour suggesting that the initial heating may be annealing the crystal or causing desorption of containments on its surface. Subsequent temperature changes follow a standard hysteresis curve.

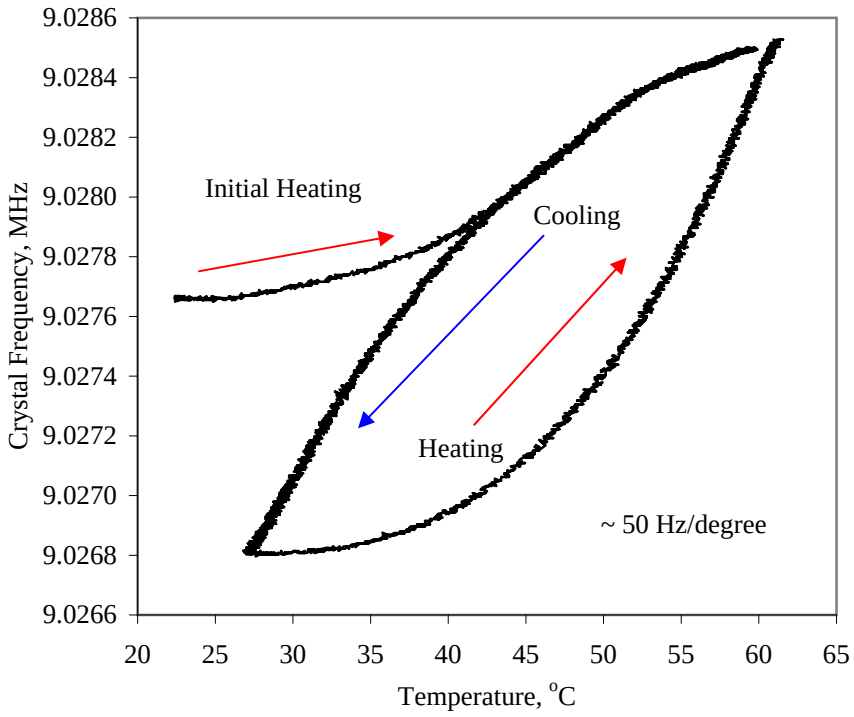

Figure V.13: A 9MHz Quartz Crystal Microbalance temperature characterisation plot to calculate frequency changes with temperature in air.

V.2.1.2 Fundamental Response

Figure V.14(a) Shows the change in frequency measurements obtained from the response of the fundamental resonance for the 9 MHz quartz crystal which have been converted to the square root viscosity-density product using the Kanazawa and Gordon equation [1]. This plot shows some agreement between the QCM derived values and the traditionally measured viscosity and density measurements with reasonable linearity. There is however large scatter around the lower values of viscosity-density product. The reason for this is unclear although it could be a result of the liquid being constrained to such a small volume above the crystal. This scatter is seen for both the calibration water-glycerol mixtures and all RTILs tested.

V.2.1.3 Third Harmonic Response

The response of the 9 MHz QCM operating on the third harmonic shows a definite linear relationship with a fit of y = 0.852x for all liquids tested with only small deviances from the line of best fit, see Figure V.14(b). A line of unity is plotted to show expected values and it is clear the QCM is not operating completely to the expected values of Kanazawa and Gordon [1]. This however, is not a problem as it is behaving linearly and this small discrepancy can be easily calibrated for by $\sqrt{\rho\eta}_Q = 0.852\sqrt{\rho\eta}_T$, where $_Q$ and $_T$ refer to QCM and traditional viscometer and densitometer measurements respectively. Figures V.14(a) and V.14(b) show that calculating the square root viscosity-density product from the fundamental response has a closer fit to unity than the third harmonic. The third harmonic response however has far less deviation from the best fit line, and with a calibration factor is the resonance of choice for comparison to traditionally measured viscosity and density values.

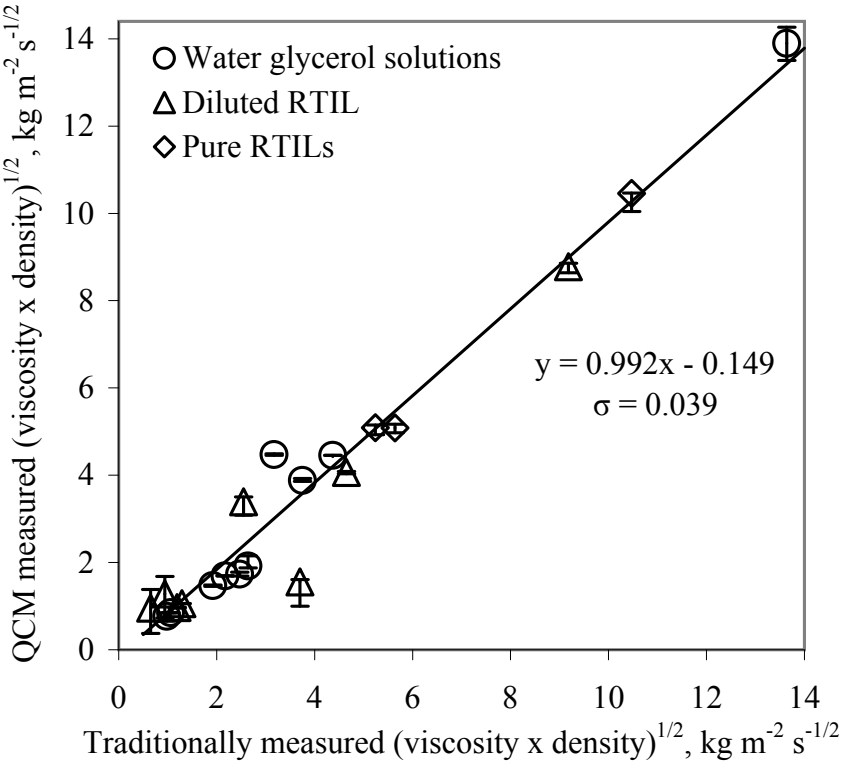

(a)

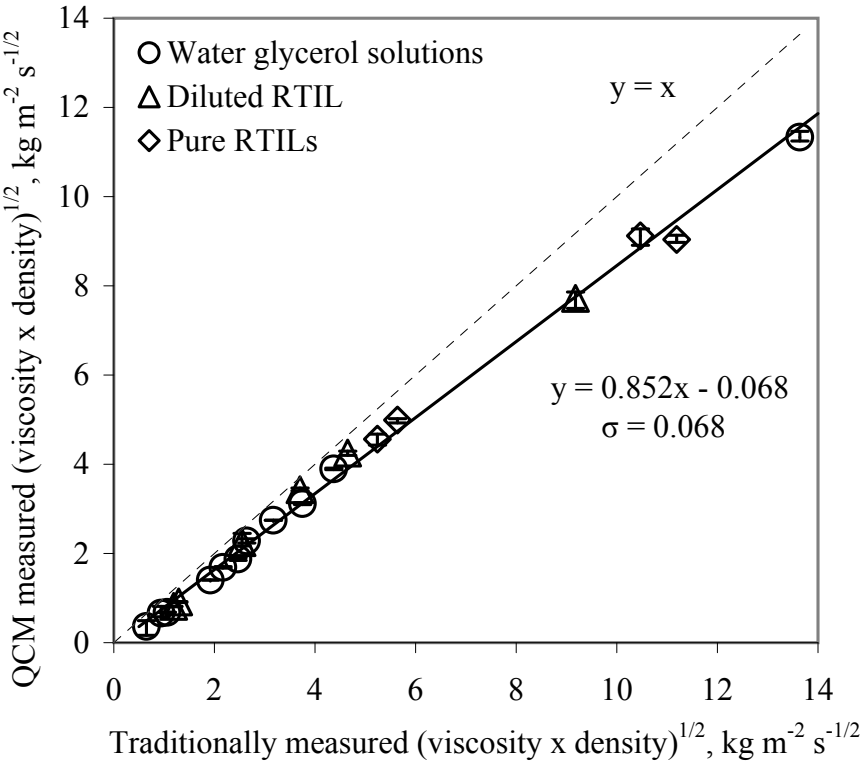

(b)

Figure V.14: (a) Fundamental and (b) Third harmonic frequency results for the 9 MHz Quartz Crystal Microbalance for the (viscosity x density)$^{1/2}$ of water-glycerol solutions, dilutions of [C_2mim][$EtSO_4$] and four pure RTILs (see Table V.2). A unity line is plotted in Figure (a) to demonstrate linearity. In Figure (b) a best fit line for all data has been plotted (- -), a unity line (-) of y = x is also plotted to demonstrate the expected relationship.

V.2.2 8 MHz Quartz Crystal Microbalance

The 8 MHz crystal has also been studied in an attempt to reduce the scatter seen on the frequency response of the 9 MHz crystal. By increasing the thickness of the crystal, the flow rate and hence the pressure which the crystal will withstand will also be increased slightly. All results for the 8 MHz quartz crystal have been collected at 30 °C, as an average of three measurements (both the minimum and maximum values are displayed as error bars on all figures). The liquids tested are described in Table V.2.

V.2.2.1 Fundamental Response

The fundamental response for the 8 MHz quartz crystal (Figure V.15(a)), shows a clear linear response between the QCM measured square root viscosity-density product and the traditionally measured values which follows the line of unity expected from the Kanazawa and Gordon equation [1]. There are however, large deviances over the range of liquids tested, and again as with the response of the 9 MHz crystal, it is unclear why these fluctuations occur.

V.2.2.2 Third Harmonic Response

Figure V.16 shows the resonant frequency, and insertion loss for the third harmonic over time for varying concentrations of RTIL, returning to the original frequency for water after each test. It is clear the third harmonic frequency response is very repeatable. When the frequency is converted into the square root viscosity-density product (Figure V.15(b)), the range of liquids tested are all seen to lie on the unity line with minimal deviance in good agreement. At high square root viscosity-density product ($\sqrt{\rho\eta} > 10$ kg m^{-2}s$^{-1/2}$) however, the resonance is extremely damped and very broad. At this point, it becomes difficult to determine the resonant frequency accurately and as a result it may represent the limit of detection for the 8 Mz QCM in the system.

It has previously been reported that the third harmonic gives a better measure of agreement for this type of application [8–10]. The results above agree, and confirm the third harmonic to be in better agreement than the fundamental response experimentally for both the 8 MHz and 9 MHz QCM in this particular experimental setup.

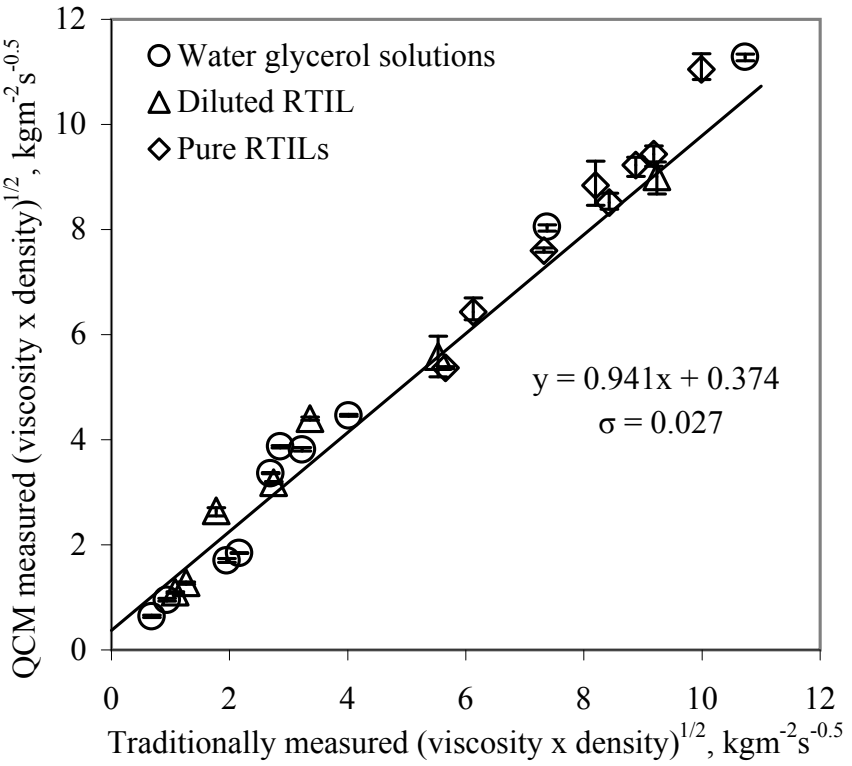

(a)

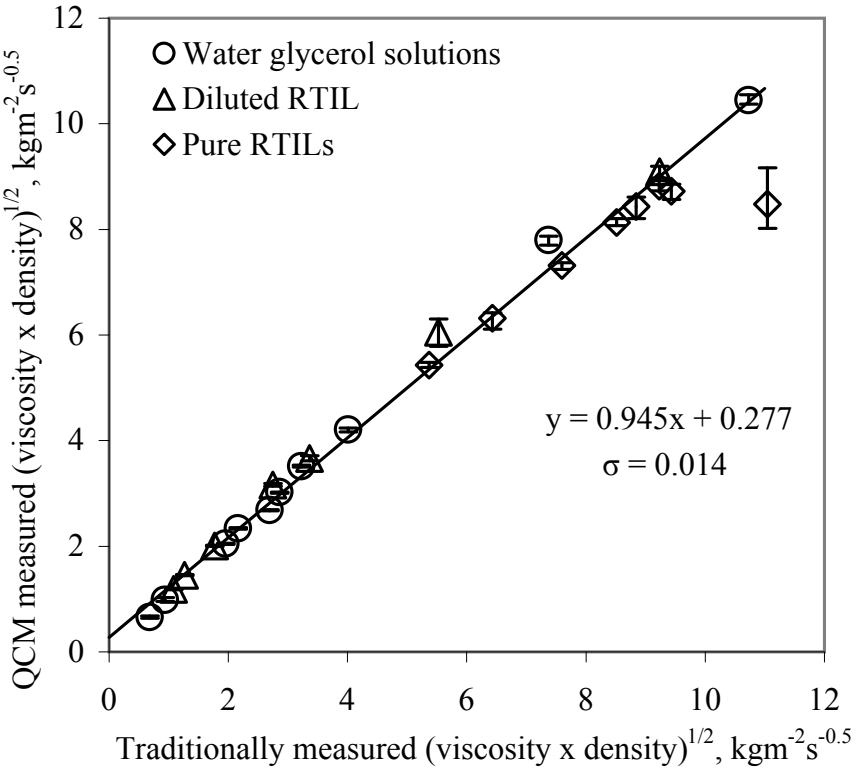

(b)

Figure V.15: (a) Fundamental and (b) Third harmonic frequency results for the 8 MHz Quartz Crystal Microbalance for the (viscosity x density)$^{1/2}$ of water-glycerol solutions, dilutions of [C_2mim][$EtSO_4$] and nine pure RTILs (see Table V.2).

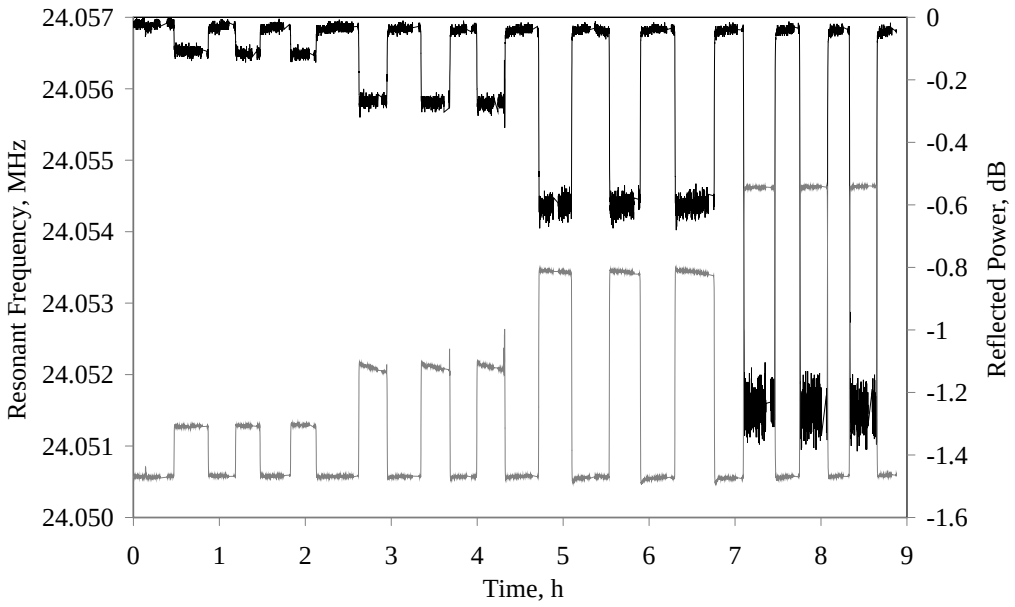

Figure V.16: A frequency and reflected power time plot showing repeatability for the third overtone resonant frequency of a 8MHz Quartz Crystal Microbalance, sensing dilutions of $[C_2mim][EtSO_4]$.

V.3 Conclusion

Using a QCM in a lab-on-a-chip system, it has been shown possible to measure the square root viscosity-density product of water-glycerol solutions and various room temperature ionic liquids using volumes as low as 30 μL. The microfluidic chip is an enclosed system in which the volume could be further reduced by optimising the tubing lengths. It is clear the third harmonic frequency response is in better agreement to traditionally measured viscosity-density for both the 8 MHz and 9 MHz crystal, with the 8 MHz operating on the third harmonic having optimum agreement. The QCM microfluidic setup offers an excellent alternative to larger volume techniques and is particularly advantageous when characterising hygroscopic liquids, whereby the viscosity decreases exponentially with water contamination. These results look promising and show great potential for this setup being included into a more complex chip design characterising the same volume of liquid using other techniques. This method could be combined with a simulation study for density such as those described by J. Jacquemin *et al.* [11] to allow viscosity to be extracted as a separate value for RTILs.

References

[1] K. Kanazawa and J. Gordon, "Frequency of a quartz crystal microbalance in contact with liquid," *Analytical Chemistry*, vol. 57, no. 8, pp. 1770–1771, 1985.

[2] R. Weast, ed., *Handbook of Chemistry and Physics*. CRC Press, 1980.

[3] S. Sutera and R. Skalak, "The history of poiseuille law," *Annual Review of Mechanics*, vol. 25, pp. 1–19, 1993.

[4] S. Younggon, "Determination of shear viscosity and shear rate from pressure drop and flow rate relationship in a rectangular channel," *Polymer*, vol. 48, pp. 632–637, 2007.

[5] C. D. Collyer AA, ed., *Rheological measurement.* Elsevier Applied Science, 1988.

[6] P. J. Carreau, D. C. R. D. Kee, and R. P. Chhabra, *Rheology of Polymeric Systems: Principles and Applications*. Hanser Gardner Publications, 1997.

[7] J. Bird, *Engineering Mathematics, Fifth Edition*. Newnes, 2007.

[8] D. Johannsmann, "Derivation of the shear compliance of thin films on quartz resonators from comparison of the frequency shifts on different harmonics: A perturbation analysis," *Journal of Applied Physics*, vol. 89, no. 11, Part 1, pp. 6356–6364, 2001.

[9] G. McHale, C. Hardacre, R. Ge, N. Doy, R. W. K. Allen, J. M. Maclnnes, M. R. Bown, and M. I. Newton, "Density-viscosity product of small-volume ionic liquid samples using quartz crystal impedance analysis," *Analytical Chemistry*, vol. 80, no. 15, pp. 5806–5811, 2008.

[10] N. Doy, G. McHale, P. Roach, M. I. Newton, C. Hardacre, R. Ge, R. W. Allen, J. M. MacInnes, and M. R. Bown, "Small volume determination of the viscosity-density product for ionic liquids using quartz crystal harmonics," in *2008 IEEE International Frequency Control Symposium, Vols 1 and 2*, pp. 440–442, 2008. IEEE International Frequency Control Symposium, Honolulu, HI, May 19-21, 2008.

[11] J. Jacquemin, R. Ge, P. Nancarrow, D. W. Rooney, M. F. C. Gomes, A. A. H. Padua, and C. Hardacre, "Prediction of ionic liquid properties. I. Volumetric properties as a function of temperature at 0.1 MPa," *Journal of Chemical and Engineering Data*, vol. 53, no. 3, pp. 716–726, 2008.

VI. EXPERIMENTAL IV: CHARACTERISATION OF ROOM TEMPERATURE IONIC LIQUIDS USING SURFACE ACOUSTIC WAVE DEVICES

The surface acoustic wave device is well known for its small size and flexibility in shape and design. These devices can be adapted to meet specific criteria. This chapter explores the behaviour of surface acoustic wave devices when sensing room temperature ionic liquids. It looks primarily at the Shear Horizontal-Surface Acoustic Wave (SH-SAW) device, a SH-SAW device with the addition of a gold film forming a metallised propagation path and a SH-SAW operating with a silicon dioxide guiding layer. SAW devices have been investigated as they can function at a much higher frequency with respect to the QCM, thus increasing their sensitivities. Since their frequency is independent of the thickness of the substrate they are created on, a thicker substrate may be used to withstand greater pressures. It is expected that the ion content of the ionic liquids may provide some problems with conductivity which might be overcome with the addition of a metallized area. This study looks at the devices on a larger volume scale giving preliminary results. Further optimisation could potentially allow for a SAW device to be used in a lab-on-a-chip set up such as those described in the previous chapters with a greater throughput. It may also be possible to reduce the sample volume required further by optimising the device properties.

VI.1 Methodology

The SAW devices required for this work were fabricated in a clean room with a standard S1813 (Micro.Chem, USA) photo resist protocol. Full fabrication steps are given below including; details of the mask design, the addition of a gold film on the propagation path and, the deposition of silicon dioxide to act as a guiding layer.

VI.1.1 Fabrication of Surface Acoustic Wave Devices

The fabrication of a surface acoustic wave device is completed by a standard S1813 (Micro.Chem, USA) photolithography lift-off process. The specific wave required is dependent on the substrate and its crystal orientation. Double sided polished 0.5 mm thickness ST-X cut 3 ” diameter quartz wafers (University Wafer, USA) were chosen to give a SH-SAW propagating along the x-flat direction (approx. £45 per wafer).

To aid adhesion of the S1813 onto the quartz substrate, the wafers were left overnight soaking in 3% v/v hexamethyldisilazane, HMDS (Sigma-Aldrich, UK) and toluene (Sigma-Aldrich, UK). The wafer was rinsed with isopropanol, IPA (Sigma-Aldrich, UK) and dried in a jet of nitrogen prior to use. The photolithography process described in Figure VI.2 was completed using a WS-650 spin processor (Laurell®, PA), and MJB4 Mask

Aligner (Suss MicroTech AG, Germany). The spin processor speed corresponds to a S1813 layer thickness of 1.5 μm and requires a UV exposure time on this machine of 1.6 seconds (total energy = 83 mJ/cm^2).

An S1813 developer, Microposit MF-321 (Micro.Chem, UK), diluted to 50% v/v concentration with distilled water was used. A dilution was needed to allow more control over the rate of development. Development requires approximately 30 seconds with agitation. S1813 is a positive photoresist, so any resist exposed to UV is not cross linked in the development stage. The developer was rinsed off with distilled water and dried in nitrogen. The patterned S1813 is seen in Figure VI.1(b) and VI.1(a). Metal deposition takes place using a K575X sputter coater. (Emitech, Quorom Technologies). A 10 nm Titanium layer was used to aid adhesion of the 100 nm gold layer onto the quartz. The exposed S1813 was removed in a bath of acetone using a sonicator. The wafer was diced with a diamond scribe to form individual SAW devices.

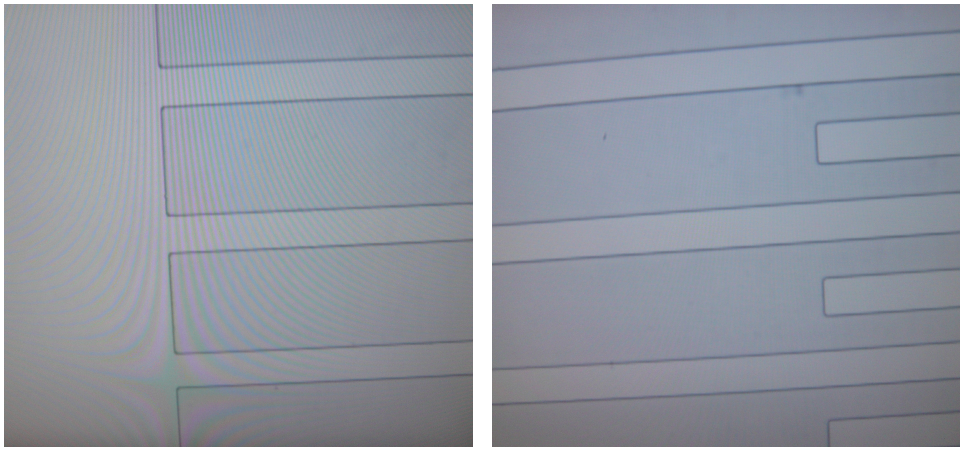

(a) (b)

Figure VI.1: Developed S1813 pattern on quartz showing (a) electrode fingers and (b) equal finger width and spacing (12.5 μm).

VI.1.2 Surface Acoustic Wave Device and Mask Design

A standard SAW design was fabricated to operate at ~ 100 MHz with single-single finger spacing on ST cut quartz. The device consists of an equal finger width and finger spacing of 12.75 μm (see Figures VI.1(a) and VI.1(b)), finger length of 2.153 mm and aperture of 2 mm. The device consisted of 88 finger pairs, with a slightly extended electrode pad to ease electrical contact. The IDTs were 7.65 mm apart, giving a large sensing area for use in the flow cell. The mask was designed to contain multiples of the device to improve the chance of obtaining the maximum number of devices from a 3" diameter quartz wafer. The mask was produced in AutoCAD® and manufactured by JD Photo-Tools (Oldham, UK) on (5 x 5)" soda lime glass. The mask design can be seen in Figure VI.3.

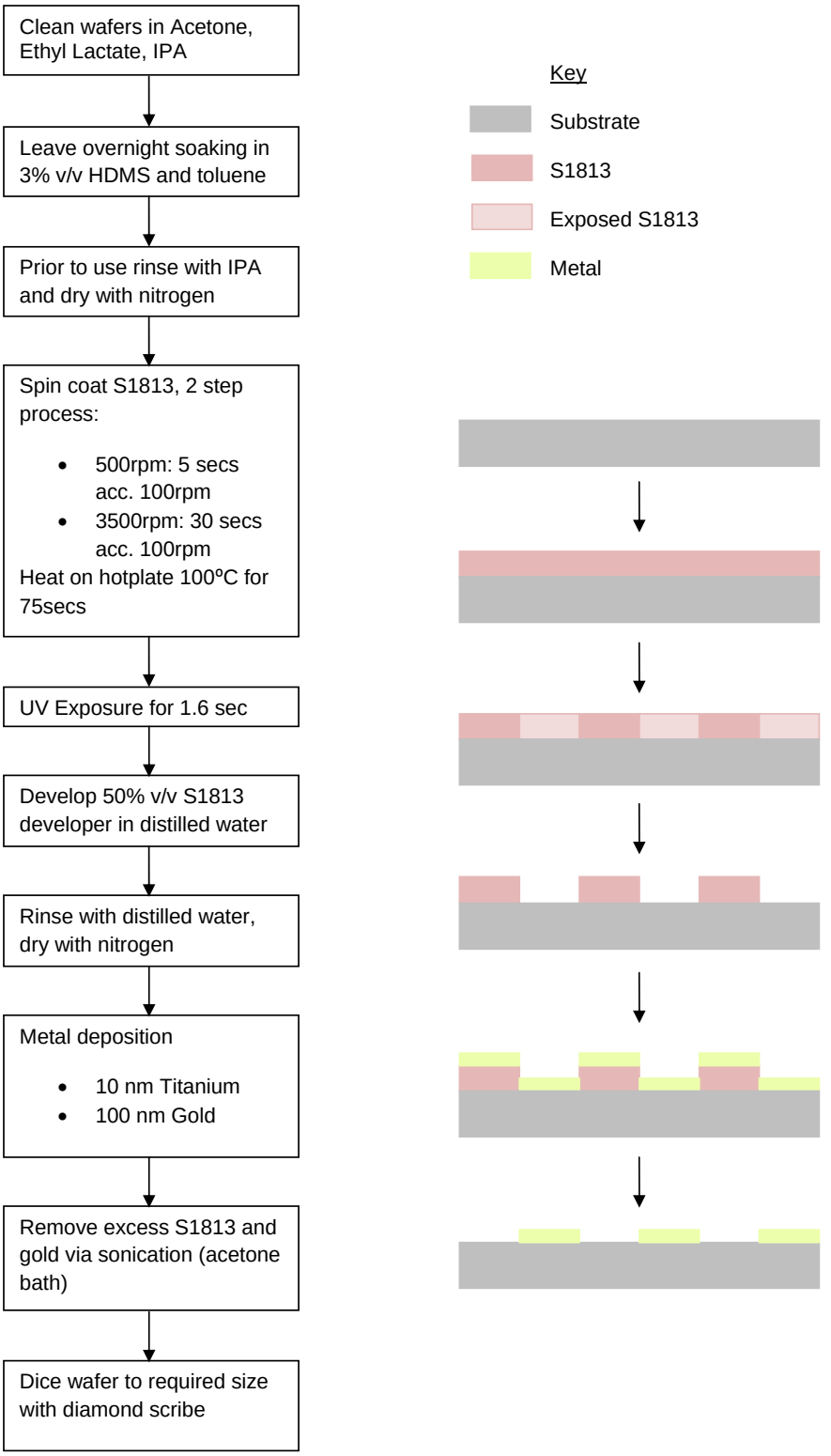

Figure VI.2: Photolithography protocol for producing surface acoustic wave devices on quartz substrate with S1813 photoresist (Micro.Chem, UK).

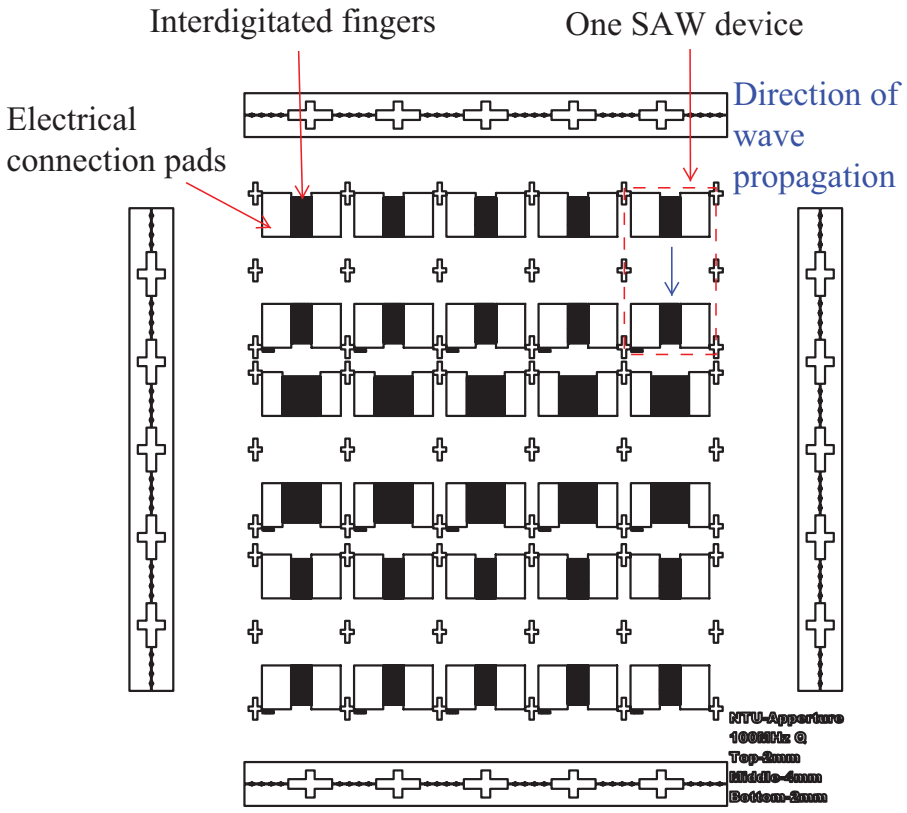

Figure VI.3: Mask design used to produce SH-SAW devices on quartz, used for exposure during the photolithography process, the mask contains two device designs.

VI.1.3 Conductivity Challenges

Two methods were tested to overcome the problems due to the conductivity of the liquids. This involved the addition of a gold film to the propagation path, and secondly the addition of a guiding layer creating a Love wave device.

VI.1.3.1 Addition of a Gold Film on the Propagation Path

At the time of completing this study, no work had been published with RTIL sensing on SAW devices. However some studies [1–6] have found increases in attenuation and limited frequency changes when liquid sensing ionic species using uncoated devices. It was therefore predicted that the ion content may cause a problem with the device experiencing electro-acoustic interactions [7] causing changes in conductivity to induce frequency changes. To limit this interaction a reference device can be used with an additional metallised propagation path to short the electric field. This is more generally used to find the conductivity of the liquid by comparing the changes in frequency shift for the two devices. Here it was hoped that by screening out the additional frequency change by use of a metallised path, it would still be possible to relate the change in viscosity-density product to a phase or insertion loss change without the need for a second device. The electrodes were masked off with adhesive tape before 10 nm of titanium and 100 nm of gold were deposited onto the propagation path using the sputter coater. The area of gold was designed to be large enough to cover the area in contact with the sample liquid. Placement of the gold is shown in Figure VI.4.

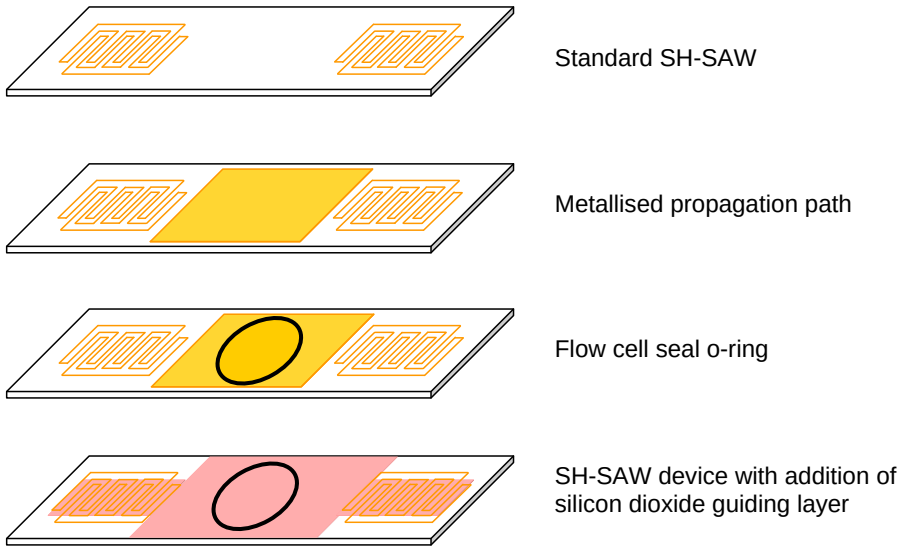

Figure VI.4: Surface Acoustic Wave design from top to bottom: a standard SH-SAW device, device with metallised path, with placement of the flowcell seal, and with SiO_2 guiding layer.

VI.1.3.2 Surface Acoustic Wave Devices with a Guiding Layer

The devices were fabricated as in Section VI.1.1 and then turned into Love wave devices by the deposition of a silicon dioxide (SiO_2) layer. This layer covers the complete surface of the device, leaving just the electrode

contacts bare, as seen in Figure VI.4. Generally, polymers are used as effective guiding layers [8, 9]. In this environment however, SiO_2 was chosen as a guiding layer as it is chemically robust [10, 11] and should withstand long exposure to RTILs.

Prior to coating the device was cleaned with ethanol, a tissue lens cloth and dried in a jet of nitrogen to remove any dust particles and finger prints. To ensure the electrical contacts were not coated with SiO_2 S1813 photoresist was applied to them using a cotton bud and soft baked on a hotplate at 65 °C for 5 mins. This allows the contacts to be easily accessed by removing the S1813 with acetone once the deposition is complete.
The SiO_2 is deposited using a modified vacuum evaporator (Edward 306) containing an R301 RF power supply and TORUS HV Circular sputter head (Kurt J. Lesker, UK). SAW devices were placed in the evaporator and the desired amount of SiO_2 was sputtered onto the devices before they were removed from the vacuum and left to cool to room temperature. A characterisation plot of the thickness of SiO_2 layer against change in insertion loss of the device was needed to optimise its sensitivity. This was achieved by removing the device from the vacuum after every additional 200 nm of deposition and recording their spectra before depositing another 200 nm. S1813 is removed from the electrode pads and the device spectra is recorded using Transmission (S21) measurements on a E5061A network analyser (Agilent, CA) using the device holder, insertion loss, phase and frequency were recorded. The contacts were then coated again with S1813 and the device returned to the vacuum for additional SiO_2 deposition. This was repeated until a characterisation plot was formed (Figure VI.10).

VI.1.4 Equipment Setup

Once the fabrication is completed a single device is placed in the setup shown in Figure VI.5. Again, one of the challenges was to create a flow cell setup that is chemically resistant. This was achieved by creating a T-piece insert from PTFE to slide into the device holder (created 'in house' from a brass block). A PTFE encapsulated rubber O-ring (Coniston profiles, UK) was placed between the T-piece and the device. The pieces were clamped tight to form a seal. PFA tubing of outer diameter 1/8 " (PFA-T2-030-500, Swagelok, USA) was used to connect to the cell via rheodyne connectors. A tubing to luer connector was manufactured from PTFE including a PFA tube fitting connector (PFA-220-2-2, Swagelok, USA). Liquids were gently pushed through the flow cell with 5 ml syringes.

Measurements of insertion loss and phase were made at a given frequency using transmission measurements on an E5061A network analyser (Agilent, CA) with the device clamped in the holder. A sample volume of 1.5 ml was needed which could be significantly reduced by minimising the tubing length and diameter if needed. Further volume reduction could also be achieved by reducing the thickness of the o-ring seal hence reducing the volume of liquid constrained over the device. The volume of liquid constrained above the SAW device in the current setup is approximately 80 μL. Flow was stopped to collect all spectra. The spectra seen on the net-

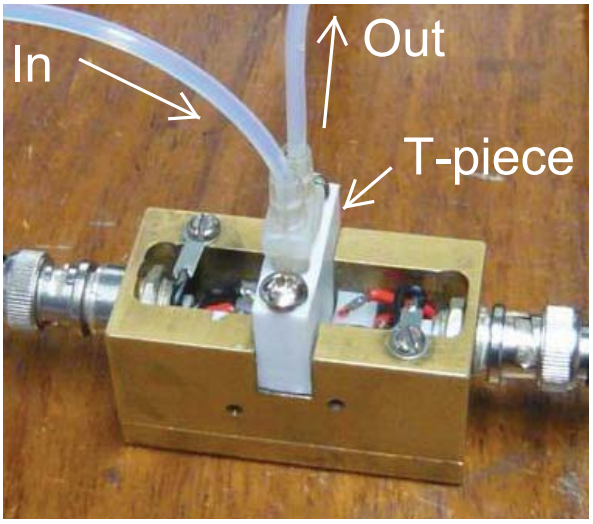

Figure VI.5: Surface acoustic wave device flowcell setup, with PTFE insert and teflon tubing making it chemically compatible with ionic liquids.

work analyser (see Figure VI.6) were saved as .csv files and later analysed using Matlab® (Mathworks, MA) to obtain the frequency of the maximum insertion loss and the phase at a chosen frequency. The frequency at which the phase was recorded was chosen to be a point on the initial resonant peak (f = 97.174 MHz for the SH-SAW and layer guided SH-SAW, 97.498 MHz for the SH-SAW with metallised path).

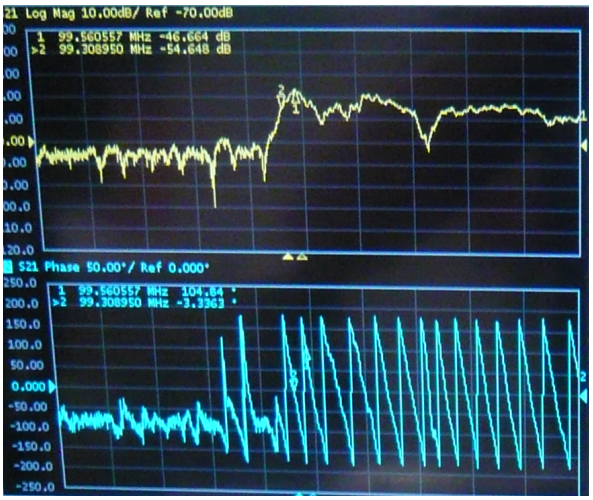

Figure VI.6: Screen shot of the surface acoustic wave device spectra seen on the network analyser showing insertion loss (top) and phase (bottom) measurements.

The flow cell was cleaned with water and methanol, flushing the flow cell with approximately 10 ml of liquid or until the phase measurement returned to its original value to insure no sample was remaining in the cell. Measurements of phase and insertion loss were made at ambient temperature (25°C) with respect to water to allow small temperature deviations to be considered. Experiments were carried out on a SH-SAW, SH-SAW with a metallised propagation path and a SH-SAW device with a silicon dioxide guiding layer of 550 nm (see Figure VI.4). To optimise the sensitivity of the device with a silicon dioxide guiding layer a characterisation plot was performed as described in Section VI.1.3.2. All devices were initially calibrated with varying con-

centrations of water-glycerol mixtures (0 - 90% v/v) to ensure the device was functioning correctly. Various concentrations (0 - 100% v/v) of $[C_2mim][EtSO_4]$ and a range of RTILs with minimal water content (see Table VI.1) were then tested.

VI.2 Results

This section is split into three studies looking at the spectral changes in the SH-SAW device, the SH-SAW device with a metallised path, and the SH-SAW device with a guiding layer of SiO_2.

VI.2.1 Surface Acoustic Wave Devices

Figures VI.7(a) and VI.7(b) show the spectra obtained for water-glycerol mixtures and various concentrations of a room temperature ionic liquid. The spectra are noticeably different depending on which type of liquid is being tested. The device is detecting a change in insertion loss, frequency, and phase for both water-glycerol solutions and RTILs with respect to the change in viscosity-density product. These changes are shown in Figures VI.8(a) and VI.8(b) and clearly show a different relationship between the two liquid types. The relationship for RTILs is most likely to be affected by the high ion content and conductivity of the liquids. As a result this device is not capable of characterising the viscosity-density product of RTILs without some form of coating or metallised path.

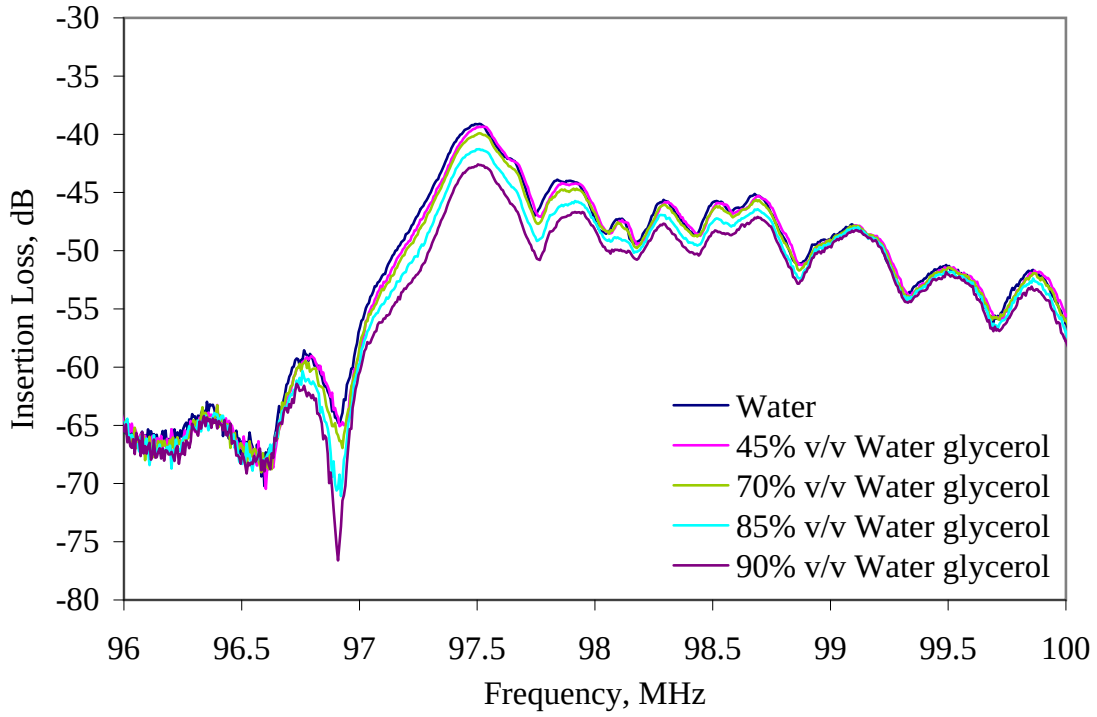

(a)

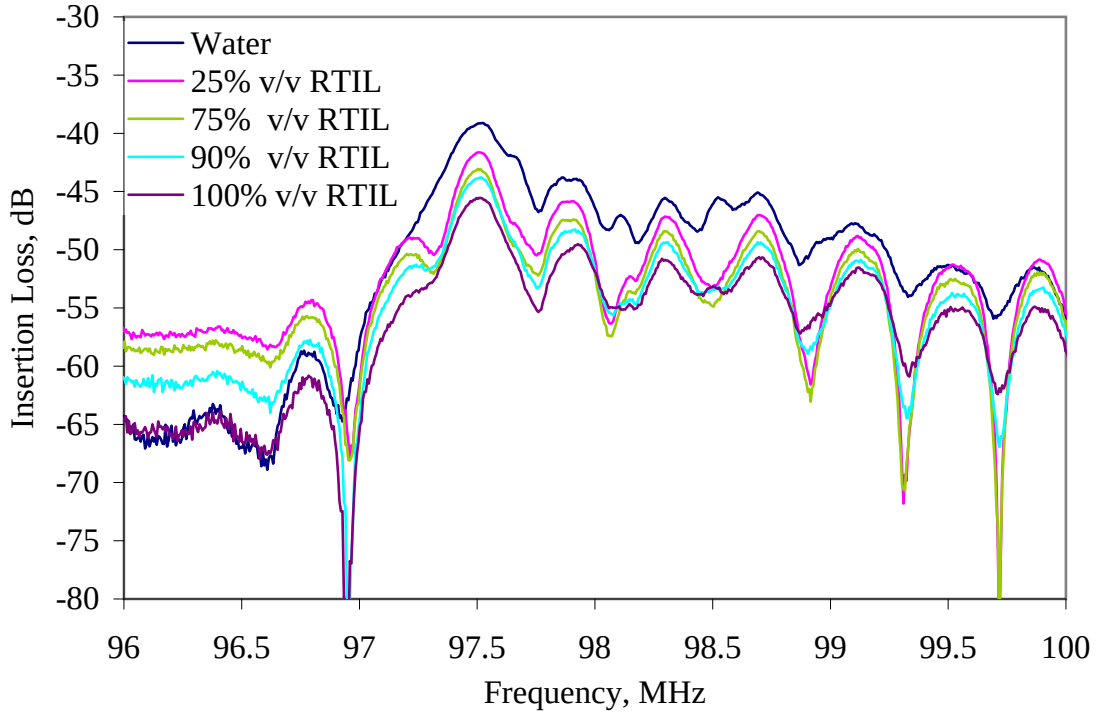

(b)

Figure VI.7: SAW Device spectra seen for (a) varying water-glycerol concentrations and (b) varying RTIL ($[C_2mim][EtSO_4]$) concentrations.

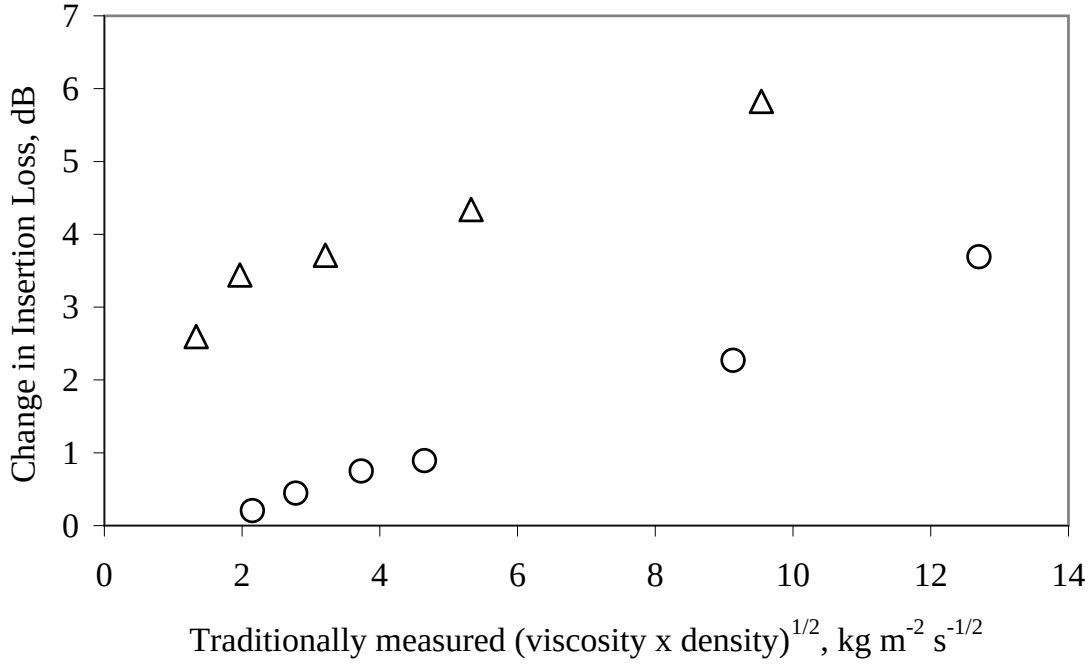

(a)

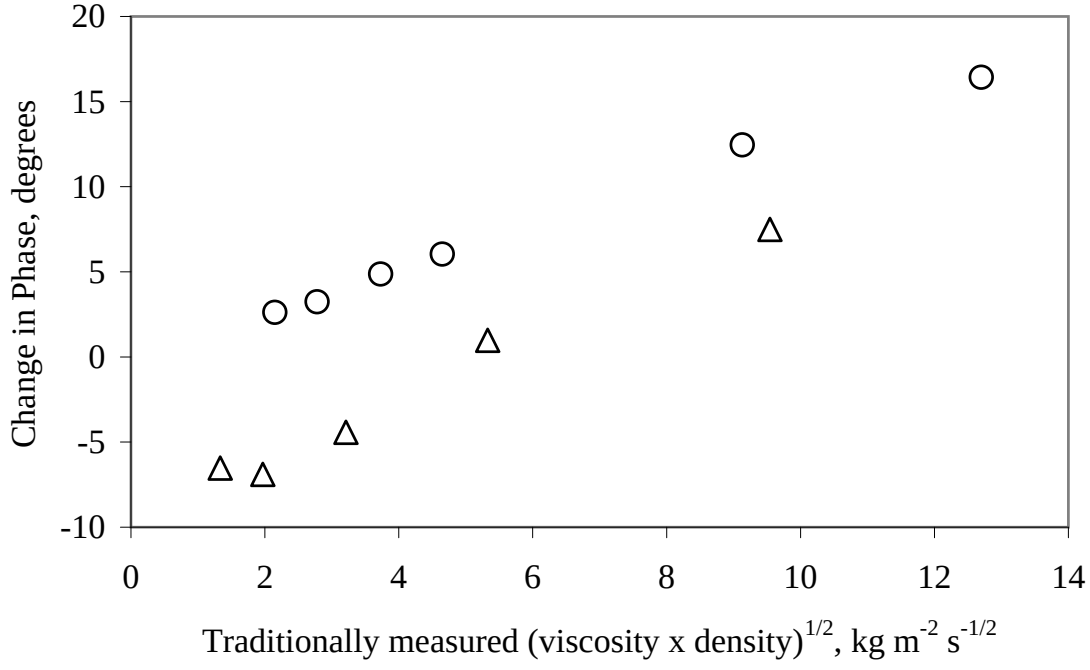

(b)

Figure VI.8: SAW Device with no guiding layer measuring the square root viscosity-density product for water-glycerol solutions (○), and dilutions of a RTIL [C_2mim][$EtSO_4$] (△) determined by (a) change in insertion loss measurements and (b) change in phase measurements (Changes are with respect to water, each point is an average of three measurements).

VI.2.2 Surface Acoustic Wave Devices with Metallised Path

Figure VI.9 shows the spectra for a SH-SAW device with a metallised path with water, 45% and 70% v/v water-glycerol and 25% v/v [C_2mim][$EtSO_4$]. The spectra show the device is not optimised with respect to the amount of gold deposition. It is however clear the device is capable of sensing water-glycerol samples using change in phase, frequency and insertion loss measurements. The ionic liquid severely damps the signal to the extent the frequency change is not truly representative of the change in square root viscosity-density product. The RTIL shown in this figure is only 25% v/v with water and as such has a low viscosity demonstrating this effect is not due to the liquid being more viscous and just signal damping. It was suggested that the metallised path may need grounding to one or both pins. This was investigated although the device responded with similar results.

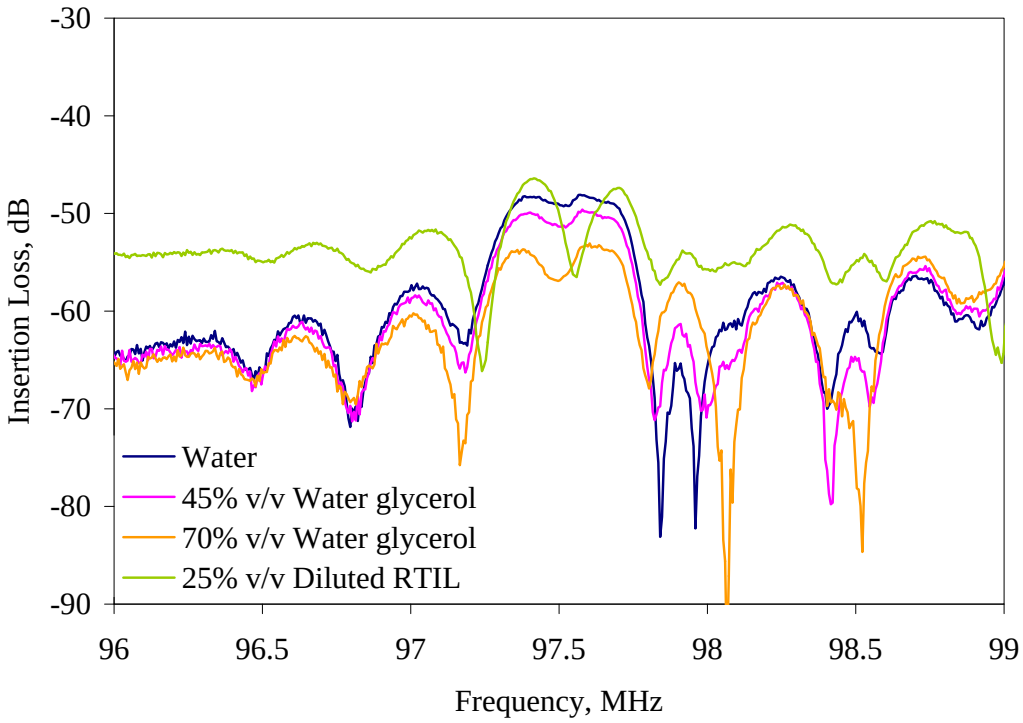

Figure VI.9: SAW Device with a metalised path, spectra produced by water-glycerol solutions, and diluted RTIL [C_2mim][$EtSO_4$].

VI.2.3 Surface Acoustic Wave Devices with a Guiding Layer

An initial characterisation plot for the thickness of SiO_2 required to optimise a layer guided SH-SAW device sensitivity is given, followed by the results obtained for various concentrations of water-glycerol and RTILs on a device with a SiO_2 layer thickness of 550 nm.

VI.2.3.1 Characterisation Plot of Guiding Layer Thickness

When working with a SAW device with a guiding layer, the thickness of the layer is critical [12]. By optimising the thickness to operate in the range of greatest change in insertion loss per additional layer thickness, the

sensitivity of the device can be optimised. Figure VI.10 shows a guiding layer thickness versus insertion loss plot to find the optimum guiding layer thickness for SiO_2. The optimum thickness is found to be approximately 550 - 800 nm as this is the region where the greatest change in insertion loss is seen.

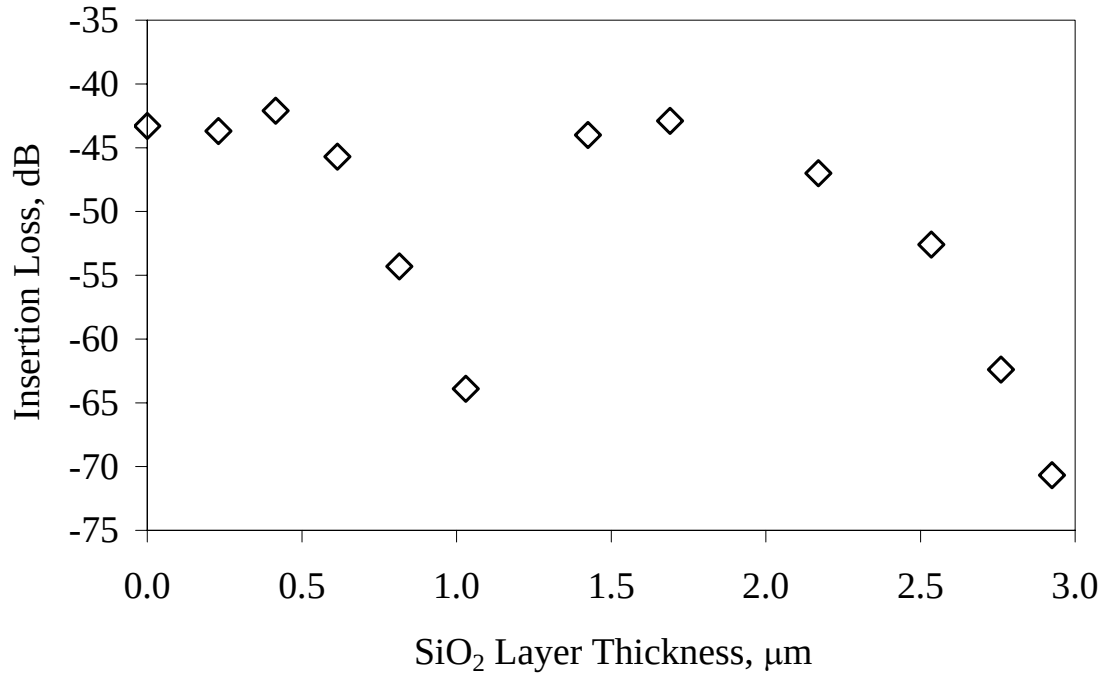

Figure VI.10: Surface acoustic wave device with a SiO_2 guiding layer showing changes in insertion loss to determine an optimum guiding layer thickness.

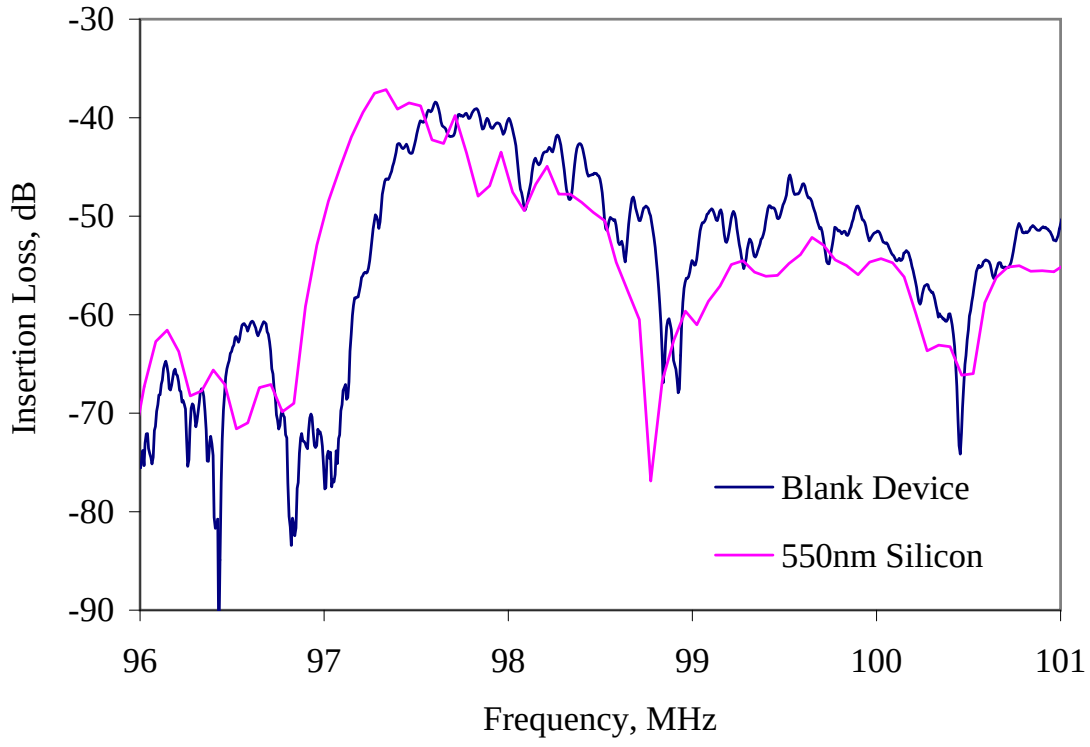

Figure VI.11: Surface acoustic wave device spectra before and after 550 nm of SiO_2 deposition.

VI.2.3.2 Liquid Phase Change and Insertion Loss Measurements

Measurements were obtained on a layer guided SH-SAW device with a SiO_2 layer of 550 nm acting as a guiding layer. Figure VI.11 shows unloaded spectra before and after the SiO_2 was added to the device. The layer has caused a small increase in insertion loss and smoothed the spectra slightly. From the change in phase seen for various concentrations of water-glycerol measurements (Figure VI.14(a)) the relationship between the square-root viscosity density product and the observed change in phase of the device can be determined. From the observed changes in phase of the device in response to RTILs, the square-root viscosity density products were calculated. These are shown in Table VI.1 with the corresponding measured viscometer and densitometer square root viscosity-density products.

Liquid	**$(\rho\eta)^{1/2}$ (kg m^{-2} s$^{-1/2}$) Viscometer-Density Meter at 25°C**	**$(\rho\eta)^{1/2}$ (kg m^{-2} s$^{-1/2}$) derived from phase measurements of Layer guided SAW 25°C**
Water-glycerol 45%	2.15	Calibration fluids
Water-glycerol 55%	2.78	
Water-glycerol 60%	3.20	
Water-glycerol 65%	3.73	
Water-glycerol 70%	4.65	
Water-glycerol 85%	9.13	
Water-glycerol 90%	12.76	
[C_2mim][$EtSO_4$] 25%	1.14	1.20
[C_2mim][$EtSO_4$] 50%	2.08	2.44
[C_2mim][$EtSO_4$]75%	4.80	5.54
[C_2mim][$EtSO_4$] 90%	5.23	5.58
[C_2mim][$EtSO_4$] 100%	9.07	8.74
[C_1mim][$MeSO_4$] 100%	10.21	10.18
[C_4mim][ACO] 100%	13.16	10.49*
[C_4mpyrr][DCA] 100%	5.78	5.88
[C_2mim][SCN] 100%	4.94	5.29
[C_4mim][TFA] 100%	9.42	8.68*
[$P_{6,6,6,14}$][NTf_2] 100%	17.04	3.34*
[C_{10}mim][NTf_2] 100%	13.87	6.15*

Table VI.1: Various concentrations (% v/v) of water-glycerol and RTILs tested on the SH-SAW device with a SiO_2 guiding layer, showing viscometer and densitometer measured square root viscosity-density product values, where * signifies the possibility of non-Newtonian behaviour as seen in Figure VI.15.

Changes in spectra for some of the ionic liquids can be seen in Figure VI.12 and show the ionic liquids behaving alike. A significant change in insertion loss and frequency can be seen with increasing viscosity. Phase spectra are shown in Figure VI.13 and show a clear change with viscosity. Phase changes were analysed at a frequency of 97.174 MHz. Phase changes with respect to water have a clear relationship with the square root viscosity-density product of the liquids with the exception of four liquids is shown in Figure VI.14(a). Changes in insertion loss also follow a similar pattern, with the majority of the liquids demonstrating good correlation

and two liquids deviating significantly as shown in Figure VI.14(b). It is possible that the liquids which do not follow the same correlation are showing non-Newtonian behaviour at this high frequency of oscillation resulting in the SAW device not sensing them correctly. It is also possible the device has reached its limit of detection. The liquids are very viscous and it may also be possible that the device is too heavily loaded.

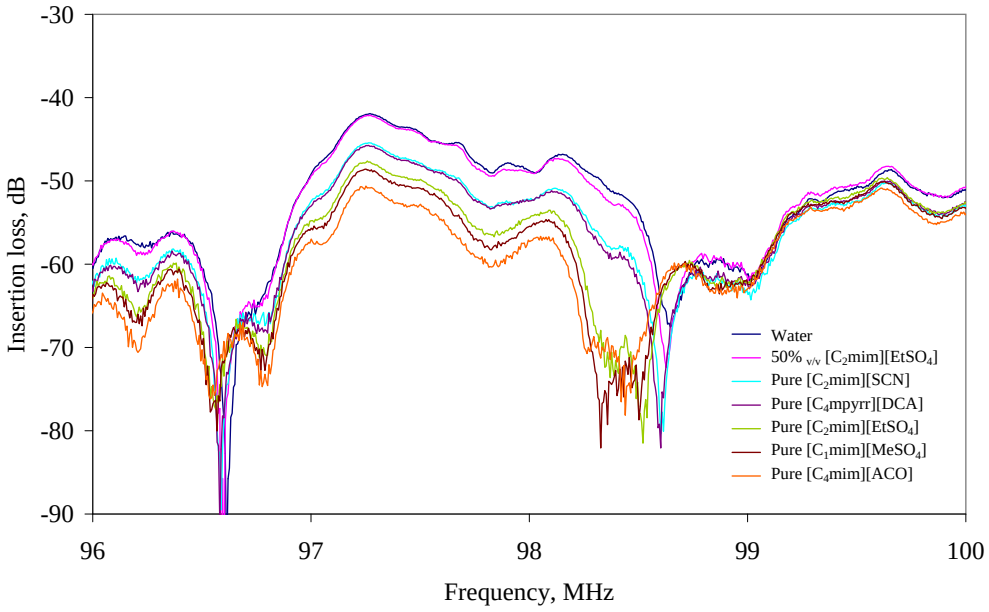

Figure VI.12: Network analyser insertion loss spectra for the SiO_2 layer guided surface acoustic wave device for several ionic liquids.

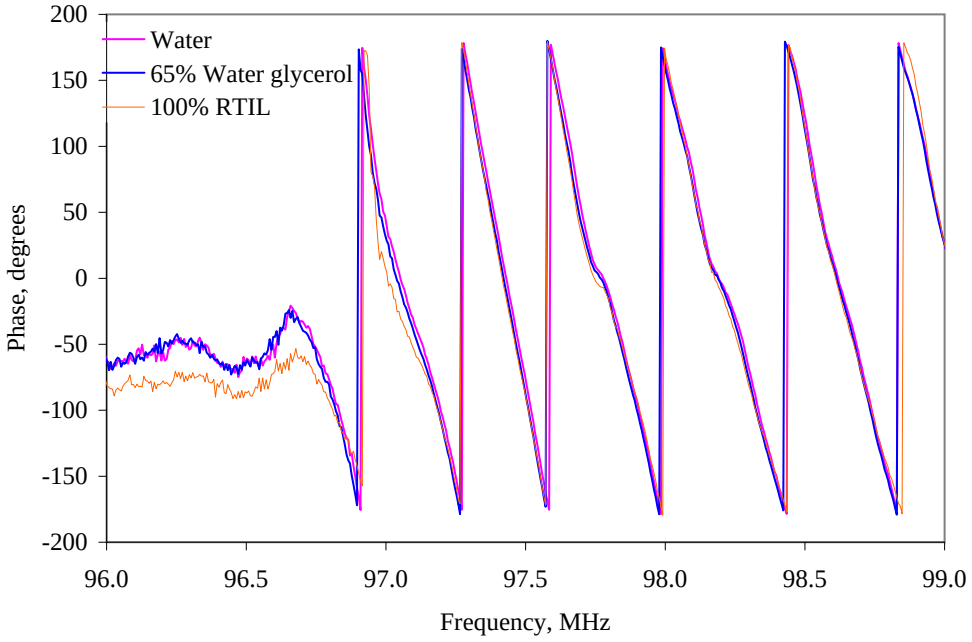

Figure VI.13: Network analyser phase spectra for the SiO_2 layer guided surface acoustic wave device for water, 65% v/v water-glycerol, and pure [C_2mim][$EtSO_4$].

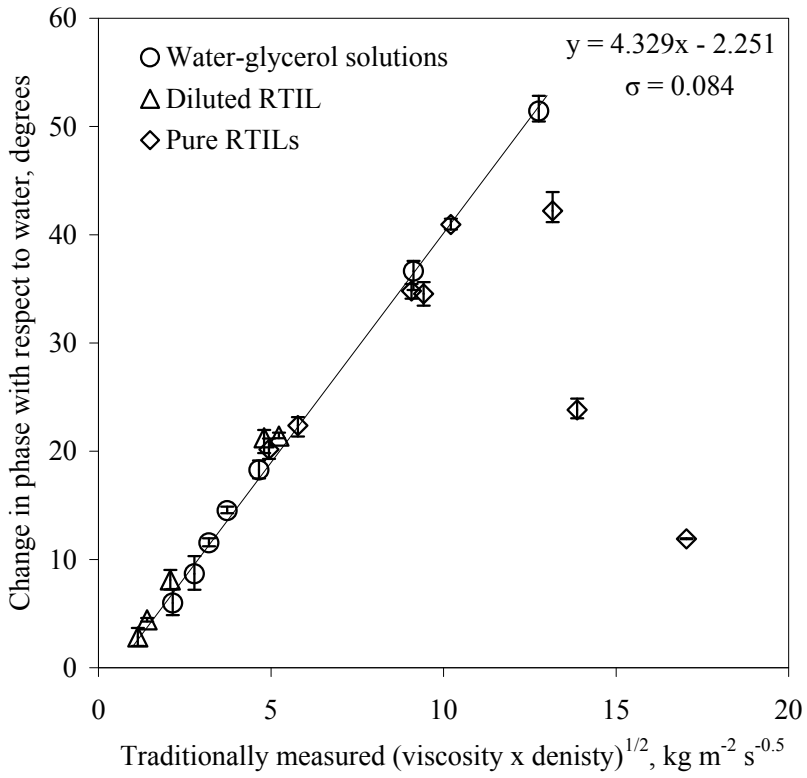

(a)

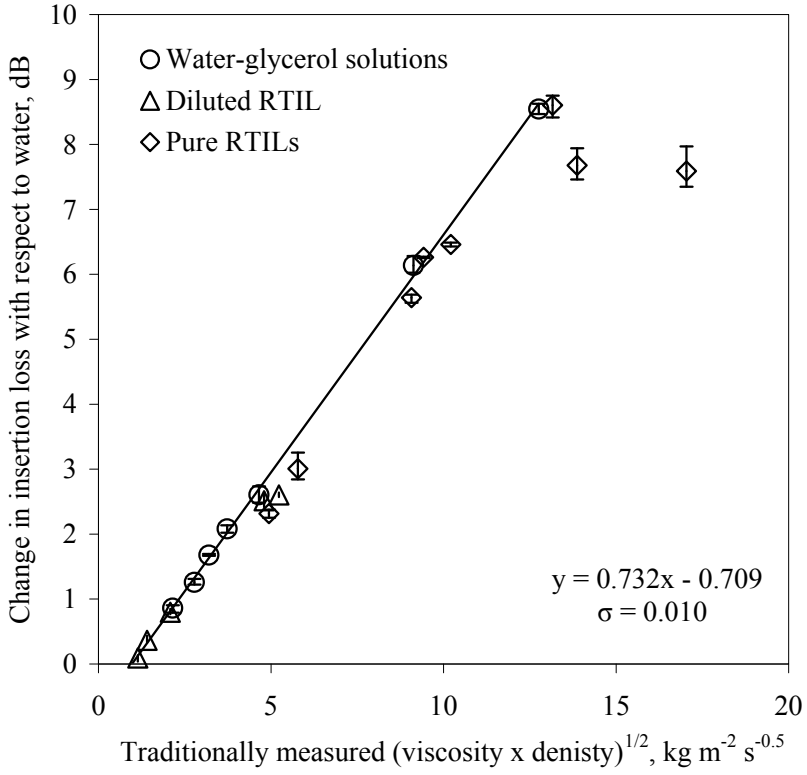

(b)

Figure VI.14: Surface acoustic wave device with a SiO_2 guiding layer showing changes in (a) phase and (b) insertion loss with response to varying square root viscosity-density product for water-glycerol solutions (○), a diluted RTIL (△), and eight pure RTILs (◇). Line of best fit and standard deviation shown only for water-glycerol solutions.

VI.2.3.2.1 Newtonian response

To determine if the liquids are behaving in a non-Newtonian manner or if the limit of detection has been reached, a plot of change in phase against change in insertion loss has been produced (see Figure VI.15).

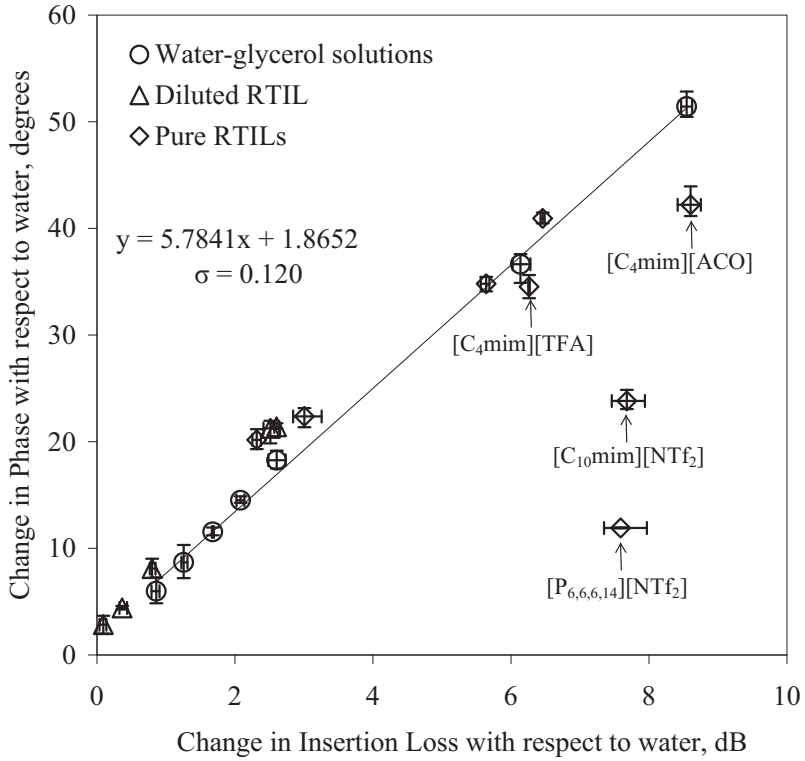

Figure VI.15: Surface acoustic wave device with a SiO_2 guiding layer showing changes in phase and insertion loss to evaluate Newtonian behaviour (see Table VI.1 for RTILs tested). Line of best fit and standard deviation calculated from water-glycerol solutions.

This plot shows water-glycerol concentrations, various concentrations of RTILs, and some pure RTILs following a simple trend, showing the liquids with Newtonian behaviour. The graphs also show some disagreement with pure RTILs ([C_{10}mim][NTf_2], [$P_{6,6,6,14}$][NTf_2], [C_4mim][ACO] and [C_4mim][TFA]) and it may be possible these are demonstrating non-Newtonian behaviour with the change in insertion loss and change in phase not following the same relationship. Three of these liquids are more viscous than the most viscous water-glycerol solution used, and it is unclear if these liquids are above the detection limit such as those described in Sections III.2.3 and V.2.2. Here, the limit of detection is found to be $\sqrt{(\rho\eta)} \approx 13$ kg m^{-2} s$^{-1/2}$.

The results for the RTILs seen here agree with those in the static pool measurements on the QCM described in Section III.2.3 for three of the four liquids. [C_{10}mim][NTf_2] is the last successful point described as Newtonian for the QCM. This particular liquid is also seen in Section V.2.2 on the 8 MHz microfluidic chip and deviates slightly from the expected square root viscosity-density product value, suggesting this liquid may be slightly non-Newtonian.

Shear rate against shear stress plots for some of the liquids were completed on the viscometer with Rheocalc

3.1 software (Brookfield, USA) over an appropriate range for each liquid to understand this behaviour more clearly. The measurements were fitted to a Bingham model [13] and agree with the data collected on the SAW device. The measurements made show $[C_4mim][ACO]$ to be slightly non-newtonian, $[C_4mim][TFA]$ and $[C_{10}mim][NTf_2]$ to be non-newtonian, and $[P_{6,6,6,14}][NTf_2]$ to be very non-newtonian. $[C_2mim][EtSO_4]$, $[C_2mim][SCN]$, $[C_4mpyrr][DCA]$, and $[C_1mim][MeSO_4]$ are clearly Newtonian from the shear rate versus shear stress plots (see Appendix C). Table VI.2 summarises the Newtonian response of the measured samples using the QCM, layer guided SAW device and rotational viscometer. Discrepancies between the responses is most likely due to the high shear rates experienced by liquids on acoustic wave devices.

Liquid	**Newtonian Response**		
	QCM	**SAW**	**Viscometer**
[C4mim][ACO]	x	x	o
[C4mim][TFA]	x	x	x
$[C_{10}mim][NTf_2]$	√	x	o
$[P_{6,6,6,14}][NTf_2]$	x	x	x
$[C_2mim][EtSO_4]$	√	√	√
$[C_2mim][SCN]$	√	√	√
$[C_4mpyrr][DCA]$	√	√	√
$[C_1mim][MeSO_4]$	-	√	√

Table VI.2: Comparison of Newtonian response seen for the QCM and layer guided SAW device. Where x is non-Newtonian response, ∘ is slight Non-Newtonian response, √ is Newtonian response and − is not tested.

VI.3 Conclusion

It is clear from the results that some form of coating or a layer guided device is needed to be able to sense room temperature ionic liquids on a surface acoustic wave device. The layer guided SH-SAW shows great potential, with a clear relationship between change in phase and insertion loss with respect to the square-root viscosity density product. This relationship breaks down at $\sqrt{(\rho\eta)} \approx 13$ kg m^{-2} s$^{-1/2}$. Above this limit no calibration liquids were measured, and as such it may be possible the limit of detection has been found. A few ionic liquids were tested above this limit and show non-Newtonian behaviour, agreeing with the traditional viscometer rheology plots for these liquids. Further Newtonian calibration liquids need to be measured to fully understand this limit. Although this setup has not decreased the sample volume required for characterisation, it has shown the layer guided SH-SAW device is capable of measuring these liquids. Miniaturisation of the device would make it possible to measure smaller volumes and gives potential for integration into future lab-on-a-chip environments for measurements on ionic liquids.

References

[1] J. Kondoh and S. Shiokawa, "Measurements of conductivity and ph of liquid using surface acoustic-wave devices," *Japanese Journal of Applied Physics Part 1 - Regular Papers Short Notes & Review Papers*, vol. 31, no. Suppl. 31-1, pp. 82–84, 1992. 12th Symp on Ultrasonic Electronics, Tokyo, Japan, Dec 02-04, 1991.

[2] A. Ricco and S. Martin, "Thin metal-film characterisation and chemical sensors-monitoring electronic conductivity, mass loading and mechanical-properties with surface acoustic-wave devices," *Thin Solid films*, vol. 206, pp. 94–101, 1991.

[3] T. Niemczyk, S. Martin, G. Frye, and A. Ricco, "Acoustoelectric interaction of plate modes with solutions," *Journal of Applied Physics*, vol. 64, no. 10, Part 1, pp. 5002–5008, 1988.

[4] S. Liew, F. Josse, D. Haworth, Z. Shana, U. Kelkar, and M. Grunze, "Applications of lithium-niobate acoustic plate modes as sensor for conductive liquids," in *IEEE 1990 Ultrasonics Symposium: Proceedings, Vols 1-3* (B. Mcavoy, ed.), pp. 285–290, IEEE, Ultrason Ferroelect & Frequency Control Soc, 1990.

[5] J. Andle, J. Vetelino, M. Lade, and D. Mcallister, "Detection of nucleic-acid hybridization with an acoustic plate mode microsensor," in *IEEE 1990 Ultrasonics Symposium: Proceedings, Vols 1-3* (B. Mcavoy, ed.), Ultrasonics Symposium, pp. 291–294, IEEE, Ultrason Ferroelect & Frequency control Soc, IEEE, 1990. IEEE 1990 Ultrasonics Symp, Honolulu, HI, Dec 04-07, 1990.

[6] F. Dickert, G. Bertlein, G. Mages, and W. Bulst, "Triphenyl methane dyes as sensor materials for solvent detection with surface-acoustic-wave devices," *Advanced Materials*, vol. 2, no. 9, pp. 420–422, 1990.

[7] M. Thompson and D. C. Stone, *Surface-Launched Acoustic Wave Sensors: Chemical Sensing and Thin-Film Characterization*. Wiley-Interscience, 1997.

[8] J. Zhao, C. Jiang, Y. Chen, H. Li, and S. He, "A study of Love wave Sensors with SU-8 guiding layers," in *2008 IEEE Ultrasonics Symposium, Vols 1-4*, Ultrasonics Symposium, (345 E 47TH ST, NY 10017 USA), pp. 1120–1123, IEEE, IEEE, 2008. IEEE Ultrasonics Symposium, Beijing, Peoples R China, Nov 02-05, 2008.

[9] M. Newton, G. McHale, and F. Martin, "Experimental study of Love wave devices with thick guiding layers," *Sensors and Actuators A-Physical*, vol. 109, no. 3, pp. 180–185, 2004.

[10] K. Kalantar-zadeh, W. Wlodarski, A. Holland, M. Austin, and H. Mendis, "Design and fabrication of a SiO2/ST-cut quartz love mode surface acoustic wave transducer for operation in liquid media," in *Commad 2000 Proceedings* (Broekman, LD and Usher, BF and Riley, JD, ed.), (345 E 47TH ST, New York, NY 10017 USA), pp. 308–311, IEEE, 2000. Conference on Optoelectronic and Microelectronic Materials and Devices, Bundoora, Australia, Dec 06-08, 2000.

[11] G. Harding and J. Du, "Design and properties of quartz-based Love wave acoustic sensors incorporating silicon dioxide and PMMA guiding layers," *Smart Materials & Structures*, vol. 6, no. 6, pp. 716–720, 1997.

[12] J. Du, G. Harding, A. Collings, and P. Dencher, "An experimental study of Love-wave acoustic sensors operating in liquids," *sensors and Actuators A-Physical*, vol. 60, no. 1-3, pp. 54–61, 1997.

[13] C. D. Collyer AA, ed., *Rheological measurement.* Elsevier Applied Science, 1988.

VII. SUMMARY AND FURTHER WORK

VII.1 Summary

The experimental work within this thesis has been presented in four separate experimental studies using small volume measurement techniques for characterising liquids. These techniques have been applied to Room Temperature Ionic Liquids with great success. The primary challenges in this project were the limited availability of liquids to test and the high viscosities of liquids, both of which have been overcome. It is very clear in each study that there is a maximum viscosity limit to both the quartz crystal microbalance (QCM) and layer guided surface acoustic wave devices used for measuring the viscosity-density product. At high viscosities it is unclear if the devices are fully loaded, and hence too damped to provide sufficient measurements, or if a breakdown in Newtonian behaviour is being observed. An alternate approach to over come this limit is to characterise the liquids at slightly higher temperatures, thus reducing liquid viscosity values to within the regime of the sensor. Both the QCM and the Love wave device have provided excellent measurements of viscosity-density values. It is clear that the acoustic wave device is the limiting factor within each study as it also sets the limiting flow rate for the lab-on-a-chip measurements (due to the thin crystal and clamping technique used). By integrating a SAW device instead of the QCM in the lab-on-a-chip setup, maximum flow rates may potentially be increased, as the frequency and sensitivity of the device is independent of crystal thickness. Discussions of alternative clamping mechanisms for the QCM may also increase the limit.

In collaboration with colleagues from Queen's University Belfast and The University of Sheffield, this experimental work has led to four peer reviewed publications [1–4]. Work has been presented at six international conferences with both oral and poster presentations, leading to three conference proceeding publications [5–7]. These conferences provided excellent opportunities to discuss work in progress and stimulate ideas.

This study contributes significantly to a future aim of having a fully operational, lab-on-a-chip set-up to characterise various properties of RTILs on a single microfluidic device. With further development, this project still has much scope and if successful, will rapidly increase the known data available on room temperature ionic liquids. Millions of liquids are yet to be characterised and as such are yet to fulfil their potential.

VII.2 Further Work

This work has provided the basis for at least three more studies: Further integration of characterisation techniques onto a single chip set up; further development of surface acoustic wave devices including optimisation and miniaturisation with the possibility of reverse sensing, where sensing takes place on the opposite side of the device to the IDTs; measurements of electrical conductivity using dual acoustic sensors. Each of these is discussed briefly in the following sections.

VII.2.1 A Laboratory-on-a-Chip System with Integrated Quartz Crystal Microbalance

One goal of this project was to overcome the technical challenges involved with a quartz crystal microbalance in a microfluidic setup. This has been achieved, and has proved very successful. An obvious next step would be to integrate this onto a single microfluidic device with many other liquid characterisation techniques such as those being developed in collaboration with other institutions. This is currently being discussed and developed with The University of Sheffield and The Queens University Belfast. This work remains focused around expanding the liquid property database [8] for RTILs. The QCM could however be an excellent technique for sensing the viscosity-density product of other less complex liquids in small volumes on chip.

Near completion of this project, an integrated chip design was produced in collaboration with The University of Sheffield and The Queens University Belfast. This has been manufactured by Micronit Microfluidics BV (The Netherlands) but unfortunately contained slight fractures in the glass. At the time of writing of this thesis a second chip is in production and will be ready for testing in June 2010.

The proposed integrated chip has two possible designs as shown in Figure VII.1 and VII.2. These vary in sample volume required. Both chips are designed to make measurements of halide concentration (electrochemical), thermal conductivity (1D conduction - steady state), specific heat capacity (1D conduction - transient), water concentration (Karl Fischer reaction - electric conduction), viscosity (using capillary viscometry (chip 1) or a dual acoustic wave sensor set up (chip 2) allowing density to also be determined) and the possibility of electrical conductivity using the open top cell (electric conduction).

The integrated glass chip needs a complex holder to allow all measurements to be made online (this is currently being developed). The glass chip is designed with open top cells to allow measurements to be decided by the user. This also gives flexibility for further developing the surface acoustic wave device. The open top cells require a large volume of liquid in relation to that needed for the remaining liquid characterisation techniques, and for this reason a ‘jumper’ has been included to bypass this cell if the measurements are not required thus conserving liquid volume. The estimated theoretical sample volume needed to make all measurements described for the first design is 45 μl, and for the second cell design 75 μl, although this may be adjusted in practice. The time needed to complete all measurements is estimated at 25 minutes per sample (this includes

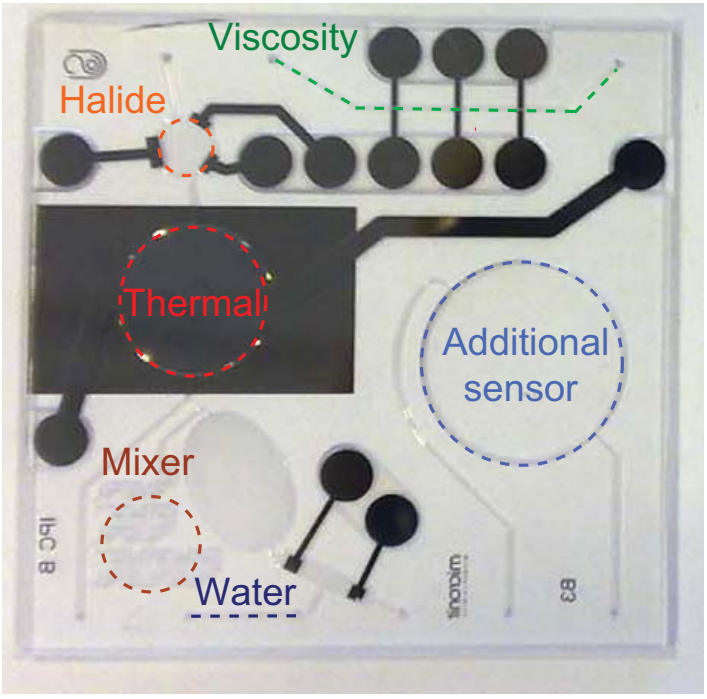

Figure VII.1: Design 1 of the integrated lab-on-a-chip for measurements of Room Temperature Ionic Liquids, where halide concentration, thermal conductivity, specific heat capacity, water concentration, viscosity-density product via acoustic wave device, and viscosity through capillary action can be measured.

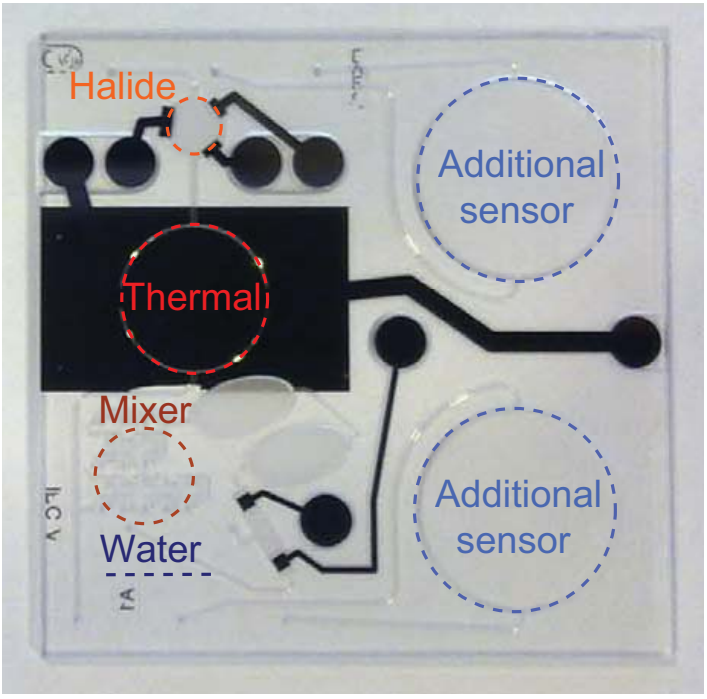

Figure VII.2: Design 2 of the integrated lab-on-a-chip for measurements of Room Temperature Ionic Liquids, where halide concentration, thermal conductivity, specific heat capacity, water concentration, viscosity-density product via acoustic wave device, and an additional open top cell for possible measurements of electrical conductivity or separate viscosity-density measurements via a dual acoustic wave device.

loading, and 10 minutes adjustment time for automated temperature control) however this theoretical estimate may change with viscosity.

This will be a very valuable system if these measurements can work with high repeatability and precision. This will rapidly advance the rate at which RTILs are characterised, and if their properties are well known, hopefully stimulate possible applications.

VII.2.2 Volume Reduction: Surface Acoustic Wave Devices

Sensing RTILs on surface acoustic waves was only attempted very briefly in this work. There is a much larger area to be explored to optimise their use with RTILs and potentially within a microfluidic setup. With the inspiration and main motivation of this project related to reducing sample volumes needed for characterisation, further sample reduction could be explored with further miniaturisation of the SH-SAW with a SiO_2 guiding layer to characterise the viscosity-density product. This project looks only at large volume sensing with the SAW, ideally a reverse sensing Acoustic Plate Mode (possibly layer guided) device. This gives a new method for electrical connection within the microfluidic setup, and is robust in terms of chemical resistance as the ionic liquid would never contact the electrodes. This could potentially allow future lab-on-a-chip designs to contain smaller open top cells, reducing volume with simpler electrical connections.

VII.2.3 Conductivity

This project has required that the challenges of acoustoelectric interactions be overcome for sensing the viscosity-density product measurements on surface acoustic wave devices. These interactions could be used to our advantage in a dual device setup to look at the changes in conductivity of the samples. This would require a reference SAW device and a SAW with a metallised propagation path. The difference between spectra should relate well to the conductivity of the liquids [9, 10]. Again these could be included into the integrated chip, with a miniaturised dual SAW device.

References

[1] N. Doy, G. McHale, M. Newton, C. Hardacre, G. Ge, J. MacInnes, D. Kuvshinov, and R. Allen, "Small volume laboratory on a chip measurements incorporating the quartz crystal microbalance to measure the viscosity-density product of room temperature ionic liquids," *Journal of Biomicrofluidics*, vol. 4, pp. 0140171–0140177, 2010.

[2] G. McHale, C. Hardacre, R. Ge, N. Doy, R. W. K. Allen, J. M. Maclnnes, M. R. Bown, and M. I. Newton, "Density-viscosity product of small-volume ionic liquid samples using quartz crystal impedance analysis," *Analytical Chemistry*, vol. 80, no. 15, pp. 5806–5811, 2008.

[3] P. Roach, S. Atherton, N. Doy, G. McHale, and M. I. Newton, "SU-8 guiding layer for love wave devices," *Sensors*, vol. 7, no. 11, pp. 2539–2547, 2007.

[4] R. Ge, R. Allen, L. Aldous, M. Bown, N. Doy, C. Hardacre, J. MacInnes, G. McHale, and M. Newton, "Evaluation of a Microfluidic Device for the Electrochemical Determination of Halide Content in Ionic Liquids," *Analytical Chemistry*, vol. 81, no. 4, pp. 1628–1637, 2009.

[5] N. Doy, G. McHale, M. Newton, C. Hardacre, R. Ge, R. Allen, and J. MacInnes, "Density and viscosity measurements of room temperature ionic liquids using patterned quartz crystal microbalances," in *Frequency Control Symposium, 2009 Joint with the 22nd European Frequency and Time forum. IEEE International*, pp. 1043 – 1045, 2009.

[6] N. Doy, G. McHale, P. Roach, M. I. Newton, C. Hardacre, R. Ge, R. W. Allen, J. M. MacInnes, and M. R. Bown, "Small volume determination of the viscosity-density product for ionic liquids using quartz crystal harmonics," in *2008 IEEE International Frequency Control Symposium, Vols 1 and 2*, pp. 440–442, 2008. IEEE International Frequency Control Symposium, Honolulu, HI, May 19-21, 2008.

[7] N. Doy, G. McHale, M. Newton, C. Hardacre, R. Ge, R. Allen, and J. MacInnes, "Separate density and viscosity determination of room temperature ionic liquids using dual quartz crystal microbalances," IEEE Sensors, The 8th Annual IEEE Conference on Sensors, Christchurch, New Zealand, 25-28 October 2009.

[8] H. Zhao, "Current studies on some physical properties of ionic liquids," *Physics and Chemistry of Liquids*, vol. 41, no. 6, pp. 545–557, 2003.

[9] S. Liew, F. Josse, D. Haworth, Z. Shana, U. Kelkar, and M. Grunze, "Applications of lithium-niobate acoustic plate modes as sensor for conductive liquids," in *IEEE 1990 Ultrasonics Symposium: Proceedings, Vols 1-3* (B. Mcavoy, ed.), pp. 285–290, IEEE, Ultrason Ferroelect & Frequency Control Soc, 1990.

[10] R. Dahint, Z. Shana, F. Josse, S. Riedel, and M. Grunze, "Identification of metal-ion solutions using acoustic plate mode devices and pattern-recognition," *IEEE Transactions on Ultrasonics Ferroelectrics and Frequency Control*, vol. 40, no. 2, pp. 114–120, 1993.

APPENDIX

A. DERIVATION OF SEPARATE VISCOSITY AND DENSITY MEASUREMENTS

In this appendix, a derivation of separate viscosity and density measurements from the Sauerbrey [1] and Kanazawa and Gordon [2] equation for a dual QCM set up is given following the approach outlined in Figure II.10.

In the following, Δf_s is change in frequency of smooth crystal, Δf_t is change in frequency of textured crystal, ρ is density of liquid, η is viscosity of liquid, h_{eff} is effective height of trap surface, f_o is frequency of unloaded smooth crystal, μ_q is shear modulus of quartz, ρ_q is density of quartz, ΔM is change in mass, and A is area of the quartz crystal.

Begin with the Sauerbrey equation for a uniform mass film,

$$\Delta f = -\frac{2f_o^2}{\sqrt{\mu_q \rho_q}} \frac{\Delta M}{A} \tag{A.1}$$

i.e.

$$\Delta f = -C_s \Delta m \tag{A.2}$$

where Δm is change in mass per unit area and C_s equals,

$$C_s = \frac{2f_o^2}{\sqrt{\mu_q \rho_q}} \tag{A.3}$$

For a liquid above a smooth flat surface the Kanazawa and Gordon equation gives,

$$\frac{\Delta f}{f_o} = -\frac{1}{Z_q}\left(\frac{f_o \rho \eta}{\pi}\right)^{1/2} = -\left(\frac{f_o \rho \eta}{\pi \mu_q \rho_q}\right)^{1/2} \tag{A.4}$$

i.e.

$$\Delta f = -\frac{1}{2}\sqrt{\frac{\rho \eta}{\pi f_o}} C_s \tag{A.5}$$

The response of a crystal with trapped liquid can be equated to a mass like layer of liquid of density ρ, with effective thickness, h_{eff}, plus a liquid response across the entire surface (Figure II.10),

$$\Delta f_t = -C_s \rho h_{eff} - \frac{1}{2}\sqrt{\frac{\rho \eta}{\pi f_o}} C_s \tag{A.6}$$

The liquid response in Equation A.6 is then assumed to be the same as the measured response due to the same liquid in contact with a crystal with a smooth flat surface, Δf_s, (Figure II.10),

$$\Delta f_t = -C_s \rho h_{eff} + \Delta f_s \tag{A.7}$$

Re-arranging gives the density,

$$\rho = \frac{(\Delta f_s - \Delta f_t)}{C_s h_{eff}} \tag{A.8}$$

Thus measuring the two frequency shifts Δf_s and Δf_t and knowing the factor C_s and texture constant h_{eff} allows the density to be extracted. Equation A.8 can also be written as,

$$\rho = \frac{\sqrt{\mu_q \rho_q}}{2 f_o^2 h_{eff}} (\Delta f_s - \Delta f_t) \tag{A.9}$$

(As in Equation II.12)

To obtain a formula for the viscosity, start with the Kanazawa and Gordon equation,

$$\Delta f_s = -f_o^{\frac{3}{2}} \left(\frac{\eta \rho}{\pi \mu_q \rho_q} \right)^{\frac{1}{2}} \tag{A.10}$$

i.e.

$$\Delta f_s^2 = f_o^3 \frac{\eta \rho}{\pi \mu_q \rho_q} \tag{A.11}$$

Substituting for density then gives,

$$\Delta f_s^2 = \frac{f_o^3 \eta \left(\frac{\sqrt{\mu_q \rho_q}}{2 f_o^2 h_{eff}} \right) (\Delta f_s - \Delta f_t)}{\pi \mu_q \rho_q} \tag{A.12}$$

i.e.

$$\Delta f_s^2 = \frac{f_o \eta \sqrt{\mu_q \rho_q} (\Delta f_s - \Delta f_t)}{\pi \mu_q \rho_q 2 h_{eff}} \tag{A.13}$$

$$\Delta f_s^2 \pi \mu_q \rho_q 2 h_{eff} = f_o \eta \sqrt{\mu_q \rho_q} (\Delta f_s - \Delta f_t) \tag{A.14}$$

Re-arranging gives the viscosity,

$$\eta = \frac{2 \Delta f_s^2 \pi \sqrt{\mu_q \rho_q} h_{eff}}{f_o (\Delta f_s - \Delta f_t)} \tag{A.15}$$

(As in Equation II.13)

In the limit of $h_{eff} = 0.5 \mu m$, Equations A.9 and A.15 are the same as those derived by Martin *et al.* [3] for the case of equal mark-space ratio texture (i.e. $L_g = L_w$).

References

[1] M. Thompson, A. Kipling, W. Duncan-Hewitt, L. Rajakovic, and B. Cavicvlasak, "Thickness-shear-mode acoustic-wave sensors in the liquid-phase - a review," *Analyst*, vol. 116, pp. 881–890, Sep 1991.

[2] K. Kanazawa and J. Gordon, "The oscillation of a frequency of a quartz resonator in contact with a liquid," *Analytica Chimica Acta*, vol. 175, pp. 99–105, 1985.

[3] S. Martin, G. Frye, and K. Wessendorf, "Sensing liquid properties with thickness-shear mode resonators," *Sensors and Actuators A-Physical*, vol. 44, no. 3, pp. 209–218, 1994.

B. RAW DATA FOR SEPARATE VISCOSITY AND DENSITY MEASUREMENTS

Raw frequency change data, for separate viscosity and density measurements seen in Chapter IV.

Liquid	Reference Δfs, Hz	Trap 1 Δft, Hz	Densitometer measured density g/cm^3	Viscometer measured viscosity, cP
Dist. Water	727	5505	0.998	1.0
Dist. Water	770	5845	0.998	1.0
Dist. Water	802	5905	0.998	1.0
40% wg	1451	6366	1.100	3.4
40% wg	1451	6066	1.100	3.4
40% wg	1461	6376	1.100	3.4
40% wg	1415	6404	1.100	3.4
55% wg	2108	6992	1.140	6.1
55% wg	2087	7037	1.140	6.1
55% wg	2083	7082	1.140	6.1
65% wg	2808	8037	1.166	12.1
65% wg	2670	8104	1.166	12.1
65% wg	2794	8135	1.166	12.1
65% wg	2659	8225	1.166	12.1
70% wg	3141	8829	1.180	16.2
70% wg	3312	8890	1.180	16.2
70% wg	3441	8750	1.180	16.2
70% wg	3230	8945	1.180	16.2
85% wg	6563	12611	1.215	67.5
85% wg	6509	12920	1.215	67.5
85% wg	6744	12940	1.215	67.5
90% wg	10060	16410	1.230	151.4
90% wg	9328	16015	1.230	151.4
90% wg	9673	15818	1.230	151.4
Ethanol	686	8252	0.786	1.1
Ethanol	796	8174	0.786	1.1
Ethanol	728	8278	0.786	1.1
[C_2mim][SCN]	3656	14008	1.118	22.9
[C_2mim][SCN]	3818	14161	1.118	22.9
[C_2mim][SCN]	3572	13851	1.118	22.9
[C_4mim][DCA]	3898	14235	1.059	27.8
[C_4mim][DCA]	3884	13972	1.059	27.8
[C_4mim][DCA]	3952	14246	1.059	27.8
[C_2mim][NTf_2]	5016	18943	1.519	29.1
[C_2mim][NTf_2]	5016	18913	1.519	29.1
[C_2mim][NTf_2]	4939	19052	1.519	29.1
[C_4mpyrr][DCA]	4268	13284	1.013	34.0
[C_4mpyrr][DCA]	4174	13397	1.013	34.0
[C_4mpyrr][DCA]	4155	13446	1.013	34.0
[C_6mim][NTf_2]	6873	20069	1.372	66.1
[C_6mim][NTf_2]	7103	19559	1.372	66.1
[C_6mim][NTf_2]	6919	19762	1.372	66.1
[C_4mpyrr][NTf_2]	7424	20559	1.395	74.1
[C_4mpyrr][NTf_2]	7336	20104	1.395	74.1
[C_4mpyrr][NTf_2]	7229	20231	1.395	74.1
[C_2mim][$EtSO_4$]	7905	19298	1.238	88.2
[C_2mim][$EtSO_4$]	7641	19067	1.238	88.2
[C_2mim][$EtSO_4$]	7313	18858	1.238	88.2
[C_{10}mim][NTf_2]	8471	20967	1.279	117.6
[C_{10}mim][NTf_2]	8748	21013	1.279	117.6
[C_{10}mim][NTf_2]	8515	20914	1.279	117.6
[C_4mim][ACO]	8981	20383	1.248	133.9
[C_4mim][ACO]	8513	20730	1.248	133.9
[C_4mim][ACO]	9184	21110	1.248	133.9

Figure B.1: Trap 1: raw frequency data for separate frequency and density measurements, where Δf_s and Δf_t are change in frequency of the smooth (reference), and patterned QCM respectively.

Liquid	Reference Δfs, Hz	Trap 2 Δft, Hz	Densitometer measured density g/cm^3	Viscometer measured viscosity, cP
Dist. Water	727	12375	0.998	1.0
Dist. Water	771	12164	0.998	1.0
Dist. Water	734	12458	0.998	1.0
Dist. Water	770	12648	0.998	1.0
Dist. Water	802	12713	0.998	1.0
40% wg	1451	14124	1.100	3.4
40% wg	1461	14120	1.100	3.4
55% wg	2108	15162	1.140	6.1
55% wg	2087	14681	1.140	6.1
55% wg	2083	15279	1.140	6.1
65% wg	2808	16355	1.166	12.1
65% wg	2670	16268	1.166	12.1
65% wg	2794	16353	1.166	12.1
65% wg	2659	16264	1.166	12.1
70% wg	3141	17039	1.180	16.2
70% wg	3312	17078	1.180	16.2
70% wg	3230	17126	1.180	16.2
85% wg	6563	21000	1.215	67.5
85% wg	6509	21212	1.215	67.5
85% wg	6744	21264	1.215	67.5
90% wg	10060	24450	1.230	151.4
90% wg	9328	24040	1.230	151.4
90% wg	9673	24015	1.230	151.4
Ethanol	686	10518	0.786	1.1
Ethanol	796	10423	0.786	1.1
Ethanol	728	10524	0.786	1.1
[C_2mim][SCN]	3572	17168	1.118	22.9
[C_2mim][SCN]	3611	17071	1.118	22.9
[C_2mim][SCN]	3575	17233	1.118	22.9
[C_4mim][DCA]	3898	16832	1.059	27.8
[C_4mim][DCA]	3884	16711	1.059	27.8
[C_4mim][DCA]	3952	16942	1.059	27.8
[C_2mim][NTf_2]	5016	23995	1.519	29.1
[C_2mim][NTf_2]	5016	23572	1.519	29.1
[C_2mim][NTf_2]	4939	23986	1.519	29.1
[C_4mpyrr][DCA]	4268	16582	1.013	34.0
[C_4mpyrr][DCA]	4174	16646	1.013	34.0
[C_4mpyrr][DCA]	4155	16574	1.013	34.0
[C_6mim][NTf_2]	6873	24454	1.372	66.1
[C_6mim][NTf_2]	7103	24014	1.372	66.1
[C_6mim][NTf_2]	6919	23847	1.372	66.1
[C_4mpyrr][NTf_2]	7424	25219	1.395	74.1
[C_4mpyrr][NTf_2]	7336	24139	1.395	74.1
[C_4mpyrr][NTf_2]	7229	24481	1.395	74.1
[C_2mim][$EtSO_4$]	7470	23061	1.238	88.2
[C_2mim][$EtSO_4$]	7905	23347	1.238	88.2
[C_2mim][$EtSO_4$]	7641	22513	1.238	88.2
[C_2mim][$EtSO_4$]	7313	22677	1.238	88.2
[C_{10}mim][NTf_2]	8471	24710	1.279	117.6
[C_{10}mim][NTf_2]	8748	24832	1.279	117.6
[C_{10}mim][NTf_2]	8515	24665	1.279	117.6
[C_4mim][ACO]	8981	24376	1.248	133.9
[C_4mim][ACO]	8513	25398	1.248	133.9
[C_4mim][ACO]	9184	24741	1.248	133.9

Figure B.2: Trap 2: raw frequency data for separate frequency and density measurements, where Δf_s and Δf_t are change in frequency of the smooth (reference), and patterned QCM respectively.

Liquid	Reference Δfs, Hz	Trap 3 Δft, Hz	Densitometer measured density g/cm^3	Viscometer measured viscosity, cP
Dist. Water	727	10788	0.998	1.0
Dist. Water	771	10967	0.998	1.0
Dist. Water	734	10960	0.998	1.0
Dist. Water	770	10978	0.998	1.0
Dist. Water	802	10977	0.998	1.0
40% wg	1451	12461	1.100	3.4
40% wg	1451	12545	1.100	3.4
40% wg	1461	12496	1.100	3.4
40% wg	1415	12570	1.100	3.4
55% wg	2108	13577	1.140	6.1
55% wg	2087	13478	1.140	6.1
55% wg	2083	13466	1.140	6.1
65% wg	2808	14465	1.166	12.1
65% wg	2670	14689	1.166	12.1
65% wg	2794	14463	1.166	12.1
65% wg	2659	14545	1.166	12.1
70% wg	3141	15221	1.180	16.2
70% wg	3312	15420	1.180	16.2
70% wg	3441	15302	1.180	16.2
70% wg	3230	15270	1.180	16.2
85% wg	6563	19030	1.215	67.5
85% wg	6509	19018	1.215	67.5
85% wg	6744	19018	1.215	67.5
90% wg	9359	21840	1.230	151.4
90% wg	9328	22153	1.230	151.4
90% wg	9673	21956	1.230	151.4
Ethanol	686	9047	0.789	1.1
Ethanol	796	8949	0.786	1.1
Ethanol	728	8992	0.786	1.1
[C_2mim][SCN]	3656	14938	1.118	22.9
[C_2mim][SCN]	3818	14743	1.118	22.9
[C_2mim][SCN]	3778	15035	1.118	22.9
[C_4mim][DCA]	3898	14734	1.059	27.8
[C_4mim][DCA]	3884	14782	1.059	27.8
[C_4mim][DCA]	3952	14734	1.059	27.8
[C_2mim][NTf_2]	5016	21173	1.519	29.1
[C_2mim][NTf_2]	5016	20972	1.519	29.1
[C_2mim][NTf_2]	4939	21130	1.519	29.1
[C_4mpyrr][DCA]	4268	14227	1.013	34.0
[C_4mpyrr][DCA]	4174	14223	1.013	34.0
[C_4mpyrr][DCA]	4155	14544	1.013	34.0
[C_6mim][NTf_2]	6873	21979	1.372	66.1
[C_6mim][NTf_2]	7103	21997	1.372	66.1
[C_6mim][NTf_2]	6919	21721	1.372	66.1
[C_4mpyrr][NTf_2]	7424	22782	1.395	74.1
[C_4mpyrr][NTf_2]	7336	22489	1.395	74.1
[C_4mpyrr][NTf_2]	7229	22193	1.395	74.1
[C_2mim][$EtSO_4$]	7470	20256	1.238	88.2
[C_2mim][$EtSO_4$]	7641	20272	1.238	88.2
[C_2mim][$EtSO_4$]	7313	20270	1.238	88.2
[C_{10}mim][NTf_2]	8471	22424	1.279	117.6
[C_{10}mim][NTf_2]	8748	22373	1.279	117.6
[C_{10}mim][NTf_2]	8515	22370	1.279	117.6
[C_4mim][ACO]	8981	22575	1.248	133.9
[C_4mim][ACO]	8513	21696	1.248	133.9
[C_4mim][ACO]	9184	22557	1.248	133.9

Figure B.3: Trap 3: raw frequency data for separate frequency and density measurements, where Δf_s and Δf_t are change in frequency of the smooth (reference), and patterned QCM respectively.

Liquid	Reference Δfs, Hz	Trap 4 Δft, Hz	Densitometer measured density g/cm^3	Viscometer measured viscosity, cP
Dist. Water	727	8558	0.998	1.0
Dist. Water	770.1	8333	0.998	1.0
Dist. Water	734	8759	0.998	1.0
Dist. Water	770	8806	0.998	1.0
Dist. Water	802	8826	0.998	1.0
40% wg	1451	10144	1.100	3.4
40% wg	1451	10084	1.100	3.4
55% wg	2108	10978	1.140	6.1
55% wg	2087	10985	1.140	6.1
55% wg	2083	10945	1.140	6.1
65% wg	2808	11851	1.166	12.1
65% wg	2670	11940	1.166	12.1
65% wg	2794	11989	1.166	12.1
65% wg	2659	11914	1.166	12.1
70% wg	3141	12488	1.180	16.2
70% wg	3312	12528	1.180	16.2
70% wg	3441	12585	1.180	16.2
70% wg	3230	12516	1.180	16.2
85% wg	6563	16179	1.215	67.5
85% wg	6509	15994	1.215	67.5
85% wg	6744	16044	1.215	67.5
90% wg	9359	18946	1.230	151.4
90% wg	9328	18959	1.230	151.4
90% wg	9673	18888	1.230	151.4
Ethanol	686	7438	0.786	1.1
Ethanol	796	7692	0.786	1.1
Ethanol	728	7582	0.786	1.1
[C_2mim][SCN]	3656	12265	1.118	22.9
[C_2mim][SCN]	3818	12022	1.118	22.9
[C_2mim][SCN]	3777	12054	1.118	22.9
[C_4mim][DCA]	3898	12038	1.059	27.8
[C_4mim][DCA]	3884	12215	1.059	27.8
[C_4mim][DCA]	3952	12291	1.059	27.8
[C_2mim][NTf_2]	5016	17976	1.519	29.1
[C_2mim][NTf_2]	5016	18136	1.519	29.1
[C_2mim][NTf_2]	4939	18079	1.519	29.1
[C_4mpyrr][DCA]	4268	12157	1.013	34.0
[C_4mpyrr][DCA]	4174	12113	1.013	34.0
[C_4mpyrr][DCA]	4155	12043	1.013	34.0
[C_6mim][NTf_2]	6985	19069	1.372	66.1
[C_6mim][NTf_2]	7103	18794	1.372	66.1
[C_6mim][NTf_2]	6919	18592	1.372	66.1
[C_4mpyrr][NTf_2]	7424	19570	1.395	74.1
[C_4mpyrr][NTf_2]	7336	19197	1.395	74.1
[C_4mpyrr][NTf_2]	7229	19010	1.395	74.1
[C_2mim][$EtSO_4$]	7641	17353	1.238	88.2
[C_2mim][$EtSO_4$]	7313	17086	1.238	88.2
[C_{10}mim][NTf_2]	8471	19574	1.279	117.6
[C_{10}mim][NTf_2]	8748	19653	1.279	117.6
[C_{10}mim][NTf_2]	8515	19599	1.279	117.6
[C_4mim][ACO]	8981	19370	1.248	133.9
[C_4mim][ACO]	8513	19262	1.248	133.9
[C_4mim][ACO]	9184	19491	1.248	133.9

Figure B.4: Trap 4: raw frequency data for separate frequency and density measurements, where Δf_s and Δf_t are change in frequency of the smooth (reference), and patterned QCM respectively.

Liquid	Reference Δfs, Hz	Trap 5 Δft, Hz	Densitometer measured density g/cm^3	Viscometer measured viscosity, cP
Dist. Water	727	7990	0.998	1.0
Dist. Water	770.1	8010	0.998	1.0
Dist. Water	734	7843	0.998	1.0
Dist. Water	770	8022	0.998	1.0
Dist. Water	802	8054	0.998	1.0
40% wg	1451	9150	1.100	3.4
40% wg	1451	9036	1.100	3.4
40% wg	1461	9061	1.100	3.4
55% wg	2108	9818	1.140	6.1
55% wg	2087	9819	1.140	6.1
55% wg	2083	9954	1.140	6.1
65% wg	2808	10830	1.166	12.1
65% wg	2670	10713	1.166	12.1
65% wg	2794	10772	1.166	12.1
65% wg	2659	10719	1.166	12.1
70% wg	3141	11331	1.180	16.2
70% wg	3312	11431	1.180	16.2
70% wg	3441	11242	1.180	16.2
70% wg	3230	11183	1.180	16.2
85% wg	6563	14612	1.215	67.5
85% wg	6509	14897	1.215	67.5
85% wg	6744	14902	1.215	67.5
90% wg	9359	17449	1.230	151.4
90% wg	9328	16864	1.230	151.4
90% wg	9673	17604	1.230	151.4
Ethanol	686	6487	0.786	1.1
Ethanol	796	7293	0.786	1.1
Ethanol	728	7644	0.786	1.1
[C_2mim][SCN]	3656	10987	1.118	22.9
[C_2mim][SCN]	3818	11279	1.118	22.9
[C_2mim][SCN]	3777	11155	1.118	22.9
[C_4mim][DCA]	3898	11033	1.059	27.8
[C_4mim][DCA]	3884	11129	1.059	27.8
[C_4mim][DCA]	3952	10958	1.059	27.8
[C_2mim][NTf_2]	5016	17901	1.519	29.1
[C_2mim][NTf_2]	5016	18069	1.519	29.1
[C_2mim][NTf_2]	4939	17819	1.519	29.1
[C_4mpyrr][DCA]	4268	10736	1.013	34.0
[C_4mpyrr][DCA]	4174	10835	1.013	34.0
[C_4mpyrr][DCA]	4155	11028	1.013	34.0
[C_6mim][NTf_2]	6873	18926	1.372	66.1
[C_6mim][NTf_2]	7103	18422	1.372	66.1
[C_6mim][NTf_2]	6919	18586	1.372	66.1
[C_4mpyrr][NTf_2]	7424	19100	1.395	74.1
[C_4mpyrr][NTf_2]	7336	18814	1.395	74.1
[C_4mpyrr][NTf_2]	7229	18779	1.395	74.1
[C_2mim][$EtSO_4$]	7470	16274	1.238	88.2
[C_2mim][$EtSO_4$]	7905	16015	1.238	88.2
[C_2mim][$EtSO_4$]	7641	16045	1.238	88.2
[C_2mim][$EtSO_4$]	7313	15669	1.238	88.2
[C_{10}mim][NTf_2]	8471	19104	1.279	117.6
[C_{10}mim][NTf_2]	8748	19127	1.279	117.6
[C_{10}mim][NTf_2]	8515	18857	1.279	117.6
[C_4mim][ACO]	8981	18452	1.248	133.9
[C_4mim][ACO]	8513	18291	1.248	133.9
[C_4mim][ACO]	9184	18281	1.248	133.9

Figure B.5: Trap 5: raw frequency data for separate frequency and density measurements, where Δf_s and Δf_t are change in frequency of the smooth (reference), and patterned QCM respectively.

C. VISCOMETER PLOTS

Viscometer plots for some water-glycerol concentrations, various concentrations of an ionic liquid and some pure liquid RTILs are measured below at 25 °C:

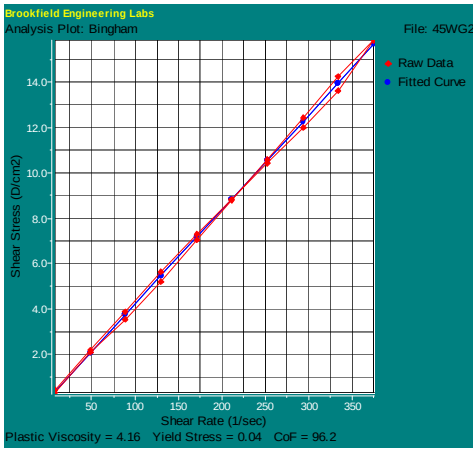

(a) 45% v/v Water-glycerol

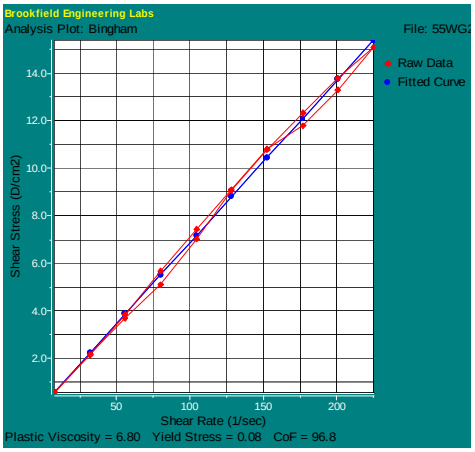

(b) 55% v/v Water-glycerol

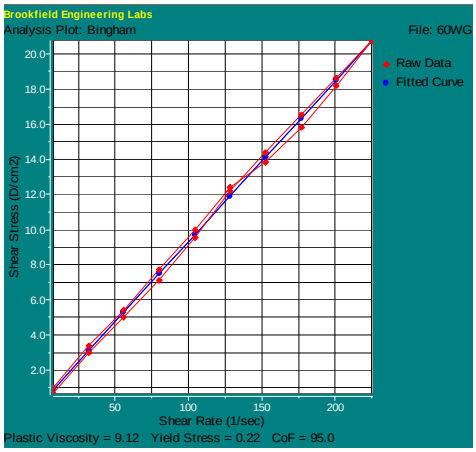

(c) 60% v/v Water-glycerol

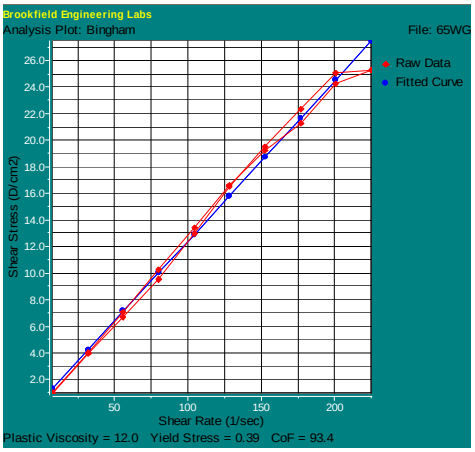

(d) 65% v/v Water-glycerol

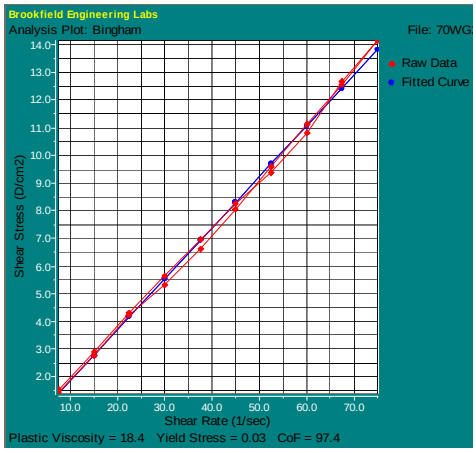

(e) 70% v/v Water-glycerol

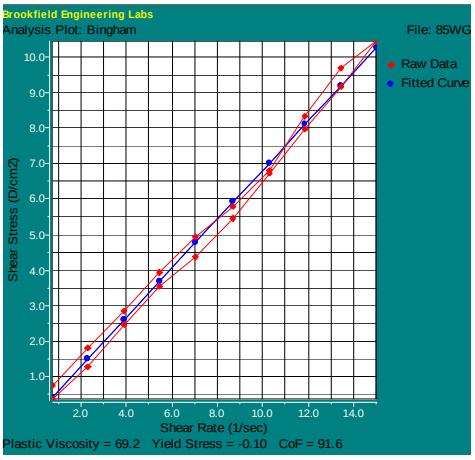

(f) 85% v/v Water-glycerol

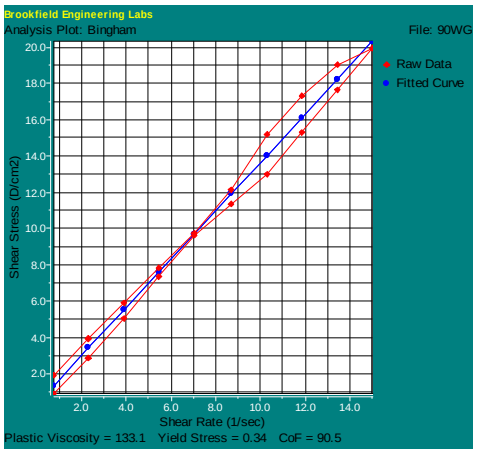

(g) 90% v/v Water-glycerol

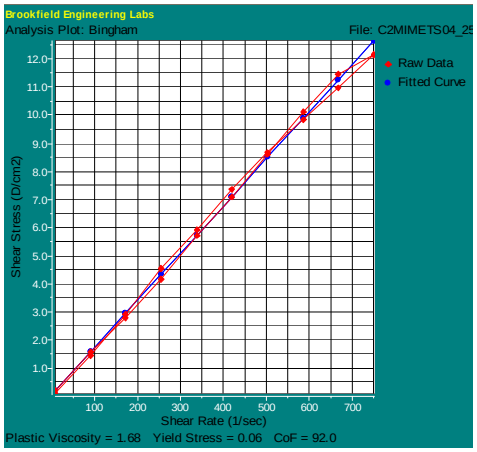

(h) 25% v/v (C_2mim)($EtSO_4$)

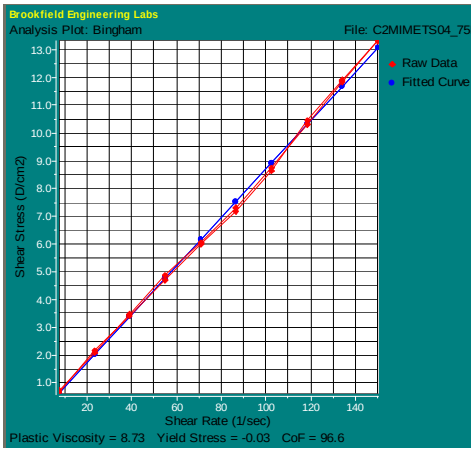

(i) 75% v/v (C_2mim)($EtSO_4$)

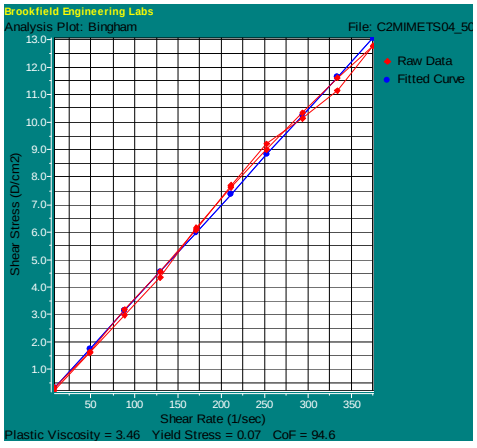

(j) 50% v/v (C_2mim)($EtSO_4$)

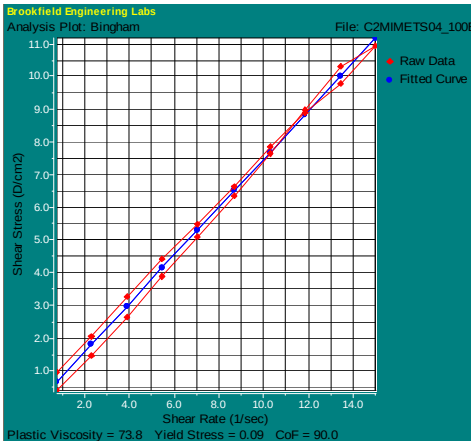

(k) 100% v/v (C_2mim)($EtSO_4$)

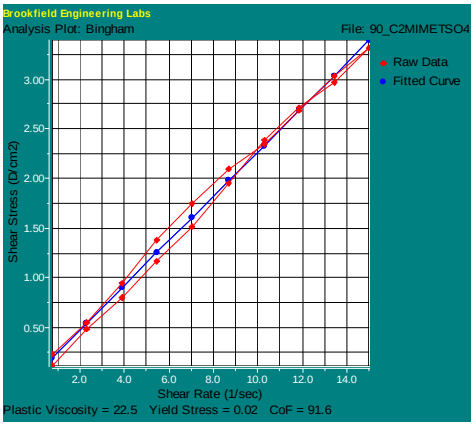

(l) 90% v/v (C_2mim)($EtSO_4$)

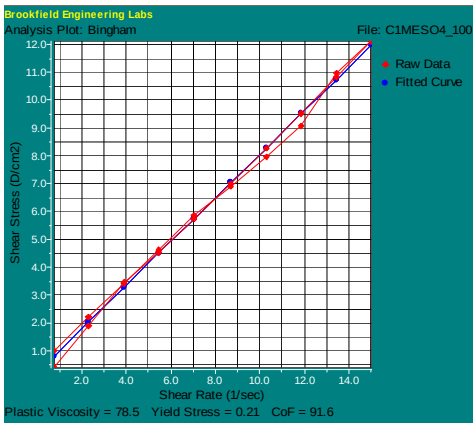

(m) (C_1)(MeSO4)

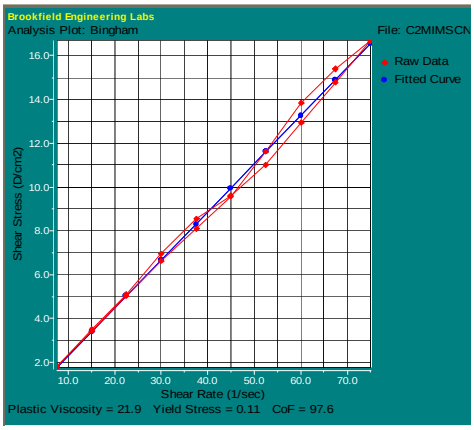

(n) (C_2mim)(SCN)

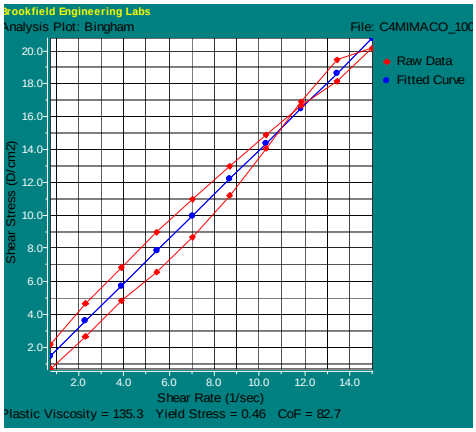

(o) (C_4mim)(ACO)

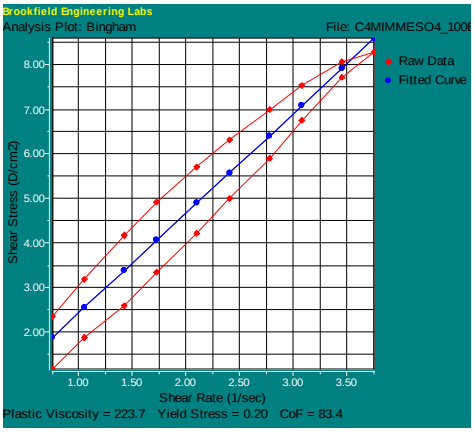

(p) (C_4mim)($MeSO_4$)

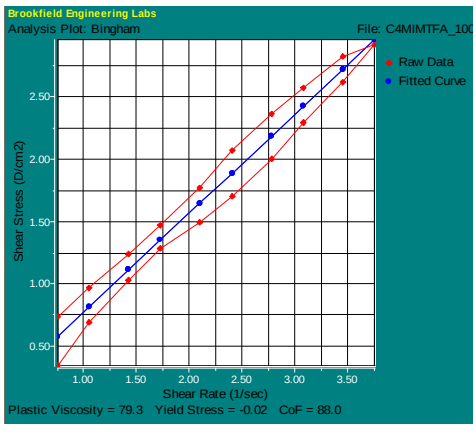

(q) (C_4mim)(TFA)

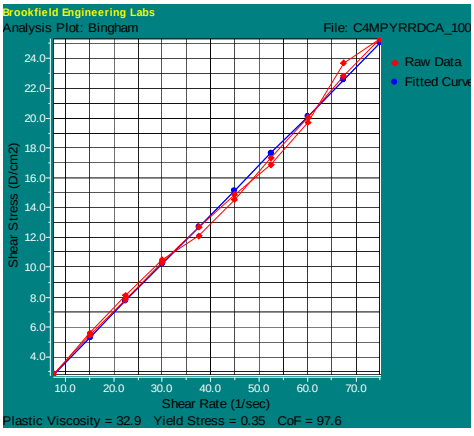

(r) (C_4mpyrr)(DCA)

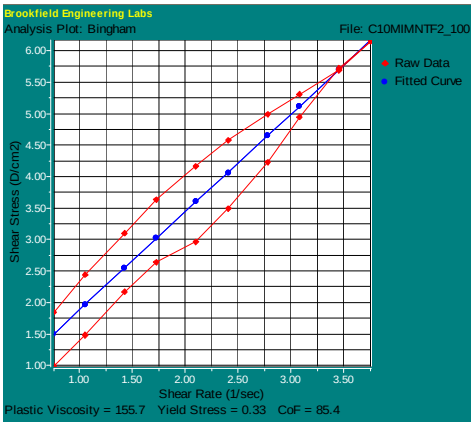

(s) (C_{10}mim)(NTf_2)

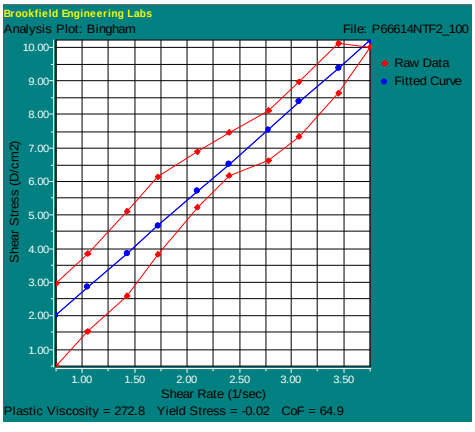

(t) ($P_{6,6,6,14}$mim)(NTf_2)

D. PUBLICATIONS

D.1 Sensors

Sensors **2007**, *7*, 2539-2547

sensors
ISSN 1424-8220

www.mdpi.org/sensors

Full Paper

SU-8 Guiding Layer for Love Wave Devices

Paul Roach*, Shaun Atherton, Nicola Doy, Glen McHale and Michael I. Newton

School of Science and Technology, Nottingham Trent University, Clifton Campus, Nottingham. NG11 8NS. United Kingdom

* Author to whom correspondence should be addressed; Email: Paul.Roach@ntu.ac.uk;
Tel: +44(0)115-848-8062; Fax: +44(0)115-848-6616

Received: 1 October 2007 / Accepted: 31 October 2007 / Published: 1 November 2007

Abstract: SU-8 is a technologically important photoresist used extensively for the fabrication of microfluidics and MEMS, allowing high aspect ratio structures to be produced. In this work we report the use of SU-8 as a Love wave sensor guiding layer which allows the possibility of integrating a guiding layer with flow cell during fabrication. Devices were fabricated on ST-cut quartz substrates with a single-single finger design such that a surface skimming bulk wave (SSBW) at 97.4 MHz was excited. SU-8 polymer layers were successively built up by spin coating and spectra recorded at each stage; showing a frequency decrease with increasing guiding layer thickness. The insertion loss and frequency dependence as a function of guiding layer thickness was investigated over the first Love wave mode. Mass loading sensitivity of the resultant Love wave devices was investigated by deposition of multiple gold layers. Liquid sensing using these devices was also demonstrated; water-glycerol mixtures were used to demonstrate sensing of density-viscosity and the physical adsorption and removal of protein was also assessed using albumin and fibrinogen as model proteins.

Keywords: Love wave, SU-8, SU-8 guiding layer, SH-SAW

1. Introduction

Surface acoustic wave (SAW) devices are widely used in sensing applications with a number of variants being used in many research fields [1, 2]. One of the simplest types of SAW device uses a Rayleigh wave, which propagates with an elliptical particle displacement through the substrate parallel

to the direction of the wave. The energy of the wave is not confined to the surface, although the amplitude of the wave decays into the depth of the substrate. These types of sensors cannot be used in liquids due to the direction of mechanical displacement allowing dampening of the wave to occur. Shear horizontally polarized SAWs (SH-SAW), propagating with a particle displacement perpendicular to the wave motion, can be used in liquids but similarly are not confined to the surface of the substrate. Love waves may be propagated when an overlayer is added on the surface of a SH-SAW or surface skimming bulk wave (SSBW) device. Such a wave will be supported if the guiding layer material has a shear speed less than that of the substrate [3]. An enhancement in device sensitivity can therefore be achieved, with Love waves offering one of the highest mass sensitivities. Love wave sensors have been used for a variety of applications including the detection of biological analytes [4, 5] liquid properties [6, 7] and evaporation kinetics [8].

Due to their ability to be used in an aqueous environment and their sensitivity, Love wave sensors are often used as biosensors. Different guiding layer materials have been reported such as polymethylmethacrylate (PMMA) [9, 10] positive photoresists [11] SiO_2 [12] and multi-layer polymer/SiO_2 structures [13]. Although silica guiding layers display low acoustic losses in the MHz range their fabrication by deposition techniques is lengthy, and thick layers (~6 μm) are required to support a Love wave if quartz substrates are used due to the materials' similar acoustic velocities [14]. Thin polymer layers (~2 μm) will support a Love wave and can be spun on relatively easily. PMMA based devices exhibit lower sensitivities compared to silica, possibly due to the high internal losses occurring in the guiding layer.

One of the disadvantages of using Love wave devices is that the interdigital transducers (IDTs) are on the same side as the sensing surface. The operation of such devices in liquids can result in electrical short circuits. Harsh liquids may even damage the IDTs. For these reasons the guiding layer is often extended across the whole face of the device to avoid the use of complicated o-rings and sealed units. The use of different materials to protect the IDTs has been reported – specifically SU-8, an epoxy based negative photo resist [15]. SU-8 was used only as a protective layer to cover the IDTs whilst silicon dioxide was deposited as a guiding layer material between the IDTs. These devices were made in a multistage process, wherein silicon dioxide was grown by chemical vapour deposition, patterned between the IDTs by photolithography, with SU-8 being applied in a later process. SU-8 is spun on to a desired thickness and soft baked to remove solvent. Reactive sites within the SU-8 polymer are created during UV irradiation, which, upon heating cross-link to form a strong, hard, chemically inert surface resilient to acids, bases and solvents. [16] By using SU-8 as a guiding layer covering the IDTs any complicated and time consuming deposition of silicon dioxide wave guide layers would be reduced to a simple spin-on process. Devices would be sensitive, durable and chemically resistant.

Here we present use of SU-8 as a Love wave guiding layer material. SU-8 is assessed in terms of the thickness required to support a Love wave, with the first mode being examined. Frequency and insertion loss of the devices were monitored with increasing guiding layer thickness. The sensitivities of devices with different thickness SU-8 guiding layers were assessed by gold deposition, and liquid sensing was demonstrated using water-glycerol mixtures and protein adsorption studies.

2. Experimental Section

Love wave devices were fabricated on ST-cut quartz with propagation orthogonal to the crystal direction. The IDTs consisted of sputtered gold (80 nm, Emitech) over titanium (10 nm, Emitech) as an adhesive layer, deposited using an Emitech K757X sputter coater. A single-single finger design was used. Finger widths and spacings were 12.8 μm, with each IDT being 4.5 mm in length, with an aperture of 4 mm and IDT centre-centre distance of 12 mm. SU-8 is a negative photoresist requiring a multistage process to form a semi-rigid layer. Parameters were defined such that the polymer was spin coated onto a device to achieve a desired thickness, soft-baked to remove solvent before UV exposure and hard-baking to allow cross linking to take place. Once hard-baked SU-8 has the advantage over other polymers often used as a guiding layer material being mechanically reliable and almost completely chemically inert. The thickness of each layer was determined by stylus and optical profilometry, being measured at 0.56 μm. The SU-8 guiding layers were successively built up using SU-8-10 (Microposit) diluted in 1-methoxy-2-propanol acetate (Aldrich, 98+%). These were spun to achieve a single layer thickness of 0.56 μm (verified using a Veeco Dektak 6M stylus profiler and an optical Veeco Dektak 3 surface analysis system.) Each layer added was prebaked at 55 ^{o}C 10 min, cooled to room temperature and exposed to UV using a Mega LV202E UV exposure unit, before being postbaked at 55 ^{o}C 10 mins and 95 ^{o}C 5 mins. Multiple 30 nm gold layers were used as a model for rigid mass, being sputtered on the centre of the Love wave propagation path up to 450 nm using an Emitech K575X fitted with a film thickness monitor. A mask was used to define a small area of 8 mm^2 onto which the gold was sputtered. Device spectra were recorded using an Agilent E5061A network analyser. Glycerol/water mixtures were pumped over the sensor using a Watson Marlow peristaltic pump. Glycerol (Sigma 98%) was diluted with distilled deionised water. Protein flow experiments were conducted with solutions being continually flown over the sensor surface at 1 ml min^{-1} by syringe pumps (Razel R100-EC). Protein solutions were prepared immediately prior to use at a concentration of 1 mg ml^{-1} in phosphate buffered saline (PBS, Sigma, tablets) using bovine serum albumin (Sigma, fraction V, lyophilized powder) and bovine fibrinogen (Sigma, type I-S, lyophilized powder) Temperature stability of 24 ± 0.1 ^{o}C was achieved using an Octagon 10 incubator. The Love wave device was used as the feedback element in an oscillator circuit consisting of cascaded amplifiers (Minicircuits ZFL-500LN), a 50 MHz high pass filter and 150 MHz low pass filter (Minicircuits BHP-50 and BPL-150), a power splitter (M/A com T1000) and a frequency counter (Agilent 53132A) interfaced to a microcomputer.

3. Results and Discussion

Signal characteristics of devices were recorded during the build up of successive layers of SU-8 photoresist. As the guiding layer thickness increases it is expected that the acoustic wave will gradually move from propagating entirely in the quartz as a surface skimming bulk wave (SSBW) to being confined at the surface of the substrate or travelling within the guiding layer as a Love wave. As this happens the velocity of the wave will decrease and so it is expected that a decrease in resonant frequency will also occur. The additional mass loading caused by the guiding layer will also contribute to a drop in frequency. Trends in frequency and amplitude of the signal over the first mode are shown in Figure 1. The signal attenuation initially decreased with increasing guiding layer thickness, reaching

a minimum of -15 dB at ~1 μm (z = 0.02). An increase in the amplitude of the signal demonstrates that more of the acoustic energy is located near the surface of the device which is consistent with previous reports using quartz substrates [11]. Additional layers of SU-8 gave rise to a gradual decrease in insertion loss due to the dampening of the overlayer, although it is well known that higher order modes can be observed with increasing thickness [3, 11].

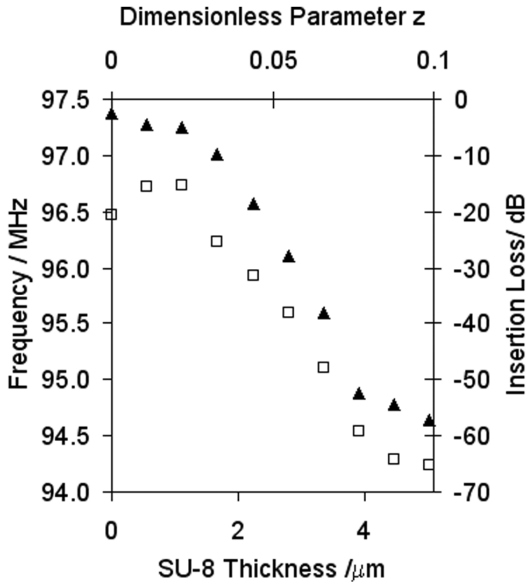

Figure 1. Signal characteristics covering the first mode of an SU-8 guiding layer Love wave device. Frequency (closed triangles) and insertion loss (open squares) shown as a function of guiding layer thickness and dimensionless parameter $z = d/\lambda_{IDT}$.

The mass sensitivity of devices with a range of guiding layer thicknesses chosen to cover the first mode has been investigated. For acoustic wave sensors without a guiding layer it usual to assume that the frequency change resulting from the addition of rigid mass is directly related to a change in phase velocity and hence a Sauerbrey type relation exists. For guided waves there may be significant dispersion and the frequency dependence of rigid mass loading onto a Love wave device may not be directly proportional [3, 17]. However if upon the addition of mass the change in guiding layer thickness is infinitesimal such that the operating point is not moved significantly down the dispersion curve, as in our experiments, then a Sauerbrey type proportionality may be observed [18]. If this is assumed then the mass loading effects of metalized layers on top of a guiding layer provide a simple route to defining the sensitivity of Love wave devices. All devices showed a linear relationship between frequency change as a function of increasing mass of gold, as shown in Figure 2.

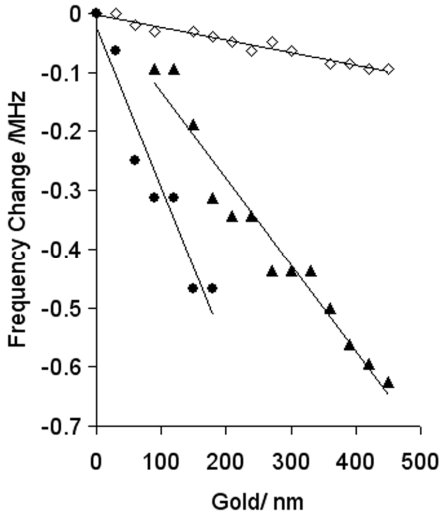

Figure 2. Relationship between mass loading and frequency of a SSBW device (open diamonds), and Love wave devices having guiding layers 1.12 μm thick (closed triangles) and 2.24 μm (closed circles).

A greater change in frequency was observed when depositing gold layers on all SU-8 devices compared to an uncoated device. The linear regions of the signal change was used to calculate the sensitivity of the devices in terms of a frequency change observed for mass loading of gold per unit area, Figure 3. From Figure 1 it would be expected that the most sensitive region would be where small changes in guiding layer thickness cause the largest changes in frequency, i.e. the middle of the mode. Indeed a sharp maximum in sensitivity was measured at ~350 Hz/ng/mm^2 at a guiding layer thickness of ~2 μm (z = 0.04), Figure 3. This corresponds well with the experimental dispersion curve data (Figure 1), relating to a point where the maximum frequency changes are observed with increasing guiding layer thickness.

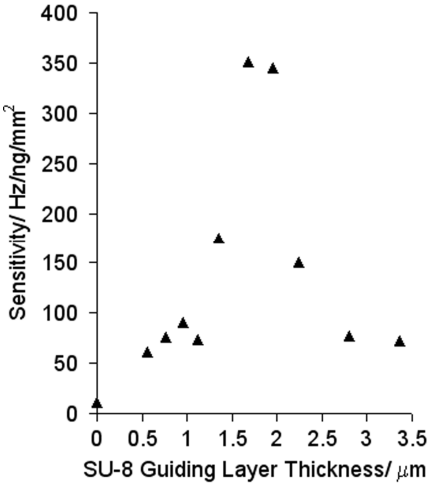

Figure 3. Frequency sensitivity of Love wave devices.

To demonstrate the use of SU-8 Love wave devices in liquid sensing, flow experiments were conducted to compare an SSBW device to a Love wave device with a 2 μm thick SU-8 guiding layer. Devices were clamped such that glycerol-water mixtures could be in contact with their sensing surface. Liquid was injected into the flow cell using a peristaltic pump with the flow direction perpendicular to the acoustic wave propagation; after the liquid was introduced the pump was halted until the next concentration was introduced. A stable signal was achieved oscillating in water, changing the liquid for 30% and 50% glycerol solutions before washing again with water, Figure 4.

The propagating acoustic waves' amplitude is attenuated by the liquid overlayer such that it decays with a penetration depth $\delta = \sqrt{\eta_l / (\pi f_0 \rho_l)}$, where ρ_l and η_l are the liquid density and viscosity respectively. For non-guided acoustic waves the Kanazawa and Gordon relationship [19] between frequency change and square root of the density-viscosity product is assumed to hold. For Love wave devices this may not be assumed due to the considerations discussed previously for mass loading. However, again, if the operating point of the sensor is not moved significantly down the dispersion curve then proportionality between the square root of the density-viscosity product and the change in frequency may be observed.

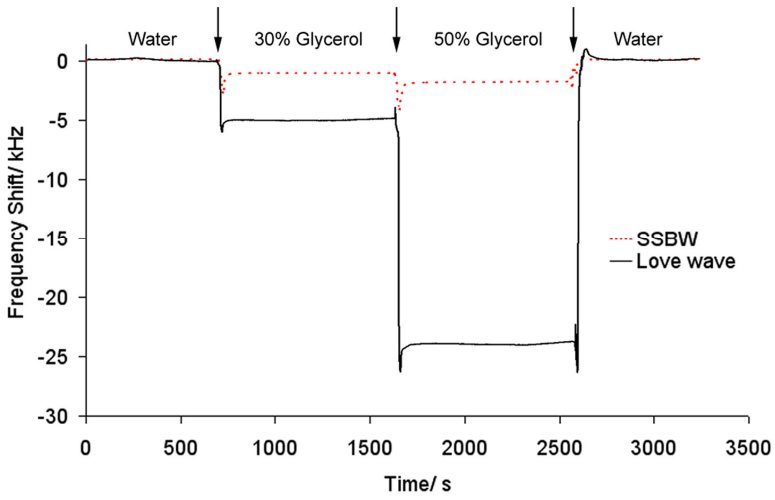

Figure 4. Liquid sensing of an SSBW device (dotted red line) and a Love wave device with an SU-8 guiding layer (solid black line), using water-glycerol mixtures. Arrows indicate points when liquid in contact with the sensor was exchanged.

As the device is oscillated in more viscous liquids the operating frequency will decrease, shown by the stepwise drops in frequency in Figure 4 as the glycerol fraction was increased. Both the devices tested returned to their original oscillating frequency when water is replaced over the sensors, indicating that no residual glycerol remained or any changes occurred to the sensor surfaces. The Love wave device shows a much higher sensitivity compared to the SSBW device, giving frequency shift more than 4 fold and 12 fold greater than the SSBW device for 30% and 50% glycerol solutions respectively (relative to water).

Initial spikes in frequency were observed due to the peristaltic pumping motion of the liquid when flushed over the crystal (causing pressure waves). Thermal drifting is often a problem during liquid sensing, wherein even small changes in temperature alter the viscosity of the media and effect the sensor itself. However, the SU-8 Love wave device showed good stability when in contact with water-glycerol mixtures, with only slight frequency drift of ~11 Hz min^{-1}. The greater stability of SU-8 compared to PMMA when in contact with water has previously been reported [20]. As SU-8 is highly chemically inert [16], it is anticipated that such devices will be stable under most chemical conditions. This may be particularly useful when measuring properties of corrosive or easily contaminated liquids such as ionic liquids.

To demonstrate the use of SU-8 Love wave devices for the detection of biomolecules, the adsorption of two serum proteins was examined. Bovine serum albumin (BSA) is a small globular protein and fibrinogen is a much larger rod-like protein, both found in high abundance in serum and are often used as model proteins in adsorption studies.[21] PBS was flown over a Love wave device having a 2 μm thick SU-8 guiding layer before the inlet of protein solution. Frequency shifts observed suggest that both albumin and fibrinogen adsorb onto the SU-8 surface upon injection over the sensor (Figure 5, point a). Following adsorption any loosely adhered or unbound protein was removed during a PBS rinse (figure 5, point b) which is shown by a slight upward shift in frequency. Albumin adsorption gave rise to a much lower change in frequency (~370 Hz) compared to fibrinogen (~1330 Hz) which is expected due to its smaller mass and differences in surface chemistry. Fibrinogen was also found to adsorb at a faster rate. These observed trends in adsorption compare well with those previously reported for these two proteins, bearing in mind the wettability of SU-8 being neither highly hydrophilic nor hydrophobic (water contact angle 80^{o} [22]). A more detailed discussion of protein adsorption profiles and how this relates to protein-surface interactions can be found elsewhere [21].

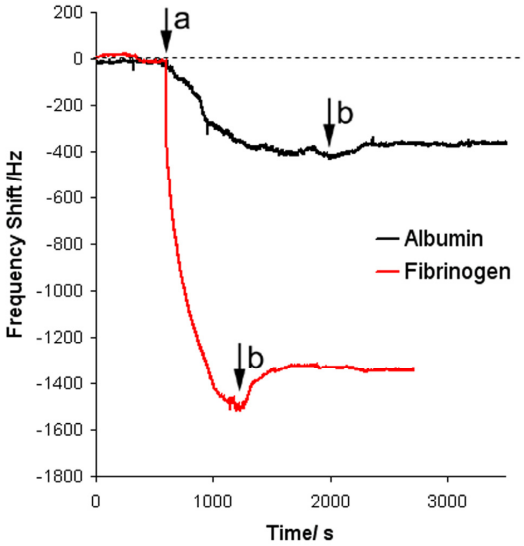

Figure 5. Protein detection using an SU-8 Love wave device. Arrows indicate points when solutions over sensors were exchanged, a) protein solution injected, prior to a) and at b) PBS solutions injected. Adsorption of albumin (black line) and fibrinogen (red line) was detected.

Conclusions

A negative epoxy-based photoresist, SU-8, was investigated as a Love wave guiding layer material. Signal characteristics were investigated in terms of guiding layer thickness. Observed trends in frequency and insertion loss were as expected for quartz Love wave devices. Frequency decreased with increasing guiding layer thickness, whilst insertion loss reached a minimum of ~-15 dB. Such low insertion losses are not common for these devices and may relate to the acoustic properties of SU-8. Sensitivity was assessed by the deposition of gold layers between the IDTs, showing a linear response in terms of frequency for all devices tested. A maximum sensitivity was achieved with a guiding layer thickness of ~2 μm (z = 0.04). Liquid sensing was also tested using water-glycerol mixtures, demonstrating the enhanced sensitivity of the Love wave device over an SSBW. Acoustic wave sensors are often used to assess viscosity-density of liquids although are often limited to those chemicals which will not damage the guiding layer The excellent stability of the devices when in contact with liquid highlights the applicability of SU-8 Love wave devices for sensing chemicals which may corrode/ dissolve/ swell or otherwise distort other polymers used as guiding layers.. The chemical stability of hard-baked SU-8 has been used by others to protect IDTs whilst another material is used as a wave guide. Protein adsorption experiments show the applicability of these sensors to detect biomolecules, showing a comparably larger frequency shift for fibrinogen adsorption than albumin and also a faster rate of adsorption for fibrinogen as expected. Here we have demonstrated the ease of fabrication and effectiveness of SU-8 based Love wave devices.

Acknowledgements

This work was funded by EPSRC grant EP/C536630/1.

References and Notes

1. Thompson, M.; Stone, D. *Surface Launched Acoustic Wave Sensors: Chemical Sensing and Thin Film Applications*, John Wiley and Sons: New York, 1997.
2. Lucklum, R.; Hauptmann, P. Acoustic Microsensors – The Challenge Behind Microgravimetry. *Anal. Bioanal. Chem*. **2006**, *384*(3), 667-682.
3. McHale, G.; Generalized Concept of Shear Horizontal Acoustic Plate Mode and Love Wave Sensors. *Meas. Sci. Technol*. **2003**, *14*, 1847-1853.
4. Melzak, K.A.; Ellar, D.J.; Gizeli, E. Interaction of Cytolytic Toxin CytB with a Supported Lipid Bilayer: Study Using an Acoustic Wave Device. *Langmuir* **2004**, *20*(4), 1386-1392.
5. Schlensog, M.D.; Gronewold, T.M.A.; Tewes, M.; Famulok, M.; Quandt, E. A Love-Wave Biosensor Using Nucleic Acids as Ligands. *Sens. Actuators B* **2004**, *101*(3), 308-315.
6. Melzak, K.A.; Martin, F.; Newton, M.I.; McHale, G.; Gizeli, E. Acoustic Determination of Polymer Molecular Weights and Rotation Times. *J. Polymer Sci. B* **2002**, *40*(14), 1490-1495.
7. Turton, A.; Bhattacharyya, D.; Wood, D. Liquid Density Analysis of Sucrose and Alcoholic Beverages using polyimide Guided Love-mode Acoustic Wave Sensors. *Meas. Sci Technol*. **2006**, *17*, 257-263.

8. Razan, F.; Rebiere, D.; Dejous, C.; Monin, D.; Joanicot, M.; Conedera, V. Determination of Menthol Kinetic Constants with Love-Wave Device. *Sens. Actuators B* **2006**, *118*(1-2), 368-373.
9. Gizeli, E.; Lowe, C.R.; Liley, M.; Vogel, H. Detection of Supported Lipid Layers With the Acoustic Love Waveguide Device: Application to Biosensors. *Sens. Actuators B* **1996**, *34*, 295–300.
10. Harding, L.G.; Du, J. Design and Properties of Quartz-Based Love Wave Acoustic Sensors Incorporating Silicon Dioxide and PMMA Guiding Layers. *Smart Mater. Struct*. **1997**, *6*, 716–720.
11. Newton, M.I.; McHale, G.; Martin, F. Experimental Study of Love Wave Devices With Thick Guiding Layers. *Sens. Actuators A* **2004**, *109*, 180–185.
12. Jakoby, B.; Ismael, G.M.; Byfiled, M.P.; Vellekoop, M.J. A Novel Molecularly Imprinted Thin Film Applied to a Love Wave Gas Sensor. *Sens. Actuators A* **1999**, *76*, 93-97.
13. Du, J.; Harding, L.G. A Multilayer Structure for Love-Mode Acoustic. *Sens. Actuators A* **1998**, *65*, 152-159
14. Du, J.; Harding, G.L.; Ogilvy, J.A.; Dencher, P.R.; Lake, M. A Study of Love-Wave Acoustic Sensors. *Sens. Actuators A* **1996**, *56*, 211-219.
15. Arana, N.; Puente, D.; Ayerdi, I.; Castano, E.; Berganzo, J. SU8 Protective Layers in Liquid Operating SAWs. *Sens. Actuators B* **2006**, *118*, 374-379.
16. LaBianca, N.; Gelorme, J.D. High aspect ratio resist for thick film applications. *Proc. SPIE*, **1995**, 2438, 846-852
17. McHale, G.; Newton, M.I.; Martin, F. Theoretical Mass, Liquid, and Polymer Sensitivity of Acoustic Wave Sensors With Viscoelastic Guiding Layers. *J. Appl. Phys*. **2003**, *93*(1), 675-690.
18. Sauerbrey, G. The Use of Quartz Oscillators for Weighing Thin Layers and for Microweighing. *Z. Phys*. **1959**, *155*, 206-222.
19. Kanazawa, K.K.; Gordon, J.G. The Oscillation Frequency of a Quartz Resonator in Contact With a Liquid. *Anal. Chim. Acta*. **1985**, *175*, 99-105.
20. Hossenlopp, J.; Jiang, L.; Cernosek, R.; Josse, F. Characterisation of Epoxy Resin (SU-8) Film Using Thickness-Shear Mode (TSM) Resonator Under Various Conditions. *J. Polymer Sci. B* **2004**, *42*, 2373-2384.
21. Roach, P.; Farrar, D.; Perry, C.C. Interpretation of Protein Adsorption: Surface-Induced Conformational Changes. *J. Am. Chem. Soc*. **2005**, *127*, 8168-8173.
22. Shirtcliffe, N.J.; Aqil, S.; Evans, C.; McHale, G.; Newton, M.I.; Perry, C.C.; Roach, P. The use of high aspect ratio photoresist (SU-8) for super-hydrophobic pattern prototyping. *J. Micromech. Microeng*. **2004**, *14*, 1384–1389.

D.2 Analytical Chemistry

Anal. Chem. **2008,** *80,* 5806–5811

Density−Viscosity Product of Small-Volume Ionic Liquid Samples Using Quartz Crystal Impedance Analysis

Glen McHale,*,† Chris Hardacre,‡ Rile Ge,‡ Nicola Doy,† Ray W. K. Allen,§ Jordan M. MacInnes,§ Mark R. Bown,§ and Michael I. Newton†

School of Science & Technology, Nottingham Trent University, Clifton Lane, Nottingham NG11 8NS, U.K., QUILL Center, School of Chemistry & Chemical Engineering, Queens University Belfast, Belfast BT9 5AG, Antrim, North Ireland, and Department of Chemical & Process Engineering, University of Sheffield, Newcastle St, Sheffield S1 3JD, U.K.

Quartz crystal impedance analysis has been developed as a technique to assess whether room-temperature ionic liquids are Newtonian fluids and as a small-volume method for determining the values of their viscosity−density product, $\rho\eta$. Changes in the impedance spectrum of a 5-MHz fundamental frequency quartz crystal induced by a water-miscible room-temperature ionic liquid, 1-butyl-3-methylimiclazolium trifluoromethylsulfonate ([C_4mim][OTf]), were measured. From coupled frequency shift and bandwidth changes as the concentration was varied from 0 to 100% ionic liquid, it was determined that this liquid provided a Newtonian response. A second water-immiscible ionic liquid, 1-butyl-3-methylimidazolium bis(trifluoromethanesulfonyl)imide [C_4mim][NTf_2], with concentration varied using methanol, was tested and also found to provide a Newtonian response. In both cases, the values of the square root of the viscosity−density product deduced from the small-volume quartz crystal technique were consistent with those measured using a viscometer and density meter. The third harmonic of the crystal was found to provide the closest agreement between the two measurement methods; the pure ionic liquids had the largest difference of ∼10%. In addition, 18 pure ionic liquids were tested, and for 11 of these, good-quality frequency shift and bandwidth data were obtained; these 12 all had a Newtonian response. The frequency shift of the third harmonic was found to vary linearly with square root of viscosity−density product of the pure ionic liquids up to a value of $\sqrt{(\rho\eta)} \approx 18$ kg m^{-2} s$^{-1/2}$, but with a slope 10% smaller than that predicted by the Kanazawa and Gordon equation. It is envisaged that the quartz crystal technique could be used in a high-throughput microfluidic system for characterizing ionic liquids.

Over the past decade, the drive toward cleaner industrial processes has led to the development of ionic liquids as alternative, environmentally friendly, solvents.[1,2] Ionic liquids provide good solvation with a range of compounds, have low volatility, are nonflammable, have a wide liquid range with temperature, and have tunable physical properties and a wide electrochemical window.[3,4] They comprise solely ions that are liquid at room temperature and can be considered designer solvents with over 1 million simple ionic liquids alone. Their use with a range of reactions, such as Heck and Suzuki cross-coupling, hydrogenations, oxidations, Friedel−Crafts, Diels−Alder, and polymerization is favored because of the control of selectivity that can be achieved and the ease of recyclability of the catalysts.[5−7] Ionic liquids have the potential for a wide range of applications including catalysis,[5−7] organic synthesis,[8] electrochemistry,[9,10] separations and extractions,[11,12] liquid crystals,[13−15] and analytical solvents and coatings.[16] However, the data on their physical properties as a function of chemical composition are limited, and extending the range of known data is difficult due to the expense and difficulty of producing large volumes of pure liquids for characterization.

Acoustic wave microsensors, such as the quartz crystal microbalance (QCM), are widely used for studying the properties of small-volume samples of liquids, the attachment of mass from the liquid phase and in situ determination of the properties of surface coatings, such as electrodeposited polymers, during the deposition process.[17−19] A QCM operates by creating a high-frequency, typically 5 MHz, shear mode oscillation of the surface. When operated in a liquid environment, this surface oscillation entrains liquid and creates an oscillation, which for a Newtonian liquid decays within a penetration depth of the interface $\delta = (\eta/$

* To whom correspondence should be addressed. E-mail: glen.mchale@ntu.ac.uk.
† Nottingham Trent University.
‡ Queens University Belfast.
§ University of Sheffield.

(1) Earle, M. J.; Seddon, K. R. *Pure Appl. Chem.* **2000**, *72*, 1391–1398.
(2) Andrade, C. K. Z.; Alves, L. M. *Curr. Org. Chem.* **2005**, *9*, 195–218.
(3) Koel, M. *Crit. Rev. Anal. Chem.* **2005**, *35*, 177–192.
(4) Wasserscheid, P.; Welton, T. *Ionic liquids in synthesis*, 2nd ed.; Wiley VCH: Weinheim, 2007.
(5) Sheldon, R. *Chem. Commun.* **2001**, (23), 2399–2407.
(6) Gordon, C. M. *Appl. Catal.* **2001**, *A222*, 101–117.
(7) Dupont, J.; de Souza, R. F.; Suarez, P. A. Z. *Chem. Rev.* **2002**, *102*, 3667–3691.
(8) Cave, G. W. V.; Raston, C. L.; Scott, J. L. *Chem. Commun.* **2001**, (21), 2159–2169.
(9) Chen, P. Y.; Lin, Y. F.; Sun, I. W. *J. Electrochem. Soc.* **1999**, *146*, 3290–3294.
(10) Endres, F. *Chem. Phys. Chem.* **2002**, *3*, 144.
(11) Wei, G. T.; Yang, Z. S.; Chen, C. J. *Anal. Chim. Acta* **2003**, *488*, 183–192.
(12) Zhao, H.; Xia, S. Q.; Ma, P. S. *J. Chem. Technol. Biotechnol.* **2005**, *80*, 1089–1096.
(13) Bowlas, C. J.; Bruce, D. W.; Seddon, K. R. *Chem. Commun.* **1996**, (14), 1625–1626.
(14) Abdallah, D. J.; Robertson, A.; Hsu, H. F.; Weiss, R. G. *J. Am. Chem. Soc.* **2000**, *122*, 3053–3062.
(15) Bradley, A. E.; Hardacre, C.; Holbrey, J. D.; Johnston, S.; McMath, S. E. J.; Nieuwenhuyzen, M. *Chem. Mater.* **2002**, *14*, 629–635.
(16) Qin, W. D.; Wei, H. P.; Li, S. F. Y. *J. Chromatogr., A* **2003**, *985*, 447–454.

10.1021/ac800490q CCC: $40.75
Published on Web 07/09/2008

Table 1. Halide Content, Water Content in Mass Fractions, Viscosity, and Density of Ionic Liquids Measured Using a Viscometer and Density Meter in This Study (at 25 °C)

ionic liquid	viscosity (cP)	density (g cm^{-3})	[H_2O] (wt %)	[halide] (ppm)
[C_2mim][SCN]	23.6	1.118	0.0307	<5
[C_4mim][DCA]	28.8	1.059	0.0256	1830
[C_4mpyrr][DCA]	36.5	1.013	0.0235	1790
[C_2mim][NTf_2]	36.5	1.520	0.0100	<5
[C_4mim][NTf_2]	50.5	1.436	0.0096	<5
[C_4mim][OTf]	83.2	1.292	0.0681	<5
[C_4mpyrr][NTf_2]	79.3	1.395	0.0010	<5
[C_6mim][NTf_2]	80.1	1.357	0.0013	<5
[C_2mim][$EtSO_4$]	98.4	1.237	0.0279	-[a]
[C_8mim][NTf_2]	95.0	1.321	0.0032	<5
[C_{10}mim][NTf_2]	120.2	1.279	0.0052	<5
[C_4mim][AcO]	139.7	1.243	0.0746	<10
[C_4mim][$MeSO_4$]	188.0	1.208	0.0067	<5
[C_4mpyrr][FAP]	221.0	1.580	0.0132	<100
[$P_{6,6,6,14}$][NTf_2]	335.9	1.065	0.0095	<5
[C_4mim][TFA]	418.5	1.068	0.0744	<5
[C_4mim][$OctSO_4$]	888.6	1.072	0.0113	<7
[$N_{1,8,8,8}$][TFA]	1708	0.966	0.0108	<5
[C_{10}mim][SCN]	683.7	1.011	0.0307	<5

[a] Halide-free preparation. [$C_n$mim]$^+$ = 1-alkyl-3-methyl imidazolium; [C_4mpyrr] = 1-butyl-1-methylpyrrolidinium; [$N_{1,8,8,8}$]$^+$ = methyl, trioctylammonium; [$P_{6,6,6,14}$]$^+$ = trihexyl, tetradecylphosphonium; [SCN]$^-$ = thiocyanate; [DCA]$^-$ = dicyanamide; [NTf_2]$^-$ = bis{(trifluoromethyl)sulfonyl}imide; [OTf]$^-$ = trifluoromethanesulfonate; [AcO]$^-$ = acetate; [$MeSO_4$]$^-$ = methylsulfate; [FAP]$^-$ = trifluorotris(perfluoroethyl)phosphate; [TFA]$^-$ = trifluoroacetate; [$OctSO_4$]$^-$ = octylsulfate.

$\pi f_s \rho)^{1/2}$ where ρ and η are the density and viscosity of the liquid and f_s is the resonant frequency.[20] In impedance analysis, both the resonant frequency and bandwidth, B, of the crystal are measured and are functions of the liquid properties. Bandwidth is a measure of the loss of energy and of the damping of the shear mode oscillation of the liquid close to the solid−liquid interface, and so some authors prefer to define a dissipation $D = B/f_s$ (also equal to Q^{-1}). When the liquid is Newtonian, a frequency decrease, Δf, and a bandwidth increase, ΔB, occur in proportion to the square root of the viscosity−density product,

$$\frac{\Delta f}{f_o} = -\frac{1}{Z_q}\left(\frac{f_s \eta \rho}{\pi}\right)^{1/2} \text{ and } \frac{\Delta B}{f_o} = \frac{2}{Z_q}\left(\frac{f_s \eta \rho}{\pi}\right)^{1/2} \quad (1)$$

where the specific acoustic impedance of quartz is $Z_q = (\mu_q \rho_q)^{1/2} = 8.84 \times 10^{-6}$ kg m^{-2} s^{-1}, f_o is the fundamental frequency and $f_s = nf_o$ is the overtone frequency at which the response is measured.[21,22] Thus, by verifying that changes in resonant frequency and bandwidth are correlated, such that $\Delta f = -\Delta B/2$, eq 1 allows a determination of whether an ionic liquid has a Newtonian response. If the ionic liquid is Newtonian, either the frequency change (the Kanazawa and Gordon equation) or the bandwidth change can be used to determine the value of the viscosity−density product and from knowledge of the density, the viscosity can be deduced.

In this work, concentrations of a water-miscible room-temperature ionic liquid, 1-butyl-3-methylimidazolium trifluoromethylsulfonate, [C_4mim][OTf], and a water-immiscible room temperature ionic liquid, 1-butyl-3-methylimidazolium bis(trifluoromethanesulfonyl)imide, [C_4mim][NTf_2], are shown to be Newtonian according to impedance spectra for a 5-MHz quartz crystal for concentrations from pure to 100% water or methanol, respectively. Results for the density−viscosity values obtained using the small-volume impedance spectra method are shown to be consistent with those obtained using a viscometer. Finally, data for 18 pure ionic liquids are presented, with Newtonian behavior being confirmed for 12 of these and the validity of a linear relationship between frequency shift and square root of viscosity−density product being confirmed up to a limit of $\sqrt{(\rho\eta)} \approx 18$ kg m^{-2} s$^{-1/2}$.

EXPERIMENTAL SECTION

Ionic Liquids. 1-Butyl-1-methylpyrrolidinium trifluorotris(perfluoroethyl)phosphate ([C_4mpyrr][FAP]), 1-butyl-3-methylimidazolium trifluoroacetate ([C_4mim][TFA]), 1-butyl-3-methylimidazolium dicyanamide ([C_4mim][DCA]), 1-butyl-1-methylpyrrolidinium dicyanamide ([C_4mpyrr][DCA]), 1-ethyl-3-methylimidazolium thiocyanate ([C_2mim][SCN]), 1-butyl-3-methylimidazolium methylsulfate ([C_4mim][$MeSO_4$]), 1-butyl-3-methylimidazolium octylsulfate ([C_4mim][$OctSO_4$]), and methyl-trioctylammonium trifluoroacetate ([$N_{1,8,8,8}$][TFA]) were obtained from Merck (98%). 1-Ethyl-3-methylimidazolium ethyl sulfate ([C_2mim][$EtSO_4$]) was prepared by reacting 1-methylimidazole with diethyl sulfate according to previously reported procedures.[23] All other ionic liquids were prepared in-house using standard literature methods from the appropriate organic halide salt.[24,25] The halide content of each ionic liquid was measured by using suppressed ion chromatography[26] and the characterization of each ionic liquid used is shown in Table 1.

(17) Martin, S. J.; Granstaff, V. E.; Frye, G. C. *Anal. Chem.* **1991**, *63*, 2272–2281.
(18) Bandey, H. L.; Hillman, A. R.; Brown, M. J.; Martin, S. J. *Faraday Discuss.* **1997**, *107*, 105–121.
(19) Bruckenstein, S.; Shay, M. *Electrochim. Acta* **1985**, *30*, 1295–1300.
(20) Kanazawa, K. K.; Gordon, J. G. *Anal. Chim. Acta* **1985**, *175*, 99–105.
(21) Bandey, H. L.; Martin, S. J.; Cernosek, R. W.; Hillman, A. R. *Anal. Chem.* **1999**, *71*, 2205–2214.
(22) Ballantine D. S.; White, R. M.; Martin, S. J.; Ricco, A. J.; Zellers, E. T.; Frye, G. C.; Wohltjen, H. *Acoustic Wave Sensors: Theory, Design, & Physico-Chemical Applications*; Academic Press: San Diego, 1997.
(23) Bonhôte, P.; Dias, A. P.; Papageorgiou, N.; Kalyanasundram, K.; Grätzel, M. *Inorg. Chem.* **1996**, *5*, 1168–1178.
(24) Earle, M. J.; Katdare, S. P.; Seddon, K. R. *Org. Lett.* **2004**, *6*, 707–710.
(25) Xu, W.; Wang, L. M.; Nieman, R. A.; Angell, C. A. *J. Phys. Chem. B* **2003**, *107*, 11749–11756.

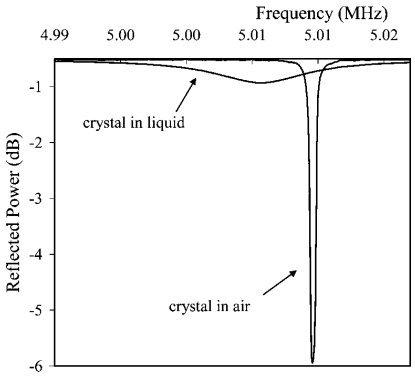

Figure 1. Quartz crystal power spectra for an unloaded crystal and one immersed in $[C_2mim][NTf_2]$.

Impedance Spectra. Polished quartz crystals having a fundamental frequency of 5 MHz and diameter of 25 mm (Testbourne Ltd. 149211-1) were used, with the frequency spectra being collected using an Agilent Technologies E5061A Network Analyzer. Resonance spectra were recorded for crystals in air and in liquid at 25 °C and fitted to a Butterworth van Dyke (BVD) model using a LabView program; exemplar data for the reflected power are shown in Figure 1 for an unloaded and a crystal immersed in an ionic liquid ($[C_2mim][NTf_2]$). The BVD model allows a load impedance to be extracted as a series combination of a resistance and an inductance and from the best fit the resonant frequency and bandwidth are obtained.[22] A brief review of this model and the procedure we used for fitting data to the resonance spectra for reflected power is reported in Roach et al.[27] Spectra were obtained for the fundamental frequency and four higher overtones. Above the third harmonic, the frequency shift could be identified, but the BVD program was unable to fit accurately enough to determine the bandwidth. Previous work comparing resonant frequency shifts of various harmonics while testing the shear compliance of thin films has suggested the third harmonic produces a more accurate frequency change in response to mass/liquid loading.[28] The test cell for holding the crystals was machined directly from PTFE leaving a 20-mm-diameter chamber and 2.5-mm-wide raised lip acting as an O-ring seal and requiring only 40 μL of test volume of liquid for satisfactory operation. To reduce the absorption of moisture, the equipment was set up inside a glovebag under argon. Crystals were cleaned in distilled water and then methanol and blown dry using nitrogen prior to each measurement. A typical measurement time for introducing the liquid to the cell and taking the resonance spectra for the full range of harmonics was under 2 min.

Viscometer and Density Data. Measurements of viscosity and density were made using a Brookfield DV-II+ programmable viscometer, and a DMA 4500 density/specific gravity/concentration meter; these methods require 1.5 and 0.5 mL of liquid, respectively. Before use, all the ionic liquids were dried using a heated oil bath at 60 °C while subjected to a vacuum (1 Torr) and left overnight to facilitate maximum water removal; water content of the ionic liquid was measured using a Karl Fischer titrator. A series of poly(dimethylsiloxane) (PDMS) oils (Aldrich) covering viscosities from 1 to 100 000 cP were used to give a comparison fluid that is known to deviate from a Newtonian behavior at high molecular weight. The temperature for both density and viscosity measurements could be controlled using a water bath and were set to 25 °C, which was the value recorded at the time the QCM measurements were made Table 2.

RESULTS AND DISCUSSION

Determination of Newtonian Liquid Behavior. The change in bandwidth or change in frequency of the QCM allows the viscosity−density product of the liquid under test to be calculated using the linear relationships given by eq 1 provided the liquid is a Newtonian fluid. To test this linearity, Figure 2a shows the change in fundamental frequency and Figure 2b the corresponding change in bandwidth as a function of square root of the density−viscosity product obtained using the viscometer and density meter for a range of concentrations of two ionic liquids (water-miscible $[C_4mim][OTf]$ diluted in water, squares, and water-immiscible $[C_4mim][NTf_2]$ diluted in methanol, triangles). These data suggest that the QCM could be used to determine the square root of the viscosity−density product of an ionic liquid directly from small-volume samples. However, a linear response in Figure 2a or Figure 2b does not directly confirm that the liquid is Newtonian and, hence, that eq 1 can be applied.

Figure 3 presents the data for the various concentrations of ionic liquids as a change in fundamental frequency against change in bandwidth. The frequency shift and bandwidth increase data are well-described by a linear relationship. To illustrate typical results for a non-Newtonian liquid, Figure 2 and Figure 3 also present data for a range of poly(dimethylsiloxane) oils (circles), which are known to deviate significantly from Newtonian behavior at higher molecular weight; this deviation can be clearly observed above a change in frequency of 3 kHz corresponding to a viscosity of 10 cP. For the ionic liquids, the majority of data in Figure 3 follow the solid line with a slope of 0.5, which is the prediction for a Newtonian liquid; the inset confirms this for concentrations up to 90%. At concentrations of ionic liquid above 90%, there is a small deviation with a slightly larger bandwidth than predicted for a given frequency shift. This is probably due to the increased difficulty in accurately fitting the resonant curves for the bandwidth for the pure ionic liquids with high viscosity (high damping), making the identification of the resonant frequency more reliable than the determination of the bandwidth. In addition, although the samples were measured in a glovebag, the high hygroscopicity of the ionic liquids and the high sensitivity of viscosity on the water content for the pure ionic liquids[29] may also contribute to the slight variance observed.

Third Harmonic Data for Viscosity-Density Product. The frequency change can be converted to square root of viscosity−density product using the Kanazawa and Gordon equation (eq 1). Figure 4 shows the square root of the density−viscosity product plotted as a function of concentration of the water-miscible $[C_4mim][OTf]$ using the QCM frequency shift measured at the third harmonic (diamonds) and the corresponding product calculated from the independent viscometer and density meter measurements (squares).

(26) Villagrán, C.; Deetlefs, M.; Pitner, W. R.; Hardacre, C. *Anal. Chem.* **2004**, *76*, 2118–2123.
(27) Roach, P. A.; McHale, G.; Evans, C. R.; Shirtcliffe, N. J.; Newton, M. I. *Langmuir* **2007**, *23*, 9823–9830.
(28) Johannsmann, D. *J. Appl. Phys.* **2001**, *89*, 6356–6364.
(29) Seddon, K. R.; Stark, A.; Torres, M. *J. Pure Appl. Chem.* **2000**, *72*, 2275–2287.

Table 2. Comparison of the $(\rho\eta)^{1/2}$ Determined from the Third Harmonic of Quartz Crystal and from Separate Measurements Using a Viscometer and Density Meter at 25 °C

ionic liquid	included in Figure 6a (Newtonian test)	$(\rho\eta)^{1/2}$ (kg m^{-2} s$^{-1/2}$) third harmonic of quartz crystal	$(\rho\eta)^{1/2}$ (kg m^{-2} s$^{-1/2}$) viscometer-density meter (±1%)
[C_2mim][SCN]	√	4.5 ± 0.6	5.1
[C_4mim][DCA]	√	5.6 ± 0.1	5.5
[C_4mpyrr][DCA]	√	5.5 ± 0.1	6.1
[C_2mim][NTf_2]	√	6.4 ± 0.6	7.4
[C_4mim][NTf_2]	√	8.2 ± 0.2	8.5
[C_4mim][OTf]	√	10.0 ± 0.9	10.4
[C_4mpyrr][NTf_2]	√	10.1 ± 0.3	10.5
[C_6mim][NTf_2]	√	9.8 ± 0.5	10.4
[C_2mim][$EtSO_4$]	√	10.7 ± 0.6	11.0
[C_8mim][NTf_2]	√	9.6 ± 0.9	11.2
[C_{10}mim][NTf_2]	√	10.9 ± 0.5	12.4
[C_4mim][AcO]	X	11.8 ± 0.2	13.2
[C_4mim][$MeSO_4$]	X	13.8 ± 0.8	15.1
[C_4mpyrr][FAP]	X	15.3 ± 2.1	18.7
[$P_{6,6,6,14}$][NTf_2]	X	10.6 ± 0.6	18.9
[C_4mim][TFA]	X	14.6 ± 0.1	21.1
[C_4mim][$OctSO_4$]	X	10.9 ± 1.1	30.9
[$N_{1,8,8,8}$][TFA]	X	15.3 ± 3.6	40.6

The inset in Figure 4shows the corresponding square root of the density−viscosity product for the QCM and non-QCM techniques; the straight line is a best fit with a slope of 0.96. The inset also provides a comparison of the density−viscosity product calculated from the third harmonic (diamonds) and from the fundamental (circles) of the quartz crystal. Both the fundamental and the third harmonic data agree within experimental error with the non-QCM measurements at lower viscosities, but at the highest viscosity, the data from the fundamental mode slightly underestimate the viscosity−density product. In contrast, the third harmonic data remain in agreement with viscometer and density meter data over the full concentration range up to pure ionic liquid. We found that the third harmonic gave better agreement with the non-QCM measurements than all the other harmonics measured. The data for the water-immiscible ionic liquid [C_4mim][NTf_2] also resulted in the same conclusions with the third harmonic data providing a low-volume sample measurement of density−viscosity product consistent with the results using the larger volumes in the viscometer and density meter; the data are shown in Figure 5. In both cases, the largest error from repeated measurements (~ ±10%) occurs for the pure liquids, which given the hygroscopic nature of these room-temperature ionic liquids and sensitive dependence on liquid composition of the viscosity, is not surprising.

Pure Ionic Liquids. A set of 18 pure ionic liquids was tested using both the small-volume quartz crystal impedance technique and the large-volume viscometer. Figure 6a shows a linear correlation between changes in resonant frequency, Δf_s, and bandwidth, ΔB, for 11 of the ionic liquids for which reliable fits of the bandwidth were obtained at the fundamental frequency (the first 11 ionic liquids in Table 1); replicate measurements have been included. All of these ionic liquids are reasonably described by the test for Newtonian behavior, $\Delta f_s = -\Delta B/2$, although the best fit to the data gives a gradient of 0.439 (solid line). Figure 6b shows the change in resonant frequency as a function of the square root of viscosity−density product measured using the viscometer and density meter for all 18 ionic liquids. There is a clear threshold at around $\sqrt{(\rho\eta)} \approx 18.7$ kg m^{-2} s$^{-1/2}$ after which two ionic liquids, [$P_{6,6,6,14}$][NTf_2] and [C_4mim][TFA], deviate slightly from the linear prediction and a further two, [C_4mim][$OctSO_4$] and [$N_{1,8,8,8}$][TFA], deviate significantly from the linear prediction. At these high levels of viscosity where resonant curves are very broad and difficult to fit accurately, however, it was possible to fit the full resonant curve for one of these, [C_4mim][$OctSO_4$], and it did satisfy the Newtonian criteria given by, $\Delta f_s = -\Delta B/2$. This would indicate that all ionic liquids tested for which the quartz crystal method was able to provide accurate results (i.e., up to $\sqrt{(\rho\eta)} \approx 18$ kg m^{-2} s$^{-1/2}$)

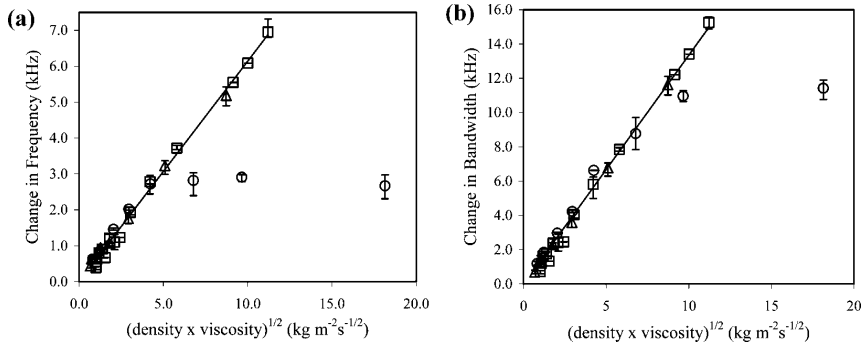

Figure 2. Changes in (a) resonant frequency and (b) bandwidth, as a function of viscosity−density product. Data show [C_4mim][OTf] up to 100% concentration in water (squares), [C_4mim][NTf_2] up to 100% concentration in methanol (triangles), and a range of poly(dimethylsiloxane) oils (circles).

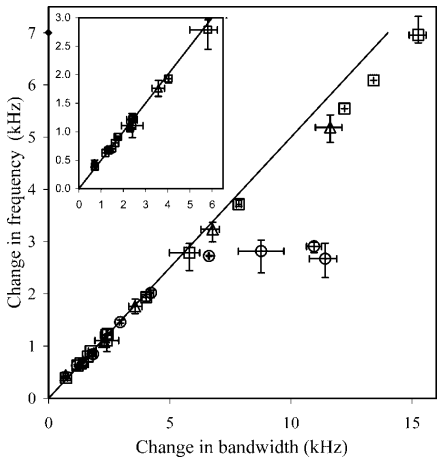

Figure 3. Data presented as change in frequency against change in bandwidth to test for Newtonian response. The poly(dimethylsiloxane) oils (circles) deviate significantly from Newtonian behavior (Kanazawa and Gordon equation shown by the solid line) at high molecular weight, but the [C_4mim][OTf] (squares) and [C_4mim][NTf_2] (triangles) remain Newtonian. The inset shows ionic liquids up to a concentration of 90%.

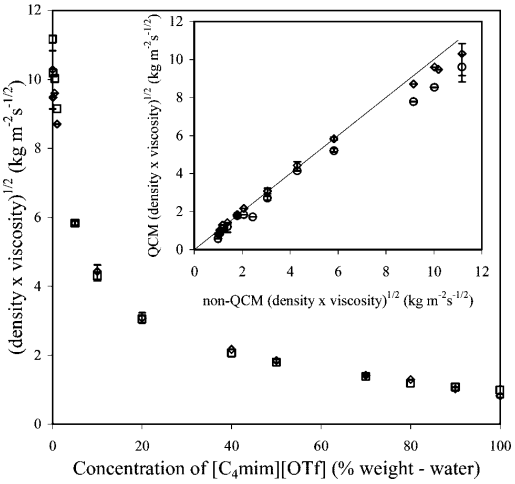

Figure 4. Density−viscosity dependence on concentration for the water-miscible ionic liquid [C_4mim][OTf] determined by viscometer (squares) and the third harmonic of the quartz crystal (diamonds). Inset shows comparison of the quartz crystal data from the fundamental (circles) and third harmonic (diamonds); solid line is a best fit with slope of 0.96.

were Newtonian. Figure 7 shows the correlation of the square root of viscosity−density product estimated using the third harmonic frequency shift of the quartz crystal with the data from the viscometer and density meter for the 16 pure ionic liquids satisfying the linear prediction or having a slight deviation from the linear prediction; Table 1 gives the average values measured for all 18 liquids measured. For data points up to $\sqrt{(\rho\eta)} \approx 18$ kg m^{-2} s$^{-1/2}$, the data can be fitted by $\sqrt{(\rho\eta)}_{QCM} = 0.92\sqrt{(\rho\eta)}_{viscometer}$, thus indicating around a 10% underestimate by the quartz crystal

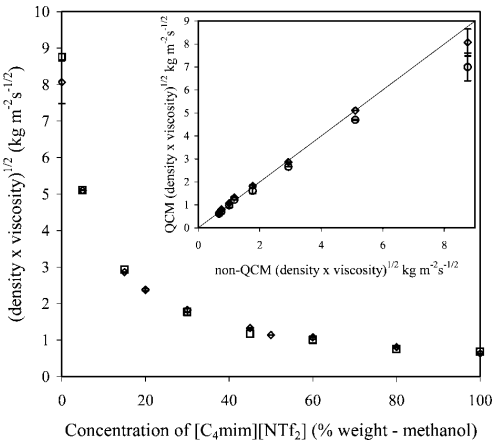

Figure 5. Density−viscosity dependence on concentration for the water-immiscible ionic liquid [C_4mim][NTf_2] determined by viscometer (squares) and the third harmonic of the quartz crystal (diamonds). Inset shows comparison of the quartz crystal data from the fundamental (circles) and third harmonic (diamonds).

impedance method compared to the viscometer. However, in a high-throughput application of the technique, such an underestimate could be corrected by using a calibrated value for the numerical coefficient in eq 1 rather than the theoretical value from the Kanazawa and Gordon equation.

Clearly the product of the density and viscosity only has limited application and usually the individual values are required, for example, in process design. Recently, predictive modeling of density data based on molar volume calculations of the constituent ions has been reported by a number of groups.[30–33] Jacquemin et al. showed using >2000 data points that the density could be predicted with an uncertainty of 0.48% as a function of temperature.[34] This level of predictability may be used in conjunction with the QCM-derived value for the $\rho\eta$ and therefore provide a predicted viscosity for a given ionic liquid. This is a significant advance given that conventional measurements of η requires >1.5 mL of ionic liquid whereas by this method the sample size may be reduced to 40 μL.

The measurements reported herein are in good agreement with previously reported data on the effect of shear rate on viscosity for ionic liquids. Seddon et al. studied the viscosity of [$C_n$mim][BF_4] ($n = 4$ to $n = 12$) and [$C_n$mim][PF_6] ($n = 4$ to $n = 12$) ionic liquids and found that for all except [C_{12}mim][BF_4] the viscosity for independent of shear rate was indicative of Newtonian behavior.[35] While for [C_{12}mim][BF_4] above 65 °C this was also true, below this temperature non-Newtonian behavior was observed due to the phase transition from the isotropic liquid phase into the liquid crystalline region. Non-Newtonian behavior has also been reported for benzyl-functionalized imidazolium-based

(30) Kim, Y. S.; Choi, W. Y.; Jang, J. H.; Yoo, K.-P.; Lee, C. S. *Fluid Phase Equilib.* **2005**, *228*, 439–445.
(31) Kim, Y. S.; Jang, J. H.; Lim, D. B.; Kang, J. W.; Lee, C. S. *Fluid Phase Equilib.* **2007**, *256*, 70–74.
(32) Gardas, R. L.; Coutinho, J. A. P. *Fluid Phase Equilib.* **2008**, *263*, 26–32.
(33) Ye, C.; Shreeve, J. M. *J. Phys. Chem. A* **2007**, *111*, 1456–1461.
(34) Jacquemin, J.; Ge, R.; Nancarrow, P.; Rooney, D. W.; Gomes, M. F. C.; Padua, A. A. H.; Hardacre, C. *J. Chem. Eng. Data* **2008**, *53*, 716–726.
(35) Seddon, K. R.; Stark, A.; Torres, M. J. *Clean Solvents* **2002**, *819*, 34–49.

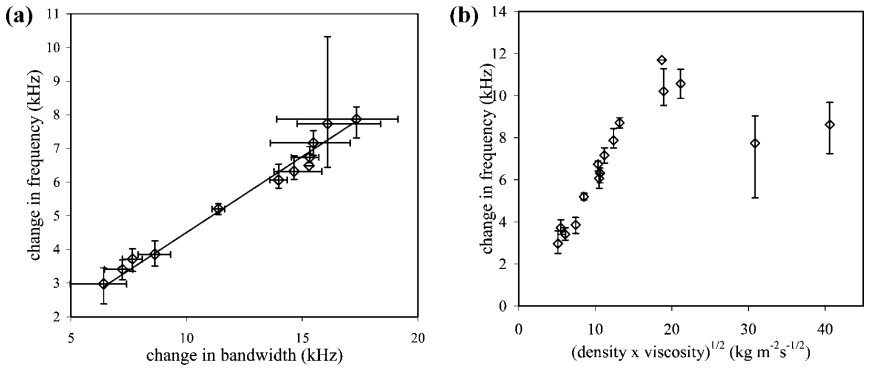

Figure 6. Fundamental mode data for 19 pure ionic liquids. (a) Correlation between change in resonant frequency and change in bandwidth demonstrating Newtonian behavior, (b) change in resonant frequency as a function of viscosity−density product. The data are described by a linear relationship up to $\sqrt{(\rho\eta)} \approx 18.7$ kg m^{-2} s$^{-1/2}$.

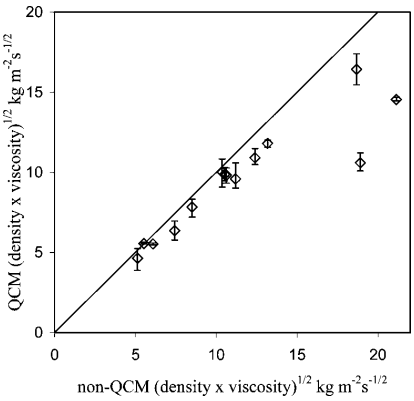

Figure 7. Correlation between density−viscosity product for 17 pure ionic liquids determined using viscometer and density meter and by using the change in resonant frequency of the quartz crystal at the third harmonic. The solid line has a slope of unity. The linear correlation breaks down for the highest viscosity ionic liquids at around $\sqrt{(\rho\eta)} \approx 18$ kg m^{-2} s$^{-1/2}$.

ionic liquids by Kulkarni et al. as well as a number of [C_{10}mim][CF_3COO], [C_{10}mim][NTf_2], and [C_{10}mim][SCN].[36] Interestingly, this is not found in the QCM data where [C_{10}mim][NTf_2] fits the linear trend of eq 1. Although, the addition of solutes to ionic liquids has been shown to result in non-Newtonian behavior, this has predominantly been for ionic liquids containing functionalized cations, for example, where strong hydrogen bonding can occur between the solute and ionic liquid.[37–39] Li et al. showed that the plastic and then Newtonian behavior was observed as the shear rate increased for mixtures of [$Me_3NC_2H_4OH$][Zn_2Cl_5] and ethanol.[39] Herein, where the ionic liquid−water interaction may be considered as weaker, only Newtonian behavior was observed. Recent calculations have shown that non-Newtonian behavior may be expected for many ionic liquids, even those thought as showing Newtonian behavior on the macroscale, if the ionic liquid is confined in microchannels, for example.[40] The QCM technique coupled with microchannel devices will enable this prediction to be studied in detail and is the subject of an ongoing study.

CONCLUSION

In this article, we have shown that quartz crystal impedance analysis can be used to determine whether mixtures of a water-miscible and a water-immiscible ionic liquid with water and methanol, respectively, have Newtonian responses when subject to a high-frequency oscillation. For ionic liquids with a Newtonian response, it has been shown that viscosity−density products can be determined from small-volume samples without the need for calibration liquids. The results also demonstrate that the third harmonic of the crystal resonance provides the greatest consistency over the full range of concentrations with results obtained using a viscometer and density meter. Data obtained for 12 pure ionic liquids were found to show Newtonian responses with correlated shifts in quartz crystal frequency and bandwidth. The change in frequency for pure ionic liquids was directly proportional to the square root of the viscosity−density product for values up to 18 kg m^{-2} s$^{-1/2}$. The ability of the quartz crystal method to determine viscosity−density products of ionic liquids should allow the development of high-throughput measurements of physical properties for ionic liquids. A natural extension of this work is to higher frequency acoustic wave devices, such as shear horizontally polarized surface acoustic wave and acoustic plate mode devices,[41,42] which can be used with smaller volumes of liquid and which can be integrated into microfluidic devices.

ACKNOWLEDGMENT

This work has been supported by the UK Engineering & Physical Sciences Research Council (EPSRC) under grants EP/D03826X/1, EP/D038294/1 and EP/D038995/1.

Received for review March 8, 2008. Accepted June 4, 2008.

AC800490Q

(36) Kulkarni, P. S.; Branco, L. C.; Crespo, J. G.; Nunes, M. C.; Raymundo, A.; Afonso, C. A. M. *Chem.:Eur. J.* **2007**, *13*, 8478–8488.
(37) Guo, Z.; Xu, X. B. *Green Chem.* **2006**, *8*, 54–62.
(38) Chagnes, A.; Tougui, A.; Carre, B.; Ranganathan, N.; Lemordant, D. *J. Sol. Chem.* **2004**, *33*, 247–255.
(39) Li, Q. M.; Wu, G. Z.; Liu, Y. D.; Luo, Y. S. *Appl. Rheol.* **2006**, *16*, 334–339.
(40) Hu, Z. H.; Margulis, C. J. *Acc. Chem. Res.* **2007**, *40*, 1097–1105.
(41) Vellekoop, M. J. *Ultrasonics* **1998**, *36*, 7–14.
(42) McHale, G. *Meas. Sci. Technol* **2003**, *14*, 1847–1853.

Anal. Chem. **2009,** *81,* 1628–1637

Evaluation of a Microfluidic Device for the Electrochemical Determination of Halide Content in Ionic Liquids

R. Ge,[†] R. W. K. Allen,[‡] L. Aldous,[†] M. R. Bown,[‡] Nicola Doy,[§] C. Hardacre,*[,†] J. M. MacInnes,*[,‡] G. McHale,[§] and M. I. Newton[§]

QUILL Research Centre, School of Chemistry and Chemical Engineering, Queen's University Belfast, Belfast, BT9 5AG, U.K., Department of Chemical & Process Engineering, University of Sheffield, Newcastle St, Sheffield S1 3JD, U.K., and School of Science & Technology, Nottingham Trent University, Clifton Lane, Nottingham NG11 8NS, U.K.

A microfluidic device designed for electrochemical studies on a microliter scale has been utilized for the examination of impurity levels in ionic liquids (ILs). Halide impurities are common following IL synthesis, and this study demonstrates the ability to quantify low concentrations of halide in a range of ILs to levels of ~5 ppm, even in ILs not currently measurable using other methods such as ion chromatography. To validate the mixer device, the electrochemistry of ferrocene was also examined and compared with spectroscopic and bulk electrochemistry measurements. An automated "sample preparation, delivery, and calibration" method was developed, and the chip successfully used for linear sweep, cyclic voltammetry (under both quiescent and steady-state flowing conditions), square wave voltammetry, and differential pulse voltammetry. An effective method of electrochemically cleaning the electrodes is also presented.

In the past decade, the use of ionic liquids (ILs) as alternative solvents and media for a wide range of applications has expanded significantly in both academia, as well as in industry.[1−5] The importance of impurities in ILs has been recognized by many researchers in this area with water, halide, and metal impurities from the synthesis of the ILs being the most prevalent. These affect both physical and chemical properties of the media, for example, drastically increasing viscosity[6] and thermal conductivity,[7] while also poisoning catalytic reactions.[8] Additionally, Jacquemin et al. have quantified the effect of halide and water content on the density of a wide range of ILs as a function of pressure and temperature, highlighting the importance of being able to measure their concentration accurately.[9,10] It should be noted that typical commercial samples contain between 10 and 1000 ppm of halide from their synthesis.[11] The purity strongly determines their cost because of the loss of IL during multistage purification.

With respect to halide content, although commonly used, the technique of using the "silver nitrate" is only qualitative and is insufficient to examine ILs for many applications.[12] However, a number of other methods have been demonstrated for the quantification of halide in ILs, although it is important to note that many have only been investigated for halide in water-miscible ILs with few studies aimed at more hydrophobic ILs, such as those based on tetraalkylphosphonium cations or trispentafluoroethyltrifluorophosphate ([FAP]$^-$) anions. These techniques include Volhard (silver nitrate) and chloride-selective electrodes,[6,13] spectrophotometry using fluorescent indicators,[14] ion chromatography (IC),[15−19] ICP-MS,[20] capillary zone electrophoresis,[21] XPS,[22] and electrochemistry.[23−25] IC has been demonstrated to be a versatile technique for the determination of halides in both hydrophobic and hydrophilic ILs. For example, Villagrán et al.

* To whom correspondence should be addressed. E-mail: c.hardacre@qub.ac.uk (C.H.), j.m.macinnes@sheffield.ac.uk (J.M.M.).
[†] Queen's University Belfast.
[‡] University of Sheffield.
[§] Nottingham Trent University.

(1) *Ionic Liquids in Synthesis*, 2nd ed.; Wasserscheid, P., Welton, T., Eds.; Wiley-VCH Verlag: Weinheim, 2007.
(2) Pârvulescu, V. I.; Hardacre, C. *Chem. Rev.* **2007**, *107*, 2615–2665.
(3) Silvester, D. S.; Compton, R. G. *Z. Phys. Chem.* **2006**, *220*, 1247–1274.
(4) Harper, J. B.; Kobrak, M. N. *Mini-Rev. Org. Chem.* **2006**, *3*, 253–269.
(5) Plechkova, N. V.; Seddon, K. R. *Chem. Soc. Rev.* **2008**, *37*, 123–150.
(6) Seddon, K. R.; Stark, A.; Torres, M. J. *Pure Appl. Chem.* **2000**, *72*, 2275–2287.
(7) Ge, R.; Hardacre, C.; Jacquemin, J.; Nancarrow, P.; Rooney, D. W. *J. Chem. Eng. Data* **2008**, *53*, 2148–2153.
(8) Anderson, K.; Goodrich, P.; Hardacre, C.; Rooney, D. W. *Green Chem.* **2003**, *5*, 448–453.
(9) Jacquemin, J.; Ge, R.; Nancarrow, P.; Rooney, D. W.; Costa Gomes, M. F.; Pádua, A. A. H.; Hardacre, C. *J. Chem. Eng. Data* **2008**, *53*, 716–726.
(10) Jacquemin, J.; Nancarrow, P.; Rooney, D. W.; Costa Gomes, M. F.; Husson, P.; Majer, V.; Pádua, A. A. H.; Hardacre, C. *J. Chem. Eng. Data* **2008**, *53*, 2133–2143.
(11) *Electrodeposition from Ionic Liquids*; Endres, F., MacFarlane, D., Abbott, A., Eds.; Wiley-VCH Verlag: Weinheim, 2008.
(12) Hilgers, C.; Wasserscheid, P. In *Ionic Liquids in Synthesis*; Wasserscheid, P., Welton, T., Eds.; Wiley-VCH Verlag: Weinheim, 2007.
(13) Mateus, N. N. M.; Branco, L. C.; Lourenço, N. M. T.; Afonso, C. A. M. *Green Chem.* **2003**, *5*, 347–352.
(14) Anthony, J. L.; Maginn, E. J.; Brennecke, J. F. *J. Phys. Chem. B* **2001**, *105*, 10942–10949.
(15) Billard, I.; Moutiers, G.; Labet, A.; El Azzi, A.; Gaillard, C.; Mariet, C.; Lutzenkirchen, K. *Inorg. Chem.* **2003**, *42*, 1726–1733.
(16) Anderson, J. L.; Ding, J.; Welton, T.; Armstrong, D. W. *J. Am. Chem. Soc.* **2002**, *124*, 14247–14254.
(17) Villagrán, C.; Deetlefs, M.; Pitner, W. R.; Hardacre, C. *Anal. Chem.* **2004**, *76*, 2118–2123.
(18) Hao, F.; Haddad, P. R.; Ruther, T. *Chromatographia* **2008**, *67*, 495–498.
(19) Stepnowski, P.; Markowska, A. *Aust. J. Chem.* **2008**, *61*, 409–413.
(20) McCamley, K.; Warner, N. A.; Lamoureux, M. M.; Scammells, P. J.; Singer, R. D. *Green Chem.* **2004**, *6*, 341–344.
(21) Berthier, D.; Varenne, A.; Gareil, P.; Digne, M.; Lienemann, C.-P.; Magna, L.; Olivier-Bourbigou, H. *Analyst* **2004**, *129*, 1257–1261.
(22) Silvester, D. S.; Broder, T. L.; Aldous, L.; Hardacre, C.; Crossley, A.; Compton, R. G. *Analyst* **2007**, *132*, 196–198.

10.1021/ac802406k CCC: $40.75
Published on Web 01/22/2009

Table 1. Comparison of the Commonly Used Techniques for the Determination of Halide in ILs

method	approximate mass of IL needed/g[a]	LOQ/ppm[a]	comments	reference
Volhard	0.3	ca. 400	IL must be water miscible	6
Spectrophotometric	n/a	ca. 300	IL must not quench fluorescence	13
Chloride selective electrode	0.1	ca. 20 for water miscible samples	Reported for water and ethanol miscible IL samples. Note for ethanol soluble samples minimum values of 1000 ppm have been reported	6
Ion chromatography	0.1	4−8	IL must dissolve in a minimum of 40% acetonitrile +60% H_2O; Long retentions times are found for highly polarizable anions such as $[NTf_2]^-$, $[FAP]^-$ in general limiting turnaround of samples	16
ICP-MS	0.1	ca. 0.01	Low LOQ was found for water soluble IL but problems were encountered for water immiscible ILs due to low solubility.	19
Capillary zone electrophoresis	0.2	ca. 5	Water miscible and immiscible ILs studied.	20
Macro-scale Electrochemistry	1.0	2−30	The viscosity of the IL to be analyzed limits the detection limit but high viscosity materials can be diluted with molecular solvents.	23
Microscale Electrochemistry	<0.05	5−17		this work

[a] Mass of IL used determines the LOQ of the techniques where the sample needs to be diluted. The LOQ values shown in the table are for the mass of IL summarized.

showed that limits of quantification (LOQ) of <8 ppm were possible for both 1-butyl-3-methyl imidazolium hexafluorophphate ($[C_4mim][PF_6]$) and tetrafluoroborate ($[C_4mim][BF_4]$) ILs.[16] However, for ILs containing large polarizable anions, such as bis{(trifluoromethanesulfonyl)imide} ($[NTf_2]^-$) the analysis time can be long and relatively large amounts of IL (~ 100 μL) are needed. In addition, the samples must have a significant solubility in water-organic solvent mixtures as they cannot be analyzed without dilution.

Spectrophotometry and electrochemical techniques such as linear sweep (LSV), square wave (SWV), and cathodic stripping voltammetry have been used to quantify the chloride concentration in both water miscible and water immiscible ILs. Both methods can be scaled down to chip level, although limits of quantification below 400 ppm have not been achieved by spectrophotometry.[6] For electrochemical techniques good sensitivity has been reported for both LSV and SWV in $[C_4mim][PF_6]$, $[C_4mim][BF_4]$, and $[C_4mim][NTf_2]$, with levels of quantification ranging between 7 and 30 ppm, the value being dependent upon the viscosity of the IL.[23] Cathodic stripping voltammetry was shown to be capable of detecting sub parts per million levels of halide, with limits of quantification reported to be ~0.3 ppm for $[C_4mim][PF_6]$, $[C_4mim][BF_4]$, and $[C_4mim][NTf_2]$.[23] In general, the electrochemistry techniques employed to date require a significant volume of IL (at least ~1000 μL) for each sample, and multiple samples are required to produce calibration curves. In addition, each sample takes a significant amount of time to measure, including electrode preparation, multiple sample preparation, cleaning and reassembly of set up, and the measurement. The techniques used, to date, for ILs and the LOQ/mass used in each with limitations are summarized in Table 1. It should be noted that all methods currently used routinely require a calibration curve; therefore, preparation times for the analysis of the IL samples can vary significantly depending on the dilutions required and the number of data points on the calibration curve.

This paper examines the use of a microfluidic device incorporating a mixer and electrochemical cell to provide an automated voltammetric method of determination of halide content in ILs using a small volume of IL. A number of considerations are required to be taken into account and assessed prior to implementation of the technology. Because of the small area of the electrodes, the limits of detection and quantification need to be examined in detail. Moreover, the issue of measurement reproducibility is important with both electrode cleanliness and sample to sample contamination, important considerations for assembled devices. Most polycrystalline electrodes require either periodic resurfacing or pretreatment to maintain optimal and reproducible behavior.[26] For the device used herein, platinum is used as the electrode material which is commonly used for both macro- and

(23) Xiao, L.; Johnson, K. E. *J. Electrochem. Soc.* **2003**, *150*, E307−E311.
(24) Villagrán, C.; Banks, C. E.; Hardacre, C.; Compton, R. G. *Anal. Chem.* **2004**, *76*, 1998–2003.
(25) Sun, H.; Yu, L.; Jin, X.; Hu, X.; Wang, D.; Chen, G. Z. *Electrochem. Commun.* **2005**, *7*, 685–691.
(26) Swain, G. M. In *Handbook of Electrochemistry*; Zoski, C. G., Ed.; Elsevier: Amsterdam, 2007.

microscale electrochemistry.[27] However, it is also prone to oxide formation and the adsorption of foreign species; thus, reproducible electrode handling is required to generate a reproducible response. As well as physical resurfacing by the use of abrasive materials, electrochemical cleaning is a method of surface regeneration. Typically, for platinum, this takes the form of deliberate oxide formation at oxidative potentials followed by oxide dissolution at reductive potentials to yield a regenerated Pt surface.[26] However, this requires the original introduction of a potential oxide forming compound, such as water. Therefore, while this method is favored for aqueous studies, its use in ideally anhydrous or non-aqueous electrochemical studies is limited. An alternative mechanism is the generation of gas bubbles, or the generation of chemically reactive reagents to clean the electrode surface. This issue has been addressed in detail in this paper.

Because of their high viscosity and low diffusivity compared with commonly employed molecular solvents, few studies have examined the use of microchannel devices with ILs. For example, de Mello et al. use electric current through IL in a microchannel to provide heating and, thereby, temperature control on a microfluidic device.[28] Chen et al. examined the mixing of a fluorescent dye in IL streams in a chain of special microchannel elements.[31] However, to date microchannel devices incorporating electrochemical cells and their use for analytical purposes have not been examined.

The preparation of known concentrations for calibration purposes in this work used an automated procedure employing syringes, syringe drives, and a mixer device. The precision of the mixture composition produced by the device is demonstrated in the paper. A further aspect of accurate measurement of a particular sample solution is deposition of a pure aliquot of that sample in the volume of the measurement cell. In order for pre-existing sample liquid not to contaminate the deposited sample adequate volume flushing of the supply path with the new sample liquid must be achieved.

EXPERIMENTAL SECTION

Materials and Synthesis. 1-Butyl-3-methylimidazolium chloride ([C_4mim]Cl), 1-butyl-1-methylpyrrolidinium chloride ([C_4mPyrr]Cl), 1-butyl-3-methylimidazolium bis{(trifluoromethyl)-sulfonyl}imide ([C_4mim][NTf_2]), 1-butyl-3-methylimidazolium trifluoromethanesulfonate ([C_4mim][OTf]), and 1-butyl-3-methylimidazolium tetrafluoroborate ([C_4mim][BF_4]) were prepared in house using standard literature methods.[29−31] ILs based on the trispentafluoroethyltrifluorophosphate ([FAP]$^-$) anion were obtained from Merck. Trihexyltetradecylphosphonium bis{(trifluoromethyl)sulfonyl}imide ([$P_{666,14}$][NTf_2]) was prepared from [$P_{666,14}$]Cl supplied by Cytec. The halide content of ILs was determined using suppressed ion chromatography (IC),[16] with the exception of the [$P_{666,14}$]$^+$ and [FAP]$^-$ based ILs which cannot currently be measured using IC. The water content was determined by volumetric Karl Fischer titration using a Mettler Toledo DL31 titrator. All ILs were found to have halide concentrations below the detection limit of suppressed ion chromatography (ca. 5 ppm). All ILs were dried under high vacuum at 70 °C prior to use, until the resulting IL contained a residual water content of <0.01 wt %. The ILs were stored in a N_2-filled glovebox where all solutions were prepared and the reservoirs were loaded.

Instrumentation. All experiments and automated syringe loading were carried out in an air-conditioned room (temperature 20 ± 1 °C).

Macro-scale electrochemical determination of chloride content was carried out in glass cells using 2 g of IL, and performed with a three-electrode arrangement with a platinum (1.6 mm diameter) working electrode and two platinum wires as counter and pseudo-reference electrodes. The cell and electrolyte were purged with argon prior to use. The Pt electrode was polished successively with 5, 1, and 0.01 μm alumina slurries on lapping pads.

Both macro-scale and on chip determination of the chloride concentration by cyclic voltammetry (CV) as well as phenol passivation and cleaning experiments were recorded with a PC controlled potentiostat/galvanostat EG&G Model 273A, using the EG&G EChem software. All other experiments were recorded with a PC controlled Autolab μAUTIII potentiostat, using Eco Chemie GPES 4.9.

Details of the Microfluidic Device. The apparatus for the automated sample preparation and delivery used Nemesys syringe drives (Cetoni) with 250 μL Gastight syringes (Hamilton) to control flow through a network constructed from two glass chips supplied by Micronit Microfluidics and interconnecting capillary tubing and fittings (Upchurch). The maximum injection rate for each syringe within the system was 0.1 μL s^{-1} based upon specified pressure tolerances for the syringes. The first glass chip contained an 18 element tear-drop mixer[32,33] supplied off the shelf (Micronit TD18), and the second chip was designed in house and included the electrochemical cell used in the experiments. Figure 1a shows a diagram of the flow network. The two syringes A and B supply the mixer to create a prescribed uniform mixture for the electrochemical cell. For example with syringe A filled with a known ferrocene and IL mixture and syringe B with a pure IL, a ferrocene solution of concentration anywhere in the range from zero to that of the syringe A solution can be supplied to the electrochemical cell. The additional syringe, C, is filled with an IL with high chloride concentration for use as an electrode cleaning agent. The volume flow rates from syringes A and B determine the concentration emerging from the mixer once steady conditions are reached and, again depending on the flow rates set, either flow from the mixer or from Syringe C can be sent to the electrochemical cell. Thus, under computer control of the three syringes considerable flexibility in the sequence of flow is available. Figure 1b shows the two chips clamped in holders facilitating the flow and electrical connections. The flow connections were made using Nanoport fittings and ferrules, PEEK

(27) Manica, D. P.; Mitsumori, Y.; Ewing, A. G. *Anal. Chem.* **2003**, *75*, 4572–4577.
(28) de Mello, A. J.; Habgood, M.; Lancaster, N. L.; Welton, T.; Wootton, R. C. R. *Lab Chip* **2004**, *4*, 417–419.
(29) Earle, M. J.; Katdare, S. P.; Seddon, K. R. *Org. Lett.* **2004**, *6*, 707–710.
(30) Bonhôte, P.; Dias, A. P.; Papageorgiou, N.; Kalyanasundaram, K.; Grätzel, M. *Inorg. Chem.* **1996**, *35*, 1168–1178.
(31) Suarez, P. A. Z.; Einloft, S.; Dullius, J. E. L.; de Souza, R. F.; Dupont, J. *J. Chim. Phys.* **1998**, *95*, 1626–1639.
(32) Chen, Z.; Bown, M.; O'Sullivan, B.; MacInnes, J. M.; Allen, R. W. K.; Mulder, M.; Blom, M.; van't Oever, R. *Microfluid. Nanofluid.* **2008**, in press.
(33) Priestman, G. H.; MacInnes, J. M.; Tippetts, J. R.; Allen, R. W. K. Fluidic oscillators for measurement, mixing and monitoring in micro reactors. Proceedings of the 7th World Congress of Chemical Engineering, Glasgow, U.K., July 10−14, 2005.

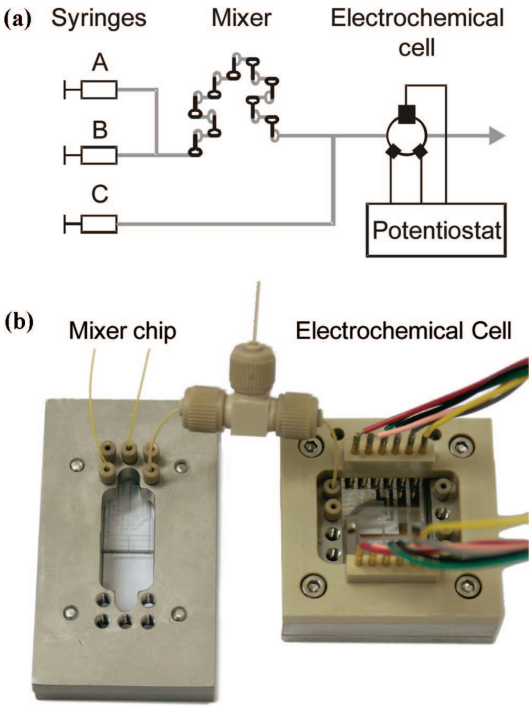

Figure 1. (a) Diagram of experimental apparatus. The two syringes A and B supply the mixer to form prescribed mixture to the electrochemical cell. Syringe C is used in the experiments to supply high concentration chloride solution to the cell for cleaning. (b) Mixer chip and electrochemical cell arrangement showing the chip holders, capillary flow connections between the two chips and the "T" junction fitting. The three input streams come in from the top of the photograph (two into the mixer chip and one into the T fitting). The outlet capillary from the electrochemical cell goes out the right-hand side of the photograph (not visible) and the electrical connection for the working, pseudo-reference, and counter electrodes are included in the wire bundles exiting to the right.

MicroTee fitting and 150 μm internal diameter PEEK capillary tubing (Upchurch). Electrical connections were made using standard spring pins (RS). The mixer is expected to produce uniformity at is outlet of less than 0.1% standard deviation in composition relative to the average for the conditions of operation.[34] The electrochemical cell cavity encloses 260 nL volume and is formed by wet etching 75 μm into one glass layer and depositing a 100 nm thick platinum pattern on a second to form the cell electrodes and electrical connections. When the layers are bonded together the cell is completed, with etched passages 250 μm wide (and 75 μm deep) leading flow to and from the cell. The electrodes overlap the edges of the cell as indicated in Figure 1a such that the contact area with fluid in the cell is 0.0033 cm^2 for the working electrode and 0.0015 cm^2 each for the pseudo-reference and counter electrodes. The holes leading from the chip channel passages up to the capillary connections in both the mixer and the electrochemical chips are powder-blasted, and these holes have volumes 1.1 and 0.3 μL, respectively.

When switching from one stream or mixture to the next it is necessary to clear out the existing solution so the desired composition is present in pure form in the electrochemical cell. Achieving this requires passing a sufficient volume along the path leading from the point of introduction of the new solution (the junction leading into the mixer in this case) through to the outlet of the cell. The larger this path volume, the more solution volume must flow to produce a given level of purity. Thus, the internal volume (capillary tubing and chip passages including connection holes, channels, and the electrochemical cell itself) between the mixer junction and cell outlet is an important parameter. This path volume is estimated to be 3.8 μL.

Two things are crucial to ensure pure deposition in the cell can be achieved. First, unused streams must be retracted from the junctions through which the desired solution flows. Otherwise diffusion of material from the unused streams into the stream that is being deposited will mean contamination of the solution used to flush the path volume. While eventually the unused streams at a junction will be cleared by the diffusion this will take an impractically long time and large amount of sample solution to achieve good sample purity in the cell. Efficient clearing, therefore, requires an initial rapid retraction of all unused streams back away from the junctions so the desired solution may pass uncontaminated.

Second, when the syringe drives are stopped mechanical relaxation occurs (in the drive mechanism, syringes, and liquid) which produces a brief continuation of flow from all syringes. The materials associated with this flow has an uncontrolled composition and must not reach the electrochemical cell. It may be possible to compensate to a large degree for the relaxation by retraction of the syringes to minimize the leaked solution volume. Herein, the experiments were conducted such that the path volume between junction and electrochemical cell was sufficiently large for the uncontrolled mixture not to reach the cell. For the flow rates, and hence pressure changes, used in the experiments the relaxation flow is estimated to expel up to 100 nL from each syringe supply. Thus up to a total of 300 nL may leak from the three solutions. Approximately twice that volume of the passage may be affected since the core of the flow travels further than the average (by exactly twice in a capillary passage, see, e.g., ref 35). With the downstream passage volume being 1 μL for the T junction and 3.5 μL for the mixer junction, the electrochemical measurement cell should be protected from the uncontrolled mixture produced during relaxation.

RESULTS AND DISCUSSION

Validation of the Injection Protocol and Mixer Chip to Accurately Prepare Known Mixtures. Although the effectiveness of the low Reynolds number mixer chip has previously been demonstrated,[33,34,36] the combination of an automated injection system plus mixer chip (Figure 1a,b) had not been validated to produce known concentrations of samples inside a subsequent chip. The protocol used was, therefore, tested using ferrocene (Fc) solutions measured using UV−vis absorption spectroscopy. A concentrated sample of ferrocene (50 mM, ca. 15000 ppm) was prepared in methanol (MeOH) and loaded into syringe A, while

(34) MacInnes, J. M.; Vikhansky, A.; Allen, R. W. K. *Chem. Eng. Sci.* **2007**, *62*, 2718–2727.
(35) MacInnes, J. M.; Du, X.; Allen, R. W. K. *Phys. Fluids* **2003**, *15*, 1992–2005.
(36) MacInnes, J. M.; Chen, Z.; Allen, R. W. K. *Chem. Eng. Sci.* **2005**, *60*, 3453–3467.

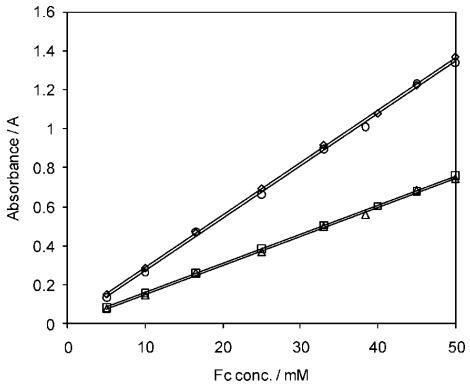

Figure 2. Comparison of the UV−vis absorbance of solutions of ferrocene prepared on-chip (440 nm(○) (R^2 = 0.998) and 325 nm (△) (R^2 = 0.997)) and off-chip (440 nm (◇) (R^2 = 0.999) and 325 nm (□) (R^2 = 0.999)), as a function of the ferrocene concentration. The concentrations were set using the control program and made by mixing a Fc solution (50 mM Fc in methanol) with pure methanol within the mixer chip.

pure MeOH was loaded into syringe B. Consecutively, eight mixing ratios were then used to prepare 1000 μL samples for off chip analysis, after passing through the entire system, and after discarding the first ca. 100 μL.

Figure 2 compares the UV−vis absorption as a function of concentration prepared on chip, as well as off chip, using micropipettes. Ferrocene is known to possess two absorption peaks in methanol, corresponding to 325 and 440 nm,[37] and both methods gave consistent data with linear plots of excellent fit demonstrating the reliability of the mixing and injection methodology under steady flow conditions.

ILs have a much higher viscosity, in general, than molecular solvent and therefore the mixing of ILs was validated within the microfluidic device using stop-flow and the electrochemistry cell. Eleven samples were prepared by mixing a 50 mM solution of ferrocene in [C_4mim][NTf_2] in syringe A with pure [C_4mim][NTf_2] in syringe B, and the concentrations measured using CV.

Figure 3 displays the correlation between both the peak area and the peak current of the Fc oxidation peak versus the Fc concentration expected from the mixing chip. In both cases a good linear fit between 0−50 mM was obtained demonstrating that efficient and predictable mixing was achievable with the high viscosity media. Figure 4 shows the effect of scan rate on the peak area and peak current using a 50 mM solution of Fc in [C_4mim][NTf_2] over 5 to 300 mV s^{-1}. In each case an ideal linear response was observed.

By increasing mass transfer, the size of the current response at the electrode can be increased. As such, steady-state voltammetry is a desirable technique for low concentrations of analyte. CVs were carried out for injection ratios for syringe A containing 50 mM solution of ferrocene in [C_4mim][NTf_2]: syringe B containing pure [C_4mim][NTf_2] of 1:0, 0.3:0.7, and 0.1:0.9

(37) Lagunas, M. C.; Pitner, W. R.; van den Berg, J. A.; Seddon, K. R. *ACS Symp. Ser.* **2003**, *856*, 421–438; Ionic Liquids As Green Solvents: Progress And Prospects.

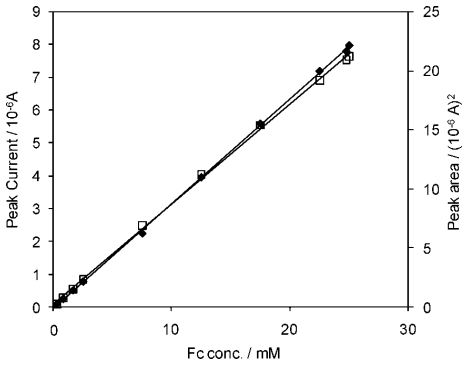

Figure 3. Calibration plots for the CV of Fc solutions, generated by mixing various volume ratios of a 50 mM solution of Fc in [C_4mim][NTf_2] with pure [C_4mim][NTf_2] within the mixer chip, displaying peak area vs predicted Fc concentration (♦, R^2 = 0.999) and peak current vs predicted Fc concentration (□, R^2 = 0.999).

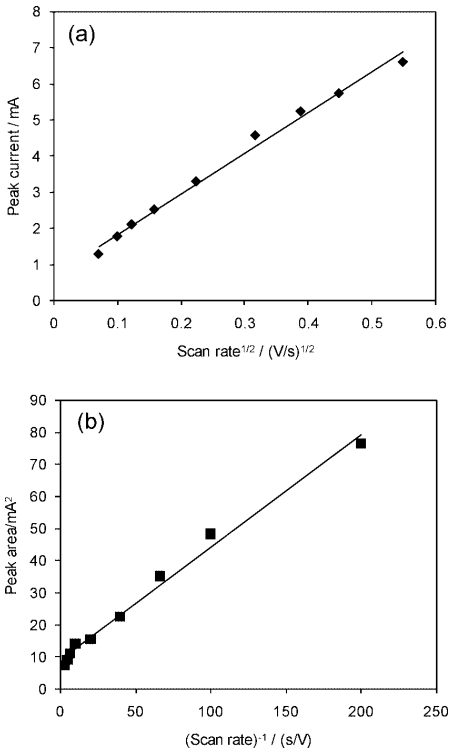

Figure 4. Plots for a 50 mM solution of Fc in [C_4mim][NTf_2], displaying (a) peak current vs the square root of the scan rate (R^2 = 0.992) and (b) peak area vs the inverse of the scan rate (R^2 = 0.989).

(Figure 5a). Under all conditions used, steady state current response was observed with a linear current response with Fc concentration. Therefore, steady state voltammetry can be carried out using this apparatus, including automated mixing of sample, while only consuming IL on the μL-scale. Figure 5b also includes the peak current values and peak area values for the three injection

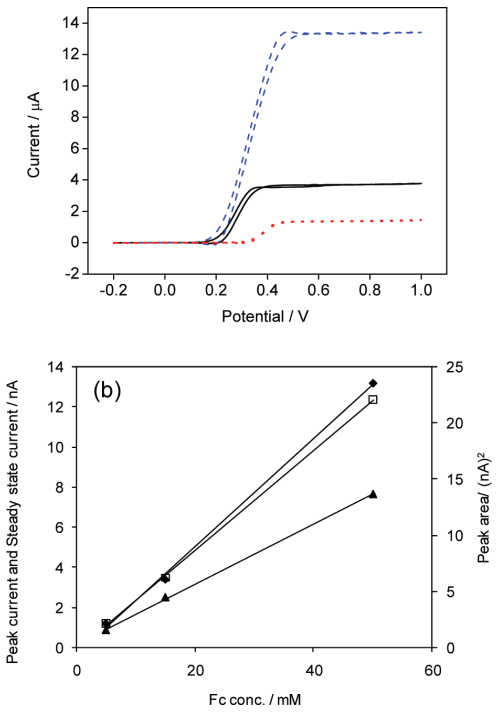

Figure 5. (a) "Steady-state" voltammetry at different injection ratios (total flow rate 1 μL/s) giving Fc concentrations of 50 mM Fc (dashed line), 15 mM Fc (solid line) and 5 mM Fc (dotted line) in [C_4mim][NTf_2]. (b) Comparison plots for "steady-state" peak current (♦, $R^2 = 0.998$), quiescent state peak currents (▲, $R^2 = 0.999$) and quiescent state peak areas (□, $R^2 = 0.999$) at each Fc concentration.

ratios when scanned under quiescent conditions. From the definition that sensitivity is the current response divided by concentration, it is observed that peak area is still a more sensitive means of concentration determination than peak current. However, steady-state voltammetry offers an improvement over quiescent peak current measurement.

Electrochemical Quantification of Halide Content by CV: Comparison between Microfluidic Device and Conventional Macro-Electrode Setup. Villagrán et al. reported that linear sweep voltammetry at a glassy carbon (GC) macro-electrode can be used to quantify chloride content in ILs using chloride oxidation with a limit of quantification at the parts per million level.[24] For example, a limit of quantification of 4.2 ppm was found for [C_4mim][NTf_2] using this methodology. This procedure was repeated in an electrochemical cell using a Pt macro-scale working electrode and two Pt wires as counter and quasi-reference electrodes to mirror the setup in the microfluidic electrochemical cell. Ten solutions of [C_4mim][NTf_2] with chloride contents between 49 ppm to 1400 ppm were prepared by adding chloride in the form of [C_4mim]Cl. The voltammetry observed was consistent with that previously reported for [C_4mim]Cl at Pt in [C_4mim][NTf_2].[38] Linear correlations were observed between peak current and chloride content at scan rates of both 5 mV s^{-1} and 100 mV s^{-1} (Figure 6). The scans at 5 mV s^{-1} were observed to be more reproducible but took approximately 260 s to complete, while scans at 100 mV s^{-1} took about 13 s and gave greater current response but poorer signal-to-noise ratios at lower Cl^- concentrations, that is, at 100 mV s^{-1}.

The same solutions were also analyzed by linear sweep voltammetry on chip. It should be noted that for these experiments a single syringe and syringe pump was used, and the mixer chip was bypassed. A strong correlation between current and chloride content was also observed over all concentrations on the microfluidic device. Panels b and d of Figure 6 display the linear sweep scans for all chloride contents at 100 mV s^{-1} and the correlation between peak current at 5 mV s^{-1} and 100 mV s^{-1} with added chloride content, respectively. The improvement in the linear correlation upon moving from the macro- to the microscale setup is attributed to the fixed position of the electrodes within the cell. In the macro-electrode more variability of the distances between the working, counter, and reference electrodes is possible and, therefore, the microfluidic device presents a clear improvement for repeated analytical work. In addition, the macro-electrode experiments typically used at least 15000 μL for a ten-point calibration with [C_4mim][NTf_2], compared with about 1000 μL (sample + chloride-spiked sample) on the microfluidic device showing the benefit of moving to the small scale.

Flushing of the Microfluidic Device. To investigate a large number of samples while minimizing the volume used, it is necessary to be able to flush out the preceding sample with the next sample. To evaluate the efficiency in flushing out the old sample, the number of volume changes required to completely remove a sample from the electrochemical cell was examined. Volume changes were delivered incrementally, six path volume changes at a time, with the flow stopped between increments to allow a CV scan to be made. While this is not ideal since mechanical relaxation causes the retracted unused streams to flow into the path volume, it was a convenient way to collect data. Three concentration samples of Fc solution in [C_4mim][NTf_2], 66 mM (~12500 ppm), 26.4 mM (~5000 ppm), and 6.6 mM (~1250 ppm), were introduced into the cell, and CV was used to measure the concentration of Fc as a function of the number of path volume changes of pure [C_4mim][NTf_2] injected as the washing solvent. Although a significant drop is observed, beyond 12 volume changes the Fc concentration appears to have reached a plateau value dependent on initial concentration as can be seen by plotting the data on semilog axes, Figure 7. The decay in contamination concentration is expected to be more rapid than exponential for this convection-diffusion process while the plateau tendency of the results shows a far slower than exponential decay. The likely cause is the incremental delivery which, because of the relaxation effect, allows deposition of some Fc solution into the path volume downstream of the mixer inlet junction following each increment.

Electrode Fouling and Regeneration Techniques. Because of the fixed nature of the electrochemical cell within the microfluidic device, it is not possible to clean the electrodes by mechanical means and, therefore, chemical cleaning is necessary. To investigate the efficiency of such cleaning, the electrodes were

(38) Aldous, L.; Silvester, D. S.; Villagrán, C.; Pitner, W. R.; Compton, R. G.; Lagunas, M. C.; Hardacre, C. *New J. Chem.* **2006**, *30*, 1576–1583.

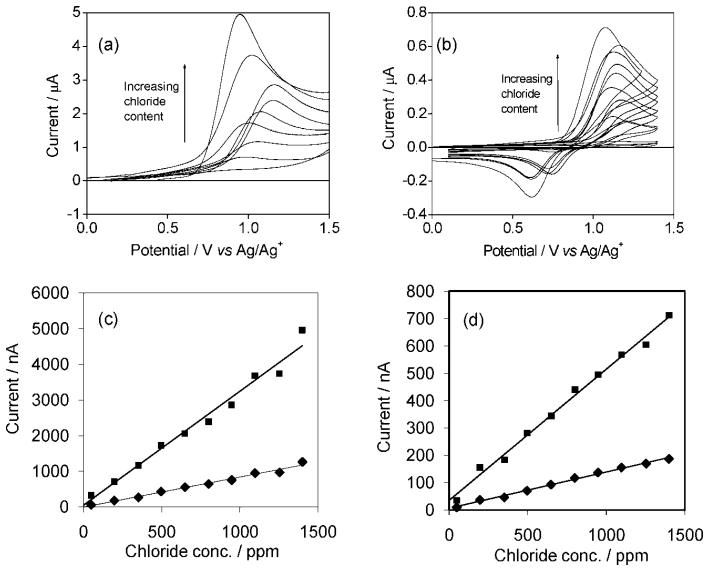

Figure 6. Linear sweep and CV of various chloride concentrations in $[C_4mim][NTf_2]$ using (a) a macro-electrode setup and (b) the microfluidic device. A comparison of peak current using (c) a macro-electrode setup at 5 mV s^{-1} (■, $R^2 = 0.985$) and 100 mV s^{-1} (♦, $R^2 = 0.978$) and (d) the microfludic device at 5 mV s^{-1} (■, $R^2 = 0.994$) and 100 mV s^{-1} (♦, $R^2 = 0.992$).

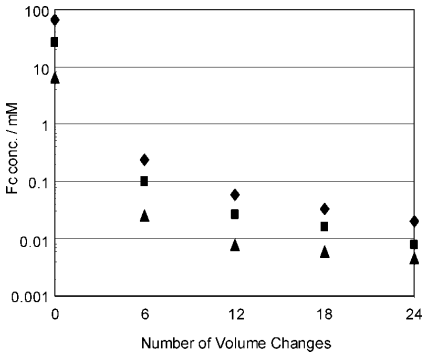

Figure 7. Concentration of Fc remaining in the chip after flushing various concentrations (66 mM(♦), 24.6(■), and 6.6 mM (▲)) of Fc in $[C_4mim][NTf_2]$ with 6, 12, 18 and 24 volume changes of pure $[C_4mim][NTf_2]$, based upon peak oxidation current.

deliberately passivated using phenol oxidation and polymerization.[39] Recently, Villagrán et al. demonstrated that in $[C_2mim][NTf_2]$ using a GC electrode, phenol displays a single oxidation peak, and bulk oxidation leads to the formation of polymerization product.[39] After injecting a 15 mM solution of phenol in $[C_4mim][NTf_2]$, three consecutive CVs showed initially a large oxidation peak at about +1.75 V versus Pt followed by no clear oxidation peaks in the second and third scans (Figure 8a). Similarly, on injecting a 15 mM solution of ferrocene in $[C_4mim][NTf_2]$ after passivation, no significant oxidation features were observed (Figure 8b). The fact that the passivation was not removed after flushing indicates that the electrode surface was fouled by a strongly adsorbed layer.

(39) Villagrán, C.; Aldous, L.; Lagunas, M. C.; Compton, R. G.; Hardacre, C. *J. Electroanal. Chem.* **2006**, *588*, 27–31.

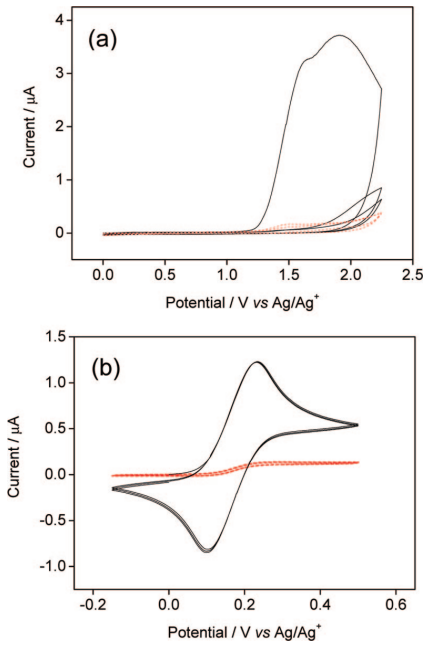

Figure 8. (a) CV of a 15 mM solution of phenol in $[C_4mim][NTf_2]$, displaying the first three consecutive scans (solid line) and three more consecutive scans after injecting 10 μL fresh phenol solution (dashed line). (b) Overlay of ferrocene scans before (solid line) and after (dashed line) electrode passivation by phenol oxidation.

Alternating the polarity of platinum electrodes has the potential to desorb some adsorbed compounds, especially charged compounds.[26] Cleaning of this type was evaluated by rapidly scanning

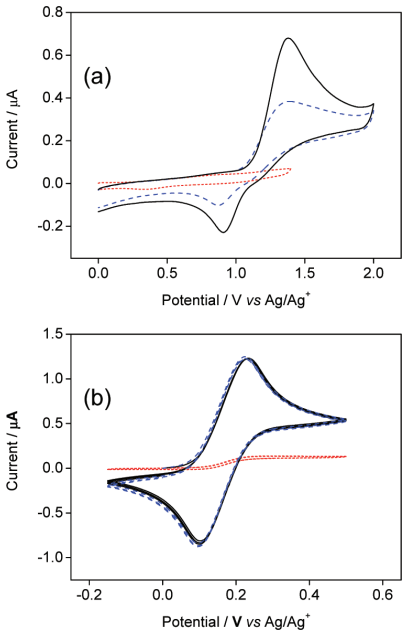

Figure 9. (a) CV of a 15 mM solution of $[C_4mim]Cl$ in $[C_4mim][NTf_2]$, after phenol passivation but prior to cleaning (dotted line), after being partially cleaned (dashed line) and after being completely cleaned (solid line). (b) CV of a 15 mM solution of Fc in $[C_4mim][NTf_2]$ prior to phenol passivation (solid line), after phenol passivation (dotted line), and after electrode cleaning (dashed line).

between +0.5 and −0.5 V, holding at each vertex for 3 s, while flowing pure $[C_4mim][NTf_2]$ at 5 μL min^{-1}. However, a quiescent scan of a 15 mM solution of ferrocene in $[C_4mim][NTf_2]$ before and after cleaning showed only a marginal improvement in the response. In contrast, chemical cleaning via the generation of gas bubbles and a reactive chemical species, in this case chlorine, showed significant improvement. An 11.5 mM solution of $[C_4mim]Cl$ in $[C_4mim][NTf_2]$ was introduced into the cell and the potential held at +2 V for 60 s, to generate Cl_2. Prior to this treatment, no chloride oxidation was observed because of the phenolic passivation; however, following sustained oxidation of the chloride to chlorine, scans of the chloride solution demonstrated gradually increasing oxidation peaks, reaching half the expected size after 7 treatments and producing chloride oxidation peaks consistent with that observed prior to phenol oxidation after 12 treatments (Figure 9). Careful control of the potential was also required as electrolysis at potentials of ≥+2.2 V, that is, beyond the oxidative window of $[C_4mim][NTf_2]$, was found to result in an overall decrease in the chloride oxidation peak because of passivation by oxidative decomposition of the IL, an effect that was only reversed by further chlorine generation at +2 V. Figure 9 indicates the effect of cleaning the electrode by showing CV scans of ferrocene at various stages of cleaning.

Optimization of Electrode Regeneration. On measuring the chloride content in the ILs using the microfluidic device, at high chloride concentrations there was sufficient generation of Cl_2 to clean the electrodes resulting in excellent reproducibility between samples. Therefore, no secondary cleaning was necessary. However, at lower chloride concentrations, typically below values of 40 ppm, the reproducibility decreased and additional surface regeneration in the form of Cl_2 generation was required. To produce sufficiently clean electrodes, a minimum chloride concentration of 400 ppm was required with the time taken for the treatment dependent on the concentration and the IL used. In general, it was found that four 15 min Cl_2 pretreatments generated using a 400 ppm Cl^- solution with flushing the chip with a fresh 400 ppm solution between each treatment was adequate to give reproducible results. This was achieved using a single syringe operation filled with the 400 ppm Cl^- IL solution.

While a 60 min long pretreatment step between samples using 400 ppm chloride solutions proved excellent for small batches of samples, the time required for the cleaning significantly reduced the turnover of samples possible. Much shorter treatment times were possible by increasing the concentration of chloride in $[C_4mim][NTf_2]$. Following fouling of the electrodes, the oxidative peak current of 40 ppm chloride was measured to probe electrode cleanliness. Using a 5 min treatment with either 2000 and 4000 ppm chloride did not result in reproducible oxidation currents (vs the established 60 min cleaning with 400 ppm Cl^-), indicating that a consistent electrode surface was not being achieved. In contrast, chlorine generation for 5 min using a 8000 ppm chloride solution resulted in a peak area within ~25% of that observed after the 60 min cleaning method. Furthermore, extending the cleaning time to 10 min resulted in a peak area ~5% of the ideal value. It should be noted that, although the cleaning protocol can be significantly speeded up by the use of solutions containing higher chloride content, more IL is used in flushing the chloride solution from the electrochemical cell to reach acceptable purity prior to analysis of the next sample.

Quantification of Chloride Using Square Wave (SWV) and Differential Pulse (DPV) Voltammetry. While both square wave (SWV) and differential pulse (DPV) gradually scan through ranges of potentials in a manner similar to linear sweep voltammetry, both techniques also subtract background current. This typically leads to improved signal-to-noise ratios and results in more sensitive and reproducible data. This was demonstrated in the quantification of halide in ILs by Villagrán et al. Therein, while LSV and SWV measurements of chloride content in $[C_4mim][NTf_2]$ gave limits of detection (LOD) of 4.2 and 4.3 ppm, respectively, SWV gave a significantly lower limit of quantification (LOQ) of 6.8 ppm relative to 25.6 ppm from linear sweep voltammetry.[39]

Halide contents between 5 and 40 ppm were investigated using SWV and DPV in $[C_4mim][NTf_2]$, $[C_4mim][OTf]$, $[C_4mim][BF_4]$, $[C_4mPyrr][NTf_2]$, $[P_{666,14}][NTf_2]$, and $[C_4mPyrr][FAP]$. A standard procedure was followed, whereby syringe A was loaded with a solution of 40 ppm of the chloride salt of the IL cation dissolved in the target IL, while syringe B was loaded with the pure IL. Syringe C was loaded with a 400 ppm "cleaning" solution of the chloride salt dissolved in the IL to be measured. Samples were then mixed at various concentrations using the automated mixer, and scans recorded using SWV and DPV, with 60 min cleaning (by Cl_2 generation) performed between

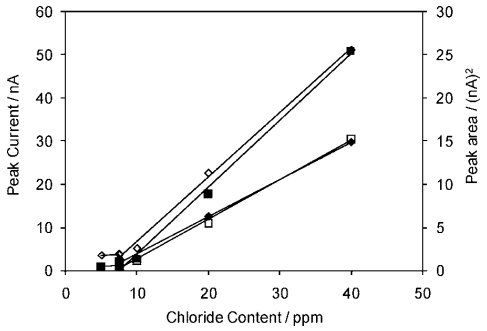

Figure 10. Comparison of the peak area and peak current as a function of chloride concentration at different frequencies, showing peak area at 32 Hz (♦, $R^2 = 0.997$) and 8 Hz (◇, $R^2 = 0.999$) and peak current at 32 Hz (■, $R^2 = 0.999$) and 8 Hz (□, $R^2 = 0.999$) for chloride in [C_4mim][NTf_2].

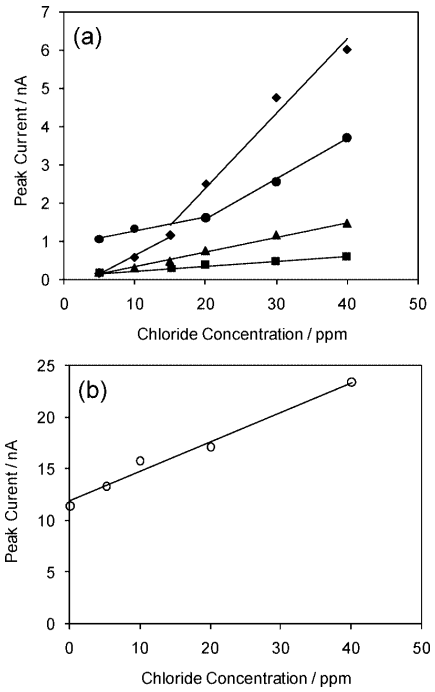

Figure 11. DPV peak current as a function of chloride concentration, for (a) [C_4mim][OTf] (♦, $R^2 = 0.977$), [C_4mim][BF_4] (●, $R^2 = 0.999$), [C_4mPyrr][NTf_2] (▲, $R^2 = 0.992$), [$P_{666,14}$][NTf_2] diluted with 20 wt % acetonitrile (■, $R^2 = 0.991$) and (b) [C_4mPyrr][FAP] (○, $R^2 = 0.981$).

the different scans/samples. In the case of [$P_{666,14}$][NTf_2], it was dissolved in acetonitrile at a weight ratio of 4:1 IL/acetontrile to decrease the viscosity of the IL and thus improve the peak current with respect to the background current. In the case of [C_4mPyrr][FAP], an 8000 ppm chloride cleaning solution was used over 10 min.

Figure 10 and Figure 11 show the peak current and peak area dependencies with respect to the concentration of added chloride in the six ILs tested. Using the criteria of signal-to-noise ratio as limit of detection (LOD)[40] and the lowest value in the linear region as the limit of quantification (LOQ), the LOD and LOQ of each IL using SWV and DPV were determined and are summarized in Table 2. The LOD and LOQ of the present technique were found to be unexpectedly low considering the small size of the electrodes and the small amount of sample used. With the exception of the tetraalkyl phosphonium based IL with LOQ values of <10 ppm, values observed were comparable to those found using the macroscale electrochemical cell.[39] For [$P_{666,14}$][NTf_2] higher LOQ/LOD values were observed, as expected, because of the higher viscosity and concomitantly smaller signal.

Table 2. LOD and LOQ for Chloride Determined for a Range of ILs Using SWV and DPV

method	IL	LOD/ppm	LOQ/ppm
SWV	[C_4mim][NTf_2]	5.7	7.3
	[C_4mim][BF_4]	3.6	5.6
DPV	[C_4mPyrr][NTf_2]	6.2	8.9
	[C_4mPyrr][FAP]	5.2	5.7
	[C_4mim][OTf]	5.0	5.2
	[C_4mim][BF_4]	5.2	5.5
	[$P_{666,14}$][NTf_2][a]	8.5	16.7

[a] Diluted with 20 wt % acetonitrile.

Benefit of the Technique. Table 1 summarizes the limitations associated with a range of halide detection techniques used in IL analysis. Both the Volhard and spectrophotometric techniques suffer from extremely high LOQ values, while also contaminating the sample with the necessary reagents. Although ion chromatography is a versatile technique for analyzing halide content in ILs, the sample commonly must be diluted with water or a combination of water and a water miscible solvent. This can result in problems where the IL does not dissolve to a sufficient extent, for example, [$P_{666,14}$][NTf_2] or [C_4mPyrr][FAP], or where the IL may decompose on dissolution. Villagrán et al. highlighted that [C_4mim][BF_4], when dissolved in a H_2O/acetonitrile mixture, decomposes rapidly with the generation of fluorine observed by IC.[17] In addition, for highly polarizable anions such as $[NTf_2]^-$ or $[PF_6]^-$, extended sample runs are required to elute the IL anion even using a gradient elution system with high concentrations of base.[17] Capillary zone electrophoresis has a wider IL range than IC enabling both water miscible and immiscible samples to be studied, but dilution of the sample was still necessary. In this case methanol was used.[21] ICP-MS provides a highly sensitive method for water miscible samples only. For water insoluble samples, the method became unreliable.[20] Similar issues were found with chloride sensitive electrodes where an LOQ ~ 20 ppm was only found for water miscible samples.[6,13] The electrochemical methods allow the analysis of the IL samples in their undiluted form with the analysis on the microfluidic device providing a more economical method with respect to sample waste compared with the macro-scale electrochemical setup. Both the macro- and microscale set-ups result in similar LOQ values; however, as demonstrated by the need to dilute the [$P_{666,14}$][NTf_2] IL to a small extent, some limitations with respect to viscosity are present with the electrochemical method. The electrochemical microfluidic

(40) Brett, C. M. A., Brett, A. M. O. In *Electroanalysis*, Oxford Chemistry Primers, No. 64; Oxford University Press: Oxford, 1998.

device allows the versalitility and similar LOQ of capillary zone electorphoresis and, to some extent, IC but uses a smaller volume of IL and offers a nondestructive methodology.

CONCLUSIONS

An automated microfluidic electrochemical device has been demonstrated which can measure the halide content of a wide range of hydrophobic and hydrophilic ILs to levels <20 ppm. As well as the electrochemical cell, the microfluidic device incorporates a mixer chip which enables rapid calibration of the device, and the mixing has been shown to be reproducible even with the highest viscosity ILs tested. A chemical cleaning protocol was established using a high concentration of chloride in the IL to produce reproducible electrode surfaces. In comparison with many other techniques used to measure halide, the electrochemical method is versatile and does not require sample pre-treatment before measurement except for high viscosity samples. By utilizing the microfluidic device, the sample size may be reduced compared with the macro-scale electrochemical setup, and the time between samples reduced to 15 min which includes the time taken to clean the electrodes, as well as the injection and analysis.

ACKNOWLEDGMENT

This work has been supported by the U.K. Engineering & Physical Sciences Research Council (EPSRC) under grants EP/D03826X/1, EP/D038294/1 and EP/D038995/1.

Received for review November 13, 2008. Accepted December 29, 2008.

AC802406K

D.3 Journal of Biomicrofluidics

BIOMICROFLUIDICS **4**, 014107 (2010)

Small volume laboratory on a chip measurements incorporating the quartz crystal microbalance to measure the viscosity-density product of room temperature ionic liquids

N. Doy,[1] G. McHale,[1] M. I. Newton,[1] C. Hardacre,[2] R. Ge,[2] J. M. MacInnes,[3] D. Kuvshinov,[3] and R. W. Allen[3]
[1]*School of Science and Technology, Nottingham Trent University, Clifton Lane, Nottingham NG11 8NS, United Kingdom*
[2]*QUILL Center, School of Chemistry and Chemical Engineering, Queens University Belfast, Belfast, BT9 5AG Antrim, Northern Ireland, United Kingdom*
[3]*Department of Chemical and Process Engineering, University of Sheffield, Newcastle St., Sheffield S1 3JD, United Kingdom*

(Received 18 December 2009; accepted 10 February 2010; published online 8 March 2010)

A microfluidic glass chip system incorporating a quartz crystal microbalance (QCM) to measure the square root of the viscosity-density product of room temperature ionic liquids (RTILs) is presented. The QCM covers a central recess on a glass chip, with a seal formed by tightly clamping from above outside the sensing region. The change in resonant frequency of the QCM allows for the determination of the square root viscosity-density product of RTILs to a limit of ~ 10 kg m^{-2} s$^{-0.5}$. This method has reduced the sample size needed for characterization from 1.5 ml to only 30 μl and allows the measurement to be made in an enclosed system. © *2010 American Institute of Physics.* [doi:10.1063/1.3353379]

I. INTRODUCTION

Room temperature ionic liquids (RTILs) are increasingly finding novel applications to chemical engineering problems for which they can be specifically tailored. RTILs are liquid at ambient temperature and comprise solely of ions. There are over 1×10^6 simple RTILs that need to be characterized to optimize their potential uses. Extending the available data on these pure liquids is difficult due to the expense of the large volumes required for traditional characterization methods. To advance quickly in this area, it is necessary to develop a method for characterizing the physical properties of the liquids quickly and efficiently using as small a volume as possible. Possible applications for RTILs include separation techniques,[1] catalysis,[2] organic synthesis,[3] pharmaceutical solvents,[4] fuels cells,[5,6] and many more. Some techniques for characterizing the RTILs have already been developed on chip including solution phase synthesis[7] and halide content.[8]

It has previously been shown that the quartz crystal microbalance (QCM) can be used to measure properties of RTILs,[9,10] which include the square root of the viscosity-density product ($\sqrt{\rho\eta}$) using a small volume method requiring only 40 μl. The viscosity of small volumes is often measured using cantilevers with a volume of only 1 ml.[11] The frequency response of a 5 MHz quartz crystal with a single sided liquid contact was characterized by the Kanazawa and Gordon equation (1),[12] which relates the change in frequency to the square root of the viscosity-density product,

$$\frac{\Delta f}{f_o} = -\frac{1}{Z_q}\left(\frac{f_s \eta \rho}{\pi}\right)^{1/2}, \tag{1}$$

where Δf is the change in resonant frequency, f_o is the fundamental frequency, the specific acoustic impedance of quartz: $Z_q = (\mu_q \rho_q)^{1/2} = 8.84 \times 10^6$ kg m^{-2} s^{-1}, $f_s = nf_o$ is the overtone fre-

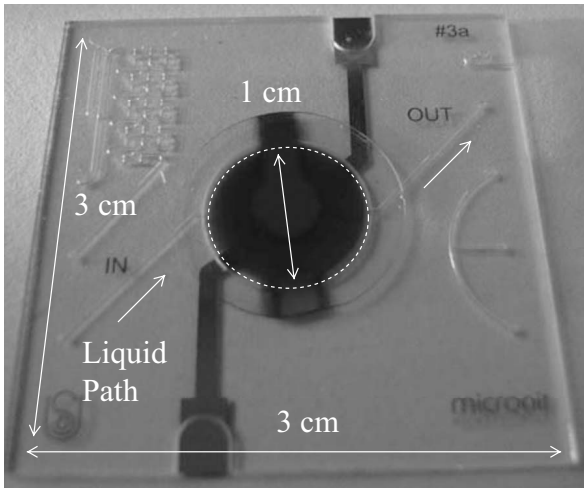

FIG. 1. Image of microfluidic glass chip; the QCM sits over the open top circular cell.

quency at which the response is measured, and ρ and η are the density and viscosity of the liquid, respectively.

In this work, we extend the previous study to incorporate the QCM on a glass microfluidic chip, reducing the required volume, allowing the measurement to be made in a sealed system, reducing the risk of water contamination, and giving the possibility of integrating other measurements onto the same chip.

II. EXPERIMENTAL

A. Microfluidic device setup

The custom designed microfluidic glass chip (3 cm $\times$ 3 cm $\times$ 1 mm) was fabricated by Micronit Microfluidics BV (The Netherlands) using two layers of glass. The chip consists of an open top circular cell with radius of 5 mm and depth of 300 μm with flow passages to and from the cell formed by wet etching (depth 125 μm), the QCM covers the open top circular cell, see Fig. 1. To connect to the flow system, standard Upchurch (WA, USA) microfluidic connectors were used, consisting of polyether ether ketone (PEEK) capillary tubing (inner diameter of 150 μm and outer diameter of 360 μm, stock 1572) with headless nuts and ferrules (outer diameter of 360 μm, stock F-123Hx and N-123–03x). To minimize risk of blockage a 2 μm filter capsule assembly (stock M-542) was used.

The chip is clamped in a holder with a specially designed top clamping system (Figs. 2 and 3).

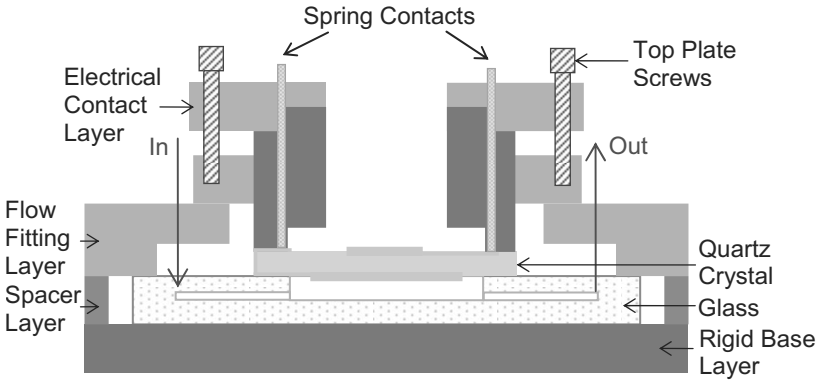

FIG. 2. Chip clamping system, including quartz crystal.

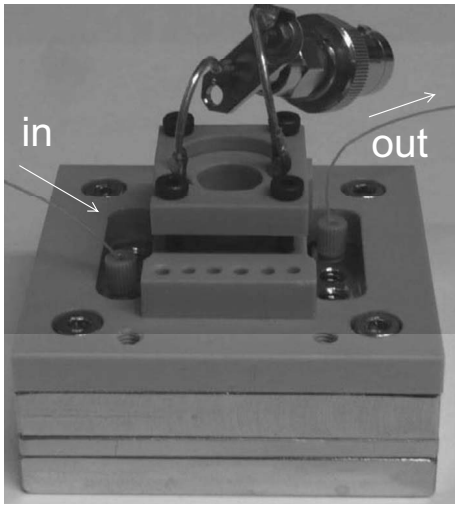

FIG. 3. Image of cell setup, with QCM clamped within the system.

This allows clamping of the QCM onto the glass chip outside the sensing region; the QCM is connected via spring contact pins.

Polished quartz disks (0.538 in. diameter) with a resonant frequency of 8 MHz were purchased from the International Crystal Manufacturing (OK, USA). Wrap around electrodes with diameters: Top 8 mm and bottom 4 mm were fabricated with 10 nm titanium and 150 nm gold using an Emitech K575X sputter coater.

Due to the chemical nature of the RTILs, it is important to use only chemically resistant materials. It has been found that by tightly clamping the PEEK against the QCM and the glass chip, a good seal is formed negating the need for any further sealing.

To ensure a stable temperature, the chip was placed in an Octagon 10 incubator (Brinsea, U.K.) and all measurements made at 30 °C. Liquid flow rate was controlled via a Nemesys syringe pump (Cetoni, Germany) with a gas tight syringe (Hamilton, Switzerland) volume dependent on the viscosity of the liquid. The chip requires a sample volume of only 30 μl and has been compared to measurements made with a Brookfield DVII+programmable viscometer (temperature controlled at 30 °C via a water bath) and DMA4500 density/specific gravity/concentration meter, which require a combined volume of 1.5 ml.

The square root viscosity-density product is calculated by measuring frequency changes and applying the Kanazawa and Gordon equation.[12] Measurements of resonant frequency changes for the QCM were obtained by tracking the frequency of the minimum insertion loss using an Agilent E5061A network analyzer for both the fundamental frequency and the third overtone. Liquid flow was stopped to allow the frequency measurements to be recorded.

Various concentrations of water glycerol solutions (0%–85% v/v) were used as calibration liquids to ensure that the QCM frequency changes were behaving according to the expected relationship.[12] Measurements of various concentrations of $[C_2mim][EtSO_4]$ (0%–100% v/v), a water miscible RTIL, and a further eight RTILs were studied (Table I). The RTILs were dried under vacuum overnight at 65 °C before use to ensure minimal water content. Immediately prior to QCM measurements, the viscosity and density were measured on a standard viscometer and densitometer ensuring that the water content for a given liquid was the same for both techniques; halide content was recorded using suppressed ion chromatography.[16]

Liquid flow rates ranged from 0.04 μl/s for highly viscous samples (>100 cP) to 2 μl/s for cleaning. Six fluid volume changes are used to ensure that there is no residue remaining from previous samples. For this purpose, water and methanol are used until the resonant frequency of the crystal returns to its unloaded value. Liquid exchange is made without opening the cell; if the cell is opened, recalibration would be needed to ensure that the QCM is operating as expected.

TABLE I. RTIL names and sources.

RTIL	Chemical name	Manufactured	Halide content (ppm)
$[C_2mim][EtSO_4]$	1-ethyl-3-methylimidazolium ethylsulfate	In house using standard literature methods[a]	Halide free
$[C_2mim][NTf_2]$	1-ethyl-3-methylimidazolium bis(trifluoromethylsulfonyl)imide		<5
$[C_4mim][NTf_2]$	1-butyl-3-methylimidazolium bis(trifluoromethylsulfonyl)imide		<5
$[C_6mim][NTf_2]$	1-hexyl-3-methylimidazolium bis(trifluoromethylsulfonyl)imide		<5
$[C_8mim][NTf_2]$	1-octyl-3-methylimidazolium bis(trifluoromethylsulfonyl)imide		<5
$[C_{10}mim][NTf_2]$	1-decyl-3-methylimidazolium bis(trifluoromethylsulfonyl)imide		<5
$[C_4dmim][NTf_2]$	1-butyl-2,3-dimethylimidazolium bis(trifluoromethylsulfonyl)imide		<5
$[C_4mpyrr][NTf_2]$	1-butyl-1-methylpyrrolidinium bis(trifluoromethylsulfonyl)imide		<5
$[C_4mpyrr][DCA]$	1-butyl-1-methylpyrrolidinium dicyanamide	Merck (98%)	1790

[a]References 13–15.

B. Seal leakage rate

The leakage rate of liquid out through the seal may be estimated using the model of radial flow in a gap of uniform height, as illustrated in Fig. 4. Determination of the velocity and pressure distribution (p) in the gap is relatively straightforward since the gap height is small in relation to radial position and the flow is necessarily in the Stokes flow regime. For these conditions one finds with approximation of order h/r the equation for radial pressure gradient in terms of leakage volume flow rate Q_L, gap height h, liquid viscosity μ, and radius r,

$$\frac{dp}{dr} = -\frac{6\mu Q_L}{\pi h^3 r}. \tag{2}$$

Integration from r_1 to r_2 then yields a relation between pressure differential and leakage flow rate,

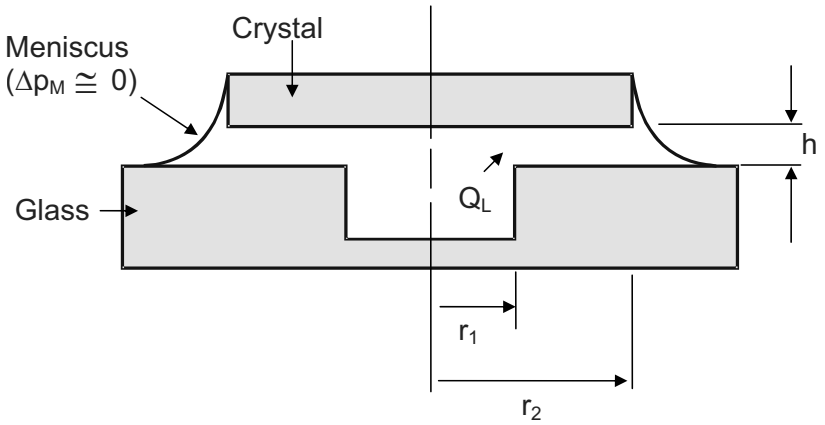

FIG. 4. Model geometry used to characterize the seal leakage rate.

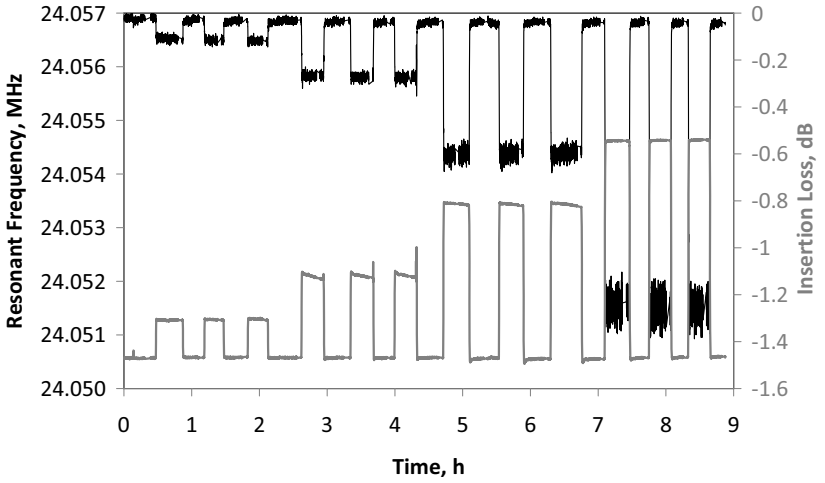

FIG. 5. A frequency and insertion loss time plot showing repeatability for the third overtone resonant frequency, sensing dilutions of $[C_2mim][EtSO_4]$.

$$Q_L = \frac{\pi h^3 (p_1 - p_2)}{6\mu \ln(r_2/r_1)}. \tag{3}$$

In practice, the gap is not uniform and varies according to the surface undulations in the glass and quartz surfaces. For the optical-quality surfaces involved in the experimental seal, the surface undulations are expected to be around 0.1 μm. Using this value for the height and a pressure difference of 1 bar, Eq. (3) gives a leakage flow rate of 1.5 pl/s in the case of a liquid with 0.1 Pa s viscosity. For continuous operation for 1 day, it can be worked out that if the leaked liquid formed a quarter-circular fillet around the perimeter of the cover disk, the fillet radius would be about 100 μm. In fact very little liquid could be detected over similar periods of operation, which suggests that in fact, the gap geometry corresponded to a yet smaller effective gap size than the 0.1 μm assumed above.

III. RESULTS AND DISCUSSION

The QCM response for various concentrations of $[C_2mim][EtSO_4]$ is shown in Fig. 5. This figure shows the frequency and insertion loss changes as a function of time operating at the third harmonic frequency. The changes in resonant frequency and insertion loss are very repeatable, with the figure showing the same liquid tested on the chip three times. On each occasion the frequency response returns to its original frequency. This consistency demonstrates that the sample volume of liquid is sufficient to provide reliable results.

Figures 6 and 7 show the calculated square root viscosity-density product from the frequency change of the QCM, operating on the fundamental and third harmonics, respectively, and compare them against the value obtained from the traditional measurements made on the viscometer and densitometer. The figures show values obtained for various concentrations of water glycerol solutions (0%–85% v/v) confirming that the QCM behaves according to the Kanazawa and Gordon relationship. The response at the fundamental frequency (Fig. 6) shows reasonable agreement with some scatter in the water glycerol solution data particularly at the lower viscosities. This scatter is significantly reduced when sensing on the third harmonic (Fig. 7). Both data sets follow the line of unity well. The RTILs present similar behavior with the scatter in the data for the fundamental significantly reduced when sensing on the third harmonic; the largest scatter is seen for the most viscous liquid measured ($\sqrt{\rho\eta} \sim 11$ kg m^{-2} s$^{-1/2}$).

It has previously been reported that the third harmonic provides a more accurate frequency change measurement.[17] This is confirmed for this application in Figs. 6 and 7. We have also seen this behavior experimentally when working with 9 MHz quartz crystals although these data have

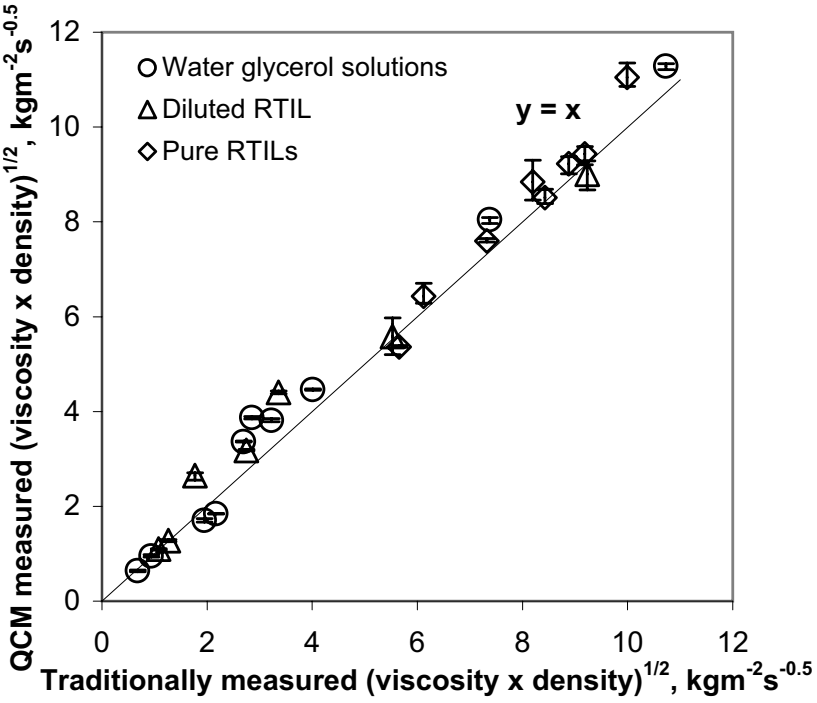

FIG. 6. Fundamental frequency data plot of the (viscosity × density)$^{1/2}$ for water glycerol solutions, dilutions of [C_2mim][$EtSO_4$], and eight pure RTILs (where traditional measurements refer to the value calculated from the viscometer and densitometer). A unity line is plotted to demonstrate linearity.

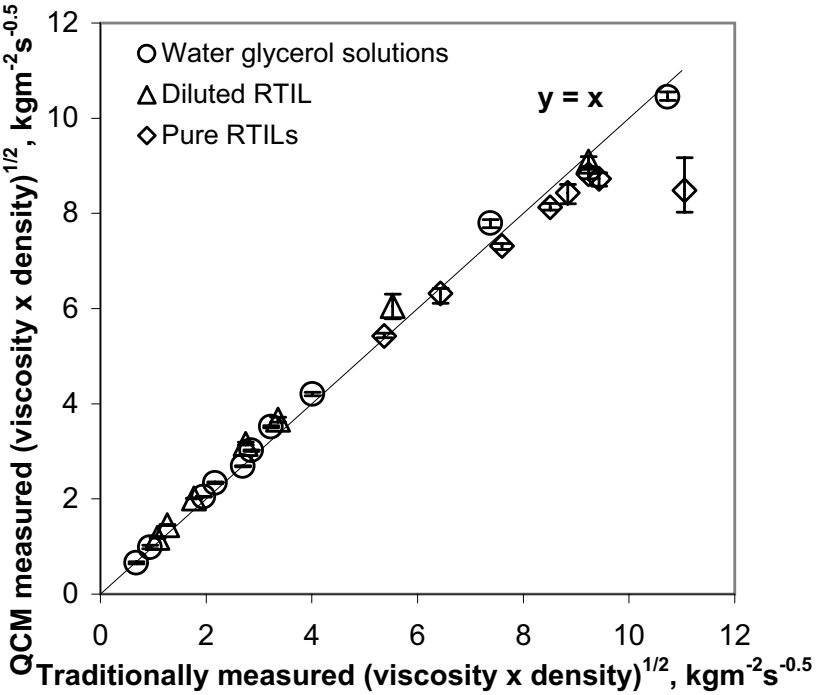

FIG. 7. Third overtone frequency data plot of the (viscosity × density)$^{1/2}$ for water glycerol solutions, dilutions of [C_2mim][$EtSO_4$], and eight pure RTILs (where traditional measurements refer to the value calculated from the viscometer and densitometer). A unity line is plotted to demonstrate linearity.

not been included. At the frequencies used, standing (compressional) waves were not a problem; however at other frequencies, this may become a problem but could be overcome with the use of a spoiler.[18] For high viscosity liquids ($\sqrt{\rho\eta} > 10$ kg m^{-2} s$^{-1/2}$), this behavior begins to break down and we believe we have reached the limit of detection for the 8 Mz QCM in the system. The agreement between the traditional viscosity-density measurements and QCM measurements is excellent despite several orders of magnitude difference in shear rates.

IV. CONCLUSION

By using the laboratory on a chip system detailed above, we have measured the viscosity-density product of RTILs using volumes as low as 30 μl, which can be further reduced by optimizing the tubing lengths. This compares well with commercially available hardware with typical volumes around 150 μl.[19] The QCM offers an excellent alternative to larger volume techniques and is particularly advantageous when characterizing hygroscopic liquids, whereby the viscosity decreases exponentially with water contamination. Ideally this method would be combined with a simulation study such as those described by Jacquemin *et al.*,[20] allowing us to extract viscosity and density as separate components for RTILs.

ACKNOWLEDGMENTS

We gratefully acknowledge the UK Engineering and Physical Sciences Research Council for funding under Grant Nos. EP/D03826X/1, EP/D038294/1, and EP/D038995/1.

[1] A. Berthod, M. J. Ruiz-Angel, and S. Carda-Broch, J. Chromatogr. A **1184**, 6 (2008).
[2] V. I. Pârvulescu and C. Hardacre, Chem. Rev. (Washington, D.C.) **107**, 2615 (2007).
[3] W. S. Miao and T. H. Chan, Acc. Chem. Res. **39**, 897 (2006).
[4] H. Mizuuchi, V. Jaitely, S. Murdan, and A. T. Florence, Eur. J. Pharm. Sci. **33**, 326 (2008).
[5] J. W. Choi, G. Cheruvalley, Y. H. Kim, J. K. Kim, J. Manuel, P. Raghavan, J. H. Ahn, K. W. Kim, H. J. Ahn, D. S. Choi, and C. E. Song, Solid State Ionics **178**, 1235 (2007).
[6] P. R. Vasudeva Rao, K. A. Venkatesan, and T. G. Srinivasan, Prog. Nucl. Energy **50**, 449 (2008).
[7] P. Dubois, G. Marchand, Y. Fouillet, J. Berthier, T. Douki, F. Hassine, S. Gmouh, and M. Vaultier, Anal. Chem. **78**, 4909 (2006).
[8] R. Ge, R. W. K. Allen, L. Aldous, M. R. Bown, N. Doy, C. Hardacre, J. M. MacInnes, G. McHale, and M. I. Newton, Anal. Chem. **81**, 1628 (2009).
[9] C. D. Liang, C. Y. Yuan, R. J. Warmack, C. E. Barnes, and S. Dai, Anal. Chem. **74**, 2172 (2002).
[10] G. McHale, C. Hardacre, R. Ge, N. Doy, R. W. K. Allen, J. M. MacInnes, M. R. Bown, and M. I. Newton, Anal. Chem. **80**, 5806 (2008).
[11] P. I. Oden, G. Y. Chen, R. A. Steele, R. J. Warmack, and T. Thundat, Appl. Phys. Lett. **68**, 3814 (1996).
[12] K. K. Kanazawa and J. G. Gordon, Anal. Chem. **57**, 1770 (1985a).
[13] P. Bonhôte, A. P. Dias, N. Papageorgiou, K. Kalyanasundram, and M. Grätzel, Inorg. Chem. **35**, 1168 (1996).
[14] M. J. Earle, S. P. Katdare, and K. R. Seddon, Org. Lett. **6**, 707 (2004).
[15] W. Xu, L. M. Wang, R. A. Nieman, and C. A. Angell, J. Phys. Chem. B **107**, 11749 (2003).
[16] C. Villagrán, M. Deetlefs, W. R. Pitner, and C. Hardacre, Anal. Chem. **76**, 2118 (2004).
[17] D. J. Johannsmann, Appl. Phys. (N.Y.) **89**, 6356 (2001).
[18] F. Eggers and Th. Funck, J. Phys. E **20**, 523 (1987).
[19] See: www.q-sense.com/dbfiles/Flow module, QFM 401 for web.pdf.
[20] J. Jacquemin, R. Ge, P. Nancarrow, D. W. Rooney, M. F. Costa Gomes, A. A. H. Pádua, and C. Hardacre, J. Chem. Eng. Data **53**, 2473 (2008).

D.4 Conference Proceedings: 2008 IEEE International Frequency Control Symposium

Small Volume Determination of the Viscosity-Density Product for Ionic Liquids using Quartz Crystal Harmonics

N. Doy, G. McHale, P. Roach and M.I. Newton
School of Science & Technology
Nottingham Trent University
Clifton Lane, Nottingham, NG11 8NS, UK.
e-mail: glen.mchale@ntu.ac.uk

C. Hardacre and R. Ge
QUILL Center, School of Chemistry & Chemical Engineering
Queens University Belfast
Belfast, Antrim, BT9 5AG, North Ireland.

R. W. Allen, J. M. MacInnes and M. R. Bown
Department of Chemical & Process Engineering
University of Sheffield
Newcastle St, Sheffield S1 3JD, UK.

***Abstract*— Data for the physical properties of Room Temperature Ionic Liquids (RTIL) as a function of chemical composition is limited, owing to the expense and difficulty of producing large volumes of pure samples for characterization. In this work we demonstrate that the viscosity-density values, obtained using impedance analysis of a quartz crystal microbalance are consistent with those obtained using a viscometer and density meter, but only requires a sample volume two orders of magnitude smaller. We also demonstrate that the third harmonic yields closest correlation out of all the harmonics from the fundamental to the eleventh.**

I. Introduction

Ionic liquids are becoming increasing popular as alternative, environmentally friendly solvents. Over the past decade, the desire for cleaner industrial processes has led to the development of Room Temperature Ionic Liquids (RTIL). RTILs consist solely of ions which are liquid at room temperature. There are over a million simple liquids and over a billion binary liquids involving more complex synthesis. Large volumes of new liquids are rarely available for characterization. The Quartz Crystal Microbalance (QCM) is well known for studying the physical properties of small volumes of liquids. We have applied this technique to characterize RTIL reducing the volume needed significantly.

In this work we describe measurements made on a QCM on the fundamental resonance and a further five harmonics (numbers 3 to 11) to find which harmonic better agrees with data obtained by traditional methods. The liquids tested were 1-butyl-3-methylimiclazolium trifluoromethylsulfonate [C_4mim][OTf], diluted with water, and water immiscible 1-butyl-3-methylimidazolium bis(trifluoromethylsulfonyl)imide [C_4mim][NTf_2] diluted with methanol.

The financial support of the UK Engineering and Physical Sciences Research Council (EPSRC) under grants EP/D03826X/1, EP/D038294/1 and EP/D038995/1 is gratefully acknowledged.

II. Theory

When a QCM is loaded with a Newtonian liquid, the crystal's resonance is related to the properties of the liquid by the use of the well known equation described by Kanazawa and Gordon [1]. If a liquid is Newtonian, a frequency decrease, Δf, and a bandwidth increase, ΔB, occur in proportion to the square root of the viscosity-density product according to (1).

$$\frac{\Delta f}{f_o} = -\frac{1}{Z_q}\left(\frac{nf_o\eta\rho}{\pi}\right)^{1/2}, \quad \frac{\Delta B}{f_o} = \frac{2}{Z_q}\left(\frac{nf_o\eta\rho}{\pi}\right)^{1/2} \tag{1}$$

where f_o is resonant frequency of unloaded crystal, ρ and η are the density and viscosity of the liquid, respectively, Δf is change in resonant frequency, ΔB is change in bandwidth, Z_q is specific acoustic impedance of quartz = $(\mu_q\rho_q)^{1/2} = 8.84\times10^6$ kg m^{-2} s^{-1} and n is the harmonic number. If the liquid is Newtonian the response of frequency and bandwidth should be related by $\Delta f = -\Delta B/2$, allowing either the change in bandwidth or frequency to be used to determine the viscosity-density product.

The fundamental resonance is most commonly used for sensing, however there are also multiples of the fundamental frequency that may be used. By varying the harmonic number in (1) it is possible to calculate the viscosity-density product from the frequency shift obtained on that harmonic. The harmonic number allows application of this single equation to data taken at various harmonics, which may provide improved sensitivity [2,3]. Previous work on thin films has shown that the viscoelastic compliance of quartz resonators can be inferred from comparison of the shifts in frequency and bandwidth on various overtones [4].

III. EXPERIMENTAL

A 5 MHz polished quartz crystal with diameter 25 mm (Testbourne Ltd., UK) was connected to an Agilient Technologies E5061A Network analyzer with which the resonant spectra were recorded. The crystal holder was designed and produced 'in house' using machined PTFE to produce a solid PTFE seal as RTIL degrade most other materials. Spectra were collected both in air and loaded with liquids at 25 °C. Concentrations of both liquids were tested between 0 and 100% w/w. To ensure the resonant frequency returned to the original value distilled water and a methanol rinse were used for cleaning. The test cell required a sample size of 40 µl, with measurements made in a glove bag under argon due to the hygroscopic nature of the RTIL [5]. Before use the liquids were dried to ensure there was no water contamination, this was confirmed using a Karl Fischer Titrator.

The viscosity and density of the tested liquids was measured using Brookfield DV-II + Programmable viscometer and a DMA 4500 density/specific gravity/concentration meter using volumes of 1.5ml and 0.5ml respectively. Measurements of all harmonics were made using the QCM loaded with air, followed by a single volume of liquid. The data obtained was analyzed using the Butterworth Van Dyke Model (BVD) [3] implemented in LabView™ (National Instruments, CA) to obtain full spectra impedance analysis [6]. Dilutions of the liquids were used to vary the viscosity and density of the fluid. Harmonics were recorded to find the harmonic that gave the results in best agreement to those obtained with the traditional methods.

IV. RESULTS

The water content of pure $[C_4mim][OTf]$ and $[C_4mim][NTf_2]$ were 0.0681 % w/w and 0.0096 % w/w respectively, both with halide contents below 5.

A. Fundamental resonance

Accurate fitting to bandwidth data was most accurate for the fundamental resonance, but higher harmonics were less easily fitted and at the highest harmonics fits were not possible. However, fits provided resonant frequencies at all harmonics. Data is presented for ionic liquids up to 90 % w/w, above which the hygroscopic nature of the liquids dominate yielding larger errors causing deviation from the expected response.

Figure 1 demonstrates the Newtonian behavior of the liquid on the fundamental resonance for both $[C_4mim][NTf_2]$ and $[C_4mim][OTf]$ diluted to various concentrations. Here data for both liquids behave in a Newtonian manner, as shown with an approximate gradient of 0.5, allowing the square of the viscosity density product to be found using the frequency shift obtained with (1).

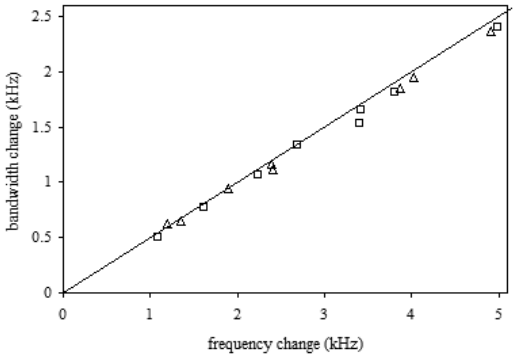

Figure 1 Fundamental data for $[C_4mim][NTf_2]$ (□) and $[C_4mim][OTf]$ (Δ) diluted to vary viscosity and density. Theoretical solid line to show expected Kanazawa and Gordan response.

B. Fundamental v's third harmonic

Figure 2 show the square root of the density-viscosity product measured by the QCM fundamental (triangles) and third harmonic (diamonds) compared to that measured using traditional methods for $[C_4mim][NTf_2]$ at varying viscosities. It is clear the data obtained on the third harmonic is in better agreement with the traditional method, with the fundamental data just below the expected values. Fig. 3 shows the equivalent plot for the $[C_4mim][OTf]$.

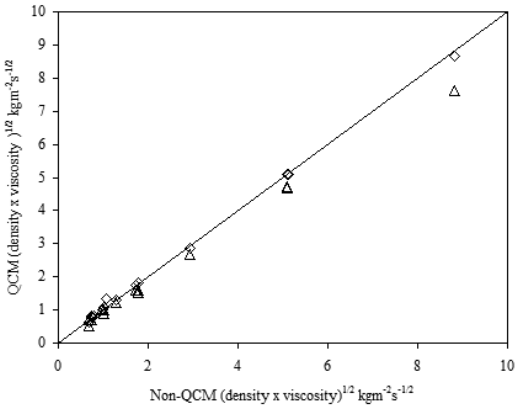

Figure 2 Fundamental (Δ) and third harmonic (◊) data determined by the QCM, showing the agreement to data for the square root of the viscosity and density obtained by traditional methods. The prediction of Kanazawa and Gordon is shown as a solid line for $[C_4mim][NTf_2]$.

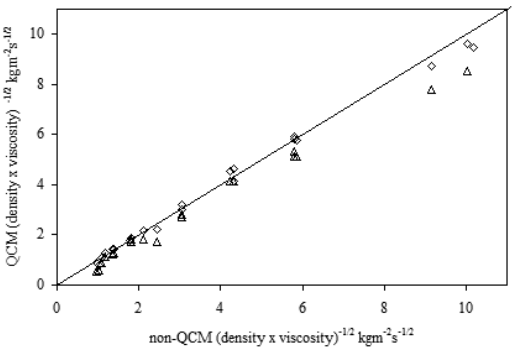

Figure 3 Fundamental (Δ) and third harmonic (◊) data determined by the QCM, showing the agreement to data for the square root of the viscosity and density obtained by traditional methods. The prediction of Kanazawa and Gordon is shown as a solid line for [C_4mim][OTf].

C. Harmonic data

Figure 4 shows the frequency change observed, against the expected square root viscosity-density product for various harmonic numbers. It is expected that all harmonic data will be linear. The fundamental, third and fifth demonstrate a similar relationship, with the fifth harmonic deviating somewhat at higher viscosities. Harmonics higher than the fifth, however, deviate completely from this line.

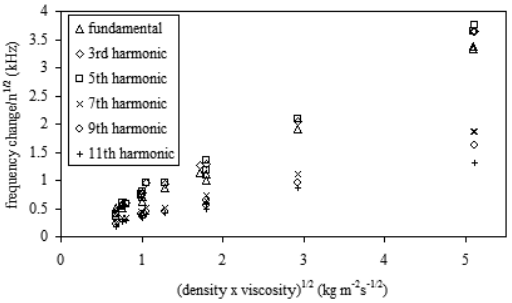

Figure 4 Frequency change observed for various harmonics of the QCM for [C_4mim][NTf_2] against the square root of the viscosity density product obtained by traditional methods.

V. Conclusion

For many room temperature ionic liquids only small volume samples are available. In this work we have shown that using such a small volume, the frequency change of a quartz crystal, measured on the fundamental resonance, allows the square root of the viscosity-density product to be calculated. Moreover, we have shown that closest agreement between the quartz crystal microbalance and traditional density-viscosity measurement using large volumes of liquid are achieved with the frequency change on the third harmonic of the quartz crystal microbalance. However, determination of the viscosity-density product using changes in bandwidth remains more reliable on the fundamental resonance.

References

[1] K. Kanazawa, and J. G. Gordon, "Frequency of a Quartz Crystal Microbalance in contact with a liquid," Journal of Analytical Chemistry, vol. 57, pp. 1770-1771, 1985.

[2] H. L. Bandey, S. J Martin, R. W. Cernosek, and A. R. Hillman, "Modeling the responses of thickness-shear mode resonators under various loading conditions," Journal of Analytical Chemistry, vol. 71, pp. 2205-2214, 1999.

[3] D. S. Ballantine, R. M. White, S. J. Martin, A. J. Ricco, E. T. Zellers, G. C. Frye and H. Wohltjen, "Acoustic Wave Sensors: Theory, Design, & Physico-Chemical Applications," Academic Press: San Diego, 1997.

[4] D. J. Johannsmann, "Derivation of the shear compliance of thin films on quartz resonators from comparison of the frequency shifts on different harmonics: A perturbation analysis," Applied. Physics. vol. 89, pp. 6356-6364, 2001.

[5] M. G. Freire, P. J. Carvalho, A. M. Fernandes, I. M. Marrucho, A. J. Queimada, J. A. P. Coutinho, "Surface tensions of imidazolium based ionic liquids: Anion, cation, temperature and water effect," Journal of Colloid and Interface Science, vol. 314, pp. 621–630, 2007.

[6] P. Roach, G. McHale, C. R. Evans, N. J. Shirtcliffe, M. I. Newton, "Decoupling of the liquid response of a superhydrophobic quartz crystal microbalance," Langmuir, vol. 23, pp. 9823-9830, 2007.

D.5 Conference Proceedings: 2009 Joint Meeting of the European Frequency and Time Forum and the IEEE International Frequency Control Symposium

Density and Viscosity Measurements of Room Temperature Ionic Liquids Using Patterned Quartz Crystal Microbalances

N.Doy, G.McHale, and M.I.Newton
School of Science & Technology
Nottingham Trent University
Clifton Lane, Nottingham NG11 8NS UK

C.Hardacre and R.Ge
QUILL Center, School of Chemistry & Chemical Engineering
Queens University Belfast
Belfast BT9 5AG, Antrim, North Ireland.

R.W. Allen, and J.M.MacInnes
Department of Chemical & Process Engineering
University of Sheffield
Newcastle St, Sheffield S1 3JD, UK.

***Abstract*— Ionic liquids are becoming of increasing interest for an extensive range of applications. Small scale characterization processes are being continually researched to find cheap and efficient methods for processing ever smaller sample volumes. This work presents a dual Quartz Crystal Microbalance (QCM) setup with one smooth, and one patterned surface using chemically compatible materials allowing separate viscosity and density measurements of room temperature ionic liquids. Measurements were corroborated with standard measurement techniques and show good agreement, demonstrating the merit of the dual QCM setup in determining the physical properties of these exciting new solvents.**

I. Introduction

In a previous report[1] we demonstrated that the viscosity-density product of small quantities of ionic liquids could be obtained using a QCM up to a limit of 18 kg m^{-2} $s^{-1/2}$ by applying the Kanazawa & Gordan equation. To separate these parameters, the method described by Martin *et al.*[2] is used whereby measurements of frequency changes using a dual QCM setup allows separate determination of viscosity and density.

II. Theory

A surface is considered smooth if the trapped liquid thickness is small compared to the liquid decay length[3] ensuring the liquid trapping response is negligible. The vertically patterned surface constrains a quantity of liquid within its structure in excess of the liquid which would be entrained by a smooth surface. This trapping effect restricts the liquid, allowing it to move only with the oscillating crystal surface. This results in the trapped liquid behaving as an ideal mass layer. For separate viscosity and density measurements, the height of the traps must be larger than the penetration depth (1) to cause an additional frequency change dependent only on the density. A dual device set-up containing one smooth and one textured QCM (Fig.1) allows viscosity and density to be resolved by comparison of these resonant frequency changes (2,3).

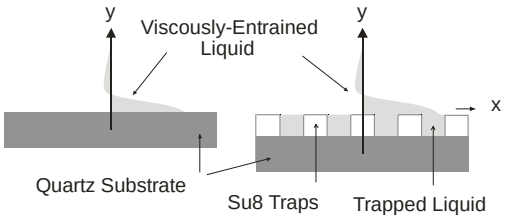

Figure 1 Diagram of (left) a smooth and (right) a patterned quartz crystal microbalance

$$\delta = (2\eta / \omega\rho)^{1/2} \tag{1}$$

$$\rho = \frac{N(\mu_q \rho_q)^{1/2}}{2 f_s^{\,2} h} \left| \Delta f_t - \Delta f_s \right| \tag{2}$$

$$\eta = \frac{2\pi h N(\mu_q \rho_q)^{1/2} (\Delta f_s)^2}{f_s \left| \Delta f_t - \Delta f_s \right|} \tag{3}$$

Where ρ is the density of liquid to be measured, η the viscosity of the liquid to be measured, *N the crystal* overtone number, h the effective height of traps, f_s the smooth crystal frequency, f_t trap bearing crystal frequency, Δf_t the change in trap bearing crystal frequency, Δf_s the change in the smooth crystal

frequency, ρ_q is the density of quartz (ρ_q = 2650kg/m^3) μ_q is the shear stiffness of quartz (μ_q = 2.95 x 10^{10}N/m^2).

III. Experimental

A. Photolithography

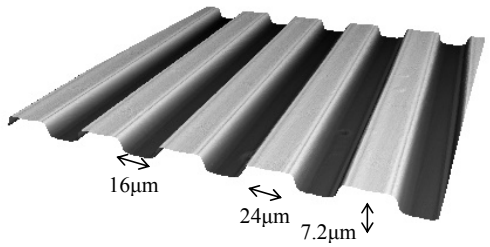

Figure 2 Optical profilometer image of textured surface

Crystals were first cleaned via sonication in a bath of Decon90 (Decon Laboratories LTD, Hove, UK) and deionised water heated to 80^{o}C for 20min. This removes any dust particles from the surface of the crystals. The reflective surface of the gold electrode causes problems with thick photoresists, leading to uneven exposure. To overcome this, an anti-reflective coating XHRIC-16 (Brewer Science, MO, USA) was applied by spinning at 3000RPM, and heating to 230^{o}C for 2 minutes before cooling slowly. This successfully prevents any unwanted reflections.

SU8-10 was applied to the surface of the QCM using a standard protocol. The traps are direction specific, and need to be placed perpendicular to the X direction of the crystal. Trap dimensions were checked for uniformity under a microscope, and measured using a Xyris 4000 WL (TaiCaan Technologies, Southampton, UK) optical profilometer (Fig. 2).

Due to the chemical reactivity of the ionic liquids there are limited materials which are compatible. To test the chemical resistance of the traps 1-hexyl-3-methylimidazolium bis[(trifluoromethyl)sulfonyl]imide ([C_6mim][NTf_2]) was left on the trap surface for 48 hours. Comparison of profiles before and after show no damage and the traps were then coated with titanium and gold.

B. Methodology

The dual QCM arrangement consists of two standard 1" polished quartz crystals operating at fundamental frequency of 5MHz. One crystal is left blank as a reference crystal, the other patterned with a resist over the electrode surface creating liquid traps (fig. 1).

A Quartz Crystal Microbalance holder made from PTFE was used to clamp the crystals. An Agilent E5062 network analyser was used to record the resonant frequency changes. Each measurement on each crystal requires only 60µl of liquid, allowing one viscosity and one density measurement to be obtained using only 120µl of ionic liquid.

The viscosity and density measurements have been corroborated using a Brookfield DV-II+ Programmable viscometer requiring 0.5ml and an Anton Paar DMA 4500 Density meter requiring a volume of 1ml giving a total volume requirement of 1.5ml.

Measurements were made with water-glycerol solutions for calibration, and then on a room temperature ionic liquid 1-butyl-3-methylimidazolium trifluoromethylsulfonyl ([C_4mim][OTf]) diluted with water. The room temperature ionic liquid was dried before use ensuring minimal water content. Measurements were recorded with the crystals in a glove box under argon.

IV. Results

A. Water-glycerol

Fig. 3 and 4, show separately determined viscosity and density for water-glycerol solutions. These act as a calibration for future measurements. Results from the dual QCM setup are compared to traditional methods. Each point shows an individual measurement repeated three times.

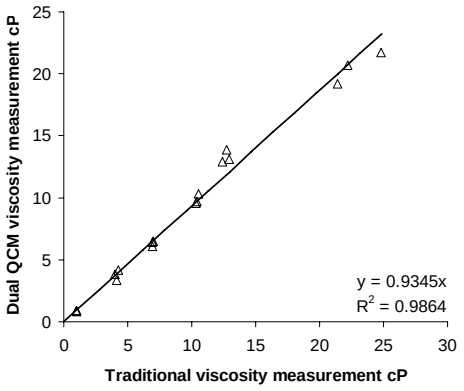

Figure 3 Water-glycerol calibration plots for viscosity measurements

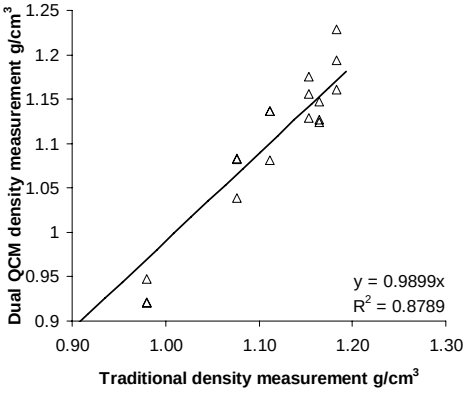

Figure 4 Water-glycerol calibration plots for density measurements

B. Room Temperatue Ionic Liquid

Fig. 5 and 6, show measurements made with diluted [C_4mim][OTf]. Results from the dual QCM setup are compared to traditional methods and show good agreement.

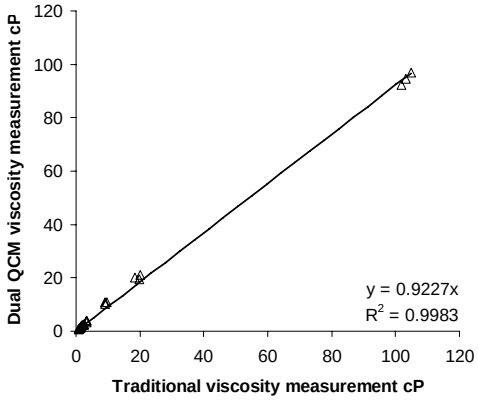

Figure 5 Varying the viscosity & density of [C_4mim][OTf] by dilutions with water: viscosity measurements

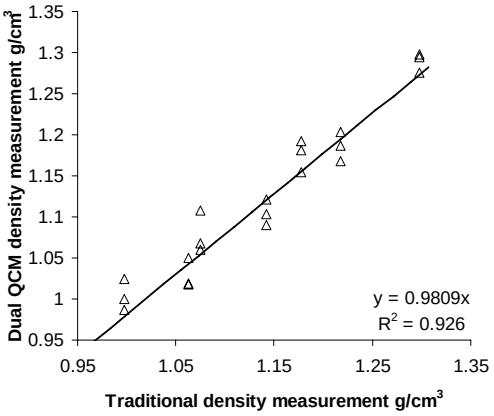

Figure 6 Varying the viscosity & density of [C_4mim][OTf] by dilutions with water: density measurements

V. Conclusion

We have presented an experimental technique demonstrating separate viscosity and density measurements of Room Temperature Ionic Liquids. These have been resolved from frequency measurements made on a dual QCM set-up. The agreement between these two measurement methods demonstrates the merit of the dual QCM setup in determining the physical properties of these exciting new solvents with an order of magnitude reduction in required sample volume.

References

[1] MCHALE, G., HARDACRE, C., GE, R., DOY, N., ALLEN, R. W. K., MACLNNES, J. M., BOWN, M. R. & NEWTON, M. I. (2008) Density-viscosity product of small-volume ionic liquid samples using quartz crystal impedance analysis. Analytical Chemistry, 80, 5806-5811.

[2] MARTIN, S. J., FRYE, G. C. & WESSENDORF, K. O. (1994) Sensing liquid properties with thickness-shear mode resonators. Sensors and Actuators A-Physical, 44, 209-218.

[3] KANAZAWA, K., & GORDAN, G. J., (1985) "Frequency of a Quartz Crystal Microbalance in contact with a liquid," Journal of Analytical Chemistry, vol. 57**,** pp. 1770-1771.

D.6 Conference Proceedings: IEEE 2009 Sensors

Separate Density and Viscosity Determination of Room Temperature Ionic Liquids using Dual Quartz Crystal Microbalances

N.Doy, G.McHale, and M.I.Newton
School of Science & Technology
Nottingham Trent University
Clifton Lane, Nottingham NG11 8NS UK

C.Hardacre and R.Ge
QUILL Center, School of Chemistry & Chemical Engineering
Queens University Belfast
Belfast BT9 5AG, Antrim, North Ireland.

R.W. Allen, and J.M.MacInnes
Department of Chemical & Process Engineering
University of Sheffield
Newcastle St, Sheffield S1 3JD, UK.

***Abstract*— The drive towards cleaner industrial processes has led to the development of room temperature ionic liquids (RTIL) as environmentally friendly solvents. They comprise solely of ions which are liquid at room temperature and with over one million simple RTIL alone it is important to characterize their physical properties using minimal sample volumes. Here we present a dual Quartz Crystal Microbalance (QCM) which allows separate determination of viscosity and density using a total sample volume of only 240µL. Liquid traps were fabricated on the sensing area of one QCM using SU-8 10 polymer with a second QCM having a flat surface. Changes in the resonant frequencies were used to extract separate values for viscosity and density. Measurements of a range of pure RTIL with minimal water content have been made on five different trap designs. The best agreement with measurements from the larger volume techniques was obtained for trap widths of around 50 µm thus opening up the possibility of integration into lab-on-a-chip systems.**

I. Introduction

Room Temperature Ionic Liquids (RTIL) have many characteristics which make them very desirable to industry providing the opportunity to reduce, or even completely eliminate, hazardous and toxic emissions into the atmosphere [1]. However, with millions of liquids potentially available, only a small percentage have been fully characterized. For this reason the limited physical property database needs to be expanded if RTIL are to be tailored for specific applications. The time needed to collect this vast amount of data and the sample volumes required, need to be reduced significantly to achieve this. Quartz crystal impedance analysis has recently been used to quantify the viscosity-density product of RTIL [2] using a small sample volume. Here we report an extension to the technique described by Martin *et al.* [3] which demonstrates a RTIL compatible setup capable of separating viscosity and density.

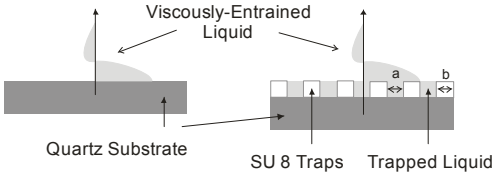

Figure 1 Diagram of smooth and patterned quartz crystal

II. Theory

The Kanazawa and Gordon equation has been successfully used for many years to allow the density-viscosity product to be determined for a range of liquids using a QCM [4]. Liquid is entrained within a penetration depth given by $\delta = (2\eta/\omega\rho)^{1/2}$, where η is the viscosity of the liquid, ρ is the density of the liquid and ω the angular resonant frequency of the QCM; for water at 5MHz this corresponds to around 250nm. Martin *et al.* [3] extended this work using two QCM, one smooth and one patterned with surface structure that trapped some of the liquid. The equations Martin et al used are shown below (1) and (2) and relate the frequency changes from the two crystals to allow separate viscosity and density measurements.

$$\rho = \frac{N(\mu_q \rho_q)^{1/2}}{2 f_s^{\,2} h} \left| \Delta f_t - \Delta f_s \right|, \tag{1}$$

$$\eta = \frac{2\pi h N(\mu_q \rho_q)^{1/2} (\Delta f_s)^2}{f_s \left| \Delta f_t - \Delta f_s \right|}, \tag{2}$$

The financial support of the UK Engineering and Physical Sciences Research Council (EPSRC) under grants EP/D03826X/1, EP/D038294/1 and EP/D038995/1 is gratefully acknowledged.

where ρ is the density of liquid to be measured, η the viscosity of the liquid to be measured, N the crystal overtone number, h the effective height of traps, f_s the smooth crystal frequency, f_t the trap bearing crystal frequency, Δf_t the change in trap bearing crystal frequency, Δf_s the change in the smooth crystal frequency, ρ_q is the density of quartz (ρ_q = 2650kg/m^3) and μ_q is the shear stiffness of quartz (μ_q = 2.95 x 10^{10}N/m^2). For these equations to be valid, the roughness needs to be sufficiently larger than the penetration depth so the trapped liquid experiences no shearing motion from the surface of the crystal.

III. Experimental

A dual QCM arrangement was used with two standard 1" (2.54cm) 5MHz quartz crystals (Tangidyne NY, USA), with one crystal patterned over the sensing region with SU-8 10 photoresist (MicroChem Corp., USA) using standard photolithography [5]. The pattern is designed to trap liquid within the structure ensuring it experiences no shearing motion and behaves as a rigid mass layer. The other crystal is left blank and used as a reference. Due to the chemical reactivity of the ionic liquids there is a limited range of materials which are compatible. To test the chemical resistance of the traps the RTIL [C_6mim][NTf_2] was left on the trap surface for 48 hours and a comparison of profiles before and after show no damage.

TABLE I. Trap design parameters

Trap Design	Trap Width µm	Separation Width µm	Effective Height µm
1	10.7	30.4	0.838
2	24.1	34.5	2.118
3	43.3	52.5	1.818
4	70.5	84.0	1.419
5	108.0	97.0	1.277

Table 1 shows the trap parameters for the five different designs investigated. Trap heights were the same for all the designs and were measured to be 8.4µm using a Dektak (Veeco, USA.) stylus profilometer. The traps are orientation specific and need to be aligned according to the crystal x-flat [6]. A volume of 120µL was used for each QCM measurement to ensure there was sufficient liquid to fill each trap and allows for a height of 57µm above their surface (for the largest trap volume). The penetration depth of the most viscous liquid tested corresponds to around 2.5 µm. Care was taken during cleaning to avoid damage to the surface of the traps. Water and ethanol were rinsed over the traps to remove all traces of the ionic liquids.

The changes in resonant frequencies of both the reference and patterned crystals were recorded with a Network Analyser (Agilent E8012) in a glove box at room temperature under an argon atmosphere to ensure minimal water contamination. A DV-II+ (Brookfield, USA) Programmable viscometer (0.5mL required volume) and a DMA 4500 (Anton Parr, Germany) Density meter (1.0mL required volume) were used to measure the liquid properties immediately prior to using the QCM setup. Various concentrations of water-glycerol and six pure RTIL (Table 2) were tested on each of the trap geometries.

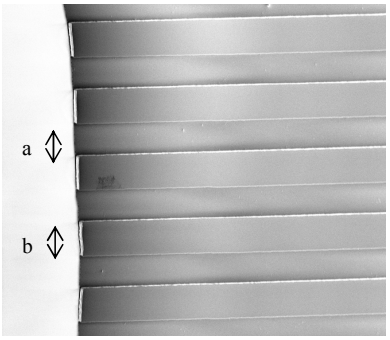

Figure 2 SEM image of traps produced with photolithography using SU8-10 (a = separation width, b = trap width)

TABLE II. RTILs with tradionally measured values for viscosity and density

Room Temperature Ionic Liquid	Chemical Name	Densitometer measured density g.cm^{-3}	Viscometer measured Viscosity cP
[C_2mim][NTf_2]	1-ethyl-3-methylimidazolium bis(trifluoromethylsulfonyl)imide	1.5190	29.1
[C_6mim][NTf_2]	1-hexyl-3-methylimidazolium bis(trifluoromethylsulfonyl)imide	1.3724	66.1
[C_{10}mim][NTf_2]	1-decyl-3-methylimidazolium bis(trifluoromethylsulfonyl)imide	1.2791	117.6
[C_2mim][$EtSO_4$]	1-ethyl-3-methylimidazolium ethylsulfate	1.2381	88.2
[C_4mim][DCA]	1-butyl-3-methylimidazolium dicyanamid	1.0591	27.8
[C_4mim][SCN]	1-butyl-3-methylimidazolium thiocyanate	1.1182	22.9

IV. Results and Discussion

Fig. 3 shows the viscosity measurement for different concentrations of glycerol in water up to a maximum concentration of 85%. For each of the trap designs there is linear relationship between the QCM derived value and the viscometer /densitometer measurements. The effective height shown in Table 1 is a geometrical fitting parameter derived from the fit in Fig. 3. Fig. 4 shows the density for the same range of water/glycerol mixtures for each of the trap designs.

From this data we can see that the smallest trap size and the largest trap size both show significant differences between the QCM derived value and the viscometer /densitometer measurements; the fit line shown here a gradient of 0.97. It is expected that there is a limit at which the traps no longer act to confine the liquid as a rigid mass. This is clearly reached by the largest traps of around 100µm. For the smallest traps the size is still much larger than the roughness used by Martin et al. however there surface was gold rather than our SU-8 10 for which water will have a much higher contact angle. This suggests that for our smallest traps, there is incomplete filling taking place, which in turn may trap some amount of air beneath the liquid; an overlayer of gold may overcome this limitation.

Fig. 5 shows the viscosity derived from the QCM plotted against that measured by the viscometer for the six different RTIL. As with the glycerol water solutions, the greatest error is seen for the smallest and largest traps with the other three trap sizes giving good agreement; the fit line has a gradient of one. In Fig. 6 the density derived from the QCM data is plotted against the data from the densitometer for the same six RTIL. As with viscosity, the greatest error is seen for the smallest and largest traps with the other three trap sizes giving good agreement; the fit line has a gradient of one.

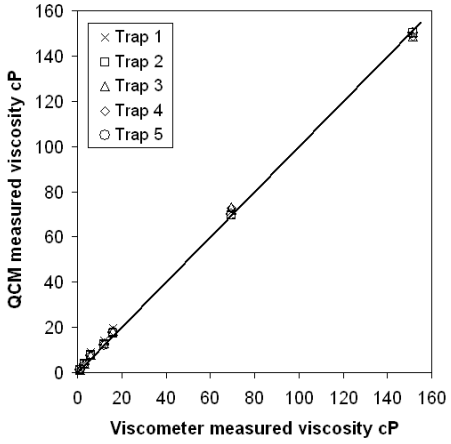

Figure 3 Viscosity measurements for different glycerol concentrations in water

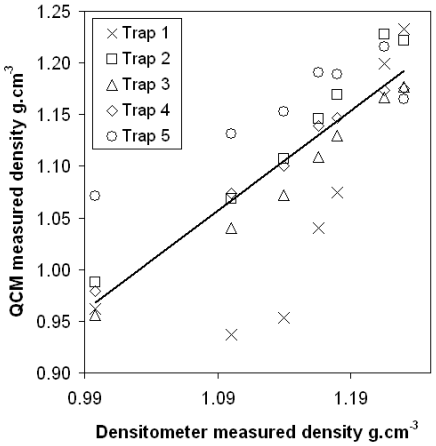

Figure 4 Density measurements for different glycerol concentrations in water

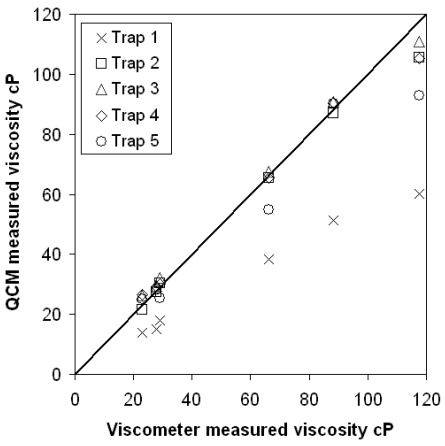

Figure 5 Viscosity measurements for the six different RTIL shown in table II

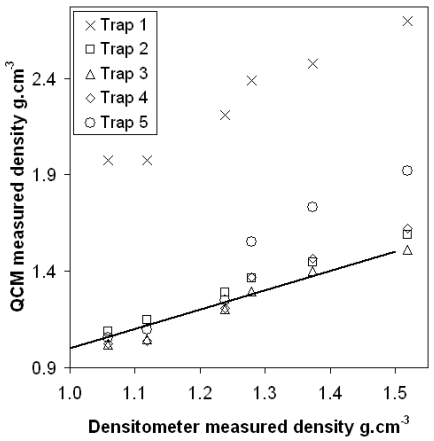

Figure 6 Density measurements for six different RTIL shown in table II

V. CONCLUSION

With the correct trap geometry the dual QCM separation technique offers a viable alternative to larger volume methods. Separate viscosity and density measurements have been made using a dual QCM set-up using a total volume size of only 240µL. This will potentially allow new liquids to be added to the physical property database [7] using smaller sample volumes.

In this paper we have reduced the current volume needed to measure viscosity and density by a factor of six and this could be further reduced by using smaller crystals thus opening up the possibility of integration into a lab-on-a-chip system.

REFERENCES

[1] J. D. Holbrey. "Industrial applications of ionic liquids," Chim. Oggi, vol. 22, pp. 35-37, 2004.

[2] G. McHale, et al. "Density-viscosity product of small-volume ionic liquid samples using quartz crystal impedance analysis," Analytical Chemistry, vol. 80, pp. 5806-5811, 2008.

[3] S. J. Martin, G. C. Frye & K. O. Wessendorf. "Sensing liquid properties with thickness-shear mode resonators," Sensors and Actuators A-Physical, vol. 44, pp. 209-218, 1994.

[4] K. Kanazawa, & G. J. Gordan. "Frequency of a quartz crystal microbalance in contact with a liquid," Journal of Analytical Chemistry, vol. 57**,** pp. 1770-1771, 1985.

[5] N. J. Shirtcliffe, et al. "The use of high aspect ratio photoresist (SU-8) for super-hydrophobic pattern prototyping," Journal of Micromechanics and Microengineering, vol. 14, pp. 1384-1389, 2004.

[6] C. Zhang, S. Schranz, & P.Hauptmann. "Surface microstructures of TSM resonators and liquid properties measurement," Sensors and Actuators B, vol. 65, pp. 296-298, 2000.

[7] H. Zhao. "Current studies on some physical properties of ionic liquids," Physics and Chemistry of Liquids, vol. 41, pp. 545-557, 2002.